RADIATION CROSSLINKED POLY(ETHYLENE OXIDE) HYDROGEL MEMBRANES

by

KATHLEEN ANNE DENNISON

B.S., Clarkson College of Technology

(1981)

S.M., Massachusetts Institute of Technology

(1984)

SUBMITTED IN PARTIAL FULFILLMENT
OF THE REQUIREMENTS FOR THE
DEGREE OF

DOCTOR OF PHILOSOPHY

at the

MASSACHUSETTS INSTITUTE OF TECHNOLOGY

March 14, 1986

Signature of Author _____
Department of Chemical Engineering
March 14, 1986

Certified by _____
Edward W. Merrill
Thesis Supervisor

Accepted by _____
William M. Deen
Chairman, Departmental Graduate Committee

RADIATION CROSSLINKED POLY(ETHYLENE OXIDE) HYDROGEL MEMBRANES

by
KATHLEEN ANNE DENNISON

Submitted to the Department of Chemical Engineering
on March 14, 1986 in partial fulfillment of the
requirements for the Degree of Doctor of Philosophy

ABSTRACT

It is possible to produce insoluble networks of poly(ethylene oxide) (PEO) by exposing aqueous solutions of PEO to ionizing radiation. During the irradiation process, bonds are formed between carbon atoms in the backbones of the polymer chains initially present, creating crosslinks between the chains. The resulting networks are highly hydrophilic and will swell in water to a volume up to 100 times the dry volume. This study concerned the important parameters controlling the structure and the mass transport characteristics of these networks. The chemistry of the process was investigated using spectroscopic techniques and size exclusion chromatography to follow changes in the molecular weight distribution of PEO samples. The structure was characterized by equilibrium swelling measurements, which provides the polymer volume fraction in the gel and the molecular weight between crosslinks, scanning electron microscopy, and differential scanning calorimetry. Effective diffusivities were measured in the swollen gels for a set of five globular molecules ranging in molecular weight from 1350 to 66000 and three linear PEO samples of molecular weight 1000, 8000, and 20000. The technique for finding the effective diffusivity was measurement of the solute uptake by the gel from a finite well-stirred reservoir of solution.

It was found that a wide range of gel structures could be obtained simply by changing the conditions of irradiation. The crosslink density of the gels in mol/mol repeat unit increased with increasing radiation dose and decreasing concentration. Chromatography work suggested that dose rate, pH, and solution additives would also affect the crosslink density. Gels with a porous structure could be made by adding K_2SO_4 to the solution, which decreases the solvent quality and causes phase separation on the same time scale as the irradiation. In the homogeneous gels, diffusion of linear PEO is controlled by the polymer volume fraction in the gel and is consistent with a reptation model of transport. Diffusion of the globular solutes is much more complicated. Diffusivities decrease with increasing polymer volume fraction and decreasing interjunction molecular weight, but neither is the controlling factor. Attempts to predict the transport behavior using a modification of the solution-diffusion model of transport were unsuccessful, which suggests that the structural dependence of transport in these gels is not simple.

Thesis Supervisor: Dr. Edward W. Merrill
Title: Carbon P. Dubbs Professor of Chemical Engineering

Acknowledgements

The author is pleased to have had the privilege of working with Professor Edward W. Merrill during this thesis project. The technical, financial, and moral support that Professor Merrill provided combined with his enthusiasm and interest in a wide range of subjects have made this project a truly valuable learning experience.

There are a number of other people who have contributed substantially to the completion of this project. Foremost among them is Kenneth Wright of the High Voltage Research Lab at MIT, whose able operation of the Van de Graaf accelerator made the project possible. Professors William M. Deen and Ulrich W. Suter provided useful suggestions in their capacity as thesis committee members. Erika Hartwieg of the MIT Biology Department Microscopy Facility was invaluable in the SEM work. Colleagues in the lab who have assisted in various capacities include Sew-Wah Tay, Cynthia Sung, Kyu-Ha Chung and Allen F. Horn.

The author also had the good fortune to work with several competent undergraduate students. In particular, significant contributions were made by Timothy Hueston in a BS thesis on various aspects of radiation crosslinking, Mark Panarusky in a UROP project which included osmometry and initial supported gel work, Peter Lukacs in a UROP project on cloud point measurements, and John Campbell in a UROP project which included salt partitioning, partition coefficient measurements, and differential scanning calorimetry.

This text of this thesis was produced with the assistance of an IBM PC/XT, SSI Wordperfect 4.1, and an IBM Quietwriter 2 printer. The illustrations were drawn by Richard Passmore, and most of the plots were made on a Hewlett-Packard 7470-A plotter driven by programs written for the IBM PC by Miguel Bibbo.

Finally, the financial support of the Millipore Corporation throughout this thesis project is gratefully acknowledged.

Table of Contents

List of Tables

List of Figures

Chapter 1. Summary

1.1. Introduction and Literature Review

For a number of years there has been interest in developing biocompatible semi-permeable membranes. There are a number of potential uses for such membranes; some of the more important ones include blood filtration (dialysis, plasmapheresis, and other more novel techniques) and controlled release drug delivery systems. If the material also shows low-protein-binding characteristics, which is likely, a large number of applications in the field of biotechnology, especially bioseparations, becomes important. Consequently, a large amount of effort has been directed toward developing low-protein-binding blood compatible membranes.

In a recent review, Merrill and Salzman [1] suggest that of the synthetic polymeric materials examined for blood compatibility, those containing some form of poly(ethylene oxide) showed the greatest compatibility. Poly(ethylene oxide) (PEO) is a synthetic polymer with the following structure

$$OH\text{-}[\text{-}CH_2\text{-}CH_2\text{-}O\text{-}]_n\text{-}H$$

where n can vary from about 5 to about 100000. This polymer is also known as polyoxyethylene (POE) and polyethylene glycol (PEG), particularly at lower degrees of polymerization (n small).

Because of the water-solubility of PEO, it must be deployed as a network for biological applications. The most popular ways of doing this have been as phase-separated block copolymer systems and as polyurethanes (also phase separated systems). Polyurethanes have been studied by Sa Da Costa [2], Mahmud [3], and Brash, et al [4], among others. Block copolymer systems examined include PEO-polyethylene terephthalate [5], PEO-polybutylene terephthalate [6], and PEO-polystyrene [7]. Two major conclusions can be drawn from these studies. First, networks containing PEO were more biocompatible than those containing poly(propylene oxide), and second, increasing the PEO content of the network increases the biocompatibility.

This previous work suggests that a network containing exclusively PEO would have desirable blood compatibility properties. Also, mass transport measurements on hydrogels formed by random crosslinking of water-soluble polymers such as polyvinyl alcohol [8,9] and polyhydroxyethylmethacrylate [10] indicate that these networks are semi-permeable and suggest that a PEO network should also be semi-permeable. These networks belong to a class of membranes referred to as solution-diffusion membranes [11], based on the postulated mechanism for transport through them. Although some previous work has been done, the mass transport behavior of these membranes has not been fully characterized either experimentally or theoretically for a number of reasons. The main thrust of this work is thus to develop, synthesize, and characterize semi-permeable PEO membranes in order to gain some insight into the network structural parameters controlling transport.

1.1.1. PEO Network Formation.

PEO networks can be made in a variety of ways, producing an equal variety of physical and chemical structures. In this work, it was desired to produce a network with a chemical structure as close as possible to that of linear PEO and a well-defined physical structure. The technique chosen to achieve this was radiation crosslinking. Treatment of polymers with ionizing radiation such as gamma irradiation or high energy electrons is a common technique, and can produce a variety of changes in the polymer, with the most important being crosslinking and main chain scission. Several reviews and books are available on this subject [35,36,37,38,39]. Irradiation of PEO has been shown to produce both carbon-carbon bonds between main chain carbons on the PEO backbone and scission of the chain [29,40,44]. When irradiated in bulk, whether as crystalline or amorphous polymer, scission was found to be the predominant process, but crosslinking could be accelerated by performing the irradiation in aqueous solution. This is apparently due to interaction of the products of water radiolysis with the PEO chain. The chemistry of the process was examined by a number of investigators [33,45,46,30], and the postulated important chemical reactions are summarized in table 1.1-1. The physical structure obtained is that of a randomly crosslinked network with a number of loose ends equal to twice the number of primary molecules (see figure 1.1-1.)

PEO Radiation Chemistry

Water Radiolysis

$$H_2O \longrightarrow H^{\cdot}, {}^{\cdot}OH, e^-_{aq} \quad (1)$$

$${}^{\cdot}OH + {}^{\cdot}OH \longrightarrow H_2O_2 \quad (2)$$

$$H^{\cdot} + H^{\cdot} \longrightarrow H_2 \quad (3)$$

$$H^{\cdot} + {}^{\cdot}OH \longrightarrow H_2O \quad (4)$$

$$e^-_{aq} + H_2O_2 \longrightarrow OH^- + {}^{\cdot}OH \quad (5)$$

$${}^{\cdot}OH + OH^- \rightleftharpoons O^{\cdot -} + H_2O \qquad pK = 11.9 \quad (6)$$

Interaction with PEO

Hydrogen Abstraction

$$CH_2\text{—}CH_2\text{—}O + {}^{\cdot}OH \longrightarrow CH_2\text{—}\dot{C}H\text{—}O + H_2O \quad (7)$$

$$CH_2\text{—}CH_2\text{—}O + O^{\cdot -} \longrightarrow CH_2\text{—}\dot{C}H\text{—}O + OH^- \quad (8)$$

Degradation

$$CH_2\text{—}\dot{C}H\text{—}O\text{—}CH_2\text{—}CH_2\text{—}O + H_2O_2 \longrightarrow CH_2\text{—}\underset{H}{C}\text{=}O + OH\text{—}CH_2\text{—}CH_2 + {}^{\cdot}OH \quad (9)$$

$$CH_2\text{—}CH_2\text{—}O\text{—}CH_2\text{—}\dot{C}H\text{—}O + e^-_{aq} \longrightarrow CH_2\text{—}CH_2\text{—}O^- + CH_2\text{=}CH\text{—}O + H_2O \quad (10)$$

Crosslinking

$$CH_2\text{—}\dot{C}H\text{—}O + CH_2\text{—}\dot{C}H\text{—}O \longrightarrow \begin{matrix} CH_2\text{—}CH\text{—}O \\ | \\ CH_2\text{—}CH\text{—}O \end{matrix} \quad (11)$$

Table 1.1-1. Proposed reaction scheme for the radiation chemistry poly(ethylene oxide) in aqueous solution. For details, see text.

Figure 1.1-1. Physical structure of randomly crosslinked PEO network. The number of loose ends is equal to twice the number of primary molecules; there may be some intramolecular crosslinking (loop formation).

1.1.2. Mass Transport Through Swollen Gels

There has been much work done in the field of membrane transport. However, only a small part of this work has been aimed at determining effective diffusivities in membranes, and much of that has looked at microporous membranes. That leaves a relatively small part of the previous work in the area of diffusion in swollen polymer gel systems. There are a number of books and reviews available on the subject of membrane transport; see refs. [11,59,60,61,62]. Swollen polymer gels can be defined as solution-diffusion membranes based on either a structural definition (no pores visible in scanning electron microscopy) [11] or an operational definition (no non-diffusive transport) [63]. Diffusive transport takes place by the dissolution of the solute species in the solvent present in the gel and diffusion through the solvent, not through the polymer itself. The two definitions are in general quite consistent with each other, and under both definitions homogeneous polymer gels fit into the solution diffusion category.

1.1.2.1. Previous Experimental Work

The current subject of interest will be limited to the concentration driven flux of solute species larger than the solvent species through highly swollen homogeneous polymer networks and to separations in which interactions between the polymer and the solute are negligible, that is, equilibrium distribution coefficients between solvent and membrane are close to the solvent volume fraction. These limitations are given for

two reasons. First, they are appropriate to the experimental system used in this study, and second, the theoretical development that will be discussed in section 1.1.2.2 requires that these conditions be met. There are several studies in the literature that meet (or claim to meet) these criteria. These include the definitive work of Colton and coworkers on transport through cellulosic membranes [66,67], the early study by Silliman on transport through glutaraldehyde-crosslinked poly(vinyl alcohol) (PVA) networks [8], the recent work by Peppas and coworkers [9] on poly(vinyl alcohol), and the work by Wisniewski and Kim [50] on polyhydroxyethylmethacrylate (polyHEMA) gels. All of these studies used the stirred batch dialysis technique of Colton [66] for measurement of the effective diffusivity. While the membranes are quite different from the PEO hydrogels used in the present study, it is instructive to consider the information obtained.

To briefly summarize, the major conclusion drawn from all of the studies except that of Reinhart and Peppas [9] is that the effective diffusivity falls rapidly with increasing solute size, and if examined in terms of the ratio of diffusivity in the membrane to diffusivity in pure solvent, the ratio fell about exponentially with increasing molecular size. This result would be expected for transport through a polymer solution. The study of Reinhart and Peppas [9] attempted to look at a different range of network structures in which transport would be restricted by the presence of crosslinks in the gel, and diffusivity should decrease more rapidly with molecular size than the earlier studies indicated. This is essentially what was found.

1.1.2.2. Theoretical Background

There are a number of ways to model transport through hydrogel membranes [61]. The most appropriate is the solution-diffusion theory first derived by Yasuda et al [70]. Three conditions are required for this theory to be appropriate. These are (1) that the transport is strictly diffusive and concentration driven, (2) there are no enthalpic interactions between the polymer and solute, and (3) that the network is highly swollen. The basis for the theory is that transport takes place through the solvent in the network. It is arrived at by starting with a rate equation for diffusion and assuming a free volume model for transport through the solvent applies. The following equation results for the ratio of the diffusion coefficient of a solute (subscript 2) in a solvent (subscript 1) swollen polymer (subscript 3) network, $D_{2,13}$, to that in pure solvent, $D_{2,1}$,

$$\frac{D_{2,13}}{D_{2,1}} = f(V_2) \exp\left[\frac{- B r_s^2 \pi}{V_{f,1}(Q-1)}\right] \qquad (1\text{-}1)$$

V_2 = characteristic volume of the solute
B = constant; includes diffusional jump length
r_s = effective solute radius
$V_{f,1}$ = free volume of solvent
Q = swelling ratio = $1/v_{2s}$

The two terms on the right hand side of equation 1-1 apply to two different effects of the network. The exponential term includes the effect of the polymer chains in reducing the amount of free volume

available for diffusion in the solvent in the network. The $f(V_2)$ term includes what is called the sieve effect. This is a restriction on transport due to the presence in the network of obstacles through which solutes cannot move. It is generally assumed that these obstacles are (or are related to) the crosslinks. The exponential term has been experimentally confirmed a number of times, but to date no successful expression for the sieve effect has been derived.

1.2. EXPERIMENTAL TECHNIQUES

The experimental system used to study the effect of network structure on diffusive transport was radiation-crosslinked poly(ethylene oxide) networks swollen in aqueous solutions. There are several advantages to this system, as well as some disadvantages. One of the most important reasons for using PEO is the low-protein-binding characteristics it appears to have, which allows the assumption that there are no enthalpic interactions between the solute molecules and the polymer chains. Radiation crosslinking has several advantages over end-linking. Network formation is accomplished without the addition of a crosslinking species, so there are no concerns about different interactions with different parts of the network or aggregation of the crosslinking species imposing a secondary structure on the network. Also, it is possible to synthesize gels with quite different structural properties that are virtually identical chemically. In terms of understanding the physical structure of the network, radiation crosslinking eliminates the ambiguity inherent in end-linking regarding the extent of reaction and junction

functionality, that is, all junctions have four chains extending from them no matter what synthetic conditions are used. One of the biggest disadvantages, which seems to be inherent in any aqueous system, is ordering or complexing of water by the chains. It is not clear a priori how this is likely to affect diffusive transport in the gel, but it certainly adds ambiguity to any liquid lattice calculations. The other disadvantages are due to the radiation crosslinking procedure. An important issue is chain scission. If it is an important process at the conditions of gel synthesis, the network structure will be different than expected as there will be some number of additional chain ends (and possibly other effects). Also, there is uncertainty about what end groups will result from scission, so the chemical structure may not be as simple as desired. However, the advantages of this system are more important than the disadvantages, some of which can be overcome by additional measurements or theoretical considerations.

1.2.1. Gel Synthesis and Characterization

Irradiation. All sample irradiation was done using 3 MeV electrons produced by a Van de Graaf accelerator at the High Voltage Research Lab at MIT. Samples were prepared from narrow-molecular-weight-distribution poly(ethylene oxide) obtained from Fluka Chemicals. Ultrapure water was prepared using a Milli-Q water polishing system (Millipore Corp) and 0.01% NaN_3 was added to all solutions to prevent bacterial growth. All other additives used were reagent grade.

Network Characterization. The interjunction molecular weight M_c, and hence the crosslink density of the networks was determined from equilibrium swelling measurements. Degree of swelling was measured by weighing pieces of gel immediately after crosslinking, when fully swollen, and after vacuum drying at 40°C for 24 hr and converting weights to volume fractions using known polymer and solvent densities. The affine deformation theory of Flory [19] as modified by Bray [48] for crosslinking in solution was used to find the interjunction molecular weight M_c and the crosslink density from the swelling measurements. It should be noted that an appropriate value for χ_1, the Flory-Huggins interaction parameter, is required in this calculation. It was therefore independently determined from osmotic pressure measurements on solutions of linear PEO at the same volume fractions important in the swelling measurements. As χ_1 was found to be nearly independent of polymer volume fraction at these conditions (v_2 ranging from 0.04 to 0.2), the average value of $\chi_1 = 0.426$ was used in all calculations. Infrared and nuclear magnetic resonance spectroscopy were done on both gels and solutions of PEO that had been irradiated. Scanning electron microscopy work was done on gels, using the technique of critical point drying to help preserve the structure of the swollen gel. Aqueous size exclusion chromatography was done using TSK PW polyether gel columns (Varian Instruments). SEC work was done on solutions irradiated below the dose required for gelation to look at relative amounts of crosslinking and scission as well as on material extracted from gel networks.

1.2.2. Effective Diffusivity Measurement

The effective diffusivities of various solutes in gels synthesized under a variety of conditions were measured using a technique based on the uptake of solute by the gel from a finite well-stirred solution volume. The solutes used for effective diffusivity measurements were proteins and narrow molecular weight distribution PEO samples and are listed in tables 1.2-1 and 1.2-2. The solvent was in all cases phosphate-buffered saline. Protein concentrations were determined by absorption at 280 nm and PEO concentrations were found using size exclusion chromatography. The conditions of synthesis of the gels used are given in table 1.2-3. In each experiment, a piece of gel of known size was placed in a known volume of solution. The data collected was the concentration in the solution at a specific time, which was converted to an effective diffusivity using the solution to the diffusion equation of Crank [90] for the infinite flat sheet geometry and the approximation of Ma and Evans [91] to account for the actual gel geometry. Additional experiments were done in which the gel was allowed to achieve equilibrium with the surrounding solution in order to determine the equilibrium distribution or partition coefficient between gel and solvent.

1.3. Results and Discussion

1.3.1. Crosslinking Characterization

Gel Dose. Figure 1.3-1 shows the results of a set of sample irradiations

Solute	Molecular Weight	Diffusivity (in Water)	Effective Radius	Ref.
Cyanocobalamin (Vitamin B12)	1355	3.79×10^{-6} cm^2/s	8.5 Å	66
Lysozyme	17000	1.04×10^{-6}	20.6	52
Chymotripsinogen	23000	0.95×10^{-6}	22.5	52
Ovalbumin	44000	0.776×10^{-6}	27.6	52
Albumin	67000	0.594×10^{-6}	36.1	52

Table 1.2-1. Globular solutes used in diffusivity measurements. The diffusivities refer to water at 25°C; effective radii are hydrodynamic radii in aqueous solution.

Nominal MW	Measured M_n (SEC)	M_w/M_n	Diffusivity (in Water)	$\langle r^2 \rangle^{1/2}$	Eff. Radius
1000	961	1.27	2.81×10^{-6} cm^2/s	42.2Å	14.6Å
8000	11211	1.05	8.22×10^{-7}	178.3	61.9
20000	21340	1.16	5.96×10^{-7}	260.8	90.5

Table 1.2-2. Summary of characterization of PEO samples used as solutes in diffusion measurements. The molecular weight measurements were done using size exclusion chromatography. Diffusivities were calculated using the correlation of Rossi, et al [35]. The effective radius refers to an effective hydrodynamic radius that is calculated assuming the molecule is behaving as an equivalent sphere in Einstein's law of viscosity.

Designation	PEO Conc.	Irradiation Dose	Solution Volume
3%,2.5	30 g/l	2.5 Mrad	7 ml
3%,5	30 g/l	5.0 Mrad	7 ml
5%,2.5	50 g/l	2.5 Mrad	7 ml
5%,5	50 g/l	5.0 Mrad	7 ml
10%,2.5	100 g/l	2.5 Mrad	7 ml
10%,5	100 g/l	5.0 Mrad	7 ml
10%,10	100 g/l	10.0 Mrad	7 ml
10%,15	100 g/l	15.0 Mrad	7 ml
15%,5	150 g/l	5.0 Mrad	7 ml
15%,10	150 g/l	10.0 Mrad	7 ml
15%,15	150 g/l	15.0 Mrad	7 ml
20%,5	200 g/l	5.0 Mrad	6 ml
20%,10	200 g/l	10.0 Mrad	6 ml
20%,15	200 g/l	15.0 Mrad	6 ml

Table 1.2-3. Conditions used for synthesis of gels used in effective diffusivity measurements. Results of the characterization are given in section 3.2.

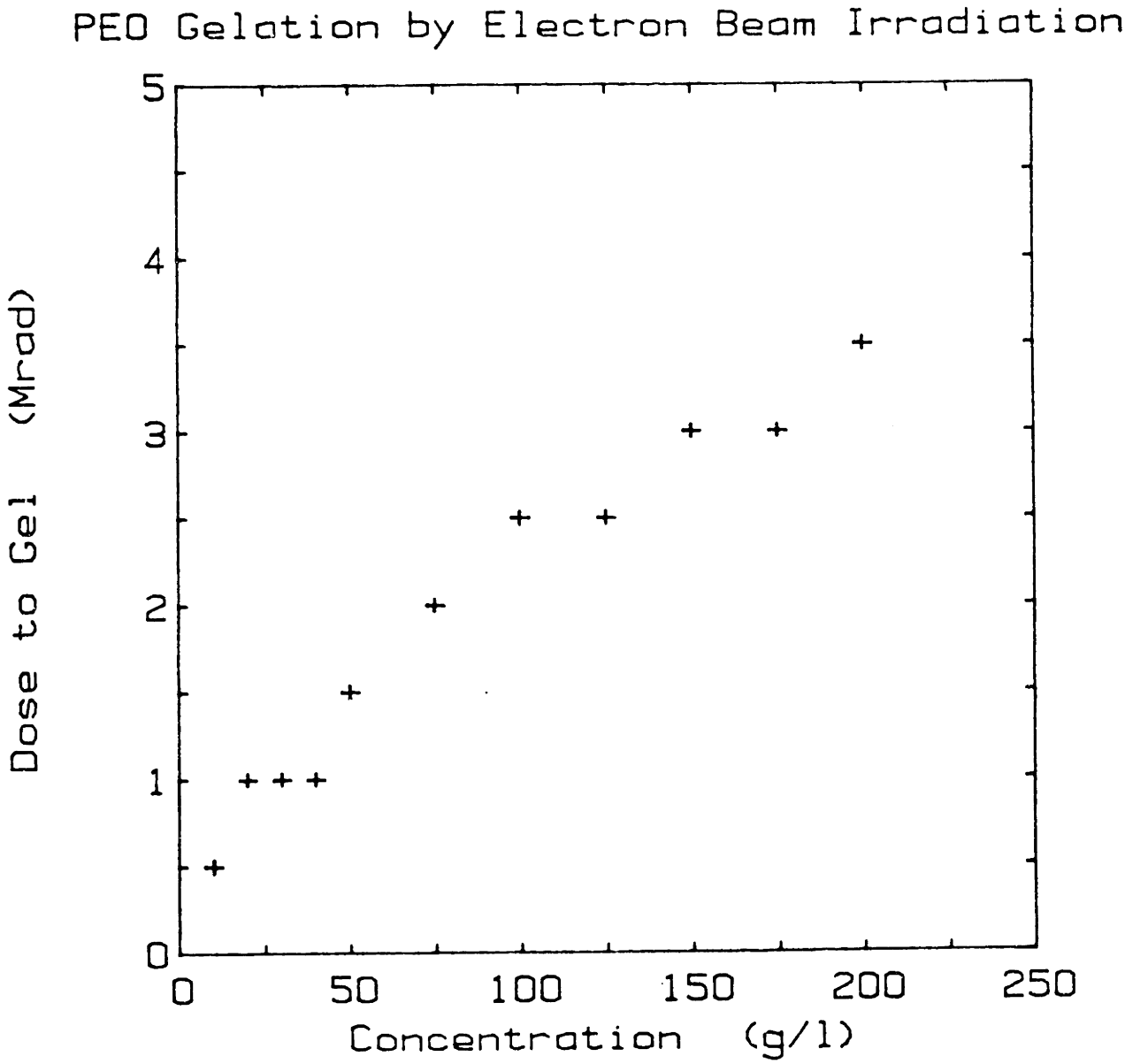

Figure 1.3-1. Approximate gelation dose as a function of PEO concentration for 35000 MW PEO in pure water. Dose rate was approximately 125000 rad/s.

done to determine the minimum dose required to gel solutions of PEO of 35000 molecular weight. As expected, the required dose to achieve gelation increases with increasing concentration in solution. This is due to the nature of gelation, which requires that a certain minimum number of crosslinks be formed per initial molecule to produce a gel. Higher concentrations have more molecules, and thus require more crosslinks to achieve gelation. Figure 1.3-2 is the energy input per crosslink as a function of concentration for the same set of samples. The most reasonable explanation for the increase in efficiency with increasing concentration is the bimolecularity in main chain radicals of the crosslinking reaction. The energy input per crosslink is more than an order of magnitude higher than that required for breaking two C-H bonds and creating a C-C bond, but about two orders of magnitude lower than the equivalent figure for gamma radiation, indicating that while electron beam radiation crosslinking is not an energy efficient process, it is much more efficient than gamma radiation crosslinking. This is due to the difference of several orders of magnitude in the dose rate for the two types of irradiation. Since high energy electron radiation is delivered at a much higher rate, the rate of radical production and thus the concentration of main chain radicals is much higher, which will favor the bimolecular crosslinking process.

Crosslink density above the gel dose. Figure 1.3-3 shows the equilibrium polymer volume fraction v_{2s} for gels fully swollen in water as a function of the crosslinking conditions. v_{2s} is seen to increase about linearly with dose and is only a weak function of initial concentration. Figure

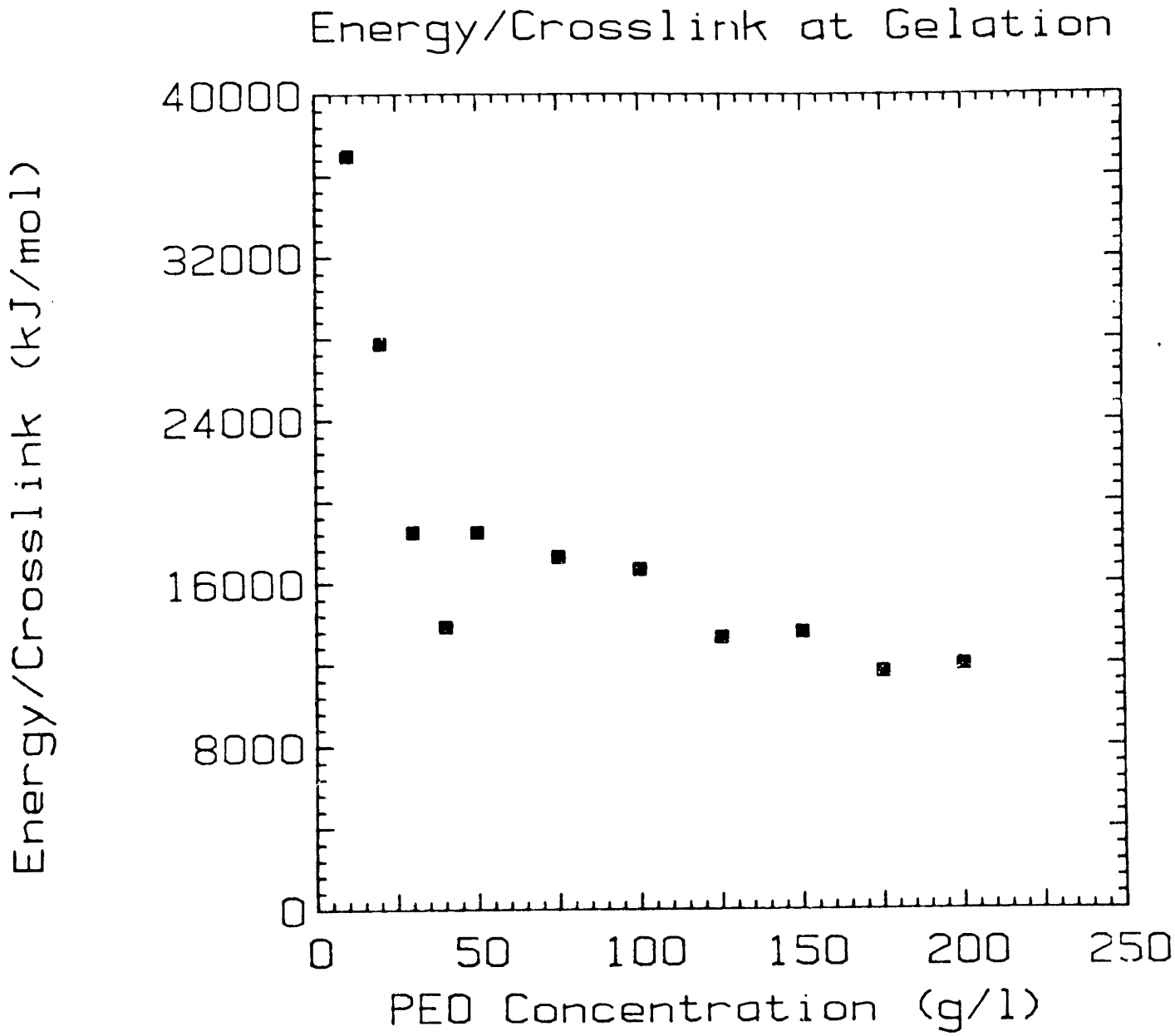

Figure 1.3-2. Gelation data replotted as energy input per mole of crosslinks as a function of PEO concentration.

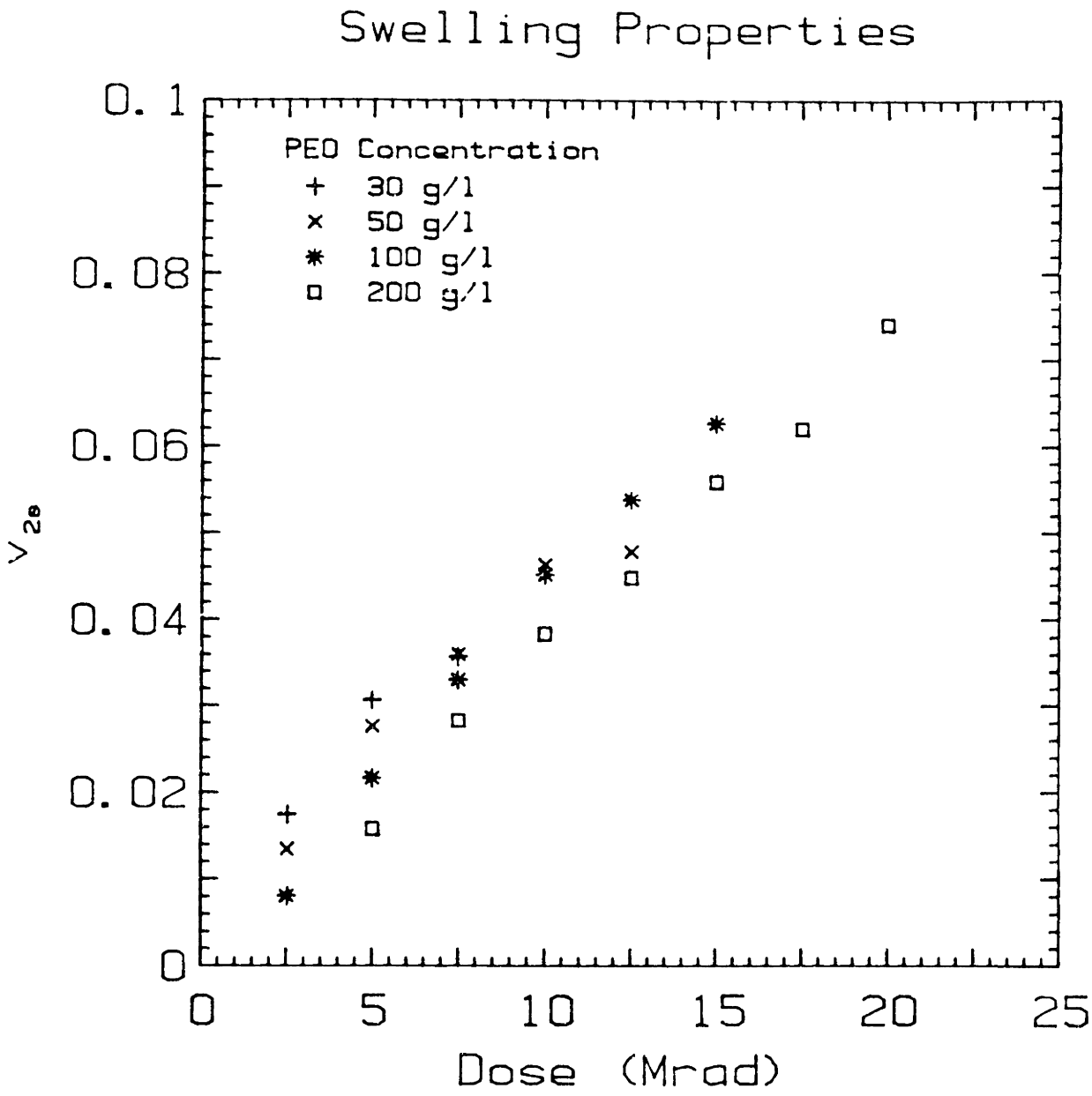

Figure 1.3-3. Polymer volume fraction for gels in equilibrium with pure water as a function of dose showing the effect of initial concentration.

1.3-4 shows the values for the interjunction molecular weight M_c calculated from the Flory-Bray affine deformation theory [48] as a function of dose. Clearly there is much more dependence of M_c on initial concentration. At sufficiently high levels of dose the value for M_c reaches a limiting plateau level. This plateau level is different for different initial concentrations, and is postulated to be the result of restricted motion of the network chains due to the high degree of crosslinking. The M_c and dose data of figure 1.3-4 can be converted to energy/crosslink, which is plotted as a function of dose in figure 1.3-5. Contrary to the expected behavior, the energy/crosslink is found to decrease with increasing dose, that is, the tighter the network, the easier it is to produce more crosslinks. It was expected that as the crosslink density increased the restrictions on chain motion would decrease the efficiency of the process. This result can probably be explained by the temperature rise produced in the samples during the irradiation process. Although no direct information about the temperature dependence of PEO irradiation crosslinking is available, it is known that both water radiolysis and polyethylene crosslinking increase in efficiency with increasing temperature [39]. The temperature rise during the present irradiations varies from about 5 to about 15°C per 2.5 Mrad dose, depending on the exact irradiation scheme used. This may be sufficient to account for the increase in efficiency with dose.

Scanning electron microscopy indicated that gels produced by irradiation in pure water were homogeneous. Spectroscopy showed no measurable amounts of any species not in linear PEO at any level of irradiation,

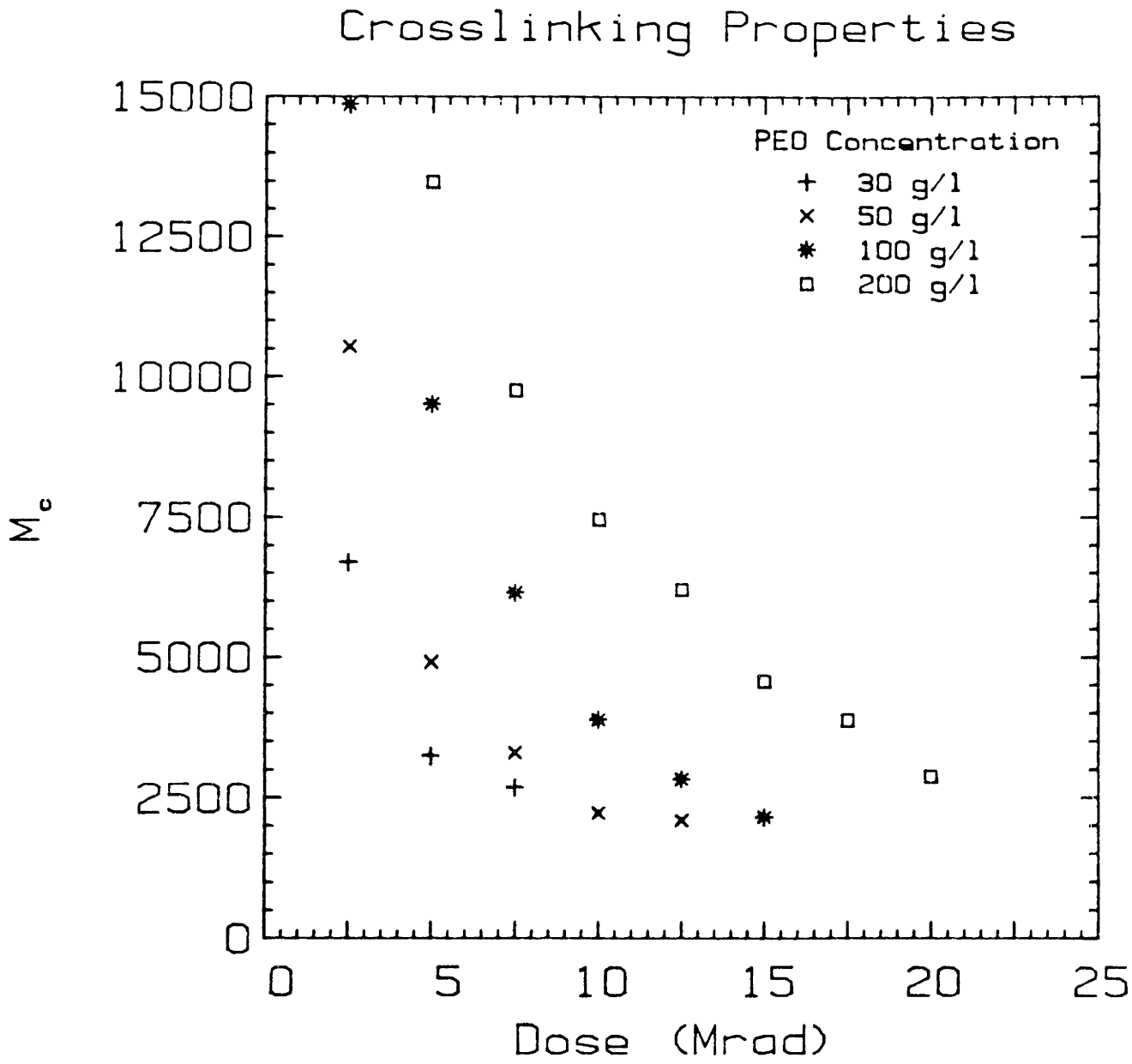

Figure 1.3-4. Values for the interjunction molecular weight M_c calculated from the swelling data of figure 3-3 using the Flory-Bray affine deformation theory.

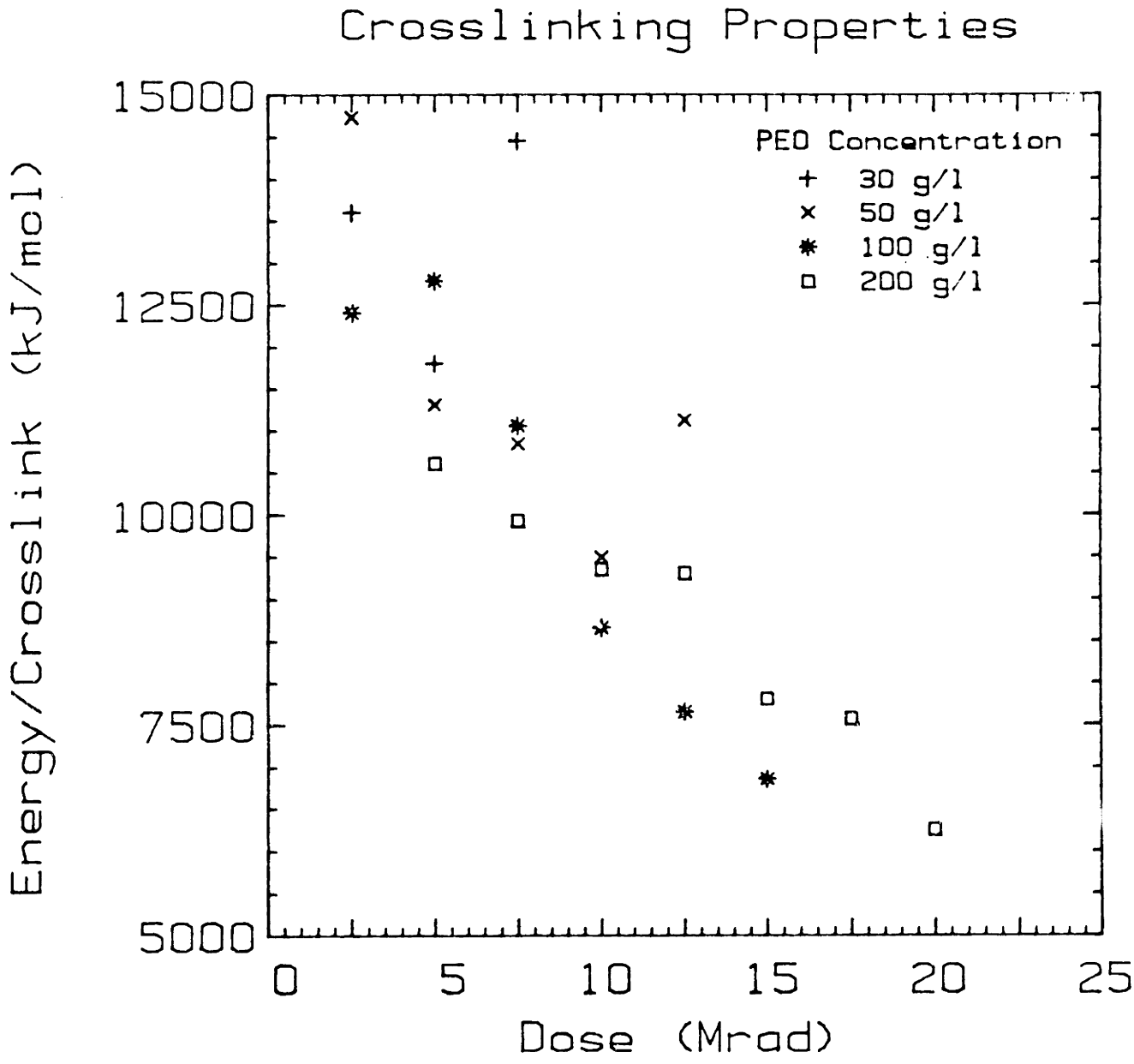

Figure 1.3-5. Data of figure 3-4 replotted as energy input per mole of crosslinks.

suggesting that the chemical structure of the gel should approximate that shown in figure 1.3-6.

Size exclusion chromatography. The SEC work was done primarily on solutions irradiated under conditions which did not lead to gelation. From the changes produced in the molecular weight distribution qualitative conclusions could be drawn about the relative amounts of crosslinking and scission as well as the overall efficiency of the process. Several parameters were varied; the important results are outlined below.

pH effect. The overall efficiency was highest at neutral pH and fell at high and low values. The ratio of crosslinking to scission was slightly higher at high pH. This could be the effect of a combination of reactions 6, 2, and 9 in table 1.1-1 (see ref. [33]).

Dose rate. The overall efficiency was about constant over the range of dose rates used, but the ratio of crosslinking to scission increased with increasing dose rate. This can be explained by the fact that crosslinking is bimolecular in main chain radicals but scission is unimolecular. Increasing the dose rate should increase the concentration of radicals and thus encourage crosslinking.

PEO concentration. Both the overall efficiency and the ratio of crosslinking to scission increased considerably over the range of concentrations used (1 to 10 g/l). There are two complementary reasons for this. The first is the bimolecularity of crosslinking. Since the ntration of water is about constant at the concentrations of PEO

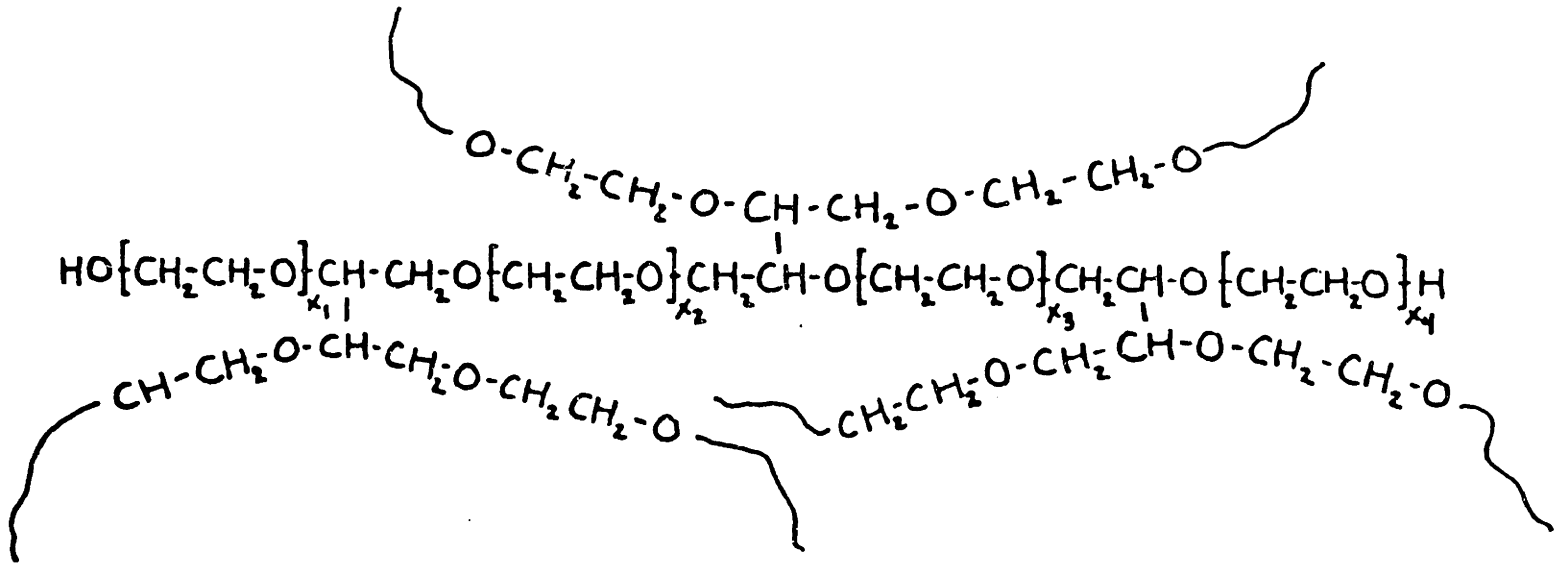

Figure 1.3-6. Expected chemical structure of radiation crosslinked PEO networks. For clarity, only a single chain is illustrated completely.

used, the concentration of water radiolysis products should be about constant. However, there are considerably more PEO chains to interact with these species, which should produce a higher concentration of main chain radicals for the same dose, leading to higher efficiency and more crosslinking. The second reason is related to the degree of overlap of the chains. At the low end of the concentration range, the chains are isolated coils, and crosslinking would be unlikely to occur.

Presence of oxygen. There was no measurable difference in molecular weight distribution between samples irradiated in oxygen and those irradiated in nitrogen. This is surprising, as a whole range of additional degradation reactions had been proposed to take place in the presence of oxygen [47]. However, it has been suggested [40] that at the dose rates used in electron irradiation it is not possible to keep solutions saturated with oxygen, and thus only the small amount initially present can react. Also, the aforementioned temperature rise will also tend to decrease the amount of dissolved O_2 available.

Solvent quality. It was found that decreasing the solvent quality by adding various amount of K_2SO_4 greatly decreased the efficiency of the irradiation. The effect on ratio of crosslinking to scission appeared to be minimal. The reduction in efficiency is postulated to be the result of the collapse of the PEO coils. This would make the chain segments less available for interaction with water radiolysis products, producing less main chain radicals.

1.3.2. Effective Diffusivity Measurement Results.

The effective diffusivity was measured for 8 different solutes in 10 gels. The gels were chosen to give as wide a range of the structural parameters v_{2s} and M_c as possible; unfortunately certain combinations of M_c and v_{2s} were either impossible to synthesize or very difficult to work with due to low structural strength. Values of the fully swollen polymer volume fraction v_{2s} in water and phosphate-buffered saline (PBS), the solvent used for all diffusivity measurements, and the interjunction molecular weight M_c for the gels used are found in table 1.3-1.

Partition Coefficients. The partition coefficient, or equilibrium distribution coefficient, between PEO gel and solvent was measured for each combination of gel and solute. It was found that there was no systematic difference between gels for the same solute (except those gels which completely excluded certain solutes). Therefore, the non-zero values for the partition coefficient were averaged for each solute and these averages used in subsequent calculations. The values were calculated as the ratio of concentration in the solvent in the gel to concentration in solution, and all values were within 20% of 1.0. This indicates that there is little interaction between the solutes and the polymer, and therefore the solution diffusion approximation should apply. Previous workers [50] had found that the partition coefficient was a function of network structural properties, in particular the degree of swelling. This was postulated to be an effect of the changing ratios of bound to free water. That effect is not seen here, but as the gels used

Gel	PEO Conc.	Irradiation Dose	v_{2s}(Water)	v_{2s}(PBS)	M_c
3%,2.5	30 g/l	2.5 Mrad	0.0172	0.0229	6926
3%,5	30 g/l	5.0 Mrad	0.0272	0.0349	3648
5%,2.5	50 g/l	2.5 Mrad	0.0137	0.0166	10425
5%,5	50 g/l	5.0 Mrad	0.0269	0.0386	5229
10%,2.5	100 g/l	2.5 Mrad	0.0074	0.0092	14655
10%,5	100 g/l	5.0 Mrad	0.0198	0.0232	10119
10%,10	100 g/l	10.0 Mrad	0.0461	0.0616	3752
10%,15	100 g/l	15.0 Mrad	0.0618	0.0849	2196
15%,5	150 g/l	5.0 Mrad	0.0187	0.0207	11671
15%,10	150 g/l	10.0 Mrad	0.0458	0.0616	4898
15%,15	150 g/l	15.0 Mrad	0.0639	0.0866	2898
20%,5	200 g/l	5.0 Mrad	0.0147	0.0175	13723
20%,10	200 g/l	10.0 Mrad	0.0483	0.0657	5436
20%,15	200 g/l	15.0 Mrad	0.0623	0.0840	3804

Table 1.3-1. Equilibrium polymer volume fraction v_{2s} in water and phsophate-buffered saline and interjunction molecular weight M_c of gels used in effective diffusivity measurements. M_c is determined from v_{2s} and the initial concentration using the swelling properties and the Flory-Bray affine deformation theory.

in this study are much more highly swollen than the poly(HEMA) gels used in the previous work, and as a much different class of solutes was used, this is not surprising.

Effective Diffusivity. The results of the effective diffusivity measurements for the globular solutes are summarized in table 1.3-2. Each diffusivity reported represents the average of 3 points. The three measurements were in general fairly consistent, varying about 20%. The error in the average values is estimated at about 30% and is higher for lower values of the diffusion coefficient, mostly due to the effect on the protein samples of being shaken at room temperature for long periods of time. Figure 1.3-7 shows a typical set of diffusivities for both the globular solutes and the PEO random coils as a function of solute size for the 15%, 10 Mrad membrane. From this plot we see the expected trend of decrease in diffusivity as solute size increases. It is interesting to note that the PEO coils diffused through the network much more easily than a protein of the same hydrodynamic radius. This is taken as evidence that the coils are not diffusing as globs but are able to uncoil and reptate [53] through the network. As this type of diffusion is not consistent with the assumptions involved in the solution-diffusion model of transport, all of the subsequent discussion will address only the globular solutes. From table 1.3-2 it is clear that the solute diffusivities and especially the maximum solute size that will penetrate a gel (molecular weight cut-off) depends strongly on the conditions of synthesis, and thus it is possible to synthesize gels with a large variety of semi-permeable properties. In general, a membrane with a high

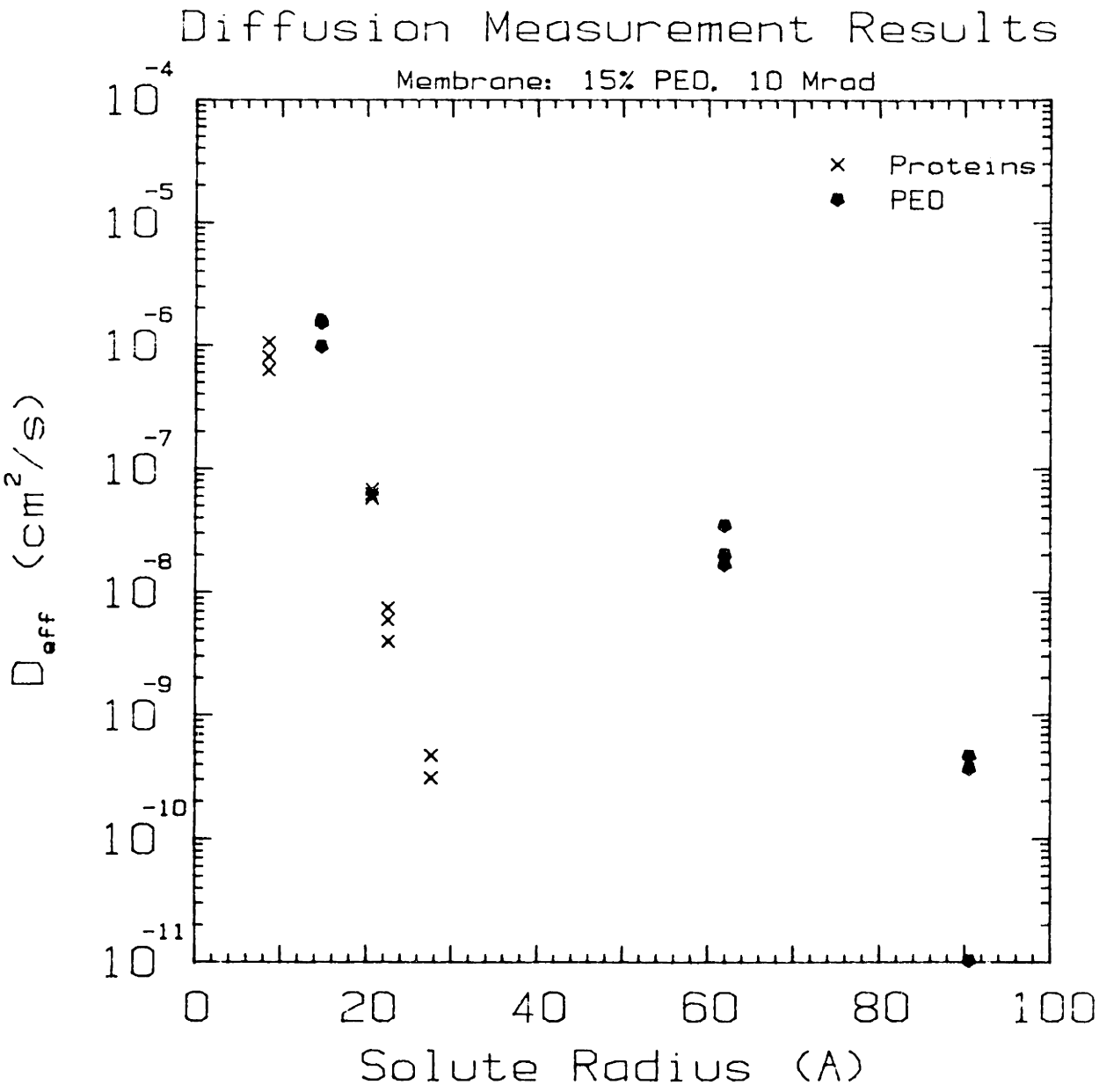

Figure 1.3-7. Effective diffusivity as a function of solute size for a 15% PEO, 10 Mrad gel. M_c = 4898, v_{2s}(PBS) = 0.0616.

Membrane	Cyanocobalamin	Lysozyme	Chymotripsinogen	Ovalbumin	Albumin
20%,5	3.29×10^{-6}	2.80×10^{-7}	1.15×10^{-7}	3.74×10^{-9}	3.01×10^{-10}
	0.867	0.296	0.121	4.82×10^{-3}	5.07×10^{-4}
20%,10	1.78×10^{-6}	4.02×10^{-7}	7.34×10^{-8}	1.52×10^{-9}	0
	0.469	0.387	7.73×10^{-2}	1.95×10^{-3}	0
20%,15	5.45×10^{-7}	2.74×10^{-8}	2.69×10^{-9}	2.18×10^{-10}	0
	0.144	2.64×10^{-2}	2.83×10^{-3}	2.82×10^{-4}	0
15%,5	9.43×10^{-7}	5.04×10^{-7}	1.33×10^{-7}	8.81×10^{-9}	6.83×10^{-10}
	0.249	0.485	0.140	1.14×10^{-2}	1.15×10^{-3}
15%,10	8.25×10^{-7}	6.29×10^{-8}	5.84×10^{-9}	3.96×10^{-10}	0
	0.218	6.05×10^{-2}	6.24×10^{-3}	6.68×10^{-4}	
15%,15	4.84×10^{-7}	3.01×10^{-8}	4.33×10^{-9}	3.78×10^{-11}	0
	0.128	2.89×10^{-2}	4.55×10^{-3}	4.86×10^{-5}	0
10%,5	9.78×10^{-7}	2.03×10^{-7}	2.35×10^{-8}	1.05×10^{-8}	0
	0.258	0.195	2.47×10^{-2}	1.35×10^{-2}	0
10%,10	9.83×10^{-7}	5.92×10^{-8}	2.55×10^{-9}	7.00×10^{-11}	0
	0.259	5.69×10^{-2}	2.68×10^{-3}	9.02×10^{-5}	0
10%,15	4.42×10^{-7}	4.09×10^{-8}	4.72×10^{-9}	0	0
	0.117	3.92×10^{-2}	4.97×10^{-3}	0	0
3%,5	2.53×10^{-7}	1.44×10^{-7}	-	2.67×10^{-8}	0
	6.67×10^{-2}	0.138	-	3.44×10^{-2}	0

Table 1.3-2. Summary of results of effective diffusivity measurements for globular solutes. The first line for each membrane is the diffusivity in the gel in cm^2/s and the second line is the ratio of diffusivity in the network to diffusivity in pure solvent.

degree of swelling and a large interjunction molecular weight has higher diffusivities than a tighter, less swollen one. When compared with the data of Colton [66] for traditional cellulosic dialysis membranes, it appears that for the same small solute (cyanocobalamin) diffusivity, a PEO hydrogel can have a lower (or zero) large solute diffusivity. Conversely, a PEO gel with the same albumin diffusivity as a cellophane membrane has a higher cyanocobalamin diffusivity. This can be summarized by saying that the size selectivity of the PEO gels used in this study is greater than that of traditional cellulosic membranes. Two things should be noted: 1. Colton's data for proteins does not appear to have been corrected for partitioning; however, this effect should not change the trends stated above. 2. As it is possible to make a whole range of PEO network structures, it is possible to make networks with a wide range of semi-permeabilities, especially if semi-permeability is evaluated in terms of molecular weight cut-off.

In order to determine what is controlling mass transport in these gels, it is useful to look at the ratio of diffusivity in the gel to diffusivity in pure solvent. The change in this ratio with solute size and swelling ratio can then be examined and compared with that predicted by equation 1-1 for the ratio of the diffusion coefficient in the membrane, $D_{2,13}$, to that in pure water, $D_{2,1}$,

$$\frac{D_{2,13}}{D_{2,1}} = f(V_2) \exp\left[\frac{- B r_s^2 \pi}{V_{f,1}(Q-1)}\right] \qquad (1\text{-}1)$$

V_2 = characteristic volume of the solute
B = constant; includes diffusional jump length
r_s = effective solute radius
$V_{f,1}$ = free volume of solvent
Q = swelling ratio = $1/v_{2s}$

to gain some insight into the controlling parameters. Figure 1.3-8 shows data for the same membrane as figure 1.3-7 replotted as the diffusion coefficient ratio as a function of solute area. If the sieve effect is unimportant, this semi-log plot would be expected to be a straight line, which is clearly not the case. This implies that some structural feature other than simply the presence of chains is affecting transport. The solid line in figure 1.3-8 was calculated from equation 1-1 assuming $f(V_2)$ is unity and using a value for $B/V_{f,1}$ found from the best fit line through Colton's data for an Avisco wet gel membrane [66] which was about 82% water. Clearly the assumption that $f(V_2)$ is unity is not correct for these membranes. That is, the sieve effect is important in transport of proteins through these highly swollen, moderately crosslinked PEO hydrogels.

1.3.3. Theoretical Development

In light of the determination that sieving is more important in controlling mass transport in these gels than is the free volume effect, an attempt was made to develop a theoretical expression for $f(V_2)$ in equation 1-1 relating easily measurable structural features of the gel to the transport properties. Minor corrections were also made to the expression for the free volume term to incorporate the appropriate

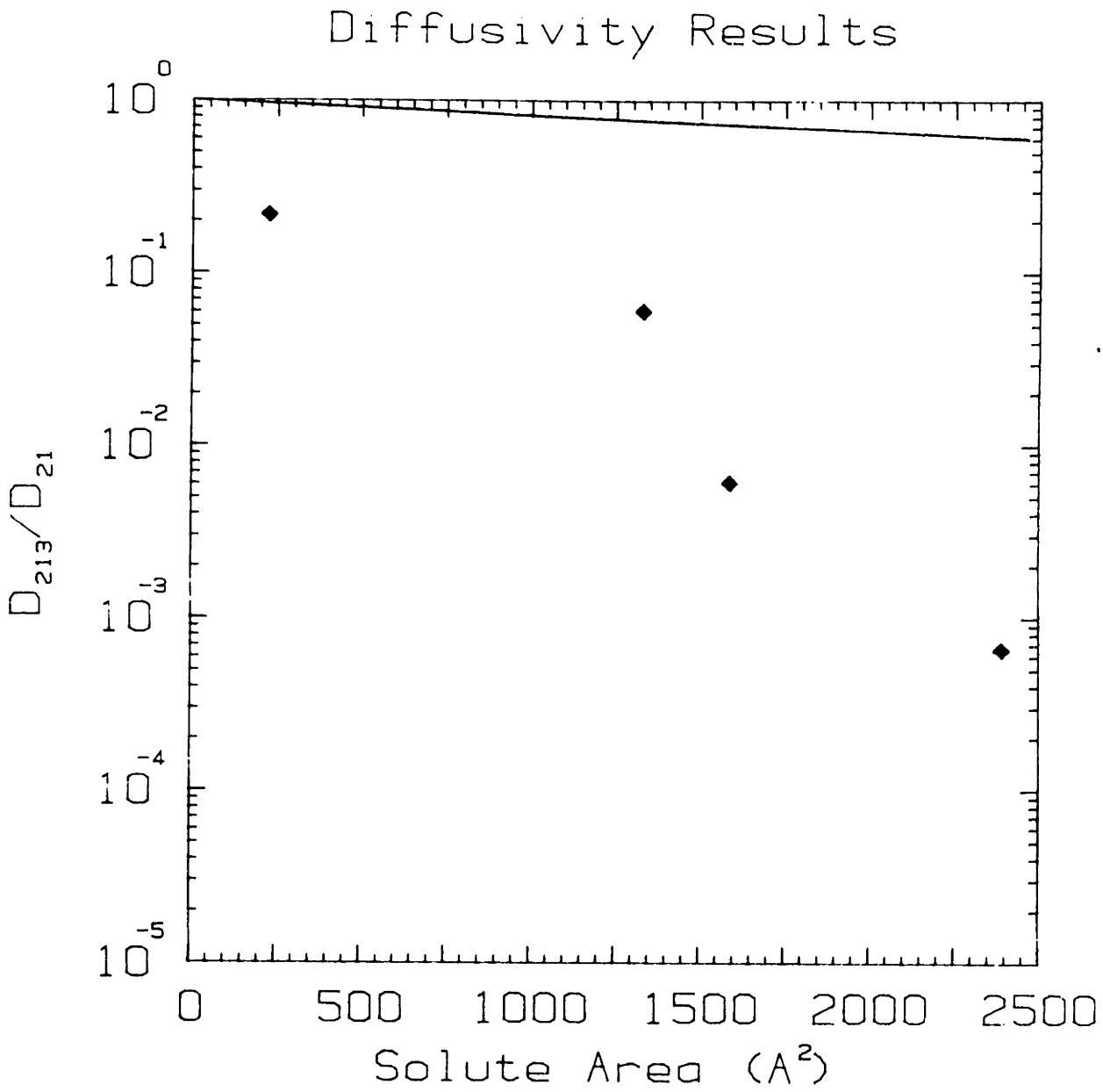

Figure 1.3-8. Data of figure 3-7 replotted as the ratio of diffusivity in the gel to diffusivity in pure solvent. The solid line is the prediction from equation 1-1, assuming $f(V_2) = 1$.

measure of the free volume. There are several ways of approaching the problem of the sieve effect. It was defined by Yasuda et al [70] to be the probability of a space between network restrictions being equal to or larger than V_2, which is a measure of the solute volume. The hardest part of deriving an expression for this term is determining what is physically restricting transport. Since the effect of the chains is included in the free volume term, the restrictions are assumed to be related to the presence of crosslinks. The mesh size ξ, which is a linear measure of the size of spaces in the network, is assumed to be related to the distance between junctions. This is illustrated for a highly idealized case in figure 1.3-9. Three different ways of determining the distribution of mesh sizes and the spaces resulting from this distribution were used. In the first, it was assumed that the mesh size was the distance between topologically connected crosslinks, and that the spaces in the mesh were this distance cubed. The second was a very similar calculation, except the mesh size was assumed to be the distance between spatially nearest junctions, whether connected or not. The third calculation used an Ogston model for the distribution of sizes of spaces in a random array of rods [101], with the rod length assumed to be the topological interjunction distances.

The topological interjunction distance calculation will be described in detail, and the differences involved in the others will be described. The mesh size and mesh size distribution, and hence $f(V_2)$ were determined using the following assumptions. First, the topological distance between crosslinks (the distance between crosslinks which are directly connected

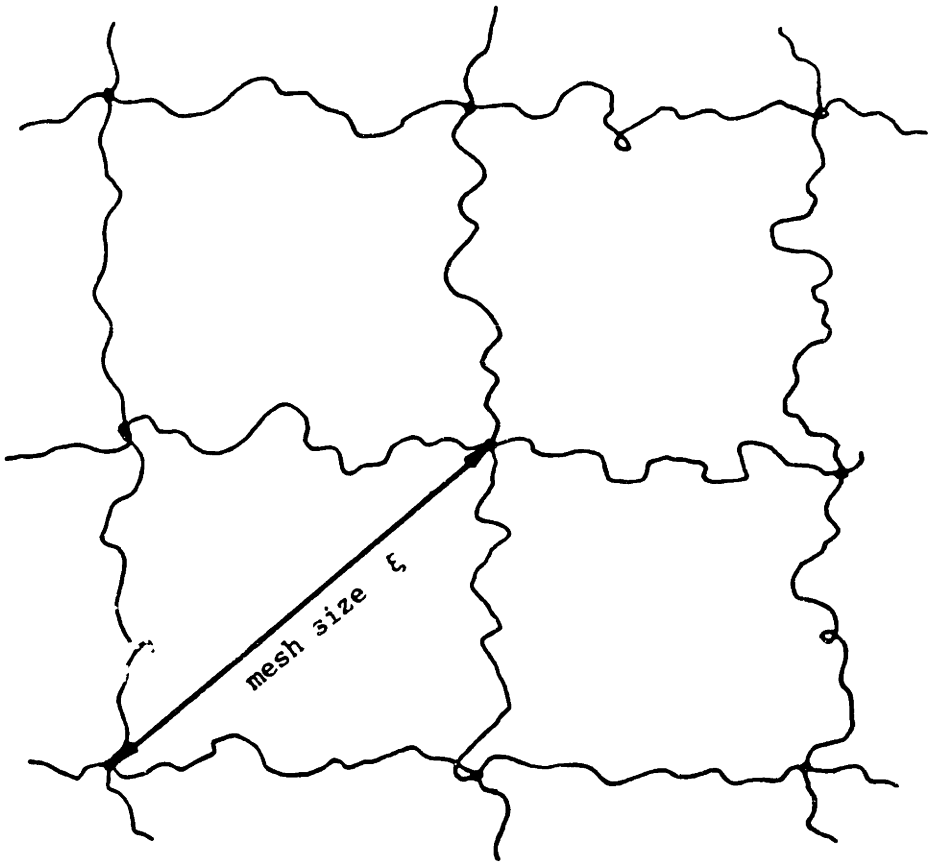

Figure 1.3-9. Schematic diagram of an idealized 2-dimensional network illustrating the mesh size and sieve effect. Molecules of diameter greater than ξ cannot penetrate mesh if junctions are immobile.

by a chain) was assumed to be the appropriate measure of the mesh size. Second, the volume measure of mesh size was assumed to be ξ^3. Third, the probability distribution of interjunction molecular weights (or degree of polymerization x), which will be called p(x), in the network was assumed to follow the most-probable distribution. It has been shown theoretically that this is true for radiation crosslinking of certain types of primary molecule distributions [35]. Fourth, it is assumed that for a single molecular weight chain the distribution of end-to-end lengths, p(r/x), which is the same as the distribution of topological interjunction distance for a network chain, is described by random coil statistics [19]. The probability distribution of topological interjunction lengths for the entire population of network chains is thus $p(r) = p(r/x)p(x)$. This result is integrated from mesh size ξ to infinity to give the probability of mesh size being larger than ξ. Figure 1.3-10 outlines this calculational procedure and presents the result. The sieve effect $f(V_2)$ is assumed to be $\Phi(\xi)^3$. Figure 1.3-11 is a plot of $f(V_2)$ as a function of solute area showing the effect of changing the interjunction molecular weight and the polymer volume fraction. Both of these effects are in the experimentally observed direction: increasing M_c and decreasing v_{2s} both increase the slope of the diffusivity ratio as a function of solute size. That is, it is easier to get large solute through a network with a high degree of swelling (low v_{2s}) and a high interjunction molecular weight. Figure 1.3-12 is a plot of the data in figure 1.3-8 with the diffusion coefficient ratio as predicted by equation 1-1 with the topological interjunction distance model as $f(V_2)$. Clearly this model seriously underpredicts the

Random coil statistics for single chain:

$$p(r/x) = 4\pi r^2 \left(\frac{3}{2\pi \langle \vec{r}^2 \rangle_x}\right)^{3/2} \exp\left[\frac{-3r^2}{2\langle \vec{r}^2 \rangle}\right]$$

= probability of length r given degree of polymerization x $(\langle \vec{r}^2 \rangle = \alpha^2 3Cxl^2)$

Most probable distribution of degree of polymerization:

$$p(x) = \left[1 - M_o\left(\frac{1}{M_c} - \frac{1}{M_n}\right)\right]^{x-1} M_o\left[\frac{1}{M_c} - \frac{1}{M_n}\right]$$

= Probability of degree of polymerization x for a given crosslink density (M)

Probability of interjuntion length r:

$$p(r) = \sum_{x=1}^{\infty} p(r/x)p(x)$$

Probability of mesh size being size ξ or larger:

$$\phi(\xi) = \int_{\xi}^{\infty} p(r)\, dr$$

$$= \int_{\xi}^{\infty} \sum_{x=1}^{\infty} p(r/x)\, p(x)\, dr$$

$$= M_o\left(\frac{1}{M_c} - \frac{1}{M_n}\right) B \sum_{x=1}^{\infty} \left\{\left[1 - M_o\left(\frac{1}{M_c} - \frac{1}{M_n}\right)\right]^{x-1} * \left[\Gamma(3/2) - \sum_{n=0}^{x} \frac{(-1)^n}{n!\,(n+3/2)} \left(A \frac{v_{2s}^{3/n}}{x} \xi^2\right)^{n+3/2}\right]\right\}$$

Figure 1.3-10. Approach used for calculation of the mesh size distribution based on the topological interjunction distance. $\langle r^2 \rangle^{1/2}$ is the root-mean-square end-to-end distance of the chain, α is the chain expansion factor, C is the characteristic ratio, l is the bond length, M_o is the repeat unit molecular weight, M_n is the primary molecule number-average molecular weight, and A and B are constants.

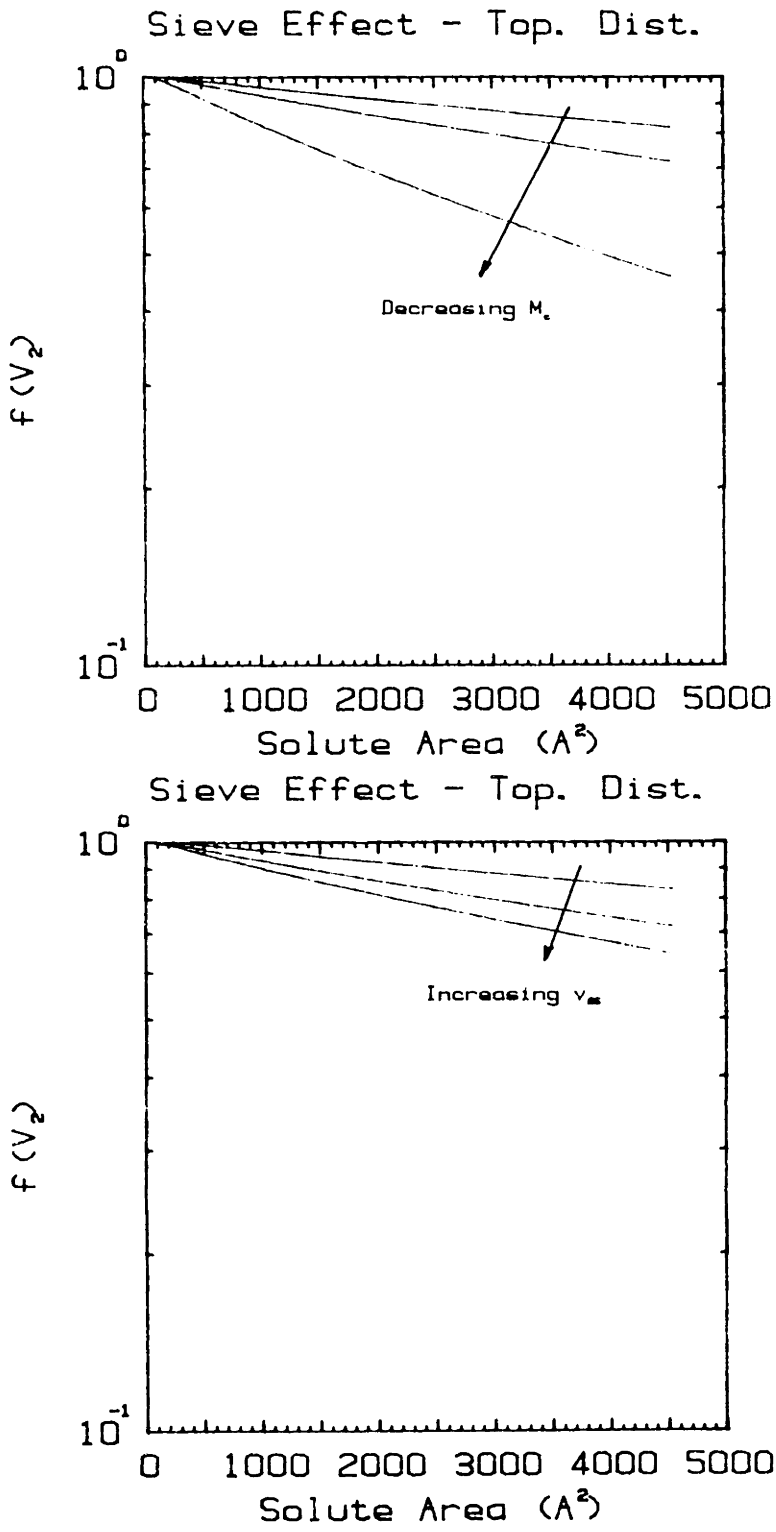

Figure 1.3-11. Scaling properties of the topological interjunction distance model for the mesh size.

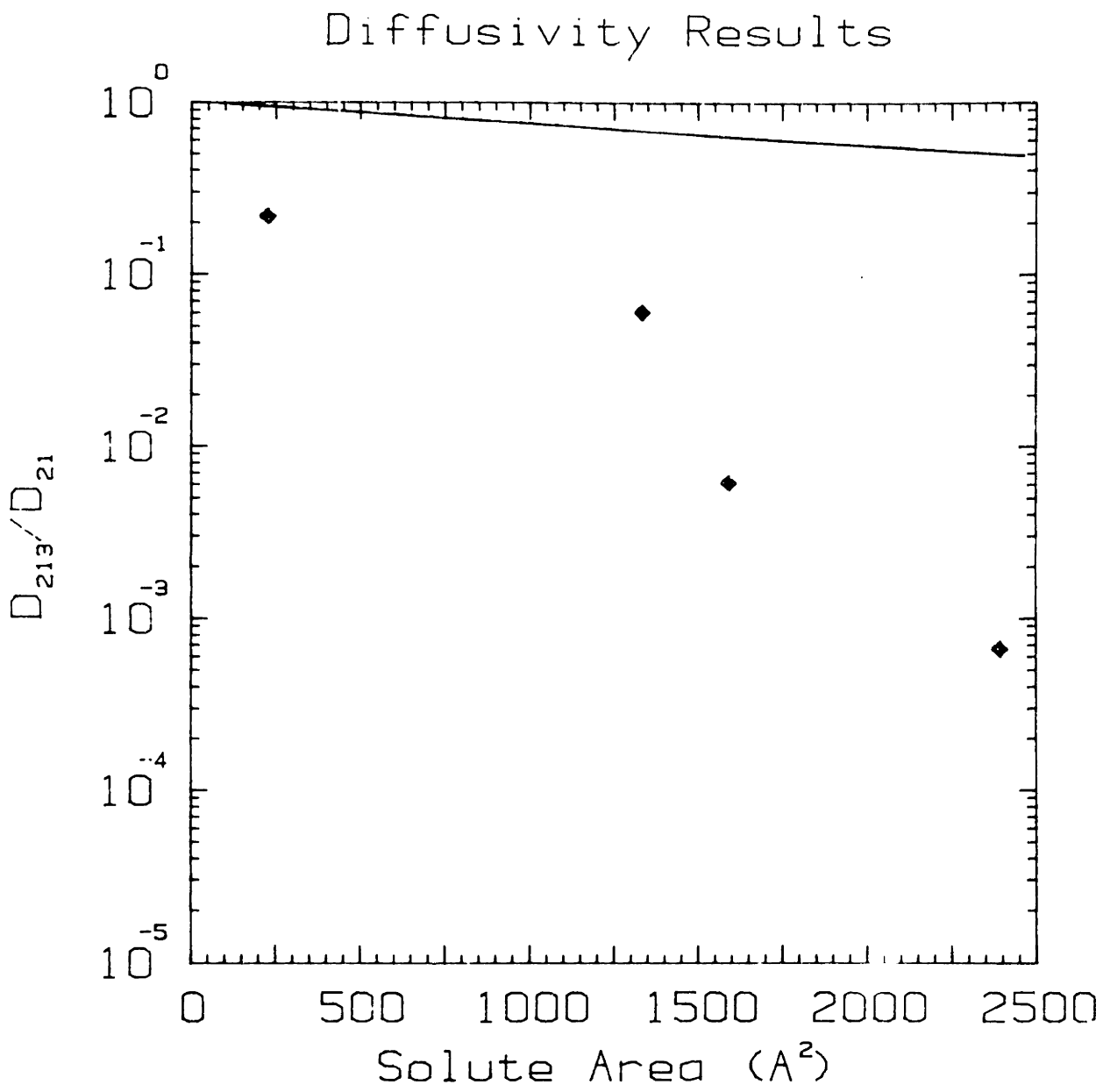

Figure 1.3-12. Comparison of predicted diffusivity ratio with data for 15%, 10 Mrad gel. Solid line is the prediction of equation 1-1 using the topological interjunction distance model for $f(V_2)$.

importance of the sieve effect. Figure 1.3-13 is the same data with the prediction using the spatially closest junction model, which essentially rescales the x-axis. The prediction is not significantly better. In fact, by changing the scaling it is possible to move the prediction to the correct order of magnitude, but the shape of the curve remains too straight, implying that even if the average space size is about right the width of the predicted distribution is too great. Figure 1.3-14 shows the M_c and v_{2s} dependencies for the Ogston-type model. This model uses the topological mesh size distribution as the rod length in the Ogston calculation for the distribution of spaces at least large enough for a spherical particle of a given size to penetrate the mesh. Figure 1.3-15 is the same plot as figures 1.3-12 and 1.3-13 for the Ogston prediction. Again, although in an average sense the magnitude of the diffusion coefficient predicted is correct, the distribution is again too broad. The implications of the theoretical development and its comparison with the experimentally obtained data are as follows. First, there is a large decrease in diffusivity ratio that is not accounted for by the free volume term of the solution-diffusion theory. This implies that there is some further effect not associated with the presence of polymer chains which is reducing transport in these gels. Secondly, the severe underprediction of this effect by both the topological interjunction distance model and the spatially closest distance model for the distribution of mesh sizes implies that either the restrictions to transport are closer together than the nearest junctions or the hole volume required for movement of a solute into a hole is larger than the cube of the solute hydrodynamic radius. A possible reason for this

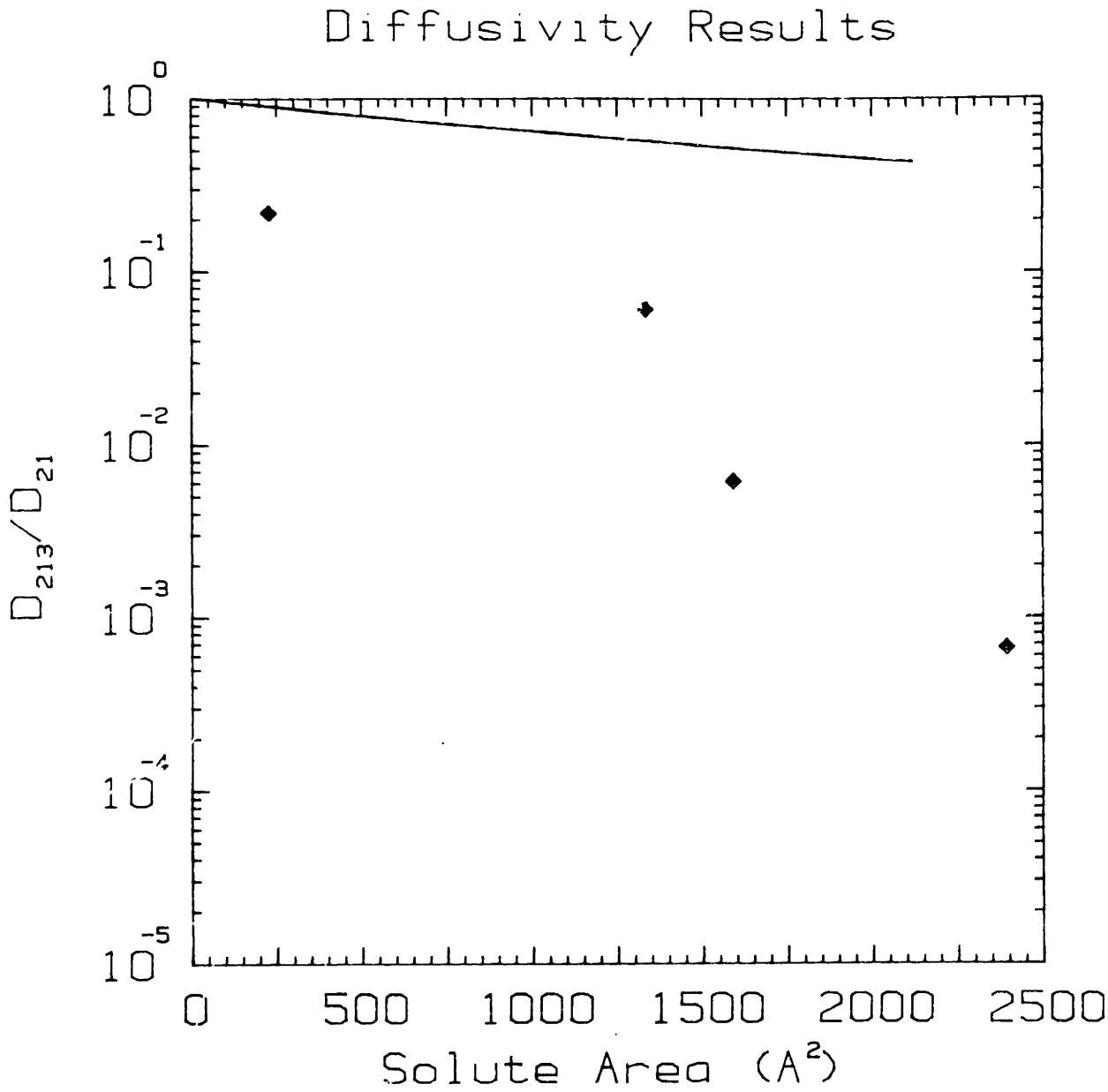

Figure 1.3-13. Comparison of predicted diffusivity ratio with data for 15%, 10 Mrad gel. Solid line is the prediction of equation 1-1 using the spatially closest interjunction distance model for $f(V_2)$.

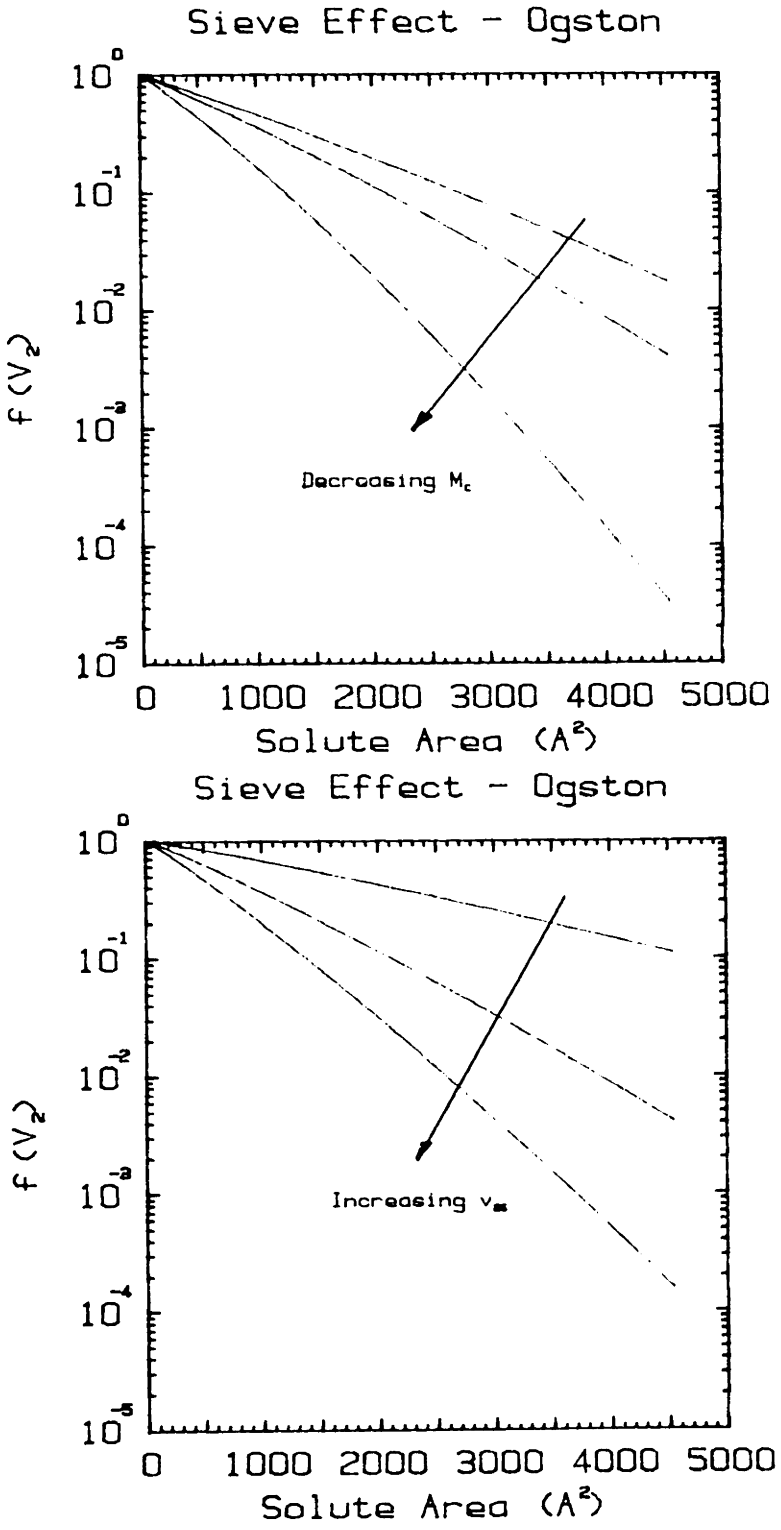

Figure 1.3-14. Scaling properties of Ogston - type model for the mesh size.

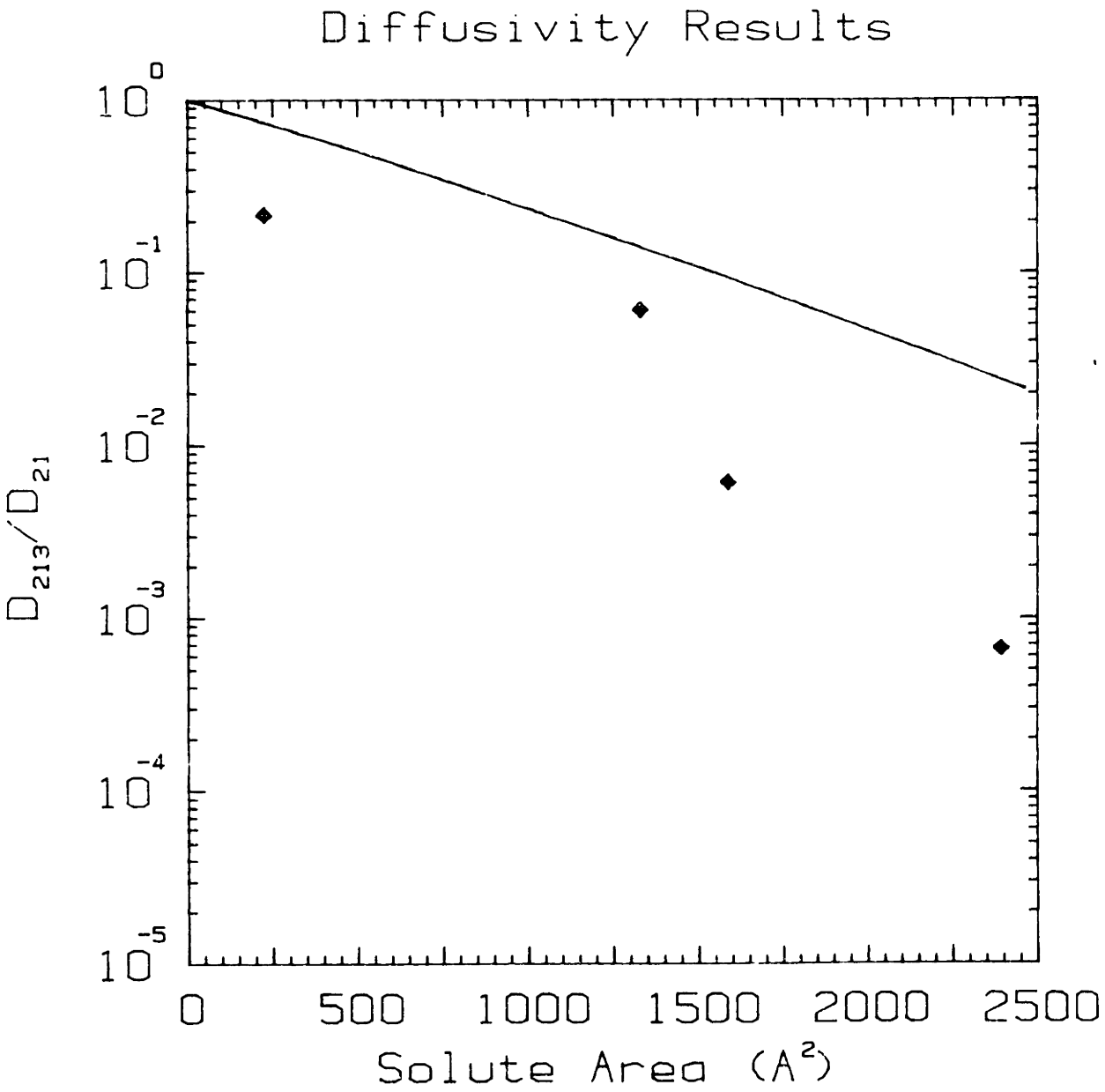

Figure 1.3-15. Comparison of predicted diffusivity ratio with data for 15%, 10 Mrad gel. Solid line is the prediction of equation 1-1 using the Ogston - type model for $f(V_2)$.

incorrect prediction is the presence of the network chains. The volume of the chains is not addressed in the hole size calculation, and neither are possible restrictions on chain movement, which could lead to blockage of some of the spaces between junctions by chains. Both of these could contribute to lowering transport rates below those predicted. Thirdly, the inability of any of the models to match the rapid drop-off in diffusivity ratio that is found experimentally implies that the calculated mesh size distributions are too broad. The fault may lie in the assumption that the distribution of end-to-end distances for a single network chain follows the same statistics as the distribution of end-to-end distances for an isolated random coil. It is likely that the motion of the junctions is quite restricted, simply by the fact that each junction is attached to four chains which are in turn attached to other junctions. So it may not be possible for a network chain to take on all the possible end-to-end lengths that a free coil can, and thus the calculated distribution would be too broad. It is possible to make the topological interjunction distance calculation assuming that all network chains are fixed at their root-mean-square end-to-end distance, but this does not show any significant improvement over the complete distribution, so perhaps some other distribution is appropriate. Unfortunately, it is not clear that any of these effects can be simply accounted for in the theoretical development.

1.4. Conclusions and Recommendations

Networks containing exclusively poly(ethylene oxide) can be easily synthesized by irradiation of aqueous solutions of the polymer with high energy electrons. The electron irradiation technique is considerably more efficient than equivalent gamma irradiations. Networks with a variety of structural properties, as measured by equilibrium swelling measurements, can be synthesized by controlling the concentration of the irradiated solution and the total radiation dose. The postulated radiation chemistry of the PEO - water system is consistent with the results obtained in the irradiation studies, although the effect of oxygen is minimal at the conditions used. It was shown that the diffusivity of globular molecules through these networks is highly dependent on at least the structural parameters M_c and v_{2s}, and there may be other structural features which are important. The gels are semi-permeable and can show greater size selectivity than traditional cellulosic dialysis membranes. This is due to the effect of some type of physical restriction to transport resulting from the presence of crosslinks (the sieve effect), an effect which had been postulated but never experimentally verified. By tailoring this effect, it would be possible to synthesize networks with a very sharp size selectivity. Theoretical modelling indicates that these restrictions are more closely spaced than the crosslinks themselves and that the distribution of distances between them is narrower than the distribution of end-to-end distances of an equivalent population of free (uncrosslinked) chains. From this it can be concluded that the mobility of the chain ends (i.e.,

the junctions) is greatly reduced for chains in a network. It is likely that the presence of the chains contributes to the sieve effect in two ways, both by decreasing the actual volume of the spaces between junctions as well as by adding another possibly impenetrable barrier.

There are several future studies which would shed further light on the observed phenomena. It would be useful to develop an endlinked system on which equivalent transport measurements could be made, as the ability to know and vary the distribution of molecular weights between crosslinks should provide further information about the mesh size distribution. An investigation into the mobility of the chains and junctions would be very useful, and the techniques of solid-state NMR should allow this to be done on gels at varying degrees of hydration (although possibly not on the radiation crosslinked system). On a more practical note, as the motivation for this work was the biocompatibility of poly(ethylene oxide), biocompatibility testing should be carried out. In order to do this, further work on supported gels and other methods of deploying PEO networks in structurally sound configurations may be necessary.

Chapter 2. Introduction and Literature Review

2.1. Introduction

For a number of years there has been interest in developing biocompatible semi-permeable membranes. There are a number of potential uses for such membranes; some of the more important ones include blood filtration (dialysis, plasmapheresis, and other more novel techniques) and controlled release drug delivery systems. If the material also shows low protein binding characteristics, which is likely, a large number of applications in the field of biotechnology, especially bioseparations, becomes important. Consequently, a large amount of effort has been directed toward developing low protein binding blood compatible membranes.

In a recent review, Merrill and Salzman [1] suggest that of the synthetic polymeric materials examined for blood compatibility, those containing some form of poly(ethylene oxide) showed the greatest compatibility. Poly(ethylene oxide) (PEO) is a synthetic polymer with the following structure

$$OH\text{-}[\text{-}CH_2\text{-}CH_2\text{-}O\text{-}]_n\text{-}H$$

where n can vary from about 5 to about 100000. This polymer is also known as polyoxyethylene (POE) and polyethylene glycol (PEG), particularly at lower degrees of polymerization (n small). More details on the structure and properties of this polymer are given in Section 2.2.

Because of the water-solubility of PEO, it must be deployed as a network for biological applications. The most popular ways of doing this are as phase-separated block copolymer systems and as polyurethanes (also phase separated systems). Polyurethanes have been studied by Sa Da Costa [2], Mahmud [3], and Brash, et al [4], among others. Block copolymer systems examined include PEO-polyethylene terephthalate [5], PEO-polybutylene terephthalate [6], and PEO-polystyrene [7]. Two major conclusions can be drawn from these studies. First, networks containing PEO were more biocompatible than those containing poly(propylene oxide), and second, increasing the PEO content of the network increased the biocompatibility.

This previous work suggests that a network containing exclusively PEO would have desirable blood compatibility properties. Also, work on hydrogels formed by random crosslinking of water-soluble polymers such as polyvinyl alcohol [8,9] and polyhydroxyethylmethacrylate [10] suggests that a PEO network should also be semi-permeable. These networks belong to a class of membranes referred to as solution-diffusion membranes [11]. Although some previous work has been done, the mass transport behavior of these membranes has not been fully characterized either experimentally or theoretically for a number of reasons. The main thrust of this work is thus to develop, synthesize, and characterize semi-permeable PEO membranes.

2.2. Properties of Poly(ethylene oxide)

Poly(ethylene oxide) is a water-soluble synthetic polymer with structure

$$OH\text{-}[\text{-}CH_2\text{-}CH_2\text{-}O\text{-}]_n\text{-}H \quad .$$

The polymer is commercially available in a variety of molecular weights ranging from about 300 to over 4,000,000. It is highly crystalline, with a melting point for high molecular weight material on the order of 66°C. In addition to water, PEO is soluble in a variety of organic solvents, including chloroform, freons, tetrahydrofuran, toluene, benzene, and others. It is insoluble in alcohols, including the single unit analogue ethylene glycol, and linear hydrocarbons. The polymer can be synthesized in a variety of ways. The two commercially important synthetic techniques are an anionic ethylene oxide ring opening, which is typically used for low molecular weight materials and which produces the narrow molecular weight distribution typical of anionic polymerizations, and a heavy metal catalyzed ring opening which produces high molecular weight polymer with a very broad distribution. For more information on the synthesis and physical properties of PEO, see ref. [12].

2.2.1. Poly(ethylene oxide) in Aqueous Solution

PEO, in common with most water soluble polymers, exhibits some unusual behavior in aqueous solution. PEO is infinitely soluble in water at low temperatures, but has a lower critical solution temperature (θ = 95°C), as illustrated in figure 2-1. This behavior has been attributed to the formation of an ordered layer of water in the vicinity of the PEO chain due to hydrogen bonding with the ether oxygen [12]. The ordering of water indicates a negative entropy of mixing, which becomes greater as the temperature is increased and the disorder in bulk water is greater.

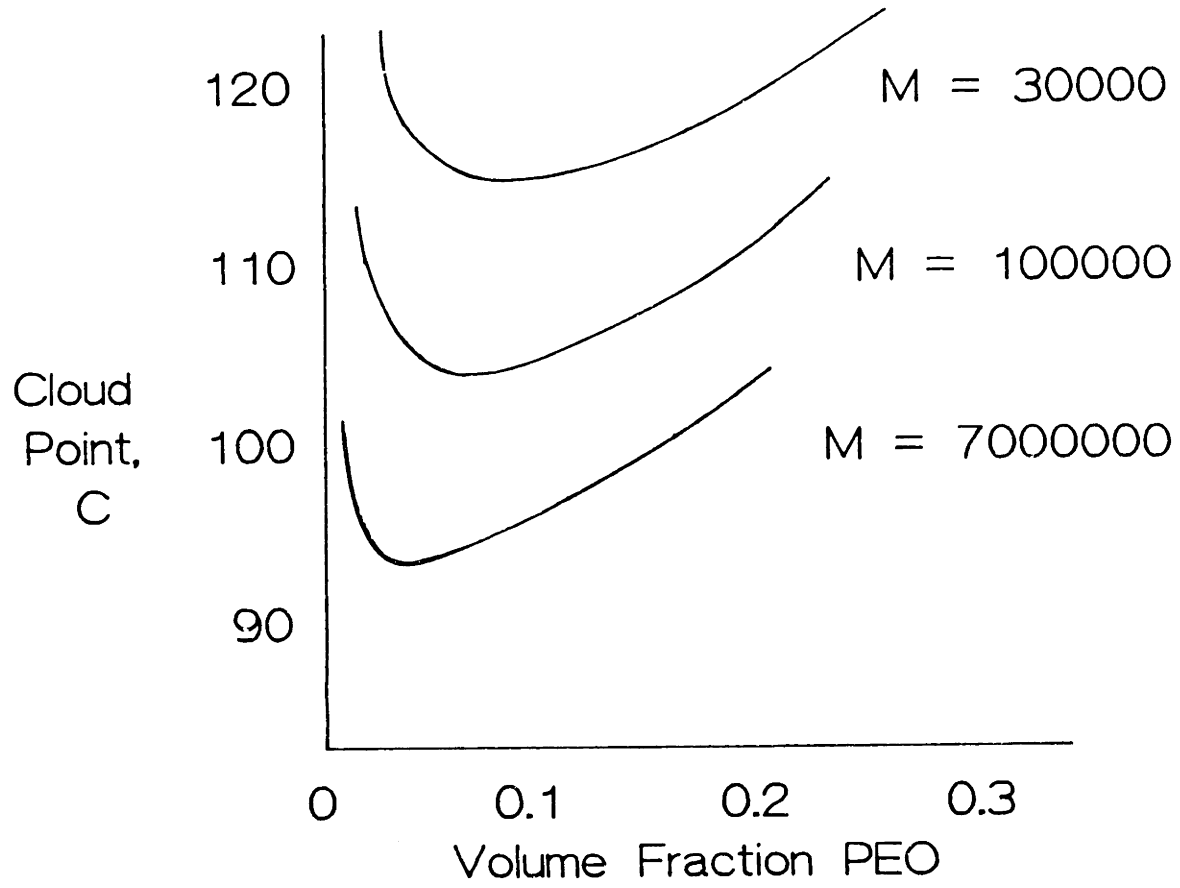

Figure 2-1. Relationship between polymer volume fraction and phase separation of aqueous solutions of PEO illustrating the lower critical solution temperature. Adapted from ref. [23].

Several studies have been carried out in an attempt to determine the pattern of the association between water and the ethylene oxide unit. Two different things have been examined: the structure of the PEO molecule in solution [13,14,15] and the structure of water in the vicinity of the PEO chains [16,17,18]. The PEO conformation studies have used techniques such as laser Raman spectroscopy [13] and nuclear magnetic resonance [14,15] to look at the chain conformation of PEO in bulk and in solution in various solvents. Two studies [13,15] conclude that the structure of the PEO chain in aqueous solutions has more crystalline nature than does the PEO chain in the melt or in organic solvent. The third study [14] reaches the opposite conclusion, that there is no evidence for a conformation different from a random coil in aqueous solution. However, despite this controversy, other studies are in agreement that there is ordering or complexation of water by the PEO chain. This has been determined by quasi-elastic neutron scattering [16], by Raman scattering [17], and by microcalorimetry [18]. The results indicate complexes of both one, three and five water molecules with each ethylene oxide unit in the backbone. Two of the investigators [17,18] proposed simple hydrogen-bonding models which adequately explain the observed behavior.

Despite the unusual interaction between PEO and water, classical Flory-Huggins liquid lattice theory [19] has been used to describe the solution behavior [12]. It is relatively successful in describing observed behavior, but it is important to be aware that the interaction parameter χ_1 cannot be interpreted as including strictly enthalpic contributions,

as it also accounts for the effect of the anomalous negative entropy. Strictly speaking, Flory-Huggins theory should not be used for the PEO - water system because of the violation of several of the central assumptions, in particular that of unbiased distribution of the two components among the lattice sites, but it is successful as a somewhat empirical means of interpreting data, provided that the error of extrapolating to dissimilar conditions is not made. Measurements of the interaction parameter χ_1 have been made by a number of investigators for the PEO-water system [20,21,22], but in light of the foregoing discussion it does not seem prudent to use these values, which were obtained under conditions somewhat different from those used in this study. The effect of temperature is especially important, and temperature differences may cause differences in the concentration dependence of χ_1.

2.2.2. Effect of Salts on PEO Solution Behavior

It is known that the addition of salts to solutions of poly(ethylene oxide) in water causes some unusual effects. Some of the better established of these effects are outlined below.

1. Decrease of cloud point. PEO undergoes a liquid-liquid phase separation from most salt solutions at a lower temperature than the equivalent solution in pure water [23]. This effect is illustrated in figure 2-2. The efficiency of various ionic species at lowering the cloud point is found to follow approximately the Hofmeister series, which describes the relative efficiency of various ions in flocculating colloidal suspensions. This behavior can further be related to the

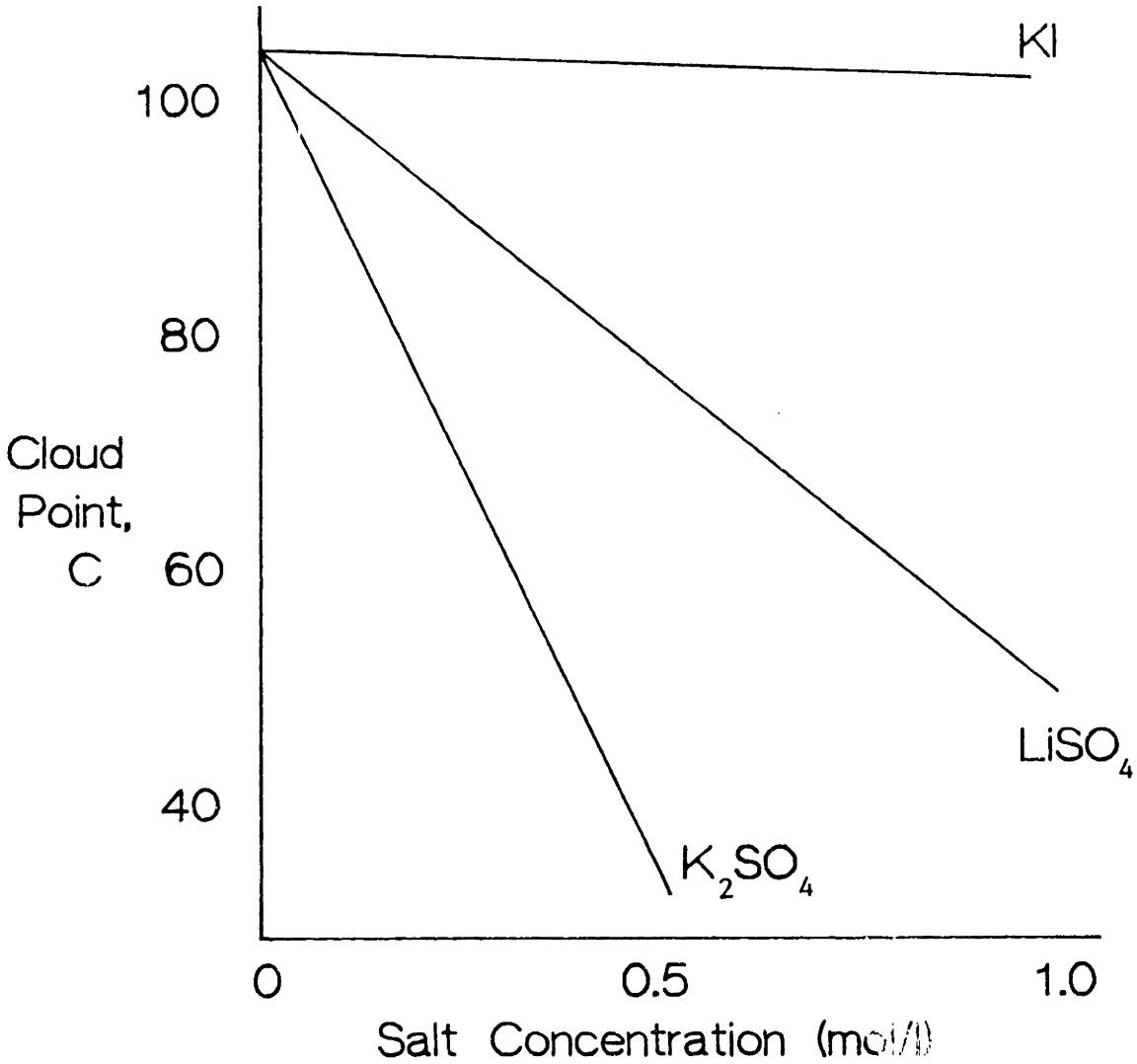

Figure 2-2. Cloud point (phase separation temperature) of PEO in salt solutions as a function of salt concentration. PEO concentration and molecular weight constant. Adapted from ref. [23].

ability of a salt to impose or disrupt structure in pure water [24]. This ability has been described in terms of the temperature at which pure water has the same number of free (non-hydrogen bonded) hydroxyl groups. If this equivalent structure temperature is below the actual solution temperature the salt imposes structure, and if it is above the salt disrupts structure.

2. Change in intrinsic viscosity. It has also been observed that the presence of salt in PEO - water solutions lowers the intrinsic viscosity; that is, the coil size of a PEO chain is smaller in the presence of salt. The effectiveness of various ions in decreasing intrinsic viscosity correlates very well with the effectiveness in decreasing cloud point [23].

3. Complexation of ions by PEO chains. There is considerable evidence that PEO can complex certain ions. This behavior has been compared with that of crown ethers [25]. PEO is relatively efficient at solubilizing salts in organic solvents and it has been demonstrated spectroscopically that cations can form complexes with some number (probably 7, based on the crystal structure) of ether oxygens in the PEO chain. It was suggested that PEO also complexed I^-, but it has since been determined that this is not the case; the complexation was actually through the cation.

It is not completely clear from the available evidence what the mechanism is for the chain collapse and precipitation of PEO in the presence of salt. As mentioned above, the decrease in phase separation temperature can be related approximately to the relative ability of a particular salt

to impose structure in water, with the salts causing the most structuring (lowest structure temperature) to be most effective. However, all salts appear to decrease the cloud point, regardless of whether they impose or disrupt structure, which cannot be explained by a strictly entropic effect of the salt. In fact, the explanation of the lower critical solution temperature in pure water being an effect of increased disorder in water at higher temperature [12] would suggest that adding salt which imposes structure should increase the solvent quality. Also, the phase separation work suggests that the cationic species is more important in determining phase separation behavior, while in the Hofmeister series and structure temperature measurements the anion is more important. These things thus lead one to suspect that there may also be an effect of ion complexation on the behavior of PEO in salt solutions. It appears that no studies looking at this effect have been done.

2.3. Crosslinking of Poly(ethylene oxide)

2.3.1 Crosslinking and network formation.

There are a variety of ways of linking polymer molecules to form an insoluble structure [19]. Typically, the ultimate result is the formation of a continuous, insoluble macroscopic network. The two most common ways of forming such a network are (i) covalently linking the individual molecules and (ii) phase separating linear copolymer molecules into two phases [26]. The two techniques produce somewhat different

structures. Covalently linked networks are insoluble in any solvent, although a good solvent for the linear polymer will swell the network. Such a network also will not flow, even above the melting and glass transition temperatures of the linear polymer. There are thus a number of applications for such a network in which the linear polymer could not be used. Phase separated networks, also known as virtual networks, have somewhat different properties. The copolymer usually consists of a component which forms a crystalline or glassy amorphous phase (hard segment) and a component which is amorphous and above its glass transition temperature (soft segment) at the conditions of application. Because the molecules are held together by the hard segment domains and are not covalently bound, it is possible to lose the network structure. If the network is in a condition that reverses the phase separation, for instance in a solvent that is good for both phases, the linear chains will dissociate and dissolve. However, in a solvent for the soft segment that is a nonsolvent for the hard segment, the network will swell much like a covalently bound network. By judicious selection of hard and soft segments, it is usually possible to make a network that will be suitable for a particular application.

Within the general class of covalently linked networks there are two different network structures, which correspond to crosslinking by linking chain ends (endlinking) and introducing crosslinks between random points on the chain backbone (random linking) [19]. Endlinking usually involves two different molecules, the bifunctional polymer chain and the junction molecule, which has a functionality of at least three. The process is

similar to a step polymerization. This type of structure is illustrated in figure 2-3a. Random crosslinking is typically a free radical process, and may or may not involve a crosslinking species in addition to the polymer chains. A typical randomly linked network is illustrated in figure 2-3b. There are several differences between the two types of covalent networks. First, in endlinking the distance between junctions is controlled by the molecular weight of the polymer molecule, whereas in random linking this distance depends on where the junctions are formed, which is random. Secondly, in random linking the junction functionality (the number of chains extending from each junction) is almost always four, and in endlinking it can be any value greater than three. Thirdly, random linking leaves loose chain ends and endlinking does not.

Poly(ethylene oxide) can be made into a network using any of the above methods. The polyurethanes of Mahmud [3] and Sa Da Costa [2] are examples of phase separated PEO networks. The silicone-PEO networks synthesized by Pekala [27], the urethane bonded networks of Graham [18], and the tri-isocyanate linked networks of Mark [28] are all examples of endlinked covalent networks with PEO as a major component. Randomly linked PEO networks have been synthesized by a number of investigators [29,30,31,32,33,34] using ionizing radiation. This last group contains the only networks formed without the addition of a non-PEO crosslinking species.

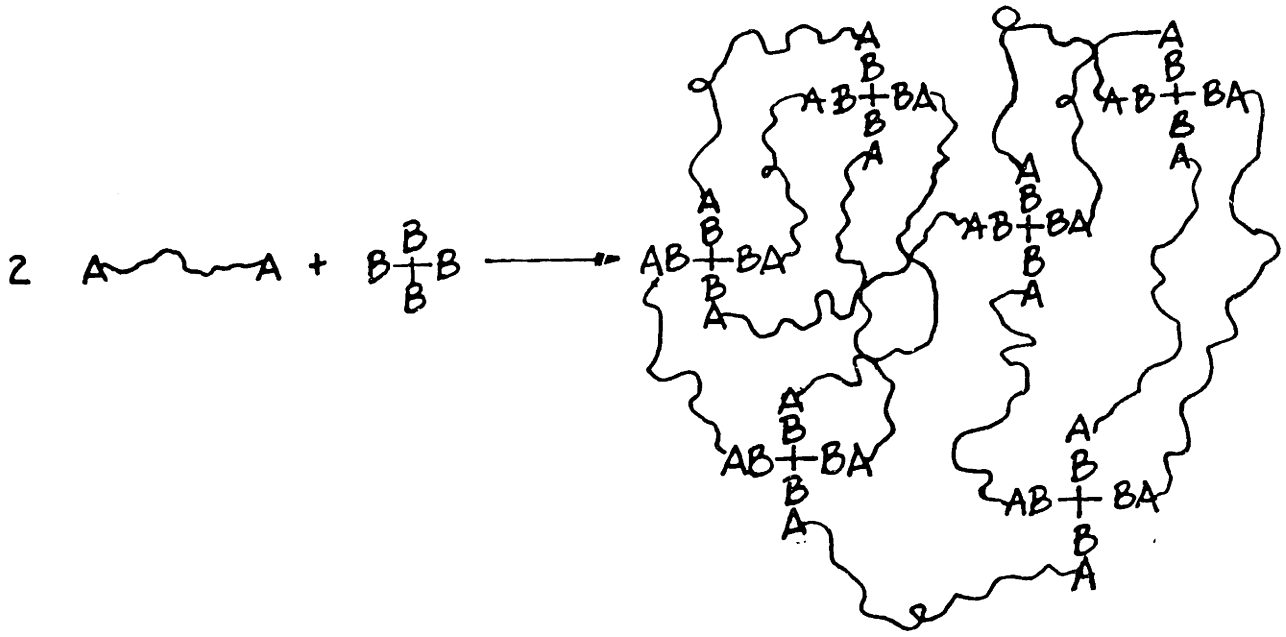

a. Structure of end-linked network.

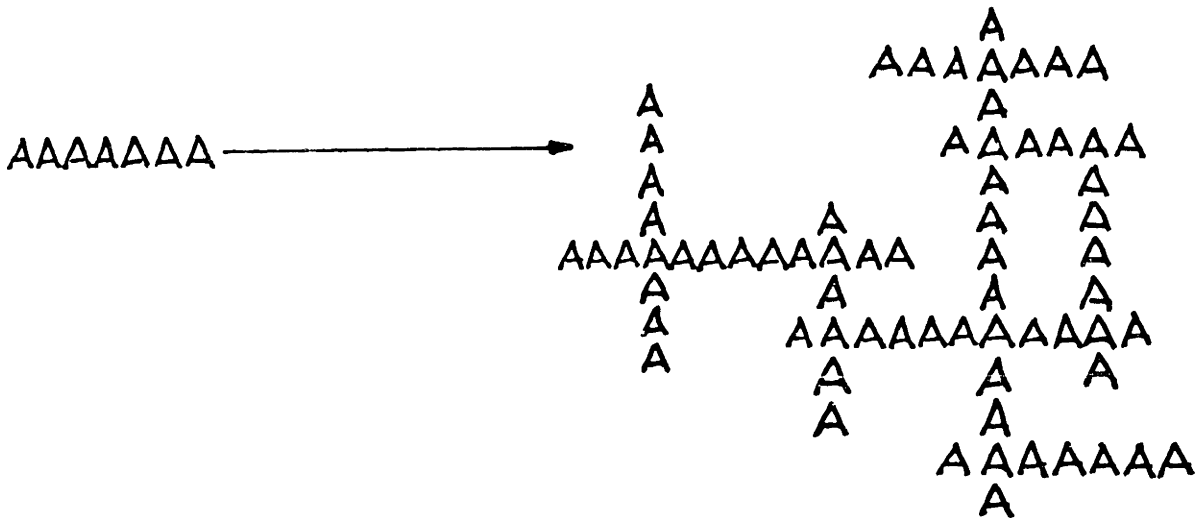

b. Structure of randomly linked network.

Figure 2-3. Possible structures of PEO networks.

2.3.2. Radiation Crosslinking

It has long been established that exposure of polymeric materials to ionizing radiation can produce some interesting changes in the properties of the polymer. Many reviews and several books have been published on the general subject of irradiation of polymers [35,36,37,38,39]. The present discussion will thus be limited to a general introduction and a more specific discussion of previous work on irradiation of poly(ethylene oxide). Most polymers, when exposed to ionizing radiation, which in the present discussion will be taken as gamma or high energy electron radiation, undergo either crosslinking, due to coupling of radicals generated on the polymer chain, or main chain scission, wherein the chain splits due to direct bond breakage or interaction with some radiolysis product, or some combination of the two [35]. The reasons a particular polymer will crosslink rather than degrade are not completely clear. Several factors seem to have an effect. It has been suggested that in order for a polymer to crosslink it must have at least one hydrogen bonded to a backbone carbon [38]. This is probably not strictly true, but the presence of an easily abstracted hydrogen or methyl group does appear to be important. Also, the relative strength of the side chain bonds (for instance C-H or $C-CH_3$) to the backbone bonds (i.e. C-C) in the polymer appears to be important in whether a polymer will crosslink or degrade. Another potentially important factor is the presence of other species which can interact with the polymer chain during irradiation. For instance, it is often desirable to exclude oxygen as it can form reactive peroxyl species that may promote degradation. These effects

have all been determined empirically, however, and the specific effect of radiation on a particular polymer species is impossible to predict.

2.3.3. Irradiation of Poly(ethylene oxide)

PEO is one of the interesting polymers that appears to undergo both crosslinking and scission reactions when irradiated. These two processes are illustrated schematically in figure 2-4. For PEO, the crosslinking involves abstraction of a hydrogen from a main chain carbon on two different chains and coupling of the two carbon radicals produced. The scission reaction may proceed in a couple of different ways depending on the irradiation conditions. One possibility is direct breakage of a C-O bond to produce a pair of radicals. The other is hydrogen abstraction leading to a backbone carbon radical followed by either spontaneous degradation or interaction with some other species to break the chain. As mentioned above, the relative amounts of the crosslinking and scission are controlled by the exact conditions under which the irradiation takes place. The previous work on irradiation of PEO will thus be discussed in terms of the conditions of the investigations.

2.3.3.1. Irradiation in Bulk

The radiation chemistry of PEO irradiated in bulk was looked at in some detail by King [40]. This study involved the irradiation of high molecular weight PEOs by both gamma and electron beam irradiation both under vacuum and in air. The irradiation was done on a dry powder of

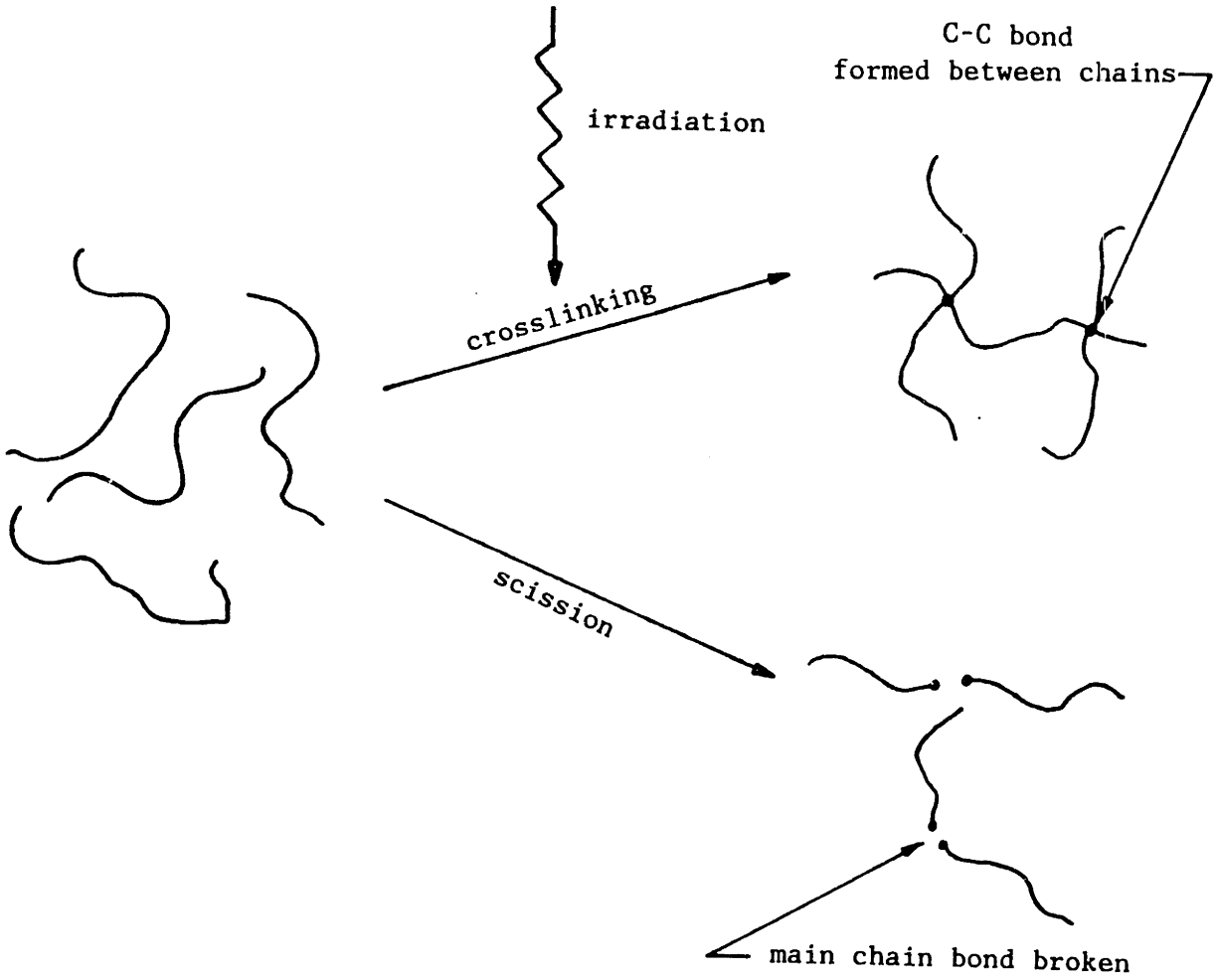

Figure 2-4. Schematic diagram of crosslinking and scission process taking place during irradiation of PEO. For the chemical reactions involved, see tables 2-1 and 2-2.

crystalline PEO. King used an investigation of the radiation chemistry of diethylene glycol [41] to interpret the data obtained. Three measurements were made on the PEO samples: bulk viscosity, shear degradation, and pituitousness (the stringiness of the sample). These were assumed to give information on the molecular weight and molecular weight distribution of the samples. The results indicate that both crosslinking and scission are taking place, but that under all the conditions studied scission is by far the dominant process. Electron beam irradiation was found to be much less efficient than ^{60}Co gamma irradiation in the scission process, but it was also observed that it was possible to render the polymer insoluble by irradiating with electrons, so crosslinking is presumed to be more efficient. The most likely explanation for this is the very large difference in dose rate (rate at which the radiation is delivered) for the two types of radiation - electron beam irradiation is typically several orders of magnitude faster than gamma. It was also observed that the presence of air increased the amount of scission considerably, and that high molecular weight species were more susceptible to scission. King calculated a G-value (also known as the radiation yield) for scission, which is the number of chain breakages per 100 eV of radiation. The calculated value for gamma irradiation in air was 200, which suggests some kind of chain process, with propagation steps important. The important point of this study is that under a wide variety of conditions scission dominated over crosslinking in the irradiation of this high molecular weight crystalline polymer. It is interesting to note that the model study on diethylene glycol indicated that the radiation yield for C-O bond breakage is five

times that of C-H bond breakage. This may help explain the predominance of scission under these conditions.

A similar investigation [42] was carried out on bulk PEO in the melt, about 30°C above the melting temperature. In contrast to the results with crystalline material, it was found to be relatively easy to form a network with electron beam irradiation in the absence of oxygen. This is perhaps attributable to the increased chain mobility in the melt, which would increase the likelihood that two main chain radicals would encounter one another and couple.

2.3.3.2. Irradiation in Solution

A number of studies have also been carried out on the irradiation of poly(ethylene oxide) in aqueous solution. The initial reason for irradiating in solution rather than in bulk was to increase the mobility of the polymer chains and thus increase the probability of main chain radicals encountering one another, leading to additional crosslinking. The first studies were done in the late 1960s [30,31,43]. They looked mostly at the general aspects of irradiation, focusing on the relation of crosslinking and scission and determining such parameters as gel doses and radiation yields. In comparing the results with those for irradiation in bulk, it appears that the ratio of crosslinking to scission is considerably higher in solution than in bulk. It was eventually agreed that this was due not to the increased chain mobility but to interaction with water radiolysis products, which increased the

efficiency of formation of main chain carbon radicals and thus the efficiency of crosslinking.

A brief description of the more complete studies follows. There are several problems with comparing the results of the studies in a quantitative way, which include the effect of different gamma sources, different PEO molecular weights, and different methods of reporting and interpreting the data, so only a brief qualitative discussion of the type of information available will be made.

The first comprehensive study published on irradiation of PEO in solution was by VanBrederode et al in 1968 [44]. The radiation source was a ^{60}Co source at a dose rate of 160 rad/s. (The rad is a unit of absorbed dose, and is equal to 100 erg absorbed/gram.) The most interesting result obtained was the energy required to produce a crosslink, which was calculated as 710 kcal/mol below the gel point and around 70 kcal/mol above the gel point. Possible explanations for the difference include scission effects, incorrect determination of the gel dose, inappropriate determination of the crosslink density above the gel dose (it was derived from dynamic mechanical measurements, but whether the effect of crosslinking in solution was considered in the theory is not clear), or an actual increase in efficiency above the gel point due to the chains being physically attached. This last point seems possible because of the low polymer concentrations used. A follow-up study [32] looked at the effect of molecular weight and found little effect on the energy per crosslink. It is interesting to note that the gel dose (dose required to

produce a macroscopic network - theoretically, one crosslink per two primary molecules) for a deaerated solution of 1% PEO, 4 million molecular weight, was 75000 rad.

A study done by King and Ward [30] indicated that in contrast to the conclusion of earlier workers [43] PEO crosslinking in solution is accomplished by an indirect interaction with water radiolysis products as the mediator. They also found that for the conditions used (deaerated solutions, ^{60}Co gamma at 30 rad/s) the ratio of crosslinking to scission was 4. Stafford [31] published a series of papers looking at the effect of various additives on crosslinking. His work supported the indirect interaction. Unfortunately, in the early part of the study he proposed a theory for the gelation phenomena observed based on the assumption of discrete, noninterpenetrating polymer coils, which is clearly not the case.

Charlesby and Byrne [29] conducted an investigation into the effect of physical state and presence of oxygen on PEO gelation. They worked with PEO of 300000 molecular weight, using a gamma source. Irradiation was done on solutions in both the liquid and frozen state, both air saturated and under nitrogen. The dose to gel for the various combinations was determined. It was found that the gel dose for liquid solutions in air was about 2.5 times the dose for the identical solution in nitrogen. There are two possible explanations for this observation. First, it is possible that the presence of oxygen somehow decreases the efficiency of the crosslinking process by competing in certain of the chemical

processes taking place. The second, and more likely, is that the presence of oxygen may increase the amount of chain scission, thus requiring more crosslinks (because one crosslink is required for each chain present) to reach gelation. It was also found that a higher dose was required for gelation of the frozen solutions. Again, there are two possible explanations. It is possible that freezing the solution will decrease the yield of water radiolysis products, giving a decrease in overall efficiency. It is also possible that the decreased crosslinking efficiency is a result of the decreased mobility of the PEO chains in the frozen state.

2.3.4. Chemistry of PEO Irradiation

As already mentioned, radiation crosslinking and scission of PEO in aqueous solution appears to proceed by an indirect process, that is, it is products of the water radiolysis that interact with the PEO chain, not the high energy electrons themselves. This fact led a number of investigators [45,46,33] to look at the radiation chemistry of PEO in solution as a model for studying aqueous radiation chemistry in general. By looking at these studies as well as the ones cited above it is possible to propose a set of reactions describing the irradiation of PEO in oxygen free aqueous solution. These are given in table 2-1. The water radiolysis products (reactions 1 - 6 in table 2-1) interact with the PEO chain to abstract a hydrogen, leaving a main chain carbon radical (reactions 7 and 8). The radicals produced can then couple (reaction 11), producing a crosslink, or undergo scission. The exact mechanism for

PEO Radiation Chemistry

Water Radiolysis

$$H_2O \longrightarrow H^{\cdot}, {}^{\cdot}OH, e^-_{aq} \quad (1)$$

$${}^{\cdot}OH + {}^{\cdot}OH \longrightarrow H_2O_2 \quad (2)$$

$$H^{\cdot} + H^{\cdot} \longrightarrow H_2 \quad (3)$$

$$H^{\cdot} + {}^{\cdot}OH \longrightarrow H_2O \quad (4)$$

$$e^-_{aq} + H_2O_2 \longrightarrow OH^- + {}^{\cdot}OH \quad (5)$$

$${}^{\cdot}OH + OH^- \rightleftharpoons O^{\cdot -} + H_2O \qquad pK = 11.9 \quad (6)$$

Interaction with PEO

Hydrogen Abstraction

$$\sim CH_2{-}CH_2{-}O\sim + {}^{\cdot}OH \longrightarrow \sim CH_2{-}\dot{C}H{-}O\sim + H_2O \quad (7)$$

$$\sim CH_2{-}CH_2{-}O\sim + O^{\cdot -} \longrightarrow \sim CH_2{-}\dot{C}H{-}O\sim + OH^- \quad (8)$$

Degradation

$$\sim CH_2{-}\dot{C}H{-}O{-}CH_2{-}CH_2{-}O\sim + H_2O_2 \longrightarrow \sim CH_2{-}\underset{H}{C}{=}O + OH{-}CH_2{-}CH_2\sim + {}^{\cdot}OH \quad (9)$$

$$\sim CH_2{-}CH_2{-}O{-}CH_2{-}\dot{C}H{-}O\sim + e^-_{aq} \longrightarrow \sim CH_2{-}CH_2{-}O^- + CH_2{=}CH{-}O\sim + H_2O \quad (10)$$

Crosslinking

$$\sim CH_2{-}\dot{C}H{-}O\sim + \sim CH_2{-}\dot{C}H{-}O\sim \longrightarrow \begin{matrix}\sim CH_2{-}CH{-}O\sim \\ \sim CH_2{-}CH{-}O\sim\end{matrix} \quad (11)$$

Table 2-1. Proposed reaction scheme for the radiation chemistry poly(ethylene oxide) in aqueous solution. For details, see text.

scission is not clear. It appears that the there must be interaction of the carbon radical with some other species present to produce scission, but it is not clear what the species is. There is evidence for both hydrogen peroxide (H_2O_2) (reaction 9) and aqueous electrons (H_2O^-) (reaction 10) being important. However, the work on irradiation in bulk suggests that the direct homolytic cleavage of the C-O bond may still be significant in solution, even though homolytic cleavage of the C-H bond is not.

In the presence of oxygen the situation is further complicated by a number of additional reactions which may become important [47]. These are shown in table 2-2. The most interesting thing to note about this set of reactions is that there are propagation steps (reactions 5,6, and 7) which was not the case in the absence of oxygen, so there is the possibility of considerably higher levels of degradation.

2.3.5. Electron Beam Irradiation of PEO Solutions

The gel synthesis studies discussed previously were done almost exclusively using ^{60}Co as a gamma source. As already pointed out, the difference in dose rate and penetration depth between gamma and electron beam irradiation make comparison of the two ridiculous. However, a reasonably complete study of the PEO gels synthesized in aqueous by electron beam irradiation was done by Hueston [34] in a study carried out in conjunction with this work. The radiation source was a 3 MeV Van de Graaf generator located in the High Voltage Research Lab at MIT and

Reactions with Oxygen

Interactions with Water Radiolysis Products

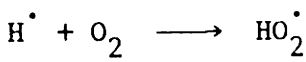

(1)

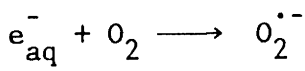

(2)

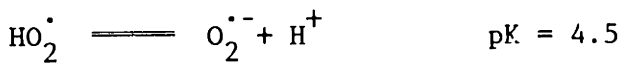

(3)

Interactions with PEO

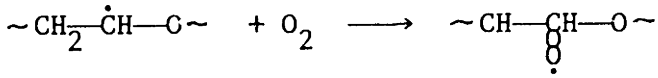

(4)

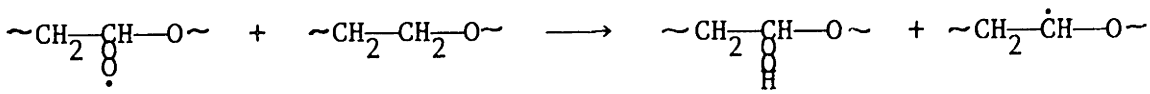

(5)

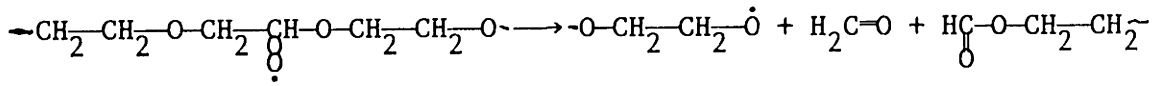

(6)

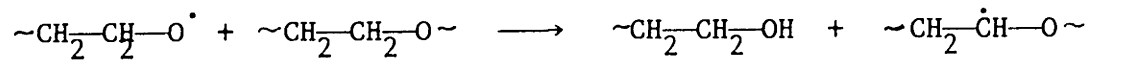

(7)

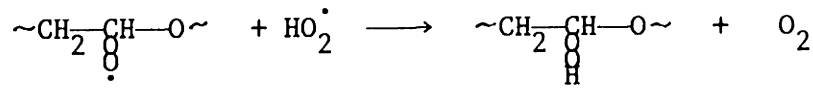

(8)

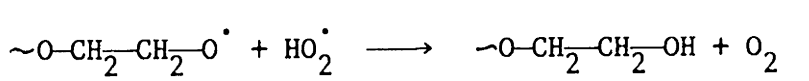

(9)

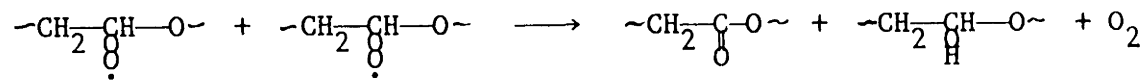

(10)

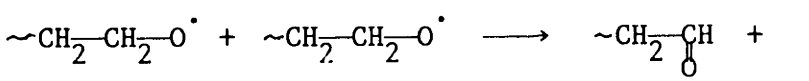

(11)

Table 2-2. Reactions proposed to take place in addition to those in table 2-1 when PEO is irradiated in solution in the presence of oxygen.

operated by Mr. Kenneth Wright. Hueston looked at crosslink density (measured by equilibrium swelling measurements) as a function of total dose, solution concentration, solution pH, and gaseous atmosphere. The trends observed are outlined below.

1. Over the range of initial concentrations studied (50 to 500 g/l) the crosslink density decreased about linearly with increasing concentration.
2. For given conditions (initial concentration, molecular weight, pH, etc.), the crosslink density increased linearly with dose up to some plateau level, above which there was no further increase in crosslink density as measured by swelling measurements.
3. The crosslink density was greater at neutral pH than in either acidic or basic solutions.
4. The crosslink density was greater in the absence of oxygen.

Physically, the gels were very fragile. They were transparent, and thicker gels (2 to 3 mm) contained numerous small bubbles. As the number of bubbles seemed to increase with dose, it was assumed that they originally contained hydrogen produced during the water radiolysis. The gels contained less than 5% extractable material immediately following crosslinking. It is interesting to note that at variance with the gamma radiation studies discussed earlier, there was only about a 20% difference in crosslink density in the presence and absence of oxygen. This is probably due to the very high dose rate (about 250000 rad/sec) used in Hueston's work. In gamma radiation, the solution can maintain

air saturation, picking up more oxygen as that initially present is used up, but in the electron beam work only the small quantity of oxygen initially present can have an effect on the irradiation chemistry. The other results are in qualitative agreement with the earlier studies mentioned.

2.4. PEO Network Characterization

2.4.1. Chemical Structure

Defining the method of crosslinking PEO solutions defines most of the chemical structure of the resulting gels. Radiation crosslinking produces a C-C bond between main chains as the crosslink unit (see section 2.3.4) and leaves the terminal hydroxyl groups untouched, and thus available for further derivitization if desired. The chains between crosslinks are exactly like uncrosslinked PEO chains. Figure 2-5 illustrates the type of chemical structure expected in these gels. It is much simpler than the chemical structure produced by any of the other crosslinking techniques mentioned earlier, and is also chemically much closer to uncrosslinked PEO. However, as pointed out in section 2.3.4, there are a number of possible degradation reactions that may be taking place during the irradiation, leaving a variety of different endgroups, so there is an ambiguity as to the chemical nature of the network.

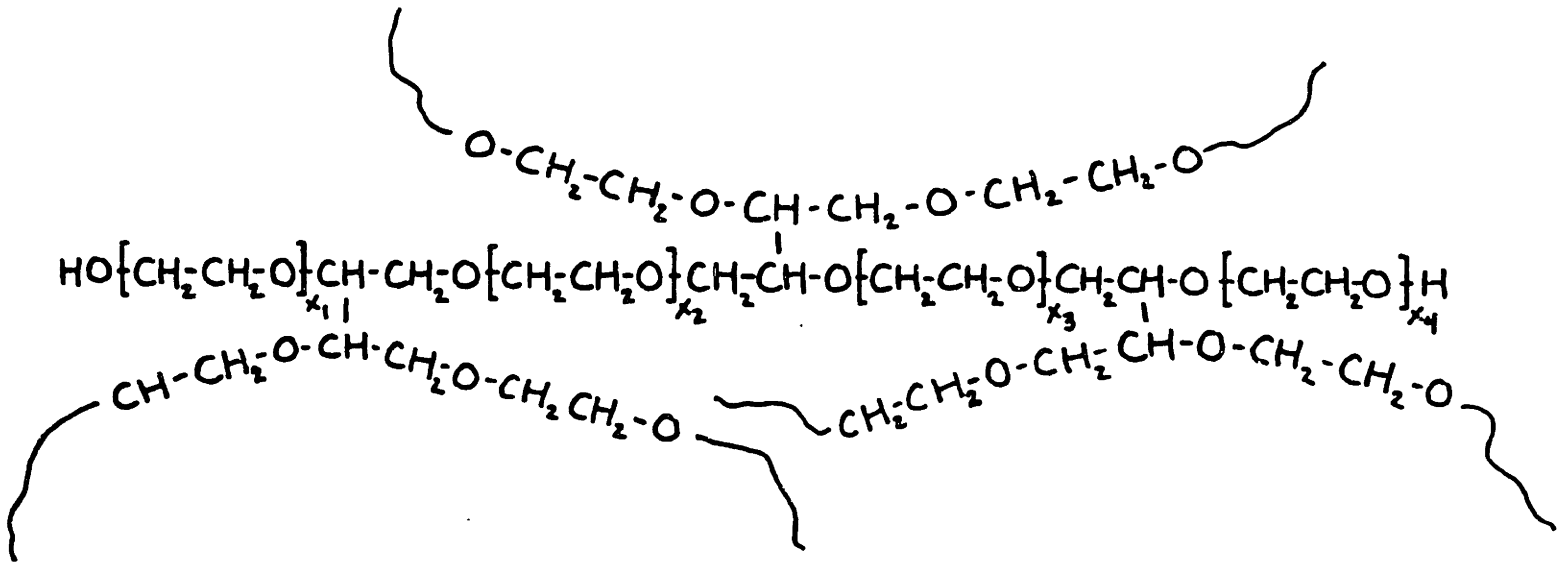

Figure 2-5. Expected chemical structure of radiation crosslinked PEO networks. For clarity, only a single chain is illustrated completely.

2.4.2. Important Structural Factors

There are a number of physical and structural properties of hydrogel networks that are important in controlling the semipermeable properties of hydrogels. The most important ones are the polymer volume fraction, the molecular weight between junctions, the conformation of the chains between junctions, the distance between junctions, the distribution of the distances between junctions, the degree to which the chains interpenetrate, and the mobility of the chains and the junctions. These properties will each be discussed briefly.

The easiest property to measure is the equilibrium polymer volume fraction in the swollen hydrogel, v_{2s}. It is defined as the volume of polymer in the swollen gel per unit total gel volume with the gel in equilibrium with excess solvent, and can be measured straightforwardly by weighing a gel in both the swollen and dried states [48]. The degree to which a particular network will swell in a given solvent depends most strongly on the crosslink density and the solvent quality; this is discussed in more detail in section 2.4.3. It is expected that the polymer volume fraction will be very important in controlling the diffusive properties of the gels. If diffusion through hydrogels actually takes place through the solvent in the swollen gel, then decreasing the amount of available solvent (by increasing the polymer volume fraction) will clearly lower the effective diffusivity. Previous workers [49,50] have suggested that the polymer volume fraction is indeed the controlling parameter in diffusion in swollen gels, and

determines the semipermeable behavior as well, as a result of the decrease in free volume available for transport. The polymer volume fraction also affects many of the other structural parameters, which will be discussed below.

The molecular weight between crosslinks, M_c, or interjunction molecular weight, is the second most straightforward property to measure. Figure 2-6 illustrates the molecular weight between crosslinks. As mentioned above, it is related to the degree of swelling of a network, and can be determined from swelling measurements by use of an appropriate theory (see section.). M_c can also be measured from a variety of mechanical tests, using the theories of rubber elasticity to relate mechanical properties to crosslink density. For a general introduction to the subject see [19]; for a detailed discussion, see [51]. The importance of M_c in controlling diffusion in hydrogels lies mainly in the dependence of the distance between junctions on the interjunction molecular weight. The junctions can be viewed as possible restrictions to diffusion; M_c controls how far apart these restrictions are.

The conformation of network chains refers to the behavior of the chains between crosslinks. Macromolecules are known to have a variety of different conformations, or chain shapes, ranging from the compact globular structures of proteins to the random coils of most synthetic macromolecules to the rod-like behavior of the polyaramides [52]. PEO is assumed to be a random coil in aqueous solution (despite the evidence mentioned above that there may be some structure in the PEO chain in

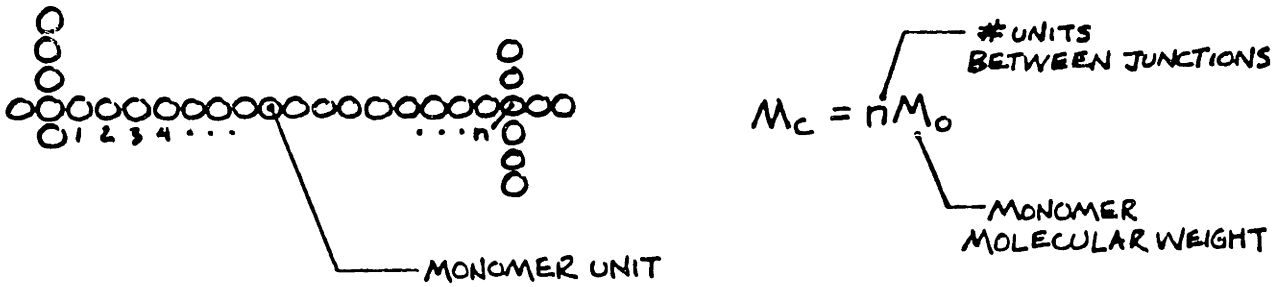

Figure 2-6. Definiton of the molecular weight between crosslinks (or interjunction molecular weight), M_c

water); however, the conformation in the swollen network will be affected by the crosslink density and the degree of swelling, so it is not possible to make the general statement that the chains in a PEO network will always behave as random coils. The effect of chain conformation on diffusion through swollen gels will be felt in several different ways. The most obvious is the effect on the distance between crosslinks, but other related issues include the homogeneity of the network, the flexibility and mobility of the chains, and the mobility of the junctions. Some of the possible chain conformations are illustrated in figure 2-7.

The distance between junctions in the network has been alluded to above. There are two different interjunction distances that can be defined for a network. These are the distance between topologically connected junctions (junctions that are at opposite ends of a network chain), d_t, and the distance between spatially nearest junctions, d_s. The difference between these two distances is illustrated in figure 2-8. Both of these distances depend on the M_c and the polymer volume fraction, and both are distributed about some average value. The average topological interjunction distance also depends on the conformation of the chains connecting the junctions, and unless this is known the distance cannot be calculated. The average spatial interjunction distance is defined by the crosslink density and the swelling ratio, so M_c and $v_{2,s}$ are sufficient to specify it. If the junctions are viewed as restrictions within the network it is clear that the distance between them will become important in controlling transport when this distance is of the same order as the

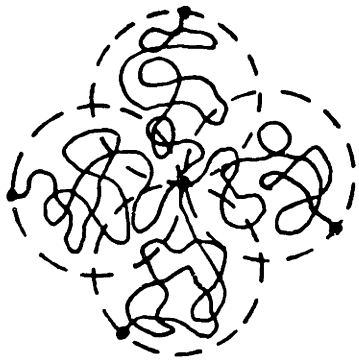

a. Discrete random coils. Coils touch only at junction points.

b. Overlapping random coils. Several coils exist in the same volume.

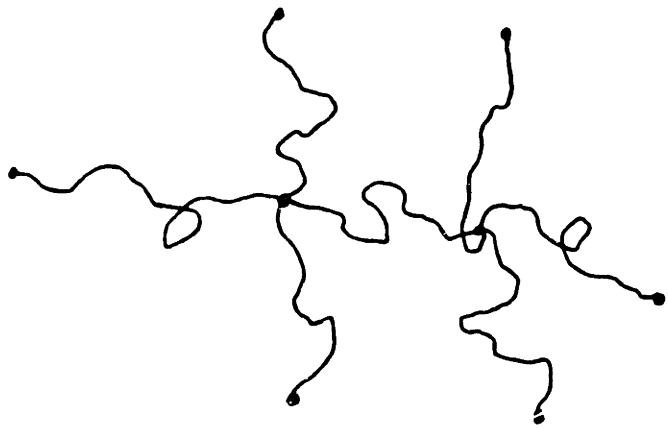

c. Highly extended chain backbones. Large empty (solvent-filled) areas exist between chains, which are not described by random coil statistics.

Figure 2-7. Schematic of some possible conformations of network chains.

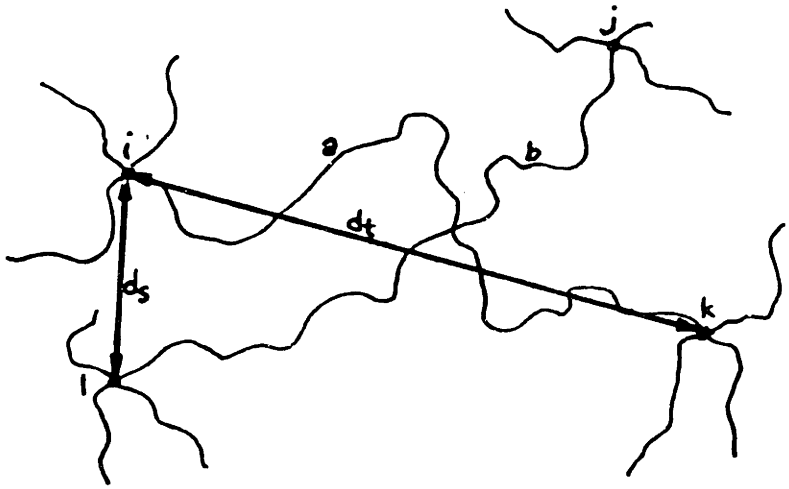

Figure 2-8 Schematic of part of a network, illustrating the distance between topologically connected junctions and spatially nearest junctions. Chains are actually overlapped some what, but are shown extended for clarity. Junctions i and k are connected by chain a, and d_t is the topological distance between them. Junctions i and l are not directly connected, but are spatial nearest neighbors, with distance d_s between them.

size of the diffusing species. This is addressed further in section 2.5.2.

As mentioned above, both interjunction distances are distributed about some average value. The nature of the distribution will depend on a number of things, which include the distribution of M_c, the chain conformation, and the degree of swelling. The distribution of topological distances will not necessarily be the same as the distribution of spatial distances. While the average distances are fairly readily obtained through simple theoretical considerations, the distribution of distances is not as simple. The distribution of topological distances should be related to the distribution of coil sizes for a polydisperse polymer sample in a good solvent, but it is further complicated by the lack of information on the distribution of M_c. It is not clear what is controlling the distribution of spatial distances. Clearly the distribution of distances will be important in determining transport in the relative size range mentioned above.

Another important parameter that is related to all of the factors already mentioned is the amount of chain interpenetration. This is a measure of the homogeneity of the network, and is somewhat controversial. Some workers [53,54] assume that a network will swell in a solvent until the chains touch only at the junction points, and thus there is no chain overlap. (This also eliminates the difference between spatial and topological junctions, as they are the same in this theory.) More traditional swelling theory [19] does not have this limitation, but in

practice there is always some amount of chain overlap. A more complete discussion of this is found in section 2.4.3. As a measure of the network homogeneity, the amount of chain interpenetration is quite important. It will determine whether there are portions of the network containing only solvent through which transport could be taking place and is also important in some of the assumptions involved in the theoretical development of sections 2.5.2 and 4.6.4.

The final factor that may be important in controlling diffusion through hydrogels is the mobility of both the chains and junctions. There are two separate parts to the mobility issue: how quickly the movements take place and what the magnitude of the motion is. Both of these parameters are difficult to measure, although there is a report of an NMR study done on PEO gels to look at relaxation times of the chains [55], which should give at least a relative measure of the rate of chain motion. As is clear from the above discussion, the junction mobility is probably at least as important as the chain mobility, because if the junctions can move out of the way they may not act as restrictions to diffusion at all. However, if there is very limited chain mobility, the chains themselves may act as restrictions to transport. Something can be assumed about the chain mobility based on the known solution behavior of PEO [16,56], but the junction mobility is more difficult to make a rational conclusion about.

2.4.3. Hydrogel Swelling Theory

As mentioned above, one of the ways of obtaining information about a polymer network is through equilibrium swelling measurements. In particular, the crosslink density and thus the molecular weight between crosslinks can be obtained from swelling measurements by applying an appropriate theory. There are several different ways of relating theoretically the equilibrium swelling properties and crosslink density of a network, however, most fall into one of two classes: rubber elasticity derived theories and solution-analogue based theories. The first type includes the affine swelling theory that is perhaps best described in Flory's book [19]. The second type is based on a scaling law proposed by DeGennes [53] which relates the behavior of a network with that of a solution at the critical overlap concentration. The important concepts of the two types of swelling theories will be discussed below, and predictions of M_c as a function of v_{2s} will be discussed.

2.4.3.1. Affine Swelling Theory.

The basis for traditional network swelling theories is an equilibrium between elastic forces of the chains holding the network together and mixing forces trying to pull the network apart by forcing solvent in. The process is depicted schematically in figure 2-9. It is most easily understood by considering it to be an osmotic process. The network is placed in contact with a large reservoir of solvent. Because the solvent

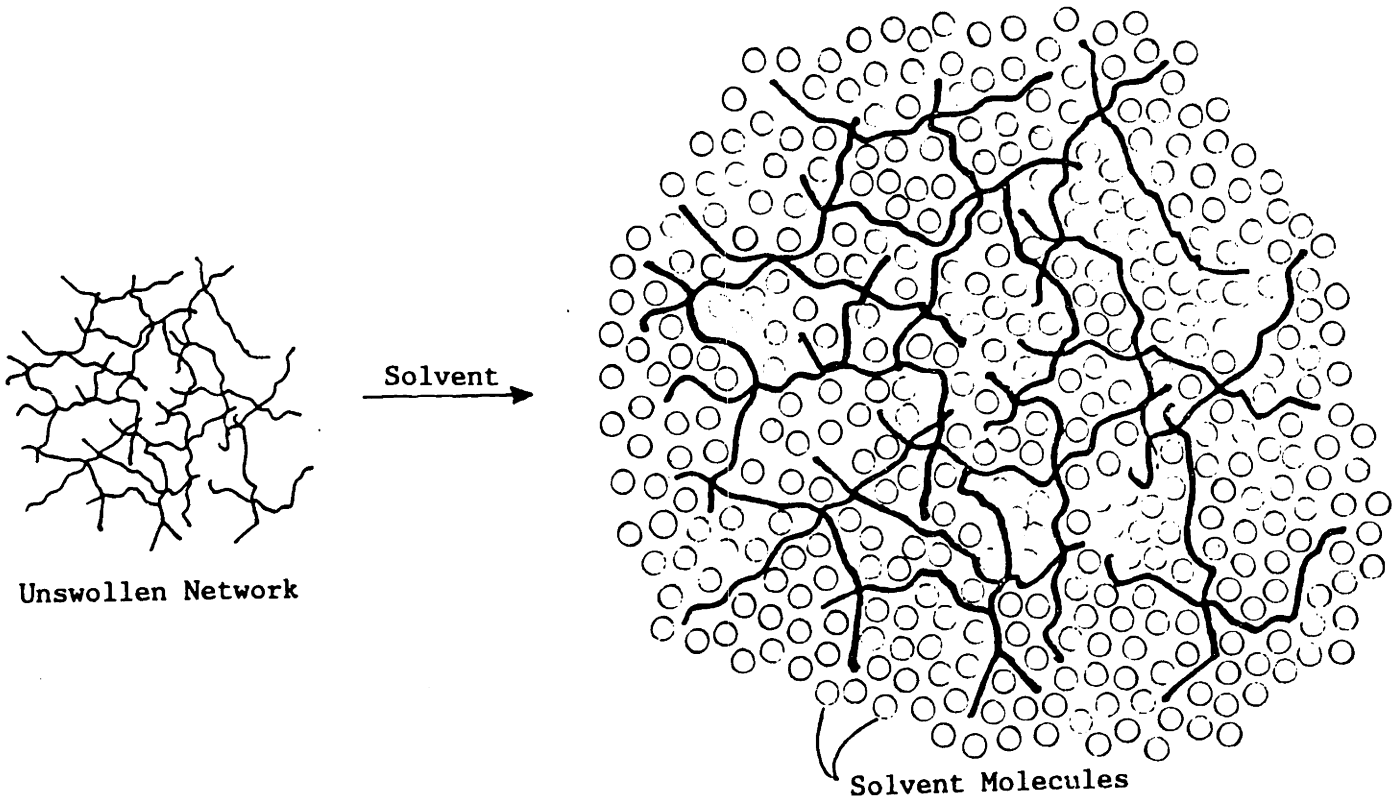

Figure 2-9. Schematic depiction of the process of network swelling. Solvent molecules penetrate the network, forcing the chains to stretch, which generates a pressure on the solvent molecules and allows them to be in equilibrium with the surrounding pure solvent.

concentration is lower inside the network, solvent is forced in to lower the osmotic pressure. However, as solvent moves in to the network the polymer chains are expanded, and because they are attached at both ends this generates an elastic retractive force pulling in. The result of this retractive force in an effective increase in the pressure inside the network. When this pressure becomes great enough to balance the osmotic pressure due to the difference in solvent concentration inside and outside the network, the network is in equilibrium with the surrounding solvent. The degree of swelling at equilibrium will clearly depend on the solvent quality (how badly the solvent wants to be in the gel) and the length of the chains between junctions.

Mathematically, following the development of Flory [19], equilibrium is reached when the chemical potential of the solvent in the network is equal to that of pure solvent.

$$\mu_1 - \mu_1^{o} = 0 = \frac{\partial \Delta F}{\partial n_1} \qquad (2\text{-}1)$$

In this equation, μ_1 is the chemical potential of the solvent in the network, μ_1^{o} is the chemical potential of pure solvent, ΔF is the free energy change, and n_1 is the number of moles of solvent. The free energy is split up into two parts, one containing the mixing terms and one containing the elastic terms.

$$\Delta F = \Delta F_{mix} + \Delta F_{el} \qquad (2\text{-}2)$$

In deriving the mixing terms Flory-Huggins liquid lattice theory is assumed to apply, which leads to the following expression:

$$\frac{\partial \Delta F_{mix}}{\partial n_1} = kT[\ln(1-v_{2s}) + v_{2s} + \chi_1 v_{2s}^2] \qquad (2\text{-}3)$$

wherein v_{2s} is the previously defined equilibrium polymer volume fraction, χ_1 is the Flory-Huggins interaction parameter, k is the Boltzmann constant and T is absolute temperature.

The elastic terms are somewhat more complicated. There are basically two things which control the elastic forces: the number of elastically effective chains and the amount they are stretched beyond the relaxed state. The relaxed state can be assumed to be the state in which the crosslinks are introduced, as there should be no stresses on the network in that state. If the relaxed state is bulk polymer, that is, if the crosslinks are introduced in bulk, the expression for the elastic terms is just that derived by Flory [19]. Bray [48] has modified this for the case in which the crosslinks are introduced in solution, so that the relaxed state is a partially swollen network. The expression derived is as follows:

$$\frac{\partial \Delta F_{el}}{\partial n_1} = \frac{kTV_1}{v}\left(\frac{1}{M_c} - \frac{2}{M_n}\right) \qquad (2\text{-}4)$$

$$\times \quad v_{2r}\left[\left(\frac{v_{2s}}{v_{2r}}\right)^{1/3} - \frac{1}{2}\left(\frac{v_{2s}}{v_{2r}}\right)\right]$$

In this expression v_{2r} is the polymer volume fraction in the relaxed

state, that is, at the concentration at which the crosslinks were introduced, V_1 is the molar volume of the solvent, and v is the specific volume of the polymer. Equations 2-1,2-2,2-3, and 2-4 can be combined to give the following expression for the interjunction molecular weight:

$$\frac{1}{M_c} = \frac{2}{M_n} - \frac{\frac{v}{V_1}\left[\ln(1-v_{2s}) + v_{2s} + \chi_1 v_{2s}^2\right]}{v_{2r}\left[\left(\frac{v_{2s}}{v_{2r}}\right)^{1/3} - \frac{1}{2}\left(\frac{v_{2s}}{v_{2r}}\right)\right]} \qquad (2\text{-}5)$$

M_c = average molecular weight between crosslinks
M_n = number average primary polymer molecular weight
v = polymer specific volume
V_1 = molar volume of solvent
χ_1 = Flory-Huggins interaction parameter
v_{2s} = polymer volume fraction in swollen network
v_{2r} = polymer volume fraction in newly crosslinked network

Equation 2-5 can thus be used to calculate the crosslink density from the swelling properties of the network. The first term on the right-hand-side is a correction for loose ends, as in any random linking process there are two loose ends for each primary molecule crosslinked. This theory has been checked experimentally for a number of polymer-solvent systems; however, PEO in water is not one of them, so there is no evidence available in the literature to prove that this is the appropriate theory for the present situation. Figure 2-10 shows some curves of predicted interjunction molecular weight as a function of swelling ratio and initial concentration for randomly crosslinked PEO networks of 35000 primary molecular weight swollen in pure water. There are two important features to note. First, in the limit of infinite swelling ($v_{2s} \rightarrow 0$), M_c approaches an asymptotic value of 1/2 the primary molecular weight. This comes from the limiting condition for gelation in

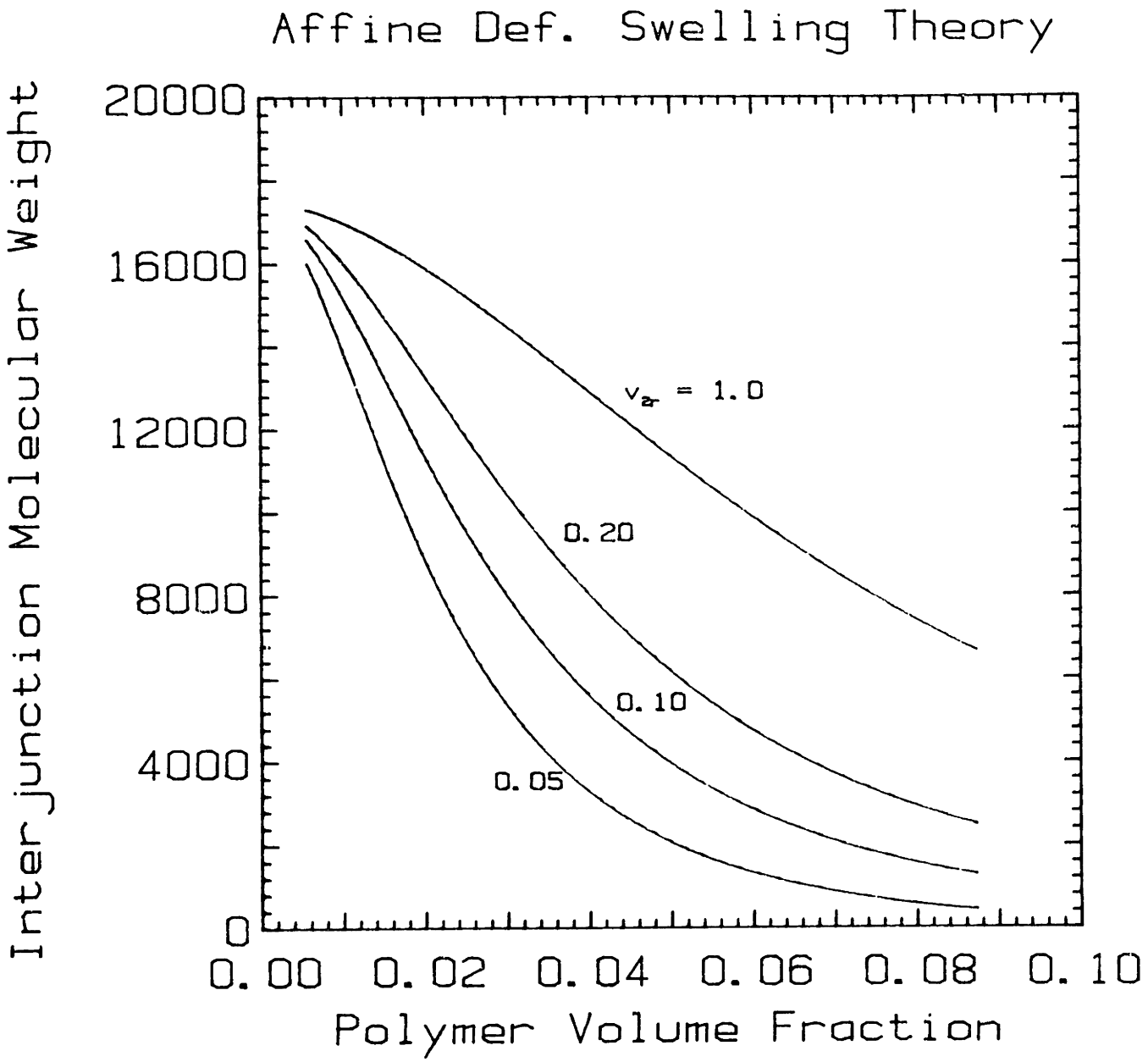

Figure 2-10. Values for the interjunction molecular weight as a function of degree of swelling of a PEO network in pure water calculated from the Flory-Bray affine deformation theory. The primary polymer molecular weight is 35000, and the initial polymer volume fraction varies from 0.05 to 1.0.

a randomly crosslinked system [19]. The second feature is the dependence on the initial concentration (or polymer volume fraction, v_{2r}). For two networks with the same crosslink density (M_c the same), as the initial polymer volume fraction increases, the degree to which the network will swell decreases. This is because in the more concentrated solution the crosslinks are closer together in the relaxed state and thus generate retractive forces at lower degrees of swelling.

2.4.3.2. Semi-dilute Solution Analogy.

The other theoretical approach is much simpler, both conceptually and mathematically. It was first suggested by DeGennes [53] and made semi-quantitative by Candau and coworkers [54,57,58]. The basis of the theory is the assumption that a network will swell until it reaches a state corresponding to a semi-dilute solution at the critical overlap concentration. At this point the individual network chains are touching only at the junction points. This theory is very attractive for its simplicity and also because it allows scaling principles derived for semi-dilute solutions to be applied to networks; however, the theory is based only on the fact that networks ought to behave like polymer solutions, and thus ignores the thermodynamic requirements for equilibrium. Bastide et al [54] add an additional level of complexity to the theory by assuming that a network swells in two steps. The first involves swelling from the bulk state, in which the network chains have their unperturbed dimensions and are also overlapped several times, to a point at which all the network chains are still in the unperturbed state

but are no longer overlapped. According to their report, this would correspond to the swelling of a network in a theta solvent. The second step is the swelling of the network from this "disinterspersed" state to the point where the network is at the critical concentration described above. They show neutron scattering results on networks swollen in theta solvents as evidence that this is indeed the case. However, there is no real physical basis for expecting this to be the case, so the mathematical development will be restricted to the theory as first developed by DeGennes, without the disinterspersion step.

According to DeGennes [55], at swelling equilibrium the topologically connected nearest junctions and the spatially nearest junctions are the same. This leads to the following expression for the equilibrium polymer volume fraction:

$$v_{2s} = \frac{M_c \, v}{N_{AV} S^3} \qquad (2\text{-}6)$$

In this expression, N_{AV} is Avogadro's number, S is the radius of gyration of the network chain, and the other variables are as previously defined. Although DeGennes does not explicitly give a form for S, the radius of gyration can be taken to be that defined by chain statistics [19]:

$$S^3 = \langle \bar{s}^2 \rangle^{3/2} = \left[\frac{\alpha^2 n_o C \ell^2}{6 M_o} \right]^{3/2} \bar{M}_c^{3/2} \qquad (2\text{-}7)$$

The variables are as follows:

$\langle \bar{s}^2 \rangle$ = mean square radius of gyration
α = expansion factor
n_o = number of bonds per repeat unit
C = characteristic ratio
ℓ = bond length
M_o = repeat unit molecular weight

According to the theory, the expansion of the chains is due to excluded volume effects, so the appropriate expression for the expansion factor α is

$$\alpha^5 - \alpha^3 = 2C_m\psi \left(1 - \frac{\theta}{T}\right)M_c^{1/2} \qquad (2\text{-}8)$$

C_m is a numerical constant for a given polymer-solvent system, ψ is the Flory entropic parameter [19], θ is the theta temperature, and other variables are as previously defined. By combining equations 2-6 and 2-7, one obtains the following expression for v_{2s}:

$$v_{2s} = k\,(\bar{M}_c)^{-1/2}(\alpha)^{-3} \qquad (2\text{-}9)$$

k is a constant for a given polymer - solvent system (39.1 for PEO in water). Using equations 2-8 and 2-9 one can make predictions for interjunction molecular weight as a function of swelling ratio. This is shown in figure 2-11, for the same system used in the Flory-Bray calculation. There are two immediately apparent differences between the semi-dilute analogy model and the affine deformation model. The semi-dilute model predicts that there is no dependence on initial polymer molecular weight or initial concentration. In fact, there is a unique relation between swelling ratio and crosslink density for any polymer - solvent pair.

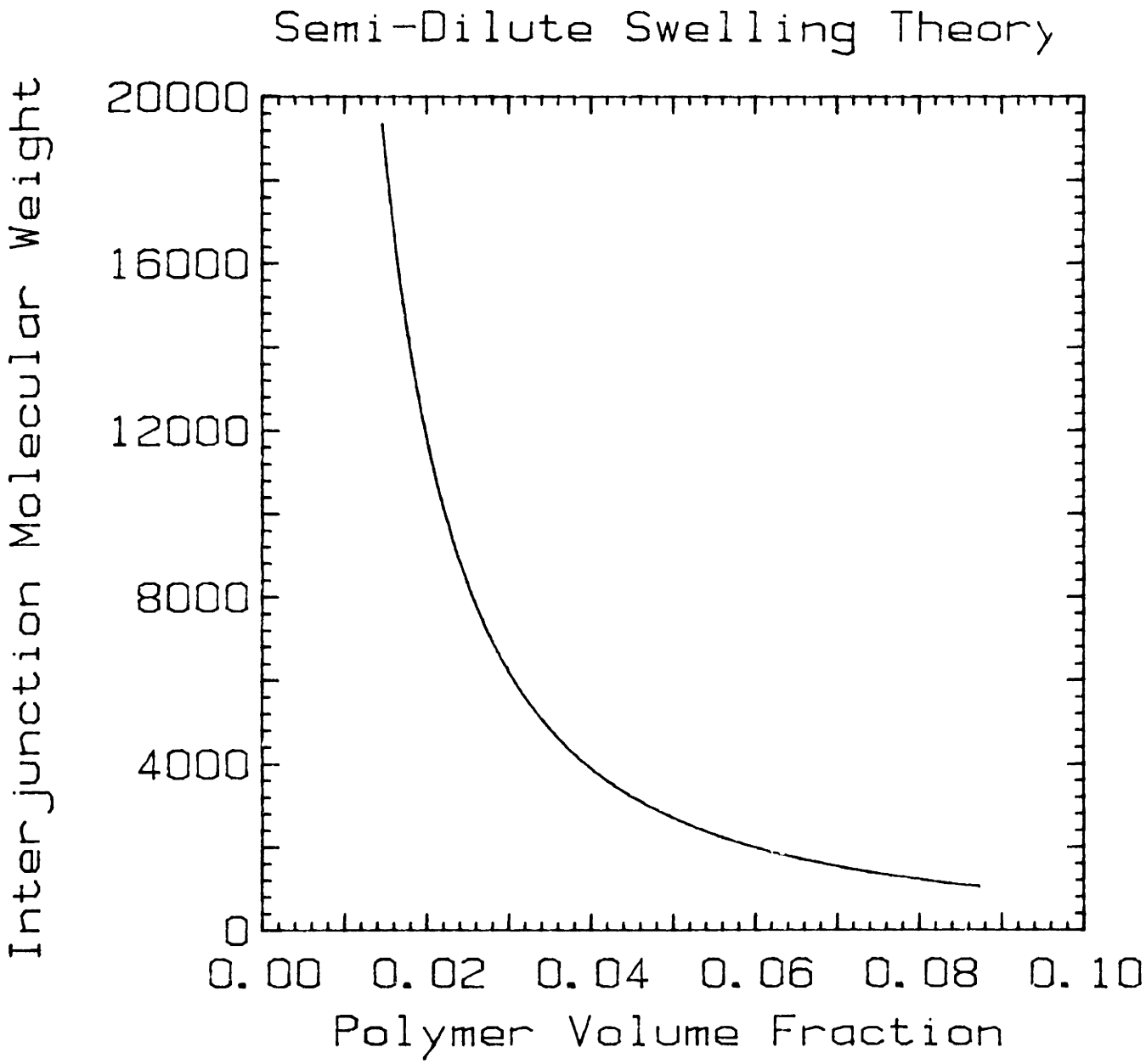

Figure 2-11. Values for the interjunction molecular weight as a function of degree of swelling of a PEO network in pure water calculated from deGennes' semi-dilute solution analogy. Changing the primary molecular weight and initial polymer volume fraction does not change the prediction.

As it has been previously demonstrated that there is a dependence of swelling ratio on initial concentration [51], the affine deformation theory will be used throughout this work for calculating values for M_c. There are a number of refinements that can be made to the theory, for instance a dual network theory could be used (see ref. [51] for a complete discussion), but as the experimental system under consideration in this work corresponds quite closely to the conditions for which the simplest theory was derived, and as there is no simple way to experimentally differentiate between similar models, the model as described above should provide as good a basis as any for correlation of the data. It should be noted, however, that while the trends measured should be real, the numerical values for the interjunction molecular weight may be incorrect by some constant factor.

2.5. Diffusion Through Swollen Gels

There has been much work done in the field of membrane transport. However, only a small part of this work has been aimed at determining effective diffusivities in membranes, and much of that has looked at microporous membranes. That leaves a relatively small part of the previous work in the area of diffusion in swollen polymer gel systems. However, as there is still an incredible amount of information available, no attempt will be made to discuss more than the most appropriate studies. There are a number of books and reviews available on the subject of membrane transport; see refs. [11,59,60,61,62].

It has been suggested [11] that semipermeable membranes can be defined as macroporous, microporous, or solution-diffusion, based on the presence and size of pores in the membrane. This is an essentially structural definition, and leads to the somewhat artificial specification of a solution-diffusion membrane as one which shows no structure at the resolution limit of scanning electron microscopy. However, a more appropriate definition of a solution-diffusion membrane is one in which bulk flow does not take place [63]; that is, all mass transport is diffusive in nature. Furthermore, the diffusive transport takes place by the dissolution of the solute species in the solvent present in the gel and diffusion through the solvent, not through the polymer itself. The two definitions are in general quite consistent with each other, and under both definitions homogeneous polymer gels fit into the solution diffusion category. There was a suggestion in some early work [64] that bulk flow of solvent may be possible in certain highly swollen polymer networks, this has since been shown to be the result of either pressure driven diffusion or pinholes in the membranes [63,65].

2.5.1. Previous Experimental Work

The current subject of interest will be limited to the concentration driven flux of solute species larger than the solvent species through highly swollen homogeneous polymer networks. The discussion will also be limited to separations in which interactions between the polymer and the solute are negligible, that is, equilibrium distribution coefficients between solvent and membrane are close to the solvent volume fraction.

These limitations are given for two reasons. First, they are appropriate to the experimental system used in this study, and second, the theoretical development that will be discussed in section 2.5.2 requires that these conditions be met. There are several studies in the literature that meet (or claim to meet) these criteria. These include the work of Colton and coworkers on transport through cellulosic membranes [66,67], the early study by Silliman on transport through radiation crosslinked poly(vinyl alcohol) (PVA) networks [8], the recent work by Peppas and coworkers [9] on poly(vinyl alcohol), and the work by Wisniewski and Kim [50] on polyhydroxyethylmethacrylate (polyHEMA) gels. (The voluminous work of Paul and coworkers, see, for example, ref. [68], will not be discussed in detail here as it includes predominantly work involving the pressure driven flux of solvents and other small molecules through various networks.) The studies closest to the present work are those on swollen PVA networks. PVA networks, like PEO, swell considerably in water, and both show relatively little interaction between polymer and solute. Also, the other two types of membranes show a tendency to form crystallites; in fact, it is the presence of such crystallites that create the network structure in cellulosic membranes [66], and poly(HEMA) membranes can be formed the same way [50]. The presence of the small crystalline regions can be expected to affect transport in different ways than the covalent bonds that form the network in radiation crosslinked PEO gels. PVA can be induced to form crystalline regions [48], but if crosslinked in solution and never dried this should not be the case. However, even the less closely related work can shed some light on the behavior of mass transport in swollen gel

systems.

The diffusion study of Colton [66] was done using a variety of cellophane-type membranes. Compared to the other networks that will be discussed, these cellulosics had a high polymer volume fraction (ranging from 20 to 50%) and as mentioned above, the structure of the membranes is not very similar to covalently crosslinked networks. However, it is the first comprehensive study on diffusion through swollen polymer membranes, and seems to be the benchmark against which most subsequent studies have been judged. The purpose of the work was to characterize the diffusive properties of solutes important in kidney dialysis applications, so a number of small molecules were examined, as well as a set of 5 small proteins. The small solutes ranged from NaCl through sugars, urea, uric acid, some polysaccharides, and a low molecular weight PEG. The proteins ranged in molecular weight from 17000 (myoglobin) to 67000 (albumin). Effective diffusivities were measured using a stirred batch dialysis cell, and a theoretically based correlation was developed to account for the fluid phase mass transfer resistance, so that the cumbersome (and non-rigorous) extrapolation involved in a Wilson plot [69] was not necessary. The most interesting results from the set of effective diffusivity measurements were that albumin was able to diffuse (although rather slowly) through all the membranes tested, and that the ratio of diffusivity in the membrane to diffusivity in pure water for the small solutes showed an exponential drop with solute size, if solute size is given by the radius [67] or the square of the radius [70]. This dependence is as predicted by diffusion through a polymer solution [71],

which will be discussed further in section 2.5.2.1. It was also observed that the rate of the drop was related to the amount of water in the membrane, with more highly hydrated membranes showing slower drops. Unfortunately, the lack of solute equilibrium distribution coefficients for the proteins makes it impossible to draw a conclusion about what was happening at larger molecular sizes.

The study by Silliman on PVA networks [8] used the same measuring technique. The gels were prepared by glutaraldehyde crosslinking of PVA in aqueous solution, and were cast on a non-woven fabric support to add strength. Silliman also crosslinked PVA gels in the presence of heparin (an anti-coagulant molecule) and measured diffusivities in these gels. Three different types of gel were tested, two of which corresponded to unsupported gels having polymer volume fraction of about 0.04 and M_c of about 20000 with and without heparin present, the other having a higher polymer volume fraction (around 7%) and lower M_c (around 15000). The range of polymer and crosslinker concentrations which could be used was somewhat limited due to the formation of micro-inhomogeneities in some gels during the crosslinking procedure. This was attributed to the presence of a microstructure in the PVA solution prior to crosslinking, but it is also possible that phase separation was beginning during the crosslinking process. However, working with gels formed in the range where inhomogeneities were not found, it was observed that the effective diffusivities in the PVA gels were higher but followed the same pattern as the membranes tested by Colton. As a reference, Silliman measured the effective diffusivity of albumin (molecular weight 67000, effective

hydrodynamic radius 36 Å) in the three gels and found that the ratio of diffusivity in the gel to that in pure solvent ranged from 0.02 (for the looser gel without heparin) to 0.009 (for the tighter gel). These are about an order of magnitude higher than the values Colton found in the cellophane membranes, which was attributed to the much higher water content of the PVA gels.

The work done by Wisniewski and Kim [50] also used a stirred batch dialysis cell to determine effective diffusivities. No attempt was made to correct for fluid phase mass transfer resistance. Two types of poly(HEMA) membranes were used, one formed simply by polymerizing HEMA in the presence of water, and the other by polymerizing HEMA with a small amount of ethylene glycol dimethacrylate as crosslinker, also in the presence of water. Only relatively small solutes were used, ranging from 20 to 500 in molecular weight. The results showed the same exponential dependence of diffusivity ratio on solute size as found in Colton's work. They also found the same dependence on degree of hydration. The measured solute equilibrium distribution coefficients were compared with those predicted using a three state theory of water inside the hydrogel. In this theory, all water in the swollen gel is found to exist in one of three states: bound, which is hydrogen bonded to the polymer chain, bulk, which has the properties of bulk water, and intermediate, which has properties intermediate between bound and bulk. The comparison with data suggested that the solutes considered had access primarily to the bulk water in the network. However, this theory does not include the possibility of interactions between polymer and solute, and such

interactions were not ruled out experimentally.

The last experimental study that will be discussed in detail is that of Reinhart and Peppas on diffusion through glutaraldehyde crosslinked poly(vinyl alcohol) gels [9]. This study was focused primarily on the effect of membrane structure on transport; consequently a single solute (bovine serum albumin) and a range of network structures were used. The molecular weight between crosslinks was found from swelling measurements to range from 2000 to 11500, and the corresponding equilibrium polymer volume fractions ranged from about 0.12 to 0.045. The diffusivity measurements were done using a stirred batch dialysis cell and the data reduction procedure of Colton [66]. The measured diffusion coefficients were found to increase with about the square of the molecular weight between crosslinks. The diffusion coefficients were quite high, up to 85% of the diffusion coefficient of albumin in water, which is quite different from the results obtained by Silliman [8] and discussed above. As was mentioned above, Silliman has been observed that PVA gels can form localized inhomogeneities in the glutaraldehyde crosslinking process, and a recent study [72] saw this manifested in anomalous diffusion behavior of albumin; it is possible that such a structural feature may have existed in the gels used by Reinhart and Peppas and that the diffusion may have been in the class of restricted diffusion through pores rather than solution diffusion.

2.5.2. Theoretical Background

The most popular way to model diffusive transport through swollen polymer gel systems is based on the assumption that transport is actually taking place through micropores. While this is probably generally accepted as an invalid approximation, because the concept of pores in a polymeric gel is a difficult one as the geometry, size, and location of such pores are constantly changing, many workers have found such analyses to produce some useful information. Most analyses are based on the models of Faxen [73] or Anderson and Quinn [74], and can yield information about the size of the "pores" in the polymer network as well as allowing correlation of diffusivity data. However, hydrodynamic analysis of one membrane system yielded a effective pore size of about 5 Å [75], and this is so far outside the range of applicability of any of the theories based on micropores [61] that the value of further such modelling even as a correlational tool is questionable. There has thus been a resurgence of interest in a theory first proposed in 1969 by Yasuda et al [70], and known most commonly as solution-diffusion. As mentioned above, this theory requires that three conditions be met. These are (1) that the transport is strictly diffusive and concentration driven, (2) there are no enthalpic interactions between the polymer and solute, and (3) that the network is highly swollen. Also, as mentioned above, the basis for the theory is that transport takes place through the solvent in the network. As the network is required to be homogeneous, the chain segments are assumed either to randomly fluctuate or be pushed out of the way of the diffusing solute. The effect of the polymer is two-fold.

First, the polymer chains decrease the amount of free volume (or perhaps more correctly the average size of a free volume element) available in the solute. This is identical to the effect predicted and observed in polymer solutions [71,76]. The second effect is due to the junction points in the network, and is essentially a limit on the size of a molecule that can get in to the network. It can be visualized simplistically in two dimensions as four tetrafunctional junctions at the corners of a square with chains making up the sides (see figure 2-12). If the junctions have limited mobility, the absolute maximum size molecule that can fit through this portion of the network is one with diameter equal to the chain length. This is generally known as the sieve effect, and is discussed in much more detail in the development of the theoretical model in section 4.6.4. In the early development, Yasuda and coworkers concentrated primarily on development of an expression for the first effect, as the available data was in a range where this appeared to be the controlling effect. It should be noted that Peppas and Reinhart in 1984 [77] arrived at essentially the same expression through a slightly different derivation. The details of the derivation are given in section 4.6.4 and appendix 7; here we will simply present the result and discuss it in terms of observed behavior and the assumptions involved.

2.5.2.1. Free Volume Term

One obtains for the ratio of the diffusion coefficient in the membrane, $D_{2,13}$, to that in pure water, $D_{2,1}$,

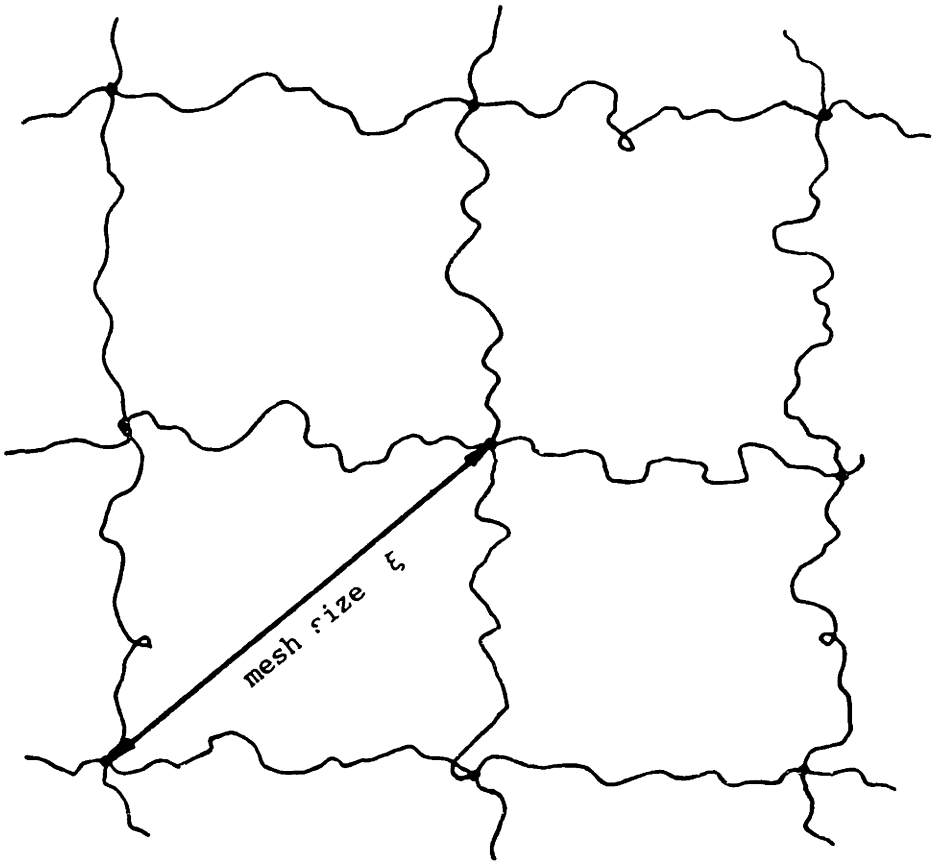

Figure 2-12. Schematic diagram of an idealized 2-dimensional network illustrating the mesh size and sieve effect. Molecules of diameter greater than ξ cannot penetrate mesh if junctions are immobile.

$$\frac{D_{2,13}}{D_{2,1}} = f(V_2) \exp\left[\frac{- B r_s^2 \pi}{V_{f,1}^{(Q-1)}}\right] \qquad (2\text{-}11)$$

V_2 = characteristic volume of the solute
B = constant; includes diffusional jump length
r_s = effective solute radius
$V_{f,1}$ = free volume of solvent
Q = swelling ratio = $1/v_{2s}$

In this expression $f(V_2)$ is the function describing the sieve effect of the polymer mesh. According to Yasuda it should be the volume fraction of the membrane containing holes larger than V_2, with V_2 a characteristic volume of the solute, although no further attempt was made to find a theoretical expression for $f(V_2)$, as the experimental data available at the time did not suggest that the sieve effect was important. The sieve term is discussed in section 2.5.2.2. The exponential term, which is the term of interest here is the conformational probability of forming a "hole" in the solvent in the network large enough for a solute molecule of effective radius r_s to pass through. Unfortunately, the development was not completely rigorous in deriving this term. There are two problems. First, the expression describing the free volume available for transport is not quite correct. The Q - dependence is appropriate, but the solvent free volume, $V_{f,1}$, is interpreted to be a free volume fraction, that is, the ratio of free volume to total membrane volume. This is clearly an incorrect interpretation, which is obvious from a simple dimensional analysis, (the appropriate dimension for the free volume is length^3) as well as from the knowledge that the term should actually express the size of the volume elements available for diffusion.

Also, this derivation requires that all the water within the membrane is available for transport and behaves the same way with regard to free volume considerations. In light of the information above on water structure in hydrophilic polymers and gels [24,50], it is not clear that this is the case. The other problem is with interpreting the constant B, which includes the diffusional jump length λ as well as some other constants arising from the free volume derivation. It is not clear whether this constant is a universal constant, or if it is a function of membrane type, solute, or both. It is assumed in both derivations that it is a universal constant. Figure 2-13 shows the type of scaling information that can be obtained from this model. There is an exponentially decreasing dependence of diffusion coefficient ratio on solute size as measured by the square of the radius for a single membrane and an exponentially decreasing dependence of diffusion coefficient ratio on $1/(Q-1)$, which is approximately the same as v_{2s}.

Clearly, then, even in the absence of sieve effect concerns (i.e., $f(V_2) = 1$) this expression is not a predictive tool. It can, however, be used to correlate data, and to determine if the dependence on the solute size and gel hydration is as predicted. This was done both by Yasuda et al. [70] and Peppas and Reinhart [77], although a fairly large fraction of the data was the same, that collected by Colton [67] on cellophane dialysis membranes. Peppas and Reinhart used some additional data on similar systems. It was found that for these semi-crystalline, not highly hydrated systems, the dependence on both solute size and swelling ratio (Q) appeared to be as suggested by the model, although the scatter

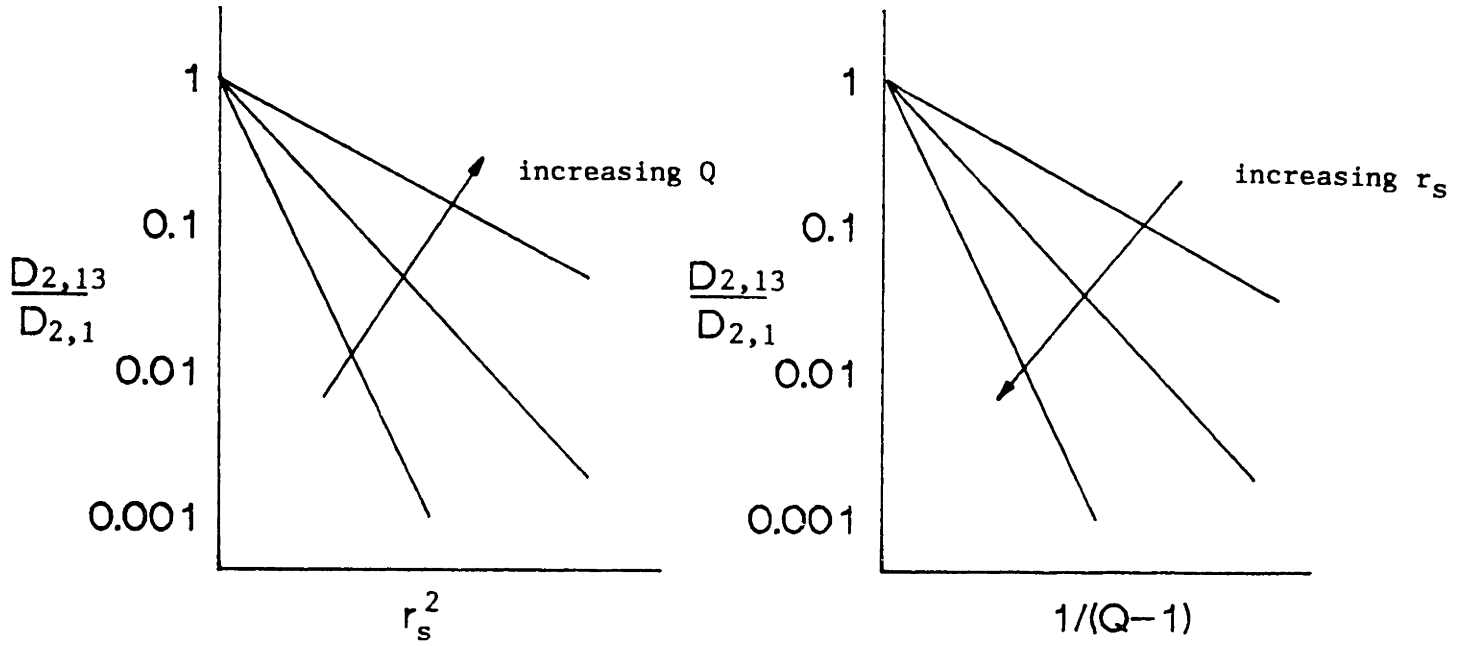

Figure 2-13. Diffusion coefficient scaling as a function of network swelling and solute size as predicted by the free volume term of the solution-diffusion equation.

in the data makes definite conclusions difficult. There is no evidence in any of the data that the sieve effect is important at these conditions.

2.5.2.2. Sieve Effect Term

As discussed above, most of the existing data on transport in water swollen membranes appears to be in a regime where the sieve effect of the membrane is not important. Consequently, very little work has been done to try to quantify this effect. The two main attempts are discussed in the aforementioned papers by Yasuda et al [70] and Peppas and Reinhart [71]. While both have a theoretical base, in practice they are really semi-empirical correlations. Both will be discussed here in detail to point out the advantages and disadvantages of each approach.

Empirical Approach of Yasuda

The approach of Yasuda et al was basically an empirical one. They interpret $f(V_2)$ in the solution-diffusion equation

$$\frac{D_{2,13}}{D_{2,1}} = f(V_2) \exp\left[\frac{- B r_s^2 \pi}{V_{f,1}(Q-1)}\right] \qquad (2\text{-}11)$$

to be equal to the probability of finding a space between restrictions in the polymer network equal to or larger than V_2, the volume of the permeating species. They then assumed various functional forms for the

distribution of hole sizes, including a Gaussian distribution, a Dirac delta (all holes have the same size - this might be the case for a model end-linked network formed from monodisperse polymer chains), and a simple linear function with sizes from zero to some maximum. All of the distributions were described by q_0, the average mesh size, which can be interpreted as the average cross-sectional area of the holes in the mesh defined by the polymer chains and junctions. This parameter arises from the simplification that the cross-sectional area of the molecule, $q_2 = \pi r_s^2$, is the important size parameter of the diffusing species (rather than the volume V_2). This discounts the importance of the length of the diffusional jump through the mesh. Unfortunately, the data available for Yasuda et al to compare with their theory was all above the limit where the sieve effect became important, so confirmation of the functional form was impossible.

The advantages to the form for $f(V_2)$ proposed by Yasuda et al are mostly in the simplicity. The fact that $f(V_2)$ should be a probability distribution arises directly from the solution-diffusion model, and the idea that the probability of interest is the probability of a mesh space being larger than the area of the molecule which must go through it is very straight-forward. The types of mesh size distributions proposed are simple functions and easy to work with; however, they have no real basis in the polymer physics of the network structure. But it does seem apparent that starting from this initial concept of a distribution of mesh sizes it should be possible to determine theoretically what the actual distribution should be. This involves first making a decision

about what network property defines the mesh that is important in controlling transport and then finding a way to predict the mesh size and mesh size distribution from known structural properties of the network. The biggest difficulty with this is the choice of the appropriate measures of network mesh size and solute size important in diffusion. Yasuda et al make no real attempt to select such parameters, although it is implied that their approach expects the distance between junctions to be appropriate for the mesh size and the effective solute area (πr_s^2) to be appropriate for the solute size.

Peppas and Reinhart Approach

The attempt by Peppas and Reinhart [77] to express the sieve effect term in easily measurable quantities is based more on polymer physics. They began with the assumption (similar to Yasuda et al) that the cross-sectional area of the mesh is proportional to the square of the distance between junctions, which is assumed to be given by $\langle r^2 \rangle$, the mean square end-to-end distance of a network chain. They further assume that this is proportional to the average molecular weight between junctions, $\bar{M}_c$, since $\langle r^2 \rangle = Cn\ell^2$ and $M = M_0 n/b$ where n is the total number bonds in the polymer chain, b is the number of bonds per repeat unit, M_0 is the repeat unit molecular weight, C is the characteristic ratio, and ℓ is the bond length. To convert to the fraction of holes above a certain size, they assume a certain minimum interjunction molecular weight, M_c^*, which corresponds to the minimum mesh size which will allow penetration of a particular solute. No attempt is made to correlate this with the solute

size, it is left as a parameter to be experimentally determined for each solute. The probability is normalized by $M_n - M_c^*$, where M_n is the primary chain molecular weight. The expression for $f(V_2)$ is thus

$$f(V_2) = k \frac{M_c - M_c^*}{M_n - M_c^*} \qquad (2\text{-}12)$$

where k is a proportionality constant.

This expression seems at first somewhat more theoretically based than that of Yasuda et al, and also directly expresses the sieve effect in terms of network properties. However, this expression has the disadvantages of the first in that the space available for solute penetration is again assumed to be the area of the tetrafunctional mesh. Also, while the problem of determining the correct solute cross-section is eliminated, it is at the expense of introducing M_c^*, a quantity which must be experimentally determined in a cumbersome procedure for each solute-network pair. The expression is thus not easily generalized, and of no use as a predictive tool, as information on the diffusion coefficient of one solute cannot be used to predict that of another, even in the same network. Furthermore, certain of the assumptions made in developing the equations are not necessarily valid. In deriving the proportionality between mesh size and molecular weight between junctions, Peppas and Reinhart assume the area of the holes should be proportional to M_c, as M_c is proportional to n which is proportional to $\langle r^2 \rangle$. Leaving aside the question of whether $\langle r^2 \rangle$ is the appropriate measure of mesh area, only in the case of a theta solvent is M_c proportional to $\langle r^2 \rangle$. In

the case of a good solvent, $\langle r^2 \rangle$ is proportional to $M_c^{1.2}$. In the case of a network swollen to equilibrium in a pure solvent there is no simple relationship, as the distance between junctions depends explicitly not only on the molecular weight between junctions but also the degree of swelling of the network, which is not necessarily a unique function of M_c. However, the power to which M_c should be raised is probably greater than 1.2. Furthermore, there is no clear reason why the denominator should contain M_n. Peppas and Reinhart suggest that at the limit $M_c = M_n$, there will be no junctions and therefore can be no transport restriction due to the mesh. They suggest that at this limit the expression for the diffusion coefficient ratio (eqn. 2-11) should simplify to the case for transport through pure solvent. Actually, the equation should simplify to the case of diffusion through a polymer solution of the same volume fraction. If the sieve effect term is one, this is essentially the case, however, Peppas and Reinhart imply that the constant k would be chosen such that the diffusion coefficient ratio (and not the sieve effect term) goes to unity when $M_c = M_n$. Additionally, there is no reason to believe that two randomly crosslinked networks with identical polymer volume fraction and molecular weight between crosslinks should show any differences in transport behavior based on primary molecular weight.

The final problem with the expression of Peppas and Reinhart is the finding by Reinhart and Peppas [9] that the expression derived for the sieve effect did not accurately represent the data described above obtained on the system of poly(vinyl alcohol) swollen in water with

albumin as solute. The explanation offered is that the mesh size may be underpredicted by the analysis given. However, as pointed out above, the diffusion coefficients measured seemed somewhat high, possibly because of inhomogeneities in the membrane. If this were the case, the experimental conditions would not be appropriate for the theoretical development and agreement would not be expected.

Chapter 3. Experimental Techniques

3.1. Experimental System

The experimental system used to study the effect of network structure on diffusive transport was radiation-crosslinked poly(ethylene oxide) networks swollen in aqueous solutions. There are several advantages to this system, as well as some disadvantages. One of the most important reasons for using PEO is the low protein binding characteristics it appears to have, which allows the assumption that there are no enthalpic interactions between the solute molecules and the polymer chains. Radiation crosslinking has several advantages over end-linking. Network formation is accomplished without the addition of a crosslinking species, so there are no concerns about different interactions with different parts of the network or aggregation of the crosslinking species imposing a secondary structure on the network. Also, it is possible to synthesize gels with quite different structural properties that are virtually identical chemically. In terms of understanding the physical structure of the network, radiation crosslinking eliminates the ambiguity inherent in end-linking regarding the extent of reaction and junction functionality, that is, all junctions have four chains extending from them no matter what synthetic conditions are used. One of the biggest disadvantages, which seems to be inherent in any aqueous system, is ordering or complexing of water by the chains. It is not clear a priori how this is likely to affect diffusive transport in the gel, but it certainly adds ambiguity to any liquid lattice calculations. The other

disadvantages are due to the radiation crosslinking procedure. An important issue is chain scission. If it is an important process at the conditions of gel synthesis, the network structure will be different than expected as there will be some number of additional chain ends (and possibly other effects). Also, as pointed out in section 2.3.4, there is uncertainty about what end groups will result from scission, so the chemical structure may not be as simple as desired. However, the advantages of this system are more important than the disadvantages, some of which can be overcome by additional measurements or theoretical considerations.

3.2. Synthesis of PEO Gels

3.2.1. Radiation Source

All gel synthesis was done using high energy electrons as the radiation source. The electrons were produced by a 3 MeV Van de Graaf generator at the High Voltage Research Lab at MIT. The generator was operated by Mr. Kenneth Wright. Figure 3-1 is a schematic of the sample transport system used. Samples are placed on the belt and carried back and forth under the beam. Dose rate (and dose per pass under the window) is controlled by the speed of the belt and the beam current, and total dose by the dose rate and the number of passes. The shape of the beam and window do not allow calculation of an exact dose rate, but an approximate measure can be made. Unless otherwise specified, irradiations were done at 2.5 Mrad/pass with a belt speed of 0.8 cm/s and a window of approximately 8

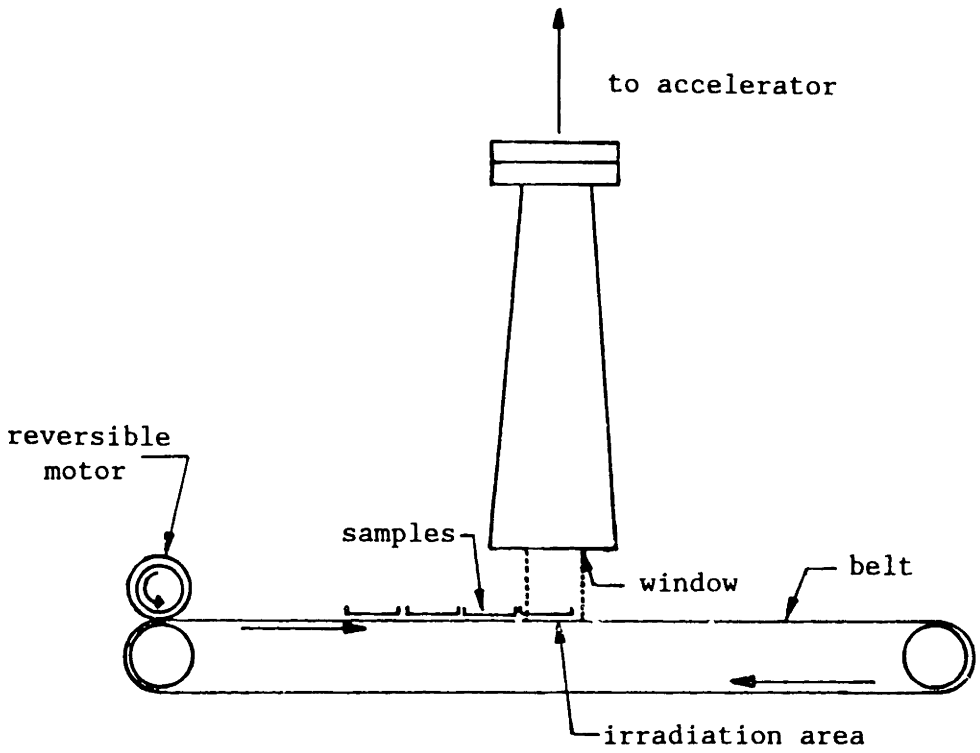

Figure 3-1. Illustration of the sample transport system of the Van de Graaf electron accelerator used in this study. Samples are placed on belt, which carries them back and forth under the beam.

cm length, giving an approximate dose rate of 250,000 rad/s. There are certain physical restrictions involved in the irradiation of these samples. Because of the shape of the beam and window samples wider than 10 cm would not get a uniform dose, so samples were kept smaller than this limit. The length of a sample was limited by the length of the belt to about 1 meter. Sample thickness is limited by the penetration depth of the electrons, which is controlled by the energy of the beam; in the case of the 3 MeV electrons used for this study the absolute penetration limit is about 0.5 cm, but the shape of the dose-depth relationship is such that it is desirable to have a sample thickness of about 2 mm or less and 2 to 3 mm of polyethylene over the sample. This gives the most uniform dose over the entire sample thickness. No attempt was made to control the irradiation temperature in any of the irradiation work. The temperature was known to rise as the irradiation takes place, and an attempt was made to quantify this by placing a thermocouple lead in a sample prepared as below but with pure water instead of PEO solution so gelation would not occur. The thermocouple output was recorded as a function of time on a strip chart recorder.

3.2.2. Preparation of PEO Samples for Irradiation

The following technique was used for all gel synthesis studies. The majority of the gels synthesized were made using the exact conditions given below, but some variations were made to study details of the synthesis (a follow-up on the study of Hueston [34] mentioned earlier) and these variations are discussed under specific experiments.

Poly(ethylene oxide) (Fluka Chemicals) of nominal molecular weight 35000 was dissolved to the desired concentration by gentle shaking in ultrapure water (produced by a Milli-Q water polishing system) with 0.01% sodium azide added to retard bacterial growth. For all but the most concentrated solutions (>10% PEO wt/vol) the dissolution process took place in less than 1 hr; more concentrated solutions were left over night. For solutions to be irradiated in the absence of oxygen, the solutions were deaerated under vacuum for at least 2 hours and saturated with the desired gas (usually N_2). The appropriate volume of solution to give a 1 to 2 mm layer was then placed in a glass Petri dish (working in a glove box under appropriate atmosphere for the O_2 excluded samples) and a double thickness of polyvinylidene chloride film (Saran wrap) was placed over each dish and sealed with a rubber band. The samples were then carried to the High Voltage Research Lab to be irradiated. The time between sample preparation and irradiation was kept to a minimum, usually between 15 and 60 min, although this did not appear to affect the results. After irradiation, the samples were returned to the lab for immediate characterization and testing.

3.3. Physical Characterization of Gels

3.3.1. Swelling Measurements

3.3.1.1. Techniques

As discussed in section 1.4.3, a considerable amount of information can

be obtained from measuring the equilibrium swelling properties of the networks. The following method was used for measuring the polymer volume fraction in the gel. Immediately after irradiation, two small pieces were cut from each sample with a cork borer. These pieces were blotted on damp filter paper to remove any surface water and weighed to an accuracy of 0.0001 g on an analytical balance. They were then placed in a known amount of ultrapure water containing 0.01% NaN_3 and allowed to swell. After 2 days the water was changed, with a sample of the original water reserved to analyze for extracted PEO, and the samples were again blotted on filter paper and weighed. The water was changed and the samples reweighed until the sample weight remained constant, which usually required only one change of water. The gel pieces were then placed in polystyrene weighing dishes and dried under vacuum at about 40°C for at least 24 hr. The samples were then immediately reweighed to avoid the absorption of any water from the atmosphere. The liquid samples reserved from the first solvent change were analyzed using the size exclusion chromatography system described in section 3.4.3.3.

3.3.1.2. Data Analysis

The three weights (immediately after crosslinking, fully swollen, and dried) were used to compute polymer volume fractions using the known densities of PEO (ρ_p = 1.2 [77]) and water (ρ_s = 1.0). The following relations between weights and volume fractions were used.

$$v_{2r} = \frac{w_p}{w_p + (w_r - w_p)(\rho_p/\rho_s)} \qquad (3\text{-}1)$$

$$v_{2s} = \frac{w_p}{w_p + (w_s - w_p)(\rho_p/\rho_s)} \qquad (3\text{-}2)$$

The variables are:

w_r, weight of the gel immediately after crosslinking
w_s, weight of the fully swollen gel
w_p, weight of the dried polymer network
ρ_p, density of the polymer
ρ_s, density of the solvent
v_{2s}, polymer volume fraction at equilibrium swelling
v_{2r}, polymer volume fraction immediately after crosslinking

The interjunction molecular weight, M_c, was obtained using the Flory-Bray swelling equation discussed in section 2.4.3.1,

$$\frac{1}{M_c} = \frac{2}{M_n} - \frac{\frac{\bar{v}}{V_1}\left[\ln(1-v_{2s}) + v_{2s} + \chi_1 v_{2s}^2\right]}{v_{2r}\left[\left(\frac{v_{2s}}{v_{2r}}\right)^{1/3} - \frac{1}{2}\left(\frac{v_{2s}}{v_{2r}}\right)\right]} \qquad (3\text{-}3)$$

M_c = average molecular weight between crosslinks
M_n = number average primary polymer molecular weight
$\bar{v}$ = polymer specific volume
V_1 = molar volume of solvent
χ_1 = Flory-Huggins interaction parameter

The solvent molar volume is taken to be 18 cm^3/mol for water at room temperature (23±1°C). The value for χ_1 was measured; see section 3.3.1.3.

From the values for M_c and v_{2s} it is possible to obtain a value for the average distance between topologically connected junctions. The following procedure is used to find these values. The root-mean-square end-to-end length of an extended polymer chain is given by

$$\langle r^2\rangle^{1/2} = \alpha\langle r^2\rangle_0^{1/2} \qquad (3\text{-}4)$$

where α is the chain expansion factor and $\langle r^2 \rangle_0^{1/2}$ is the unperturbed end-to-end distance, given by

$$\langle r^2 \rangle_0^{1/2} = (Cn\ell^2)^{1/2} \qquad (3\text{-}5)$$

where C is the characteristic ratio, n the number of bonds in the interjunction chain (3 times the number of repeat units, or $3(M_c/44)$, for PEO), and ℓ is the bond length. α, the expansion factor, is the amount the chain is stretched above its unperturbed state. In the present context of network swelling, α is not the same as the intramolecular expansion factor for isolated polymer coils in solution, which can be determined from various theoretical considerations. For a swollen network, if the swelling is affine, which means the individual chains are stretched proportionally to the entire network, the expansion factor can be related to the degree of swelling of the network

$$\alpha = Q^{1/3} = 1/(v_{2s})^{1/3} \quad . \qquad (3\text{-}6)$$

Q is the swelling ratio, which is the inverse of the polymer volume fraction. Combining equations 3-4, 3-5, and 3-6 allows one to calculate a value for the average distance between topologically connected junctions.

3.3.1.3. Measurement of the Flory-Huggins Interaction Parameter

The Flory-Huggins interaction parameter, χ_1, was measured for PEO in solution in water. χ_1 was measured using an osmometric technique. The osmometer and associated plumbing is depicted schematically in figure 3-2. The osmometer is a steel cell with a porous metal lower plate on which the membrane rests. It was designed to up to 1000 psi internal pressure, and was supplied by Millipore Corp. Two membranes were used, both of which were low molecular weight cut-off cellulose membranes obtained from Amicon Corp. The YM-2 membrane had a nominal molecular weight cut-off of 1000 and the YM-5 of 5000. Neither membrane allowed any measurable passage of any of the polymer samples used. The PEO samples (Fluka AG) had nominal molecular weights of 14000, 20000, and 35000, and were shown by SEC to have narrow molecular weight distributions, with $M_w/M_n < 1.15$ for all three. Solutions were prepared in ultrapure water with 0.01% NaN_3 added. The same ultrapure water with NaN_3 was used as the solvent against which the osmotic pressure was measured throughout. Solutions were prepared weight to volume and polymer concentrations converted to volume fractions using $\rho_p = 1.2$ g/cm^3. In a typical measurement, the porous metal plate of the osmometer was sonicated in water to completely fill the pores with solvent. The plate was then replaced in the osmometer and sufficient water added to bring the level of the meniscus in the capillary tube (see figure 3-2) even with the level of the plate. The membrane, which was soaked in water prior to use, was placed flat against the porous plate, the o-ring placed over it, and the upper chamber tightened on to the lower chamber.

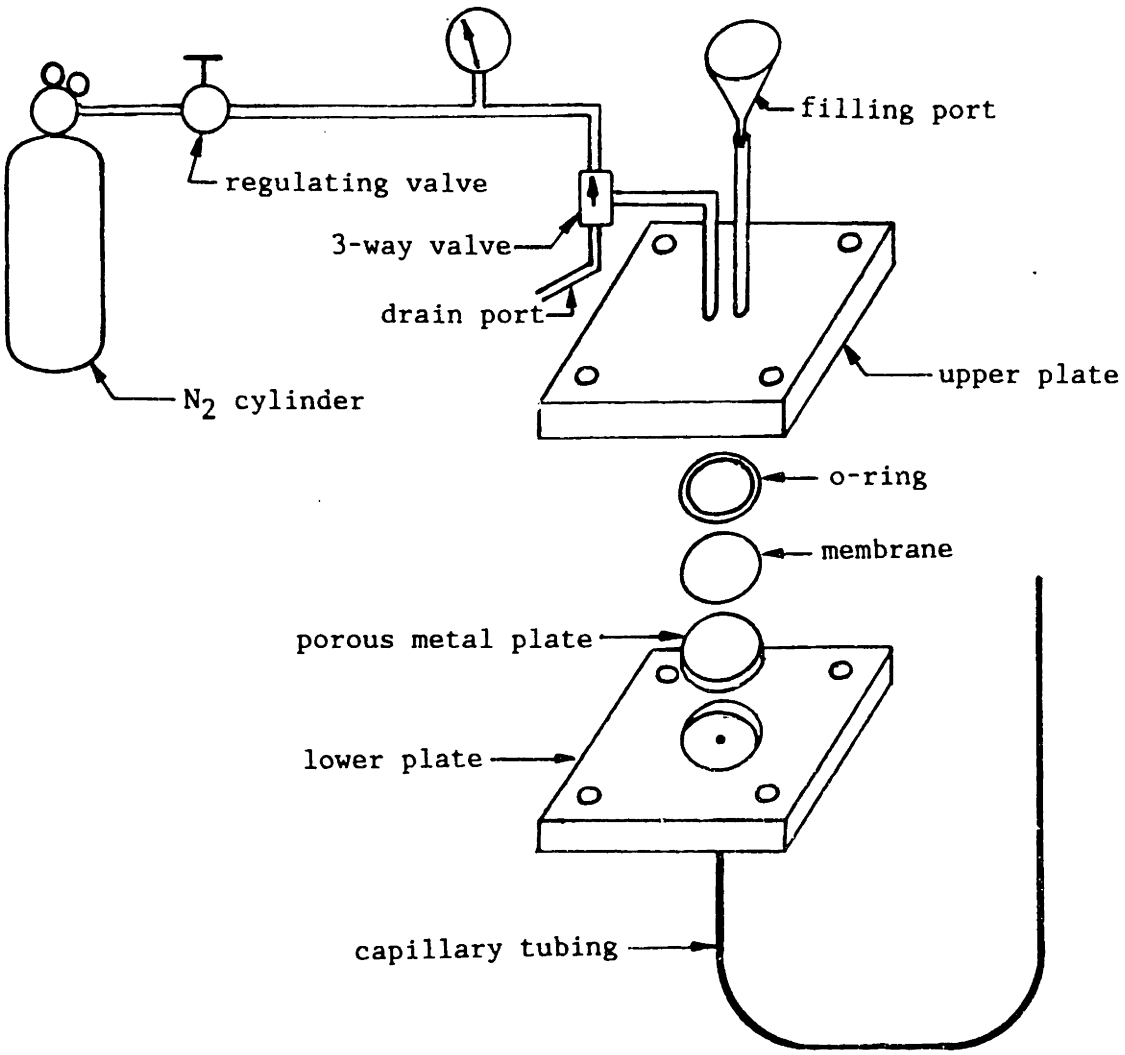

Figure 3-2. Schematic diagram of osmometer used in measurement of Flory-Huggins interaction parameter.

Both the filling and drain ports to the chamber were then opened and the cell was quickly filled with polymer solution, allowing enough to wash out the drain to ensure the cell was full. After filling, the drain was closed first followed by the filling port. The filling procedure was accomplished as quickly as possible to prevent osmotically driven flux of water back into the polymer solution being washed through. After filling, the level of the meniscus in the tubing fell due to backflow of water across the membrane into the polymer solution. Pressure was applied from a nitrogen tank through a regulating valve by opening the three-way valve to the pressure source. The meniscus was brought back to the initial level by increasing the pressure and the system allowed to equilibrate. This process was repeated, increasing the pressure each time until the meniscus remained stationary at the original level. The time required to reach osmotic equilibrium varied from about 20 min to over 1 hr depending on the concentration of PEO used. The pressure required to reach equilibrium for each solution (the osmotic pressure of the solution) was read from the pressure gauge in the gas inlet line.

The osmotic pressure readings were converted to values for the interaction parameter using the following relations from liquid lattice theory [19]. The osmotic pressure can be related to the chemical potential difference of the solvent by classical thermodynamics considerations

$$\pi = -(\mu_1 - \mu_1^0)/V_1 \qquad (3\text{-}7)$$

where μ_1 and μ_1^0 are the chemical potential of solvent in the polymer solution and pure solvent respectively, π is the osmotic pressure, and V_1 is the solvent molar volume. The chemical potential difference, from liquid lattice theory, is given by

$$\mu_1 - \mu_1^0 = RT[\ln(1-v_2) + (1-1/x) + \chi_1 v_2^2]. \qquad (3\text{-}8)$$

v_2 is the volume fraction of polymer in the solution and x is the ratio of molar volume of polymer to molar volume of solvent. These two equations are combined and solved for χ_1, giving

$$\chi_1 = -1/v_2^2[V_1\pi/RT + \ln(1-v_2) + (1-1/x)v_2]. \qquad (3\text{-}9)$$

So values for the Flory-Huggins interaction parameter can be simply calculated from the osmotic pressure measurements at known polymer volume fraction.

3.3.2. Scanning Electron Microscopy

Scanning electron microscopy was performed on the PEO networks at the MIT Department of Applied Biological Sciences Microscopy Facility with the assistance of Erika Hartweig. In order to avoid artifact due to collapse of the gel during air or vacuum drying, all samples were prepared using the technique of critical point drying. Gel samples, fully swollen in water, were dehydrated by equilibration with ethanol-water solutions of gradually increasing ethanol concentration up to absolute ethanol, in

which the samples were left for at least 24 hr prior to critical point drying. The samples were then placed in a pressure chamber and equilibrated with liquid CO_2. After allowing sufficient time for mixing of CO_2 and ethanol, the temperature was raised and the CO_2 taken through the critical point to the gas phase without undergoing a phase transition. This takes the sample from a liquid environment to a gaseous one without the surface tension between liquid and air being an issue. The gaseous CO_2 was then vented to atmosphere. For more details about the critical point drying technique, see ref. [79]. Following drying, the samples were coated with a layer of a gold/palladium mixture using a standard evaporative coating technique. The instrument used for all SEM work was an ISI DS-130.

3.3.3. Differential Scanning Calorimetry

Differential scanning calorimetry was done using a Perkin-Elmer DSC available in the Polymer Central Facility at MIT. Two different studies were performed, one on dried gels and one on gels swollen to equilibrium in water. The dried gels had been vacuum dried as described above. Samples of approximately 10 mg of each gel were scanned at a heating rate of 20°C/min over a temperature range of 30 to 80°C. The cooling rate was 320°C/min. All samples were taken through the heating and cooling cycle once prior to collecting data to help ensure a consistent initial condition for all gels. The calorimeter was calibrated with an Indium standard. Peaks were automatically detected and integrated and the results reported as calories absorbed/gram of sample. These values were

converted to percent crystallinity using a literature value of the heat of fusion of 8.29 kJ/mol of repeat units [78].

3.4. Chemical Characterization of Crosslinking and Networks

3.4.1. Infrared Spectroscopy

Both dried crosslinked networks and irradiated solutions were examined using infrared spectroscopy. The instrument used was a Perkin-Elmer Model 1430 Ratio Recording Infrared Spectrophotometer interfaced with a Perkin-Elmer Model 3600 Data Station for data collection and manipulation. Network samples were prepared in one of four ways. All samples were vacuum dried at about 40°C for 24 hr. This temperature was below that at which changes in the IR spectrum (mostly appearance of a carbonyl peak due to oxidation of the chain) upon drying at different temperatures were first apparent. The best technique was to mount a thin film of the network and look directly at the film. This was unfortunately only possible with very thin films, so many of the samples were analyzed by crushing the sample while wet with a mortar and pestle, drying the gel, and either making a Nujol mull, which was applied as a smear directly to a NaCl crystal, or making a KBr pellet with the sample embedded in the pellet [80]. Of these two techniques, the KBr pellet was preferred as the Nujol mull superimposes the spectrum of the Nujol mineral oil on the sample spectrum, but it was not always possible to grind the gels fine enough to make a KBr pellet. The fourth sample handling technique used involved the use of a multiple internal

reflectance (MIR) accessory. In this accessory, the sample is positioned on one side of a crystal. The infrared beam enters the end, which is angled, and reflects across the crystal several times along the length of the crystal (see figure 3-3). Due to the difference in refractive index between the sample and crystal, the beam penetrates the sample slightly (about 1 μm, depending on the refractive indices) each time it is reflected, and an infrared spectrum of the sample is generated [81]. While the surface analytical aspects of this technique are not important in the context of the present work, the technique was useful in that network samples too thick (and therefore too absorptive) for direct infrared measurements could be mounted whole in the MIR attachment and a spectrum obtained. This technique was used whenever possible when direct spectra of the films could not be obtained.

Liquid samples, whether of the PEO starting material or irradiated polymer samples that were not gelled, were handled as follows. The samples were vacuum dried using the same conditions as for crosslinked samples. They were then dissolved in $CHCl_3$ at a concentration of about 1%. A few drops were placed on a salt crystal and the chloroform allowed to evaporate. If necessary, more solution was added until sufficient polymer had been deposited on the crystal to produce a good absorbance spectrum. Irradiated samples in which additives were initially present in the aqueous solution, for instance those at high pH which contained NaOH, were desalted using Pharmacia PD-10 disposable Desalting Columns packed with Sephadex G-25M prior to vacuum drying. Size exclusion chromatography on control samples indicated no significant loss of the

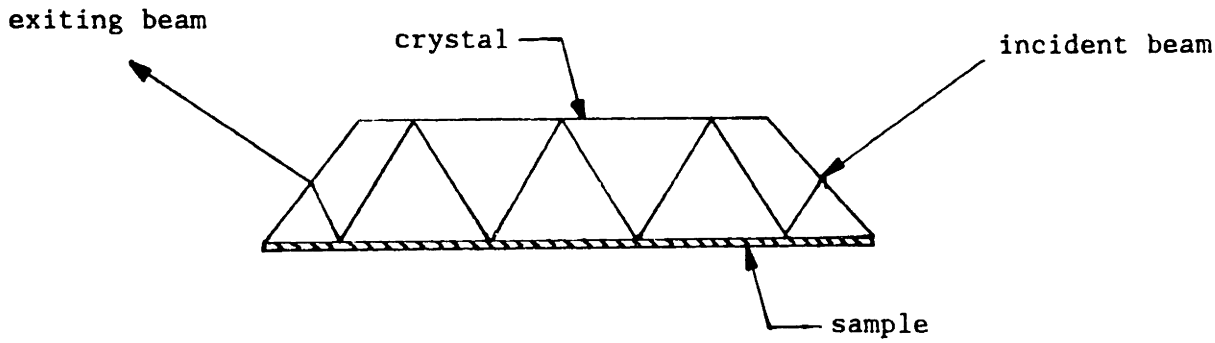

Figure 3-3. Illustration of crystal and sample positions in multiple internal reflectance IR accessory. Beam is reflected several times along the crystal and penetrates the sample slightly at each reflection.

polymer during the desalting step.

3.4.2. NMR on PEO Solutions

Nuclear magnetic resonance spectra were taken on several samples of PEO that had been irradiated below the gel dose. Samples, originally in aqueous solution, were desalted if necessary and dried as described above. The resulting PEO was dissolved in deutero-chloroform (Aldrich) and submitted to the Chemical Spectrometry Lab at MIT for analysis. Both ^{13}C and ^{1}H spectra were obtained, the former at a frequency of 67.9 MHz and the latter at 250 MHz.

3.4.3. Size Exclusion Chromatography Study of Crosslinking

The technique of size exclusion chromatography (SEC), which separates molecular species based on size, can be used to obtain the molecular weight distribution of a polydisperse polymer sample. This technique is described in detail in ref [82]. SEC has been used with success in the past to study scission of polymer chains by hydrolysis [83], neutron irradiation [84], and in various flow fields [85]. In the present study, with the competing processes of crosslinking and scission, the use of SEC to obtain the molecular weight distribution becomes very important, as average molecular weight measurements may not accurately reflect the relative importance of the two processes.

3.4.3.1. Sample Irradiation

Solutions of poly(ethylene oxide) of 35000 nominal molecular weight (Fluka AG) were made in ultrapure water with 0.01% NaN_3 added to retard bacterial growth. All solutions were deaerated for at least 1 hr prior to use, and the desired atmosphere (N_2, N_2O, or O_2) was sparged through the solution. Solutions were adjusted to the desired pH using HCl or NaOH. Other additives (H_2O_2, 5% by volume; $CuCl_2$, 1% wt/vol; K_2SO_4, 0.2 to 0.6 M) were added after dissolution of PEO but before pH adjustment and sparging with gas. Working in a glove box under the appropriate gaseous atmosphere three ml of solution were placed in 2 oz screw cap jars and the jars sealed. The sealed jars were irradiated as described above. The total radiation dose ranged from 100000 to 5000000 rad and the dose rates used for this study were 10000 and 50000 rad/s.

3.4.3.2. Preparation of Samples for SEC

The irradiated samples were filtered through 0.22 μm Millex GV filters (Millipore Corp) and the samples containing acid, base or other salts were desalted using Pharmacia PD-10 prepacked disposable Sephadex G-25M desalting columns as outlined in the manufacturers' instructions. A control sample indicated no significant change in PEO molecular weight distribution due to this procedure, although there was a dilution of the samples of about 1.5 to 1.

3.4.3.3. SEC System

The chromatographic separation was performed on a Waters 150C ALC/GPC. The solvent used was ultrapure water, which was filtered through a 0.45 μm filter and deaerated for about 2 hr immediately before use. A column set of 3 TSK PW aqueous SEC columns (Varian) was used. The three columns were designated G5000PW, G4000PW and G3000PW, with the higher number indicating larger pore size and thus higher molecular weight fractionation range. According to the manufacturer, the columns are packed with a semirigid hydrophilic polyether gel [86], but infrared spectrum analysis of a sample of the column packing material removed from a column suggests that it is a poly(hydroxy acrylate) of some type, most likely butyl acrylate. The plate count of the column set was about 18000 plates according to the manufacturers procedure for column testing. The column set was calibrated using 12 narrow molecular weight distribution PEO standards (Varian) ranging in molecular weight from 1000 to 1000000. An example calibration curve is shown in figure 3-4. The column set was recalibrated at least once a week when the chromatographic system was being used. The flow rate of solvent was 1 ml/min and injection volume was 0.1 ml. Concentration was monitored on a continuous flow refractometer which is integral to the 150C system, and which measures refractive index difference between the column eluent and a pure solvent reference. The output of the refractometer was a voltage versus time signal with a full scale voltage of 10 mV. This signal was read by an IBM PC/XT using a Data Translation DT2805 analog to digital converter board. The signal was sampled once a second for the duration of the

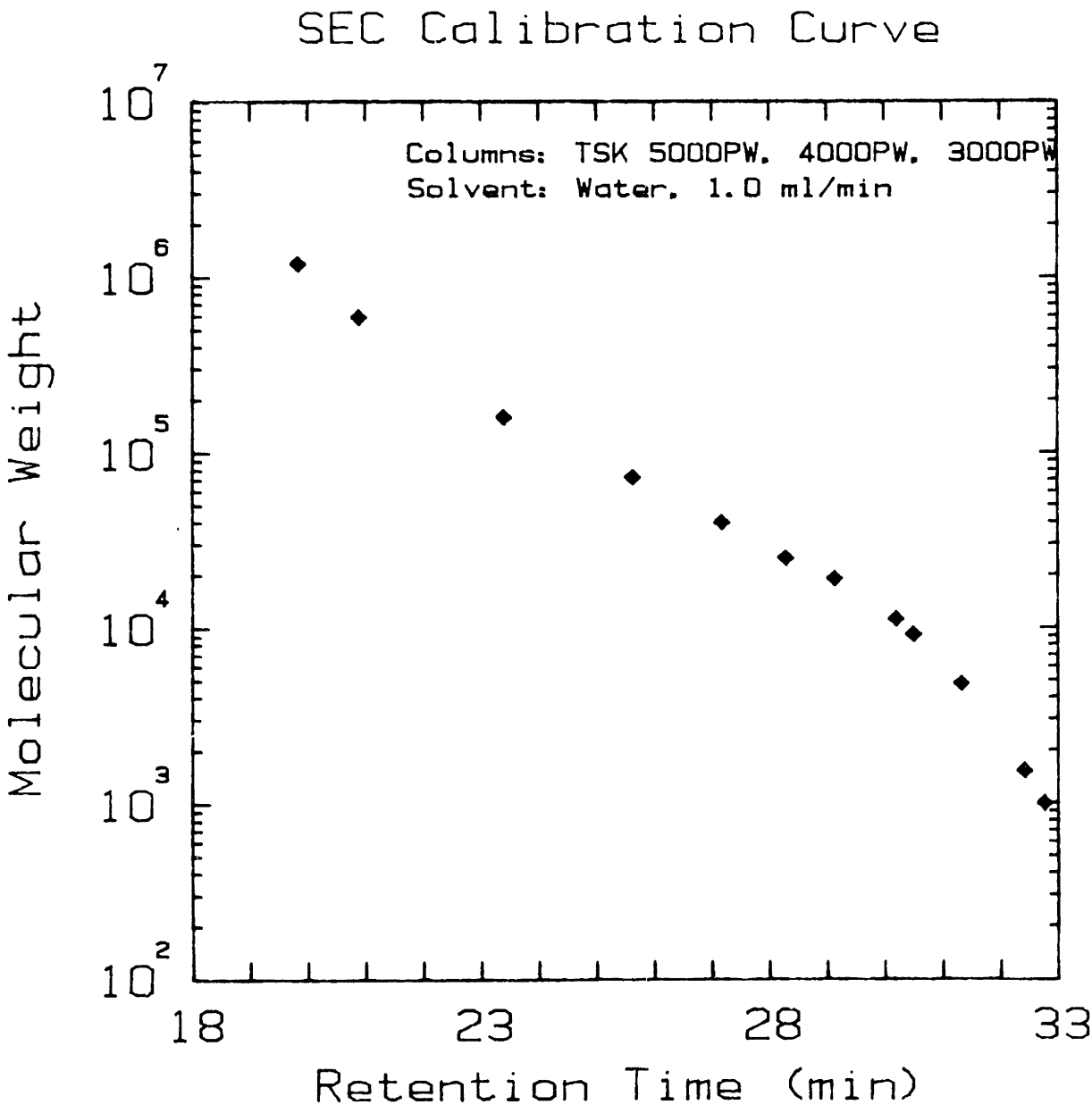

Figure 3-4. Example of an SEC molecular weight calibration. Samples are well-characterized narrow-molecular-weight-distribution poly(ethylene oxide) standards.

chromatographic run (40 min with the columns listed). The PC was programmed to analyze the data and produce an output in mass fraction versus molecular weight format. The complete program listing and a more thorough description are included in appendix 1. In brief, the baseline was corrected by performing a linear regression on user selected portions of the chromatogram and subtracting the voltage values so computed from the corresponding data points. This allowed for correction of drifting or nonlinear baselines. Peaks were detected automatically as a departure from the baseline value or could be user defined. After the peak start and end points were determined, the voltage values were divided by the total area under the peak to give mass fraction (as the output from the refractometer is proportional to mass concentration). Retention time was converted to the corresponding molecular weight using a third order fit of log(molecular weight) versus retention time data collected on the aforementioned PEO standards, and using this and the area information weight and number average molecular weights were calculated. The mass fraction as a function of molecular weight data was saved in a format which could subsequently be used for comparison with other samples and plotting.

3.5. Synthesis and Characterization of Supported PEO Membranes

For certain of the studies done on the PEO networks it was desirable to have stronger and thinner gels than it was possible to produce as free standing networks. Consequently, techniques for making supported PEO gels were investigated. The desired characteristics of the supporting

material was something that would add strength to the membrane system without significantly changing the properties, in particular the transport properties. Also, it was important to have a uniform PEO layer thickness, and it was preferred that it be simple to measure the PEO thickness. Support materials examined included woven and non-woven polyester cloths and woven nylon. Other materials were dismissed from consideration because of low water permeability.

3.5.1. Synthesis of Supported Membranes

The following procedure was used in the preparation of all supported membranes. PEO solutions were prepared as described in section 3.2.2. Circles of 9 cm diameter were cut of each of the support materials. The thickness of the support materials was measured using a dial comparator (Ames Manufacturing, Waltham MA). The dial comparator is graduated in 0.001" (mils), which is equivalent to 25 μm, and readings could be estimated to the nearest 0.1 mil. The non-woven polyester cloth (Remay) was found to have considerable variation in thickness. The average thickness was about 200 μm (8 mil) but the variation was plus or minus 50 μm. As the thickness of the PEO layer deposited on the membranes was on the order of 50 to 100 μm, this variation was too great. Consequently, each cloth disc was measured individually at 5 points. Those pieces showing internal variation greater than about 10 μm were discarded. Also, the pieces were separated into groups of discs with thickness within 10 μm. The other materials, which were woven, did not show the variability in thickness and thus were not individually measured. About

10 ml of the appropriate PEO solution was placed in a 100 mm Petri dish and four of the cloth circles placed in solution. Because of the tendency of the materials to float care was taken to ensure that all of the discs were completely saturated with PEO solution. The PEO-soaked discs were removed one at a time, allowed to drain, about 2 to 3 seconds for solutions of concentration less than 10% wt/vol and 5 to 10 seconds for the more concentrated (and more viscous) solutions, and placed on a 4" by 15" piece of flat window glass. The volume of solution retained by each support disc varied from about 0.5 to about 1 ml depending on the PEO concentration and support material. Care was taken to ensure that no air bubbles were trapped between the membrane and the glass plate and the support was again checked for complete saturation with PEO solution. Four identical membranes were made on each glass plate. A set of pieces of rubber tubing was placed around the edges of each plate to serve as spacers and feet (see figure 3-5). A piece of 7 mil thick mylar sheet the same size as the glass plate was set on top of the spacers and the whole assembly was wrapped in Saran wrap. The completed plates were transported to the High Voltage Research Lab and irradiated as outlined in section 3.1. The time between sample preparation and irradiation was kept as short as possible because of the tendency of the more dilute samples (which retained less solution) to dry out. The time between preparation and irradiation was usually about 15 min and was always less than 30 min. A control sample of PEO solution in a Petri dish prepared and irradiated as described in section 3.1 was made for each PEO solution used. Following irradiation, the samples were returned to the lab and removed from the glass plates by first soaking the gels with water and

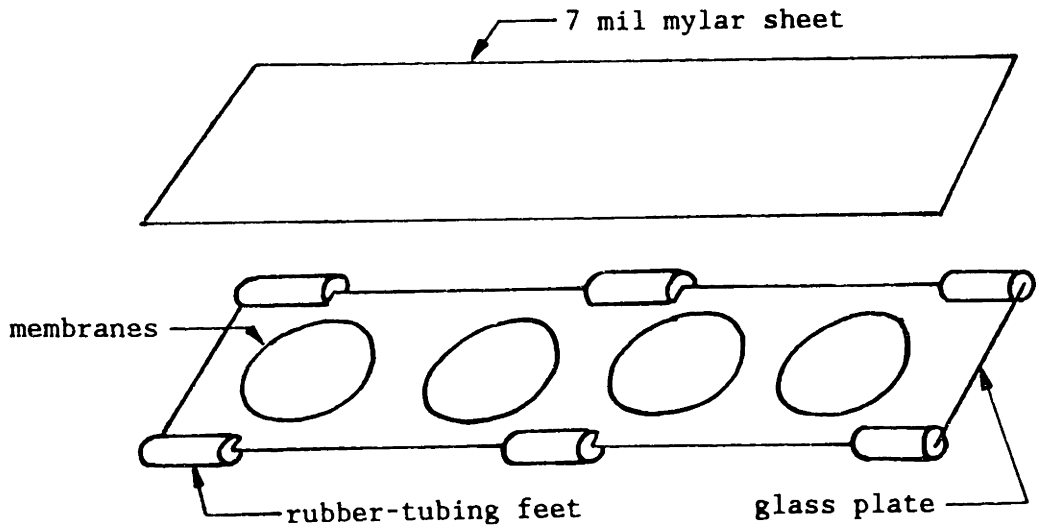

Figure 3-5. Apparatus used for synthesis of supported PEO membranes. Exploded view. The mylar sheet rests on the top of the rubber feet, about 0.5 cm above the membranes, and the whole assembly is wrapped in saran wrap prior to irradiation.

then gently lifting them off the plate. The samples were placed in water with 0.01% NaN_3 to swell and extract any unattached PEO. The free standing controls were used for swelling measurements as described in section 3.3.1.

3.5.2. Characterization of Supported Membranes

Most of the characterization techniques carried out on the free standing PEO gels were also done on the supported membranes, with minor changes necessary because of the support material. The changes are discussed below.

Scanning Electron Microscopy. SEM work was done on the supported gels using the same instrument, dehydration procedure, and critical point drying technique as in section 3.3.2. Small samples were cut from the larger pieces of membrane prior to the dehydration procedure. After critical point drying and before coating the samples were mounted so that both the upper (away from the glass plate during irradiation) and lower (next to the plate) surfaces and a cross-section were visible. Unfortunately there was a tendency of the membranes to curl as the PEO layer, which was predominantly on one side of the support, shrank somewhat during the sample preparation, so it was difficult to obtain good cross-sections.

Thickness Measurement. The thickness of the supported membrane when fully swollen in water was measured using the dial comparator described

above.

Infrared Spectroscopy. IR spectra were obtained on dried membranes using the multiple internal reflectance accessory as outlined in section 3.4.1. Spectra of control supporting material and both sides (upper and lower) of the supported membranes were taken.

Swelling Measurements. Because of the support material, the simple swelling procedure described in section 3.3.1 could not be used on the supported gels. The free standing controls were thus used for determination of crosslink density. However, it was desirable to know if the degree of swelling of the gel was affected by the presence of the support material, so the swelling ratio of the supported gel was measured. This was done by weighing pieces of the support material prior to saturating them with PEO, weighing the membranes made on these pieces of support immediately after irradiation, and reweighing them after swelling to equilibrium in water. Weights of the samples were measured using the blotting procedure given in section 3.3.1. The supported gels were then vacuum dried and the dried membranes reweighed. The dried membranes were reswelled to see if drying affected the membrane properties. The weight of the support material was subtracted from all membrane weights to give the weight of the gel in the relaxed, swollen, and dried states, which were converted to volume fractions using equations 3-1 and 3-2.

PEO Layer Integrity Testing. Several different methods were used to

check whether the PEO coating on the support material was complete and without pinholes. The simplest measurement was a hydraulic permeability measurement, wherein the membrane was sealed in a chamber and exposed to a small head of water (see figure 3-6a). The water permeability of the unsupported PEO gels was unmeasurably low under these conditions, so any measurable flux of water through the membrane was assumed to be due to incomplete coverage or pinholes. A related measurement was an inverse bubble point test, where the supported membrane was held against a fritted plate by a vacuum drawn on the opposite side of the plate (see figure 3-6b). Any evidence of air bubbles on the downstream side of the plate was taken as indication of a leak, as whole unsupported gels did not allow passage of any air.

3.6. Synthesis and Characterization of Porous PEO Gels

3.6.1. Synthetic Conditions

It was found that PEO gels with a highly porous structure could be made under certain irradiation conditions. The following experimental program was designed to determine what conditions were appropriate for the production of such gels. The sample preparation and irradiation procedure used was identical to that outlined in section 3.2 except for the following. Various concentrations of K_2SO_4 were added to the PEO solutions prior to irradiation. The salt molarity ranged from 0.2 to 0.6 molar. Also, the effect of dose rate (through changing the dose per pass) was looked at. Approximate dose rate was varied from 50000 rad/s

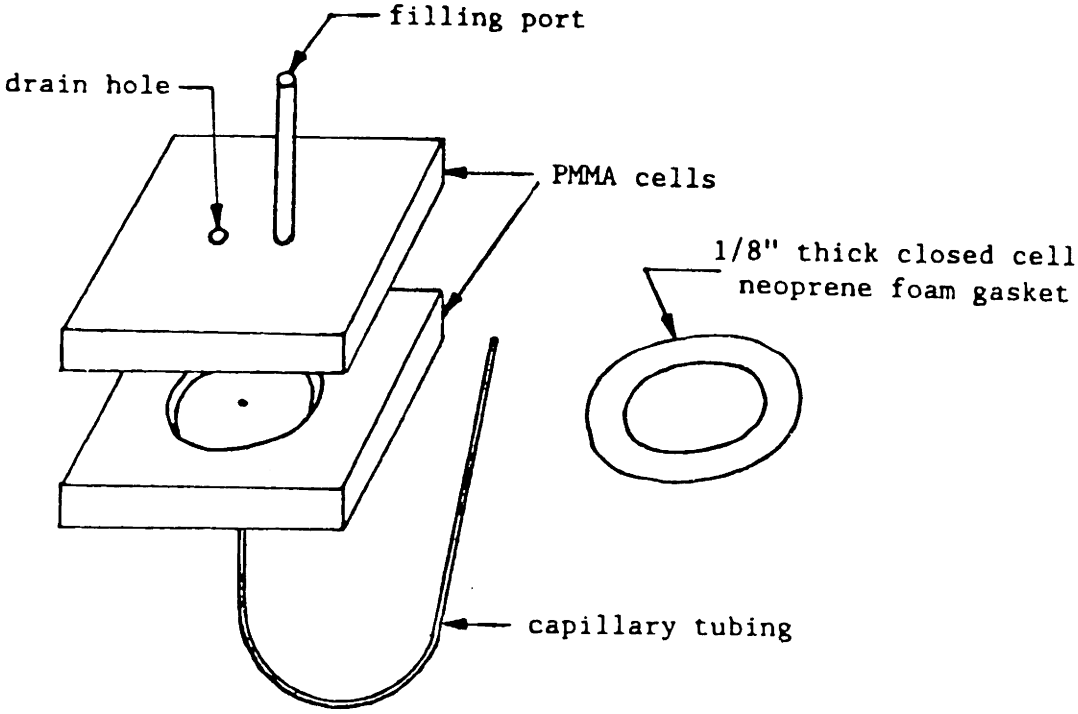

a. Hydraulic permeability cell. Membrane is placed between two neoprene gaskets and clamped into cell. Lower chamber is initially filled with water; upper chamber is put into place, filled, and the drain hole plugged. If membrane leaks, level of water in filling tubing falls and water drips from capillary tubing. Each chamber holds about 10 ml.

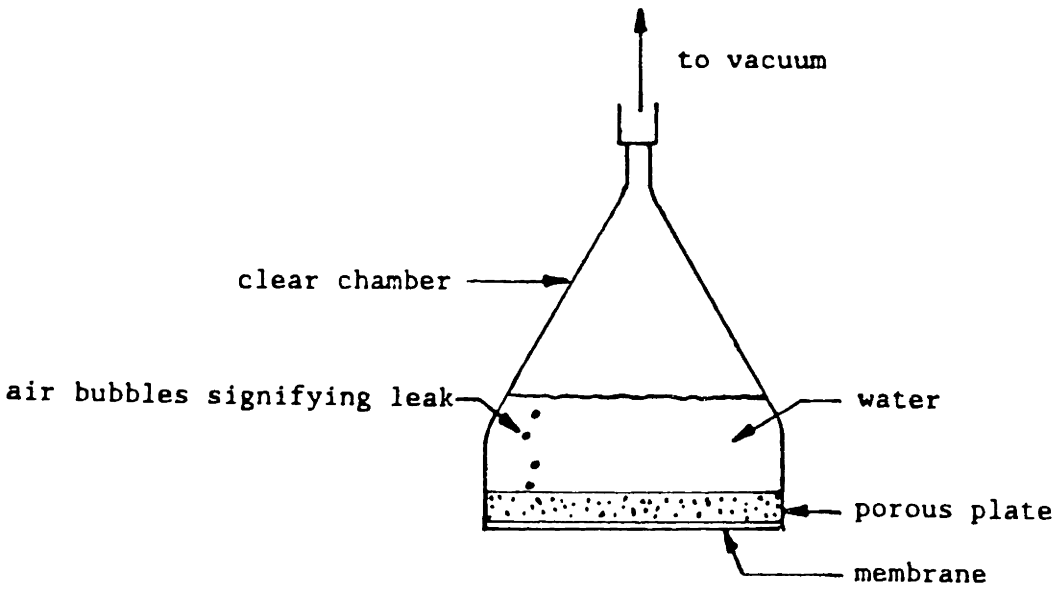

b. "Bubble point" measurement apparatus. Membrane is held to porous plate by internal vacuum, Leaks are detected by air bubbles in the water inside the chamber.

Figure 3-6. Apparatus for integrity testing of supported membranes.

to 250000 rad/s.

3.6.2. Characterization of Porous Gels

It was desired to characterize the structure of the porous gels. This was done using many of the same procedures given above for the characterization of homogeneous gels. The techniques used and any variations are summarized below.

Scanning Electron Microscopy. SEM work was carried out using the same procedure as given in section 3.3.2. However, the sample preparation prior to critical point drying was varied. Some samples were dehydrated and critical point dried from the swollen state as usual. Other samples were vacuum dried, reswollen, and critical point dried. Others were freeze dried, then either reswollen and critical point dried or used without the reswelling and subsequent drying steps. In all cases, efforts were made to look at both surfaces (arbitrarily designated upper and lower - it was impossible to know which surface had originally rested against the glass of the Petri dish) and a cross-section.

Swelling Measurements. The swelling procedure outlined in section 3.3.1 was used to measure the equilibrium volume fraction of polymer in the porous gels. However, as there is water in the pores as well as water swelling the gel the polymer volume fractions cannot be used to determine the crosslink density. The equilibrium polymer volume fraction of gels that had been dried and reswollen was also measured.

Pore Volume Measurement. The pore volume was measured by a solute equilibrium distribution technique. By measuring the equilibrium partitioning between gel and solution of a solute that can enter the pores but that does not penetrate the walls of the pores (the swollen gel itself) the volume of the gel structure accessible to that solute can be obtained. This volume should be equal to the pore volume of the gel. The procedure used was to measure gel volumes by measuring the thickness of fully swollen gel discs of known diameter using the dial comparator referred to previously. This known volume of gel was allowed to equilibrate with a known (and approximately equal) volume of 0.1% bovine serum albumin (Sigma) solution. After reaching equilibrium, which was checked by taking periodic samples, the concentration in the solution was measured by measuring the absorbance at 280 nm. The following mass balance was used to calculate the pore volume, assuming the solute had access only to the pores but all the pores were accessible, and that the pores were sufficiently large that partitioning due to steric effects was negligible, that is, the concentration inside the pores was the same as the concentration in the solution.

$$C_{si}V_s = C_{sf}V_s + C_{pf}V_p \qquad (3\text{-}10)$$

C_s refers to the concentration of solute in solution, the subscripts i and f refer to initial and final concentrations respectively, V_s is the volume of solution, C_p is the concentration in the pores (assumed to be the same as C_{sf}) and V_p is the pore volume. V_p can be written as $V_g f_p$,

where V_g is the gel volume and f_p is the pore volume fraction, or porosity. From these relationships and the known solution concentrations and solution and gel volumes it is possible to calculate f_p.

3.7. PEO - Salt Solution Interactions

Two complementary sets of experiments were conducted on the behavior of PEO in aqueous solutions containing various salts.

3.7.1. Cloud Point Measurements.

A series of measurements were done to determine the dependence of the temperature at which PEO solutions undergo phase separation (cloud point) on salt type, salt concentration, and PEO concentration. All measurements were made on PEO of 35000 nominal molecular weight. Salt solutions were made at the desired molarity in ultrapure water. PEO was then dissolved weight/volume in the salt solutions. About 3 ml of the solution to be tested was placed in a 16 by 100 mm test tube and the tube placed in a stirred water bath over a heater. A thermometer was inserted into an identically prepared test tube to measure temperature. The bath was slowly heated and the temperature at which the solution became cloudy was noted. The bath was then cooled and the temperature at which the solution cleared was noted. The transitions were quite sharp (within about 0.2°C) and reproducible, and the phase separation temperatures measured on heating and cooling were also within 0.2°C.

3.7.2. Salt Partitioning.

A series of measurements was done to determine the partitioning behavior between PEO and free solution.

3.7.2.1. Techniques.

A free standing gel made as discussed in section 3.2 was used for all measurements. The gel used was made using 15% PEO 35000 wt/vol in ultrapure water. It was given a total dose of 5 Mrad at a dose rate of about 250000 rad/s. The properties of this gel are given in section . The gel was swelled extensively in ultrapure water with 0.01% NaN_3 prior to use. Salt solutions were made in ultrapure water with 0.01% NaN_3 added. Gel weights were measured as described in section 3.3.1.1. Known weights were placed in small vials with an approximately equal volume of the salt solution, the vials capped tightly, and the system allowed to equilibrate. 0.2 ml samples of the solution were removed after equilibration and diluted with 100 ml pure water for conductivity measurements. Conductivities of salt solutions of known concentration were measured as a calibration.

3.7.2.2. Data Analysis.

The partition coefficient, defined as the ratio of the concentration in the gel to the concentration in solution at equilibrium, is obtained by rearranging the following mass balance.

$$C_{si}V_{si} = C_{sf}V_{sf} + C_{gf}V_{gf} \qquad (3\text{-}11)$$

where C_s refers to the salt concentration in the solution, C_g refers to the salt concentration in the gel, the subscripts i and f refer to initial and final states, V_s is the solution volume, and V_g is the volume of the gel. As the equilibrium swelling of the gel is affected by the presence of salts the final gel volume had to be measured. This was done by measuring the weight as described in section 3.3.1.1 and converting to volume using the known polymer volume fraction in water, the weight of the gel in water, the weight in the salt solution, and the densities of PEO, pure water, and the salt solution. The salt solution densities were measured by weighing a known volume of the solution. The procedure essentially involved converting the volume fraction in water to a weight fraction by using the densities. From this and the weight of the gel in water the weight of the polymer in the gel was calculated. From the weight in the salt solution, and knowing the densities and the weight of polymer in the gel, the final volume of the gel in the salt solution could be computed, as could the polymer volume fraction in the gel. The final solution volume could be calculated by making an overall mass balance, that is, the weight lost by the gel was gained by the solution, and the volume change was calculated from the solution density. Equation 3-11 can be rearranged to give

$$K = C_{gf}/C_{sf} = (V_{si}C_{si}/C_{sf} - V_{sf})/V_{gf} \qquad (3\text{-}12)$$

from which K, the equilibrium distribution coefficient, or partition coefficient, is obtained.

3.8. Measurement of Effective Diffusivities in Gels

A number of techniques for measuring the effective diffusivity of various solute molecules in the gels were attempted before settling on a simple solute uptake by the gel from a finite solution volume technique. The lack of strength of these gels made it impossible to use many of the more common techniques, such as stirred b tch dialysis measurements, and preliminary investigations showed the technique used to be reasonably accurate and reproducible. The experimental technique will be described in detail, and the data analysis method will be discussed both here and in more detail in appendix 3.

3.8.1. Experimental Technique.

3.8.1.1. Materials Used.

Solutes. The solutes used were selected to give a range of solute size that should be appropriate for studying the effect of sieving in the gels. A preliminary protein penetration study using bovine serum albumin showed that the gel structures that were routinely produced included a few which allowed albumin to penetrate the gels and others which did not, so it was assumed that proteins of the size of albumin and smaller would be appropriate for the study. (A larger protein, catalase, was also used initially, but electrophoresis indicated degradation over relatively short periods of time, so it was eliminated from the study.) It was also desirable to choose molecular species that were well characterized in

terms of molecular size and diffusion coefficient in aqueous solution, and ones which might reasonably be expected to meet the assumptions required by the solution-diffusion theory. The solutes selected are listed in table 3-1, along with some of the important properties. In light of reports suggesting that diffusion of random coiling macromolecules in microporous media is quite different from diffusion of globular molecules [87,88], it was also desirable to look at how random coils behaved in these non-porous swollen gel systems. Consequently, three narrow molecular weight distribution PEO samples with effective hydrodynamic radii of the same order as the proteins were also used as solutes. The properties of these molecules are given in table 3-2, and the complete characterization data is in appendix 2. The proteins and cyanocobalamin (vitamin B12) were all used at a concentration of 1 g/l in phosphate-buffered saline (PBS) (0.125 M NaCl, 0.025 M PO_4^{3-} as NaH_2PO_4 and Na_2HPO_4, and 0.01% NaN_3 wt/vol in ultrapure water). The solutions were stored at 4°C and small aliquots removed from the stock solution and warmed to room temperature for use as needed. Electrophoresis conducted on the stock solutions after completion of the measurements showed no degradation had taken place. The poly(ethylene oxides) were used at 10 g/l in PBS and were stored at room temperature in the dark. Size exclusion chromatography carried out periodically throughout the measurements indicated no degradation of the PEO solutions.

Gels. The PEO networks used were synthesized and characterized as described in sections 3.2, 3.3, and 3.4. The exact conditions of synthesis of the gels used are summarized in table 3-3. The results of the characterization of these gels are discussed in section 4.6.1. In

Solute	Molecular Weight	Diffusivity (in Water)	Effective Radius	Ref.
Cyanocobalamin (Vitamin B12)	1355	3.79×10^{-6} cm^2/s	8.5 Å	66
Lysozyme	17000	1.04×10^{-6}	20.6	52
Chymotripsinogen	23000	0.95×10^{-6}	22.5	52
Ovalbumin	44000	0.776×10^{-6}	27.6	52
Albumin	67000	0.594×10^{-6}	36.1	52

Table 3-1. Globular solutes used in diffusivity measurements. The diffusivities refer to water at 25°C; effective radii are hydrodynamic radii in aqueous solution.

Nominal MW	Measured M_n (SEC)	M_w/M_n	Diffusivity (in Water)	$\langle r^2 \rangle^{1/2}$	Eff. Radius
1000	961	1.27	2.81×10^{-6} cm^2/s	42.2Å	14.6Å
8000	11211	1.05	8.22×10^{-7}	178.3	61.9
20000	21340	1.16	5.96×10^{-7}	260.8	90.5

Table 3-2. Summary of characterization of PEO samples used as solutes in diffusion measurements. The molecular weight measurements were done using size exclusion chromatography. Diffusivities were calculated using the correlation of Rossi, et al [100]. The effective radius refers to an effective hydrodynamic radius that is calculated assuming the molecule is behaving as an equivalent sphere in Einstein's law of viscosity. (See appendix 2.)

Designation	PEO Conc.	Irradiation Dose	Solution Volume
3%,2.5	30 g/l	2.5 Mrad	7 ml
3%,5	30 g/l	5.0 Mrad	7 ml
5%,2.5	50 g/l	2.5 Mrad	7 ml
5%,5	50 g/l	5.0 Mrad	7 ml
10%,2.5	100 g/l	2.5 Mrad	7 ml
10%,5	100 g/l	5.0 Mrad	7 ml
10%,10	100 g/l	10.0 Mrad	7 ml
10%,15	100 g/l	15.0 Mrad	7 ml
15%,5	150 g/l	5.0 Mrad	7 ml
15%,10	150 g/l	10.0 Mrad	7 ml
15%,15	150 g/l	15.0 Mrad	7 ml
20%,5	200 g/l	5.0 Mrad	6 ml
20%,10	200 g/l	10.0 Mrad	6 ml
20%,15	200 g/l	15.0 Mrad	6 ml

Table 3-3. Conditions used for synthesis of gels used in effective diffusivity measurements. Results of the characterization are given in section 4.6.

addition to the usual characterization, the equilibrium swelling properties of these gels in PBS was measured, using the same method as the swelling measurements in water. The gels chosen for diffusivity measurements were selected to give as wide a range of structural properties as possible while still meeting the criteria required for application of solution-diffusion theory.

3.8.1.2. Concentration Measurements.

The concentrations of all protein solutions and cyanocobalamin were measured by UV absorbance at 280 nm on a Perkin-Elmer Lambda 3 UV-Visible Spectrophotometer. Extinction coefficients were measured for each species and were found to agree well with those available in the literature [89]. Concentrations of PEO were measured using size exclusion chromatography. The Waters 150C ALC/GPC system mentioned above was used with a single column (TSK 3000 PW) and with PBS as solvent. The solvent flow rate was 1 ml/min, and injection volumes were 0.1 ml. In addition to a molecular weight calibration, the system was calibrated for concentration using the same PEO samples used in the diffusivity measurements at known concentration. The area under the peak was determined using the SEC data reduction program described in appendix 1 on operator selected peaks so that the peak start and end time was identical for all peaks of the same molecular weight. A linear best fit was made for the concentration - area data. This calibration was repeated each time a set of samples of that molecular weight was run; an example of the type of calibration obtained is shown in figure 3-7. From

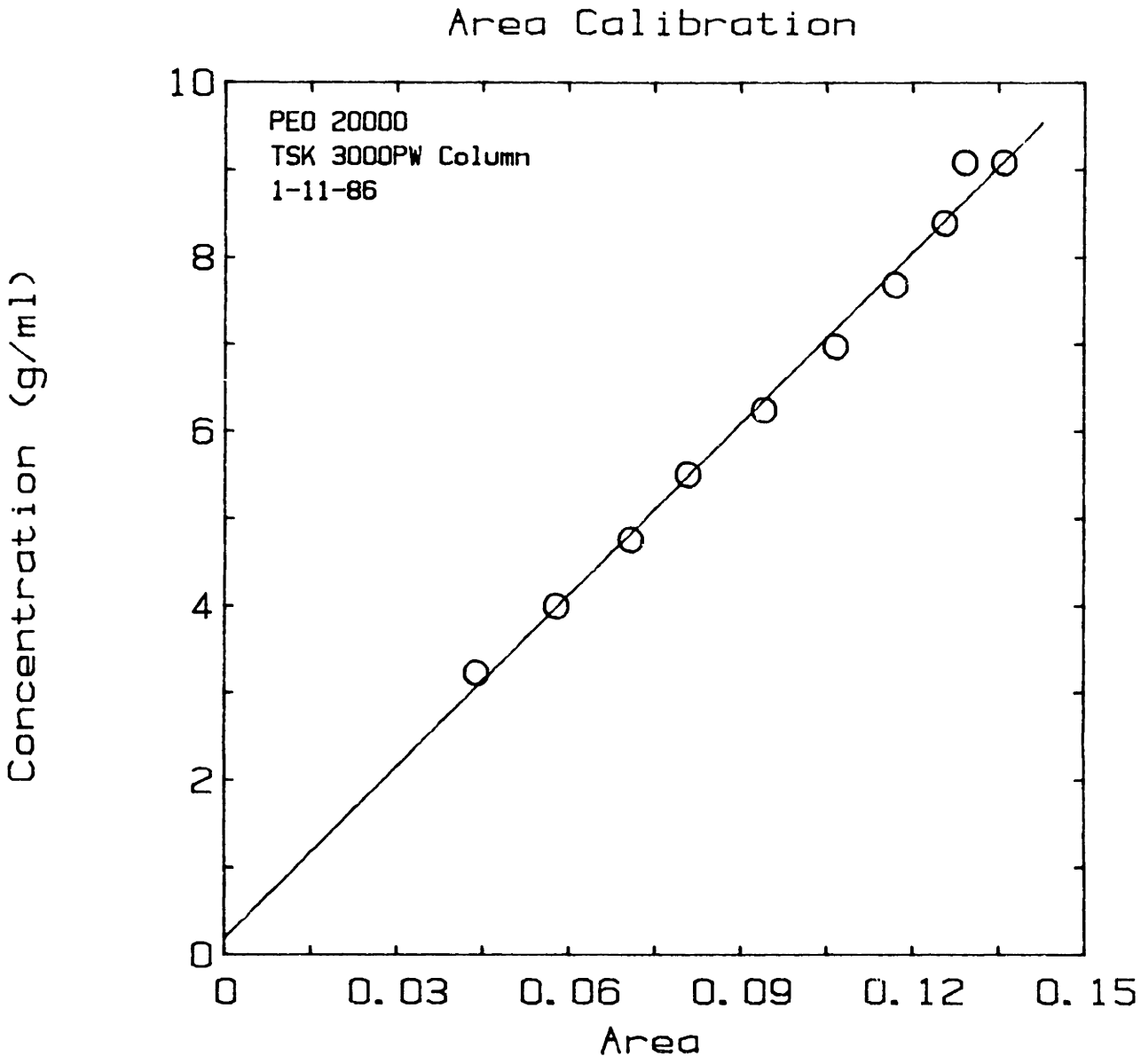

Figure 3-7. Example of a concentration calibration for a single TSK 3000PW column. Solvent is phosphate-buffered saline at 1 ml/min, injection volume is 50 µl, PEO molecular weight is 20000, the same as the samples.

this calibration the concentration of the unknown samples could be calculated from the measured area under the chromatographic peak.

3.8.1.3. Diffusivity Measurement Techniques.

The procedure used to make the diffusivity measurements was as follows. The PEO network to be used was equilibrated with PBS for at least a week prior to testing. The swollen gel was then cut into discs of 1.1 cm diameter using a #6 cork borer. The gels were saturated with PBS throughout this procedure. The cut pieces were then blotted one at a time on damp filter paper and the thickness measured using the dial comparator mentioned above. Some of the looser gels were compressed slightly in the measuring process, so care was taken to note the thickness at which the upper plate of the comparator just touched the gel. Thicknesses ranged from about 0.8 to 1.5 mm for different gels depending on the degree of swelling of the particular gel, and there was a thickness variation of about 0.2 mm from piece to piece of the same gel. Gels were divided into groups having the same thickness within 0.02 mm and put back into PBS solution to maintain equilibrium swelling conditions. For each diffusivity measurement, three pieces of gel of the same thickness were removed from PBS, blotted on damp filter paper, and placed on the bottom of a 20 ml glass scintillation vial. 0.3 ml of the solute to be tested was added and the vial was sealed and immediately placed in a shaker (Warner-Chilcott) operating at highest speed. This speed was found to be above the speed setting necessary to get consistent results for the apparent diffusivity, so fluid phase transport resistance

was assumed negligible. After an appropriate period of time the sample was removed from the shaker and 0.2 ml of the solution removed for concentration measurement as described above. Each solute - gel combination was tested in triplicate, usually at slightly different equilibration times. All measurements were done at room temperature, 23±1°C.

3.8.1.4. Partition Coefficient Measurements.

The equilibrium distribution or partition coefficient foe each solute was measured using the same procedure as the diffusivity measurements except the samples were allowed to reach equilibrium. A change was made to the procedure to make this simpler. Because of the tendency of the protein solutions to denature when shaken for long periods at room temperature, the samples requiring more than about 24 hr to reach equilibrium (typically bovine serum albumin and ovalbumin) were refrigerated without shaking for the period required to reach equilibrium. Clearly this time was much longer than that required if the equilibration could have been done at room temperature in the shaker. The samples were warmed to room temperature prior to concentration measurement.

3.8.2. Data Analysis.

3.8.2.1. Partition Coefficients.

The partition coefficient, defined here as the ratio of the concentration

of solute in the solvent in the gel to the concentration of solute in solution, was computed from the following mass balance.

$$V_s C_{si} = V_s C_{sf} + V_g v_{1s} C_g \qquad (3\text{-}13)$$

V_s is the solution volume, C_s is the solution concentration, V_g is the gel volume, v_{1s} is the volume fraction of solvent in the gel, and C_g is the concentration of solute in the solvent in the gel. The subscripts i and f refer to initial and final states. Any change in the equilibrium swelling of the gel due to the presence of the solute is unmeasurably small, so the initial and final volumes of the gel are the same. The definition of the equilibrium distribution coefficient $K = C_g/C_{sf}$ leads to the following equation.

$$K = [(C^s{}_i/C_{sf}) - 1][V_s/(V_g v_{1s})] \qquad (3\text{-}14)$$

K can thus be calculated from the measured concentrations and volumes and the known polymer and solvent volume fractions in PBS.

3.8.2.2. Calculation of Effective Diffusivity.

The effective diffusivity in the gel is found by solving the diffusion equation for the situation at hand. An analytical solution for the case of diffusion from a finite well-stirred volume of solution into an infinite slab is available [90], as are solutions for certain other one-dimensional geometries, including the infinite cylinder and the sphere [90]. Although the discs used in this study approach the infinite slab (plane sheet) geometry, fairly large errors are introduced by assuming

this solution applies. A numerical solution to the problem of diffusion into an arbitrary three-dimensional object from a finite volume stirred solution has been developed by Ma and Evans [91]. They find that for short dimensionless times ($\theta = Dt/\sigma^2 < 0.2$) the analytical and numerical solutions for all shapes collapse to a single line if the length σ used in the dimensionless time is the ratio of the volume of the body to its surface area. At larger dimensionless times the solutions diverge, with geometrically similar shapes remaining close. For instance, a cylinder with length to diameter ratio of 1/16 is within 10% of the solution for the plane sheet for all values of θ. Therefore, the analytical solution of Crank [90] for the plane sheet was used in this work, with the correction of Ma and Evans for the dimensionless time. The full calculational procedure is given in appendix 3. In brief, the solution of Crank gives the fractional uptake of solute by the sheet as a function of the dimensionless time defined earlier, the ratio of the volumes of solution and sheet, α_k, which includes any partitioning effects and is thus defined as $\alpha_k = V_s/KV_g$, and a set of q_n, the roots to the equation $\tan(q_n) = -\alpha_k q_n$. This solution is shown in equation 3-15.

$$\frac{M_t}{M_\infty} = 1 - \sum_{n=1}^{\infty} \frac{2\alpha_k(1+\alpha_k)}{1 + \alpha_k + \alpha_k^2 q_n^2} \exp(-\theta q_n^2) \qquad (3\text{-}15)$$

The variables are

M_t = mass of solute in sheet at time t
M_∞ = mass of solute in sheet at equilibrium
α_k = ratio of solution volume to sheet volume accessible to solute
θ = dimensionless time = Dt/σ^2
q_n = roots to $\tan(q_n) = -\alpha_k q_n$
t = time
D = diffusivity in sheet
σ = ratio of sheet volume to surface area

The measured variable is the concentration, which can be related to the fractional uptake as follows. At any time t, the mass of solute in the sheet (gel) is $V_s(C_{si} - C_{st})$ where C_s is the concentration in solution initially (C_{si}) and at time t (C_{st}) and V_s is the volume of solution. From the definition of the partition coefficient and α_k,

$$M_\infty = V_s C_{si}/(1+\alpha_k) \qquad (3\text{-}16)$$

and thus

$$\frac{M_t}{M_\infty} = \frac{C_{si} - C_{st}}{C_{si}} (1+\alpha_k) \quad . \qquad (3\text{-}17)$$

So M_t/M_∞ can be calculated from the measured concentrations, volumes, and partition coefficient. The time is also known, and σ is calculated by the following formula from the known height h and diameter d of the gel discs.

$$\sigma = dh/(2d + 4h) \qquad (3\text{-}18)$$

Since α_k is known, the roots to $\tan(q_n) = - \alpha_k q_n$ can be found. Equation 3-15 can then be solved iteratively for θ, from which D, the effective diffusivity, can be found. For the current situation, in which α_k is different for each sample, the roots (q_n) must be found independently for each diffusivity calculation. A computer program was written to find D given the gel dimensions, the time, and $M_t/M\infty$. The program and details of the calculations are included in appendix 3. Briefly, Newton's method is used to calculate the roots of $\tan(q_n) = - \alpha_k q_n$. These values are used in another Newton's method calculation on equation 3-15 to find the value for θ. The summation is tested for convergence inside the root-finding routine. The effective diffusivity D is calculated from θ.

Chapter 4. Results and Discussion

4.1. Physical Characterization of Radiation Crosslinking of PEO

4.1.1. Gel Dose.

The dose required for gelation of solutions of PEO 35000 in pure water is shown as a function of concentration in figure 4-1. These measurements were made at a dose rate of about 125000 rad/s, which is about half the value used in the bulk of the irradiations. Although there is considerable scatter in the data due to the fact that the measurements could be made only to the nearest 0.5 Mrad, it is obvious that the gel dose does not simply increase linearly with concentration. The dose required per gram of PEO irradiated decreases slightly as the concentration of the irradiated solution increases. At 200 g/l, for example, the gel dose is approximately 3.25 Mrad. As 1 Mrad is 10 J/g sample irradiated, and approximating the weight fraction of PEO as 0.2 g PEO/g solution, we find that the energy input to reach gelation is about 160 J/g PEO. At 30 g/l, the gel dose is about 0.75 Mrad, and the corresponding energy input is about 250 J/g PEO. This suggests that the efficiency of the crosslinking process is somewhat lower at lower concentration. It is informative to further convert these values to the energy input per crosslink formed. This is done using the assumption that to reach the gel point requires on average 1 crosslink per two primary molecules for this tetrafunctional system [19]. Using a primary molecule number average molecular weight (M_n) of 37000 g/mol (see appendix 2), and since there are half the number of crosslinks as chains,

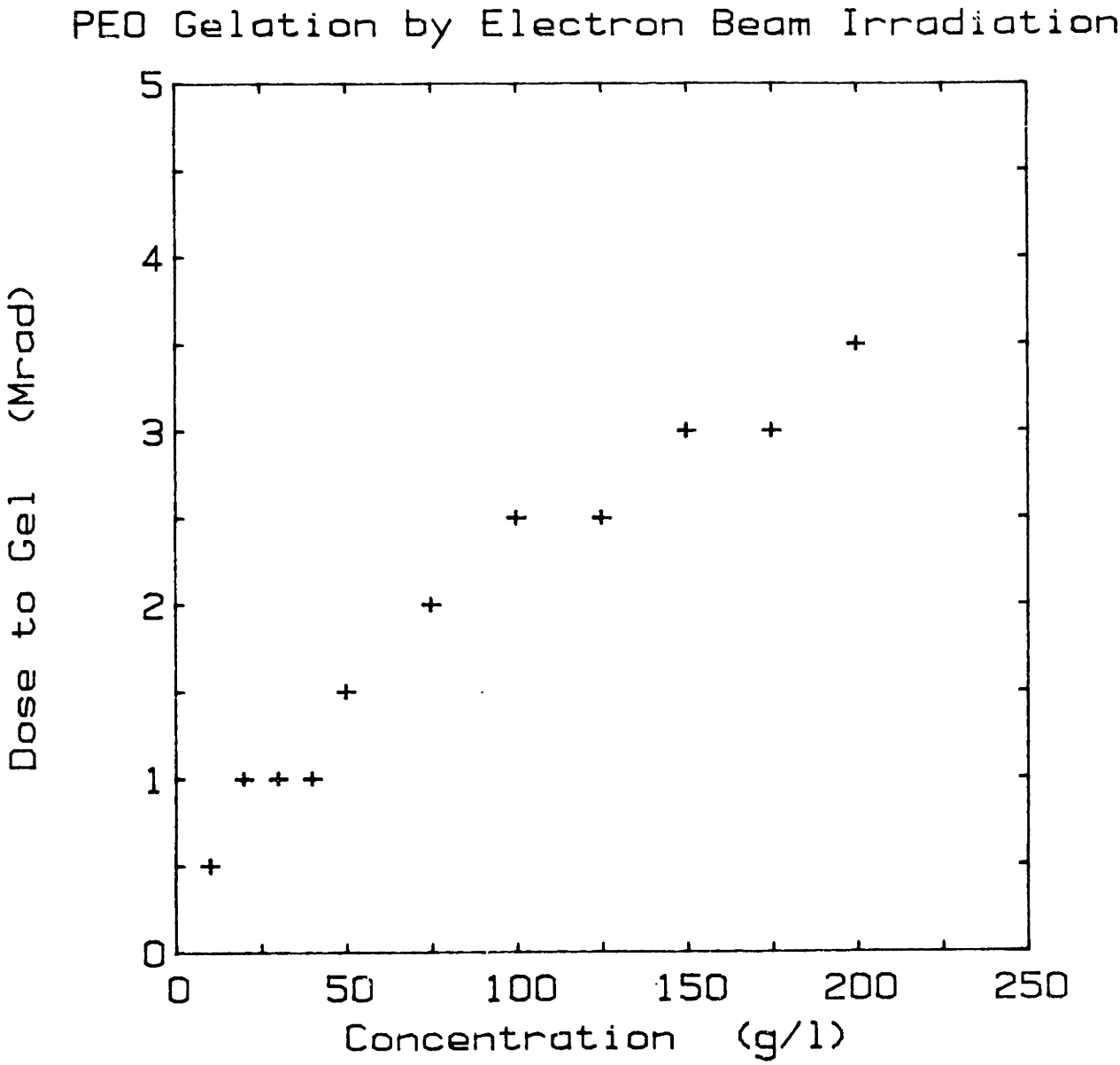

Figure 4-1. Approximate gelation dose as a function of PEO concentration for 35000 MW PEO in pure water. Dose rate was approximately 125000 rad/s.

the energy required per crosslink is 18500 kJ/mol at 30 g/l and 11800 kJ/mol at 200 g/l. The energy per crosslink is plotted as a function of solution concentration in figure 4-2. Note that in these calculations it is assumed that all energy absorbed by the solution can contribute to crosslinking, because of the assumed indirect chemistry wherein energy is first absorbed by the water and transferred to the PEO (see section 2.3.4). Several interesting things can be noted about these values. The values are all considerably higher than the value of 710 kcal/mol (3000 kJ/mol) reported by VanBrederode [44] for ^{60}Co irradiation of PEO solutions (discussed in section 2.3.3.2), which is surprising, as previous work suggests that electron beam irradiation should be more efficient than gamma. However, it appears that VanBrederode's calculations were done without accounting for energy absorbed by water and transferred to PEO, that is, it was assumed that only energy directly absorbed by the PEO was effective in producing crosslinks. If the number is recalculated including the indirect effect of water (which involves simply dividing the previously calculated number by the weight fraction of PEO in the solution) VanBrederode's value is increased by two orders of magnitude to 300000 kJ/mol. This value is clearly considerably higher than those calculated for the present case, suggesting very strongly that electron beam irradiation is a much more efficient means of crosslinking PEO in solution than is gamma irradiation. The difference in efficiency is probably attributable to the difference in dose rate of about 3 orders of magnitude. The measured energy/crosslink can be compared to the bond energies of the bonds broken and formed. The enthalpy of dissociation of a C-H bond is about 416 kJ/mol; that of a C-C bond is about 347 kJ/mol

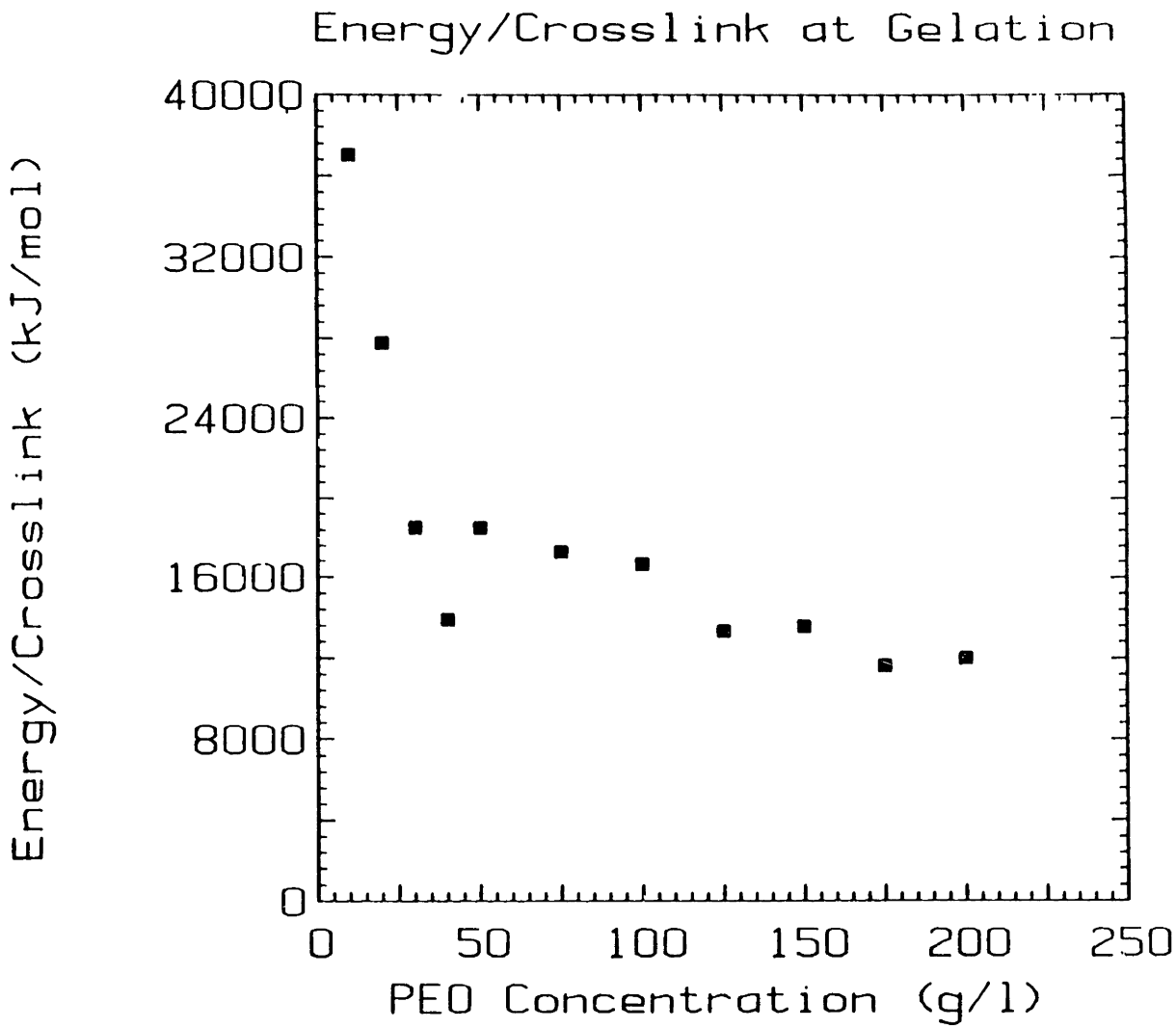

Figure 4-2. Gelation data replotted as energy input per mole of crosslinks as a function of PEO concentration.

[92]. To form a crosslink, two C-H bonds are broken and one C-C bond is formed, so an energy input of about 485 kJ/mol is required. This value is more than an order of magnitude lower than the measured energy/crosslink, that is, about 5% of the absorbed energy is actually used in making crosslinks. It is encouraging that the measured value is greater than the required energy input, and there are several reasons for the discrepancy between the values. The reasons for the low efficiency include the possibility of chain scission, which was not considered in the calculation. This would have a two-fold effect, first in explaining where some of the energy ended up, and second because scission would decrease the effective value for M_n, which would mean there are more crosslinks required to achieve gelation than expected. The presence of scission would also help explain the concentration dependence of the energy required, as scission is expected to be more predominant at lower PEO concentration. It is difficult to quantify this effect, as neither the amount of scission or the exact chemistry of the process are known. A related possibility is intramolecular crosslinking, or the formation of loops in primary molecules. Considering the length of the primary chains, it seems fairly likely that loop formation could take place, but as these are not effective crosslinks, they would not contribute to the progress toward gelation. Again, this would be expected to be more important at lower concentrations, where the degree of chain interpenetration is less. Other reasons for low efficiency include incident energy dissipated as heat and energy used in the radiolytic dissociation of water.

4.1.2. Equilibrium Swelling Results.

All of the gels irradiated beyond the gel dose were analyzed using equilibrium swelling measurements. As shown earlier, two related pieces of information are obtained from these measurements, the equilibrium polymer volume fraction, v_{2s}, and the crosslink density, from which the interjunction molecular weight, M_c, is obtained. Calculating the crosslink density requires a theory relating the degree of swelling with the number of elastically effective chains. In this case the affine deformation theory modified for networks crosslinked in solution (see section 2.4.3.1) is used. As an accurate value of the Flory-Huggins interaction parameter χ_1 is required to give correct results, this parameter was measured in an independent set of osmotic pressure measurements.

Results of χ_1 Measurement. The Flory-Huggins interaction parameter was obtained as a function of concentration for a PEO samples of three different but relatively low molecular weights. The 35000 molecular weight sample was the same polymer used in the irradiation work. All measurements were made at room temperature, 23±1°C. Table 4-1 is a summary of the results obtained for the osmotic pressure π and the interaction parameter χ_1. The data for χ_1 as a function of solution concentration (polymer volume fraction) are plotted in figure 4-3. As expected, there is no effect of molecular weight on the interaction parameter. It is clear from this plot that in the range of polymer concentrations used the dependence of χ_1 on concentration is quite small.

Molecular Weight	Polymer Volume Fraction, v_2	π (psig)	χ_1
14000	0.083	15	0.419
14000	0.104	26	0.416
14000	0.125	42	0.410
14000	0.146	51	0.434
14000	0.167	63	0.449
20000	0.083	15	0.419
20000	0.167	65	0.446
35000	0.042	3	0.428
35000	0.083	14	0.427
35000	0.104	24	0.425
35000	0.125	37	0.426
35000	0.146	51	0.434
35000	0.167	67	0.442

Table 4-1. Summary of osmotic pressure data used for determination of Flory-Huggins interaction parameter χ_1. All measurements were on PEO in pure water.

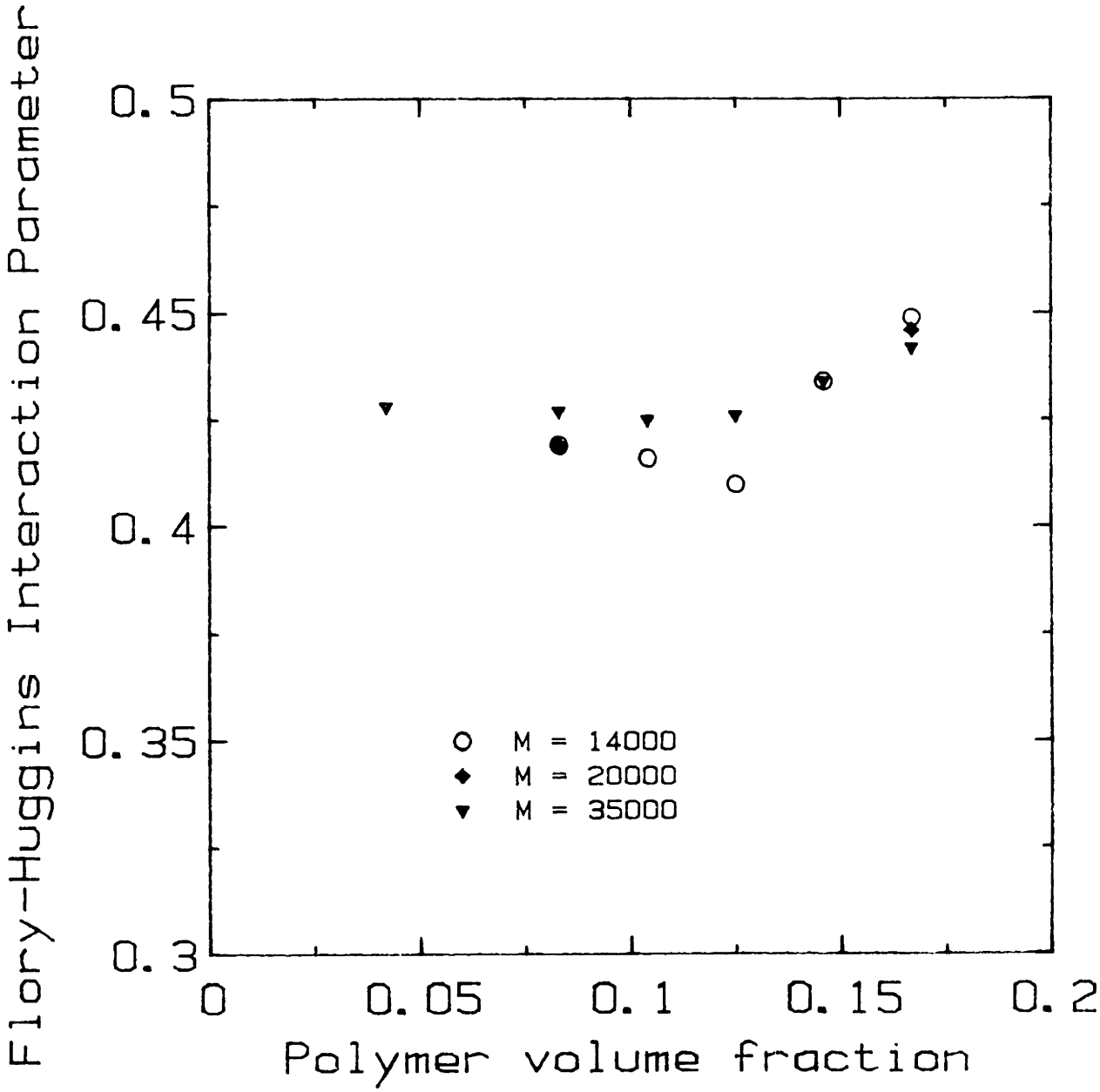

Figure 4-3. Flory-Huggins interaction parameter χ_1 for the system PEO - water as a function of polymer volume fraction. χ_1 was obtained from osmotic pressure measurements as discussed in the text. Different symbols correspond to different polymer molecular weights.

Fits of χ_1 as a function of v_2 were done using polynomials of order 1 through 4; the quality of the fit as measured by r^2 increased as the degree of the polynomial increased, but considering the scatter in the data no real significance can be attributed to any of the fits. The value for χ_1 used in all subsequent work was 0.426, the average of the values obtained. The lack of concentration dependence was at variance with the previous work of Malcom and Rowlinson [22] in which they reported a strong linear increase of χ_1 with increasing polymer volume fraction. However, their data were obtained at 80.3°C, which is quite different from the temperature used in this study. In light of the interactive changes that are known to take place with increasing temperature and considering the fact that χ_1 in this case includes effects of both enthalpic and entropic interactions (see section 2.2) it is not surprising that not only the magnitude but also the concentration dependence of the interaction parameter would vary with temperature.

Gel Properties. A fairly thorough parametric study of electron beam irradiation of PEO was done by Hueston [34] for the same system used here. The early work of this thesis confirmed Hueston's results. All the results reported here are for networks crosslinked in the presence of oxygen at a dose rate of 250000 rad/s, with no attempt at temperature control. Figure 4-4 shows the equilibrium polymer volume fraction plotted as a function of the radiation dose for networks formed at several different initial concentrations. It should be noted that there is some variability in v_{2s} for networks made under the same conditions on different occasions. (Networks made using the same conditions at the

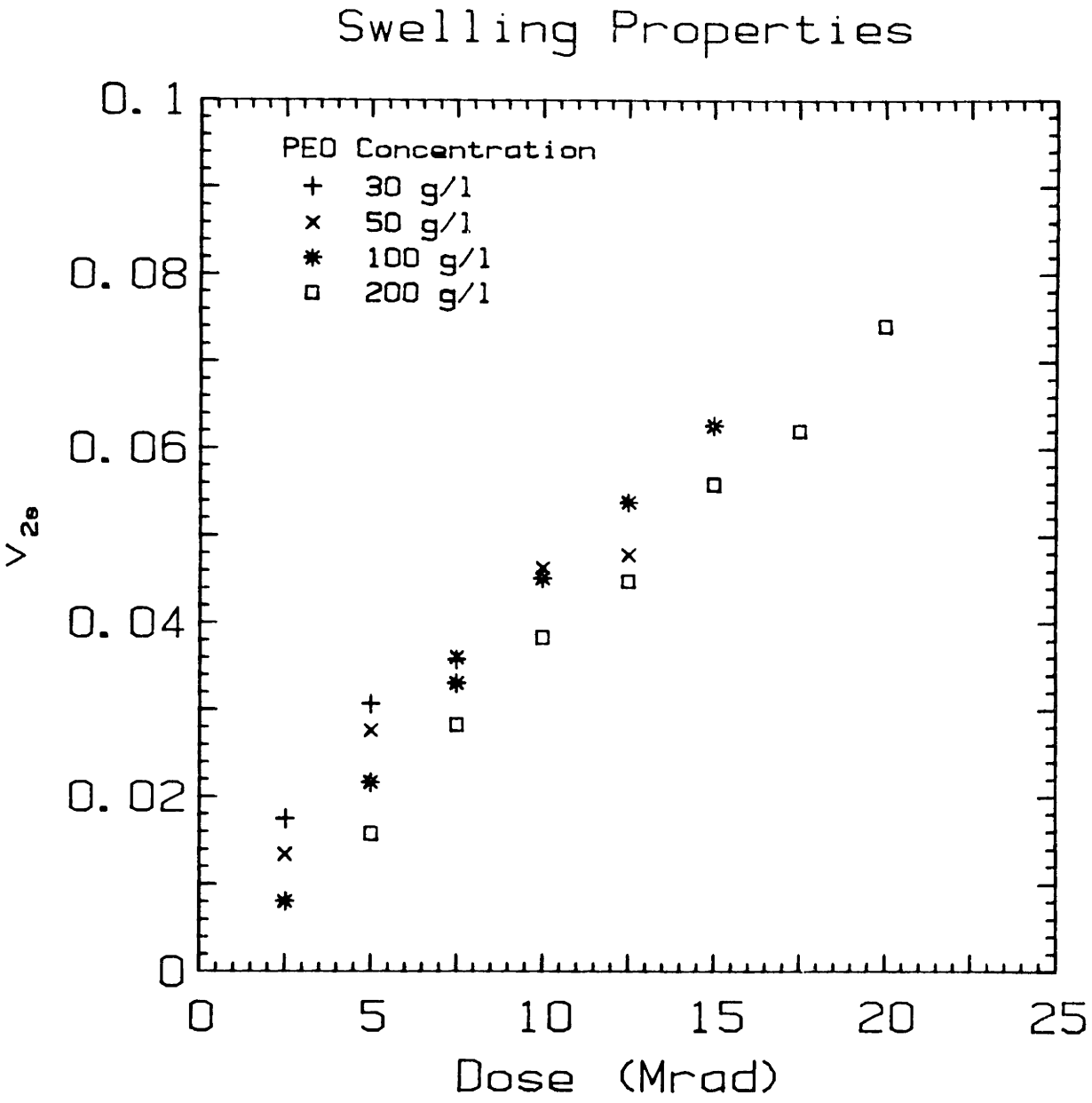

Figure 4-4. Polymer volume fraction for gels in equilibrium with pure water as a function of dose showing the effect of initial concentration.

same time did not show this variability.) This can be attributed to differences in the actual dose received by the samples due to inaccuracy in the control of the irradiation procedure.

Figure 4-5 shows the interjunction molecular weight calculated using equation 3-3 as a function of dose for the same networks. The presence of limiting, or plateau, levels of crosslinking are becoming evident in this plot for the least concentrated solutions. These plateau levels are different for different initial concentrations. The plateau level indicates that the crosslinking process has become considerably less effective. This has been attributed to the ratio of crosslinking to scission falling due to limited chain mobility in the network. That is, chain motion is decreased due to the presence of crosslinks, and since two main chain radicals on different network chains must be coupled to produce a crosslink but scission requires only a single main chain radical interacting with some non-PEO species, this would tend to decrease the ratio of crosslinking to scission. Figure 4-6 shows the same type of data for some networks made using somewhat higher doses, which allows the plateau level to be reached for solutions of higher concentration. The effect of increased initial concentration is seen in both an increase in the dose required to reach the plateau level of crosslinking and an increase in the value of the plateau M_c. The increase in the dose required to reach the plateau is related simply to the fact that there are more primary molecules to crosslink in a more concentrated solution, so it takes a higher dose to achieve the same crosslink density. The increased plateau M_c may be related to the higher

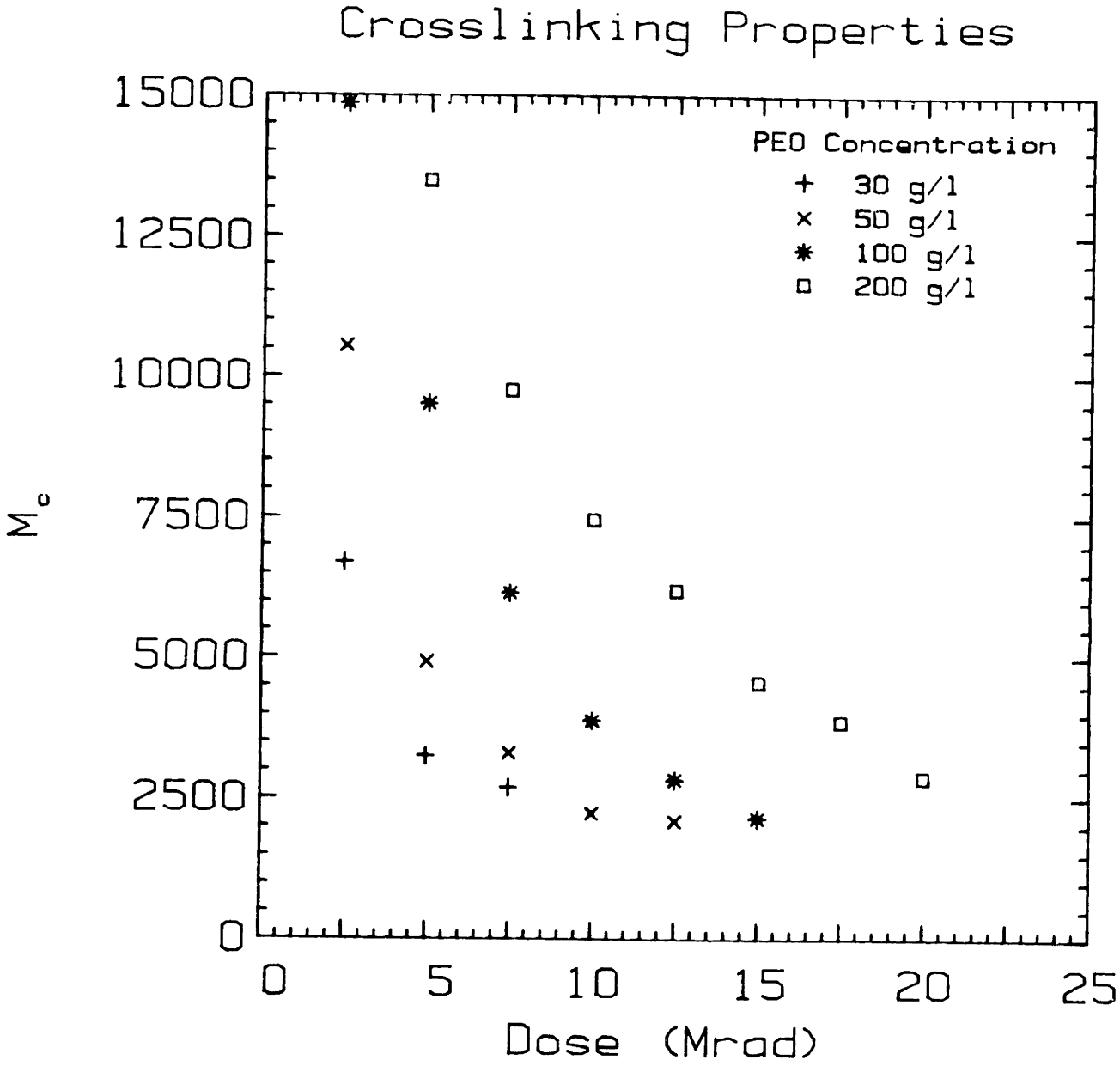

Figure 4-5. Values for the interjunction molecular weight M_c calculated from the swelling data of figure 4-4 using the Flory-Bray affine deformation theory.

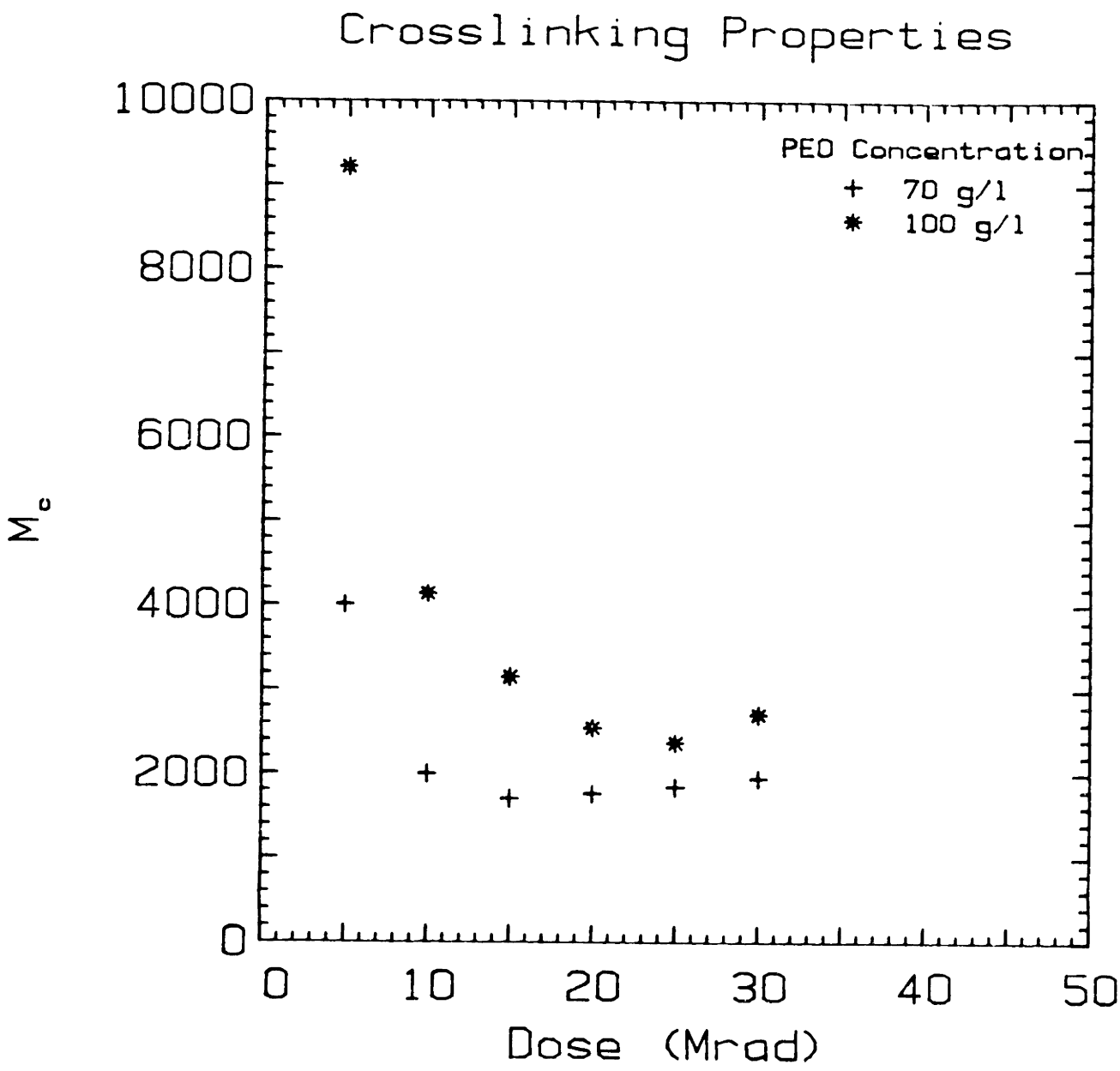

Figure 4-6. Interjunction molecular weight as a function of dose for networks synthesized using high doses to illustrate the plateau level of crosslinking. Dose rate = 250000 rad/s, M_n = 37000.

polymer volume fraction in the solutions crosslinked, which could decrease the mobility of the chains, as the mobility is probably a function both of the molecular weight of the chains and the restrictions imposed by interpenetrating coils. Figure 4-7 replots the data of figure 4-4 as crosslink density in mol crosslinks/mol repeat units as a function of radiation dose. It is clear from this plot that even below the plateau dose there is a somewhat non-linear relationship between crosslink density and dose for a particular solution concentration. Also, the slope of the curve is different for different solution concentrations. That is, even at low degrees of crosslinking, the efficiency of the process is not independent of PEO concentration, which confirms what was seen in the gel dose measurements, and is at slight variance with the results of Hueston [34], although this may be a result of Hueston's use of the wrong concentration dependence of the Flory-Huggins interaction parameter in the swelling theory equation.

The values for interjunction molecular weight as a function of concentration and dose can be converted to energy per crosslink in a manner similar to that used for the gel dose measurements. In this case, the number of crosslinks formed per primary chain is found from $(M_c/M_n - 1)/2$. M_c/M_n is the number of network chains into which one primary chain is formed. $M_c/M_n - 1$ is the number of junctions required per primary molecule to make that number of chains. The factor of 1/2 accounts for two primary chains participating in each crosslink. Multiplying the number of crosslinks per primary chain by the number of moles of primary chains gives the moles of crosslinks formed. The energy input per gram

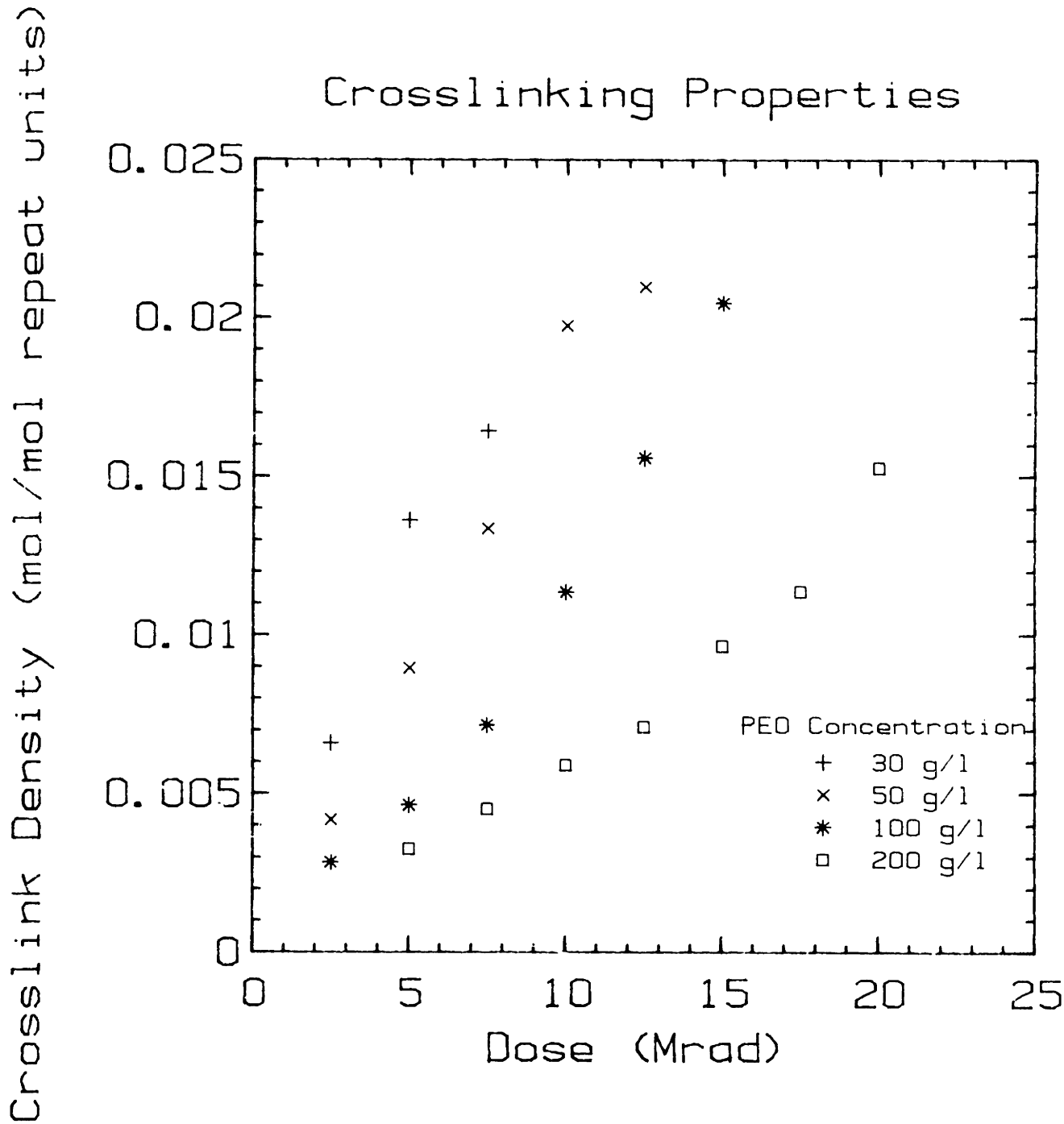

Figure 4-7. Crosslink density in mol crosslinks/mol repeat units as a function of the total radiation dose for the gels in figure 4-4.

of PEO is found as in section 4.1.1, giving the following equation for the energy/crosslink.

$$\frac{\text{energy}}{\text{crosslink}} = \frac{\text{Dose/Conc}}{\frac{1}{2}\left(\frac{1}{M_c} - \frac{1}{M_n}\right)} \qquad (4\text{-}1)$$

The dose is in units of energy absorbed per mass of irradiated material and the concentration is the weight fraction of PEO in the solution. Table 4-2 summarizes the results of the swelling measurements and subsequent calculations for the same gels as shown in figure 4-4. The energy/crosslink is plotted as a function of crosslinking conditions in figures 4-8a and b. It is immediately apparent that the energy input per crosslink decreases with increasing dose and concentration. The two lowest concentrations again show the effect of the plateau level of dose in the increase in energy/crosslink at the highest doses. The possible reasons for the concentration effect were discussed in section 4.1.1. It is not immediately clear why the energy/crosslink should decrease with dose. The effect is not extremely large; the lowest values are about 50% of the highest values. The first possibility to consider is that the theoretical relationship between degree of swelling and interjunction molecular weight is incorrect and the values computed for the number of crosslinks produced are wrong. The good agreement between the values for energy/crosslink obtained from the gel dose measurement, which does not rely on swelling measurements for the crosslink density, and the values obtained for the lowest degrees of crosslinking in this series suggests that these low dose values are probably reasonable. This in turn suggests that the affine deformation theory used to calculate M_c from

Concentration	Dose	v_{2s}	M_c	crosslink density	energy/crosslink
3 g/l	2.5 Mrad	0.0174	6684	6.582×10^{-3} mol/mol	13596 kJ/mol
3	5.0	0.0306	3230	1.362×10^{-2}	11796
3	7.5	0.0357	2680	1.642×10^{-2}	14446
5	2.5	0.0134	10536	4.176×10^{-3}	14731
5	5.0	0.0276	4913	8.950×10^{-3}	11304
5	7.5	0.0360	3293	1.336×10^{-2}	10844
5	10.0	0.0463	2230	1.973×10^{-2}	9492
5	12.5	0.0478	2098	2.097×10^{-2}	11121
10	2.5	0.0080	14854	2.829×10^{-3}	12408
10	5.0	0.0216	9503	4.629×10^{-3}	12787
10	7.5	0.0330	6146	7.159×10^{-3}	11055
10	10.0	0.0451	3876	1.135×10^{-2}	8659
10	12.5	0.0538	2826	1.557×10^{-2}	7649
10	15.0	0.0626	2152	2.045×10^{-2}	6855
20	5.0	0.0158	13486	3.265×10^{-3}	10610
20	7.5	0.0283	9751	4.514×10^{-3}	9930
20	10.0	0.0383	7461	5.896×10^{-3}	9346
20	12.5	0.0448	6196	7.102×10^{-3}	9303
20	15.0	0.0559	4563	9.645×10^{-3}	7807
20	17.5	0.0620	3872	1.137×10^{-2}	7568
20	20.0	0.0741	2882	1.527×10^{-2}	6251

Table 4-2. Summary of the swelling results and calculated network parameters for a selected set of gels.

swelling measurements is probably predicting the right values for M_c for a wide range of initial PEO concentrations at degrees of crosslinking close to the gel point. Whether the theory is good farther from the gel point is not clear, so no real conclusion can be drawn about the validity of the energy/crosslink calculations at higher crosslink densities. The same trend, increased efficiency with dose, was observed by VanBrederode [44], although he saw an order of magnitude difference in efficiency. However, it is not clear how crosslink densities were determined in that study, so it should not be viewed as strong confirmation of the results obtained in this study.

It is important to look at the possible effects of scission on these calculations, as it is expected that the presence of scission would become more important as the total dose increases. Looking at equation 3-3, it can be seen that if scission is assumed to have an effect equivalent to decreasing the primary molecular weight (increasing the number of loose ends), the value of M_c calculated for a particular degree of swelling would fall, increasing the crosslink density, and decreasing the calculated value of energy/crosslink, which suggests that efficiency may increase even more with dose than figure 4-8 indicates. However, equation 3-3 was not derived for the case of simultaneous crosslinking and scission, and it is not clear what the effect of scission on the elastic term would be. It would depend strongly on the location of the broken bonds, which is difficult to predict in the present situation with both crosslinking and scission taking place.

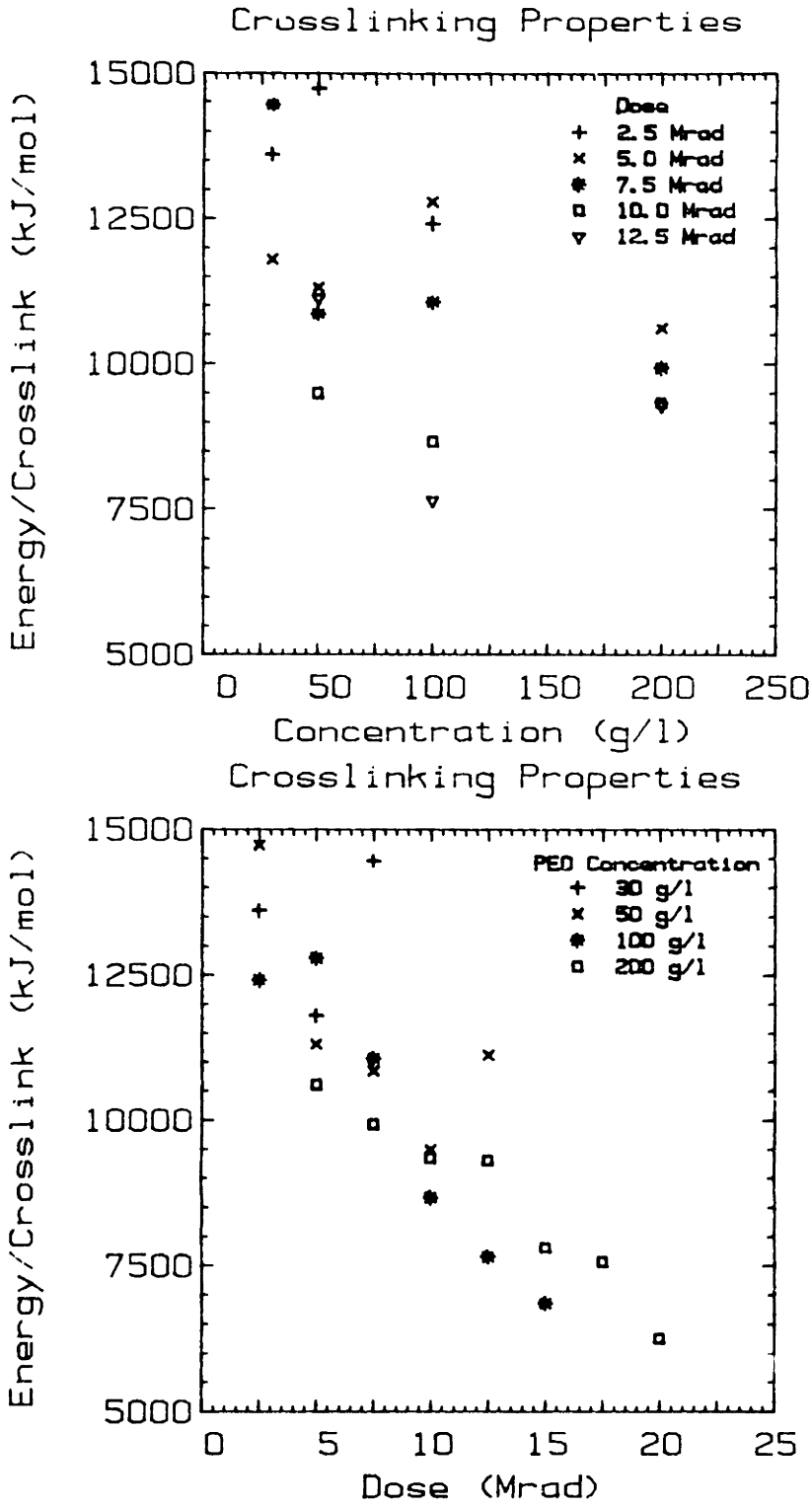

Figure 4-8. Energy input per mol of crosslinks formed as a function of initial PEO concentration and total irradiation dose. The networks are the same as in figure 4-4.

It appears, then, that if the values for interjunction molecular weight calculated from the affine deformation theory are correct, the efficiency of the crosslinking process increases with degree of crosslinking up to some plateau level. This effect can probably be attributed to increase in temperature with dose. By inserting a thermocouple into a sample during an irradiation, it was possible to monitor the sample temperature and confirm that the temperature rises about 15°C with each 2.5 Mrad of dose (one pass) at the dose rate of 250000 rad/s used in this work. Depending on the time between passes under the beam, which in turn depends on the number of samples and the location of a particular sample on the belt, the temperature falls 5 to 10°C between each 2.5 Mrad. The effective temperature rise is thus between 5 and 10°C per 2.5 Mrad. Thus a sample given 15 Mrad could be on average about 15 to 20°C warmer during the irradiation than a sample given 2.5 Mrad. It is not clear if this is sufficient to cause the two-fold increase in efficiency observed, but as it is known that the efficiency of water radiolysis increases with increasing temperature, it will certainly have an effect. However, in the absence of independent confirmation of the crosslink density at high degrees of crosslinking, no real conclusions can be drawn about the efficiency of the process.

4.1.3. Scanning Electron Microscopy.

Figures 4-9 and 4-10 are scanning electron micrographs of radiation crosslinked PEO networks. Figure 4-9 is a surface shot, with the right side a 10 times magnification of the small box on the left. Figure 4-10

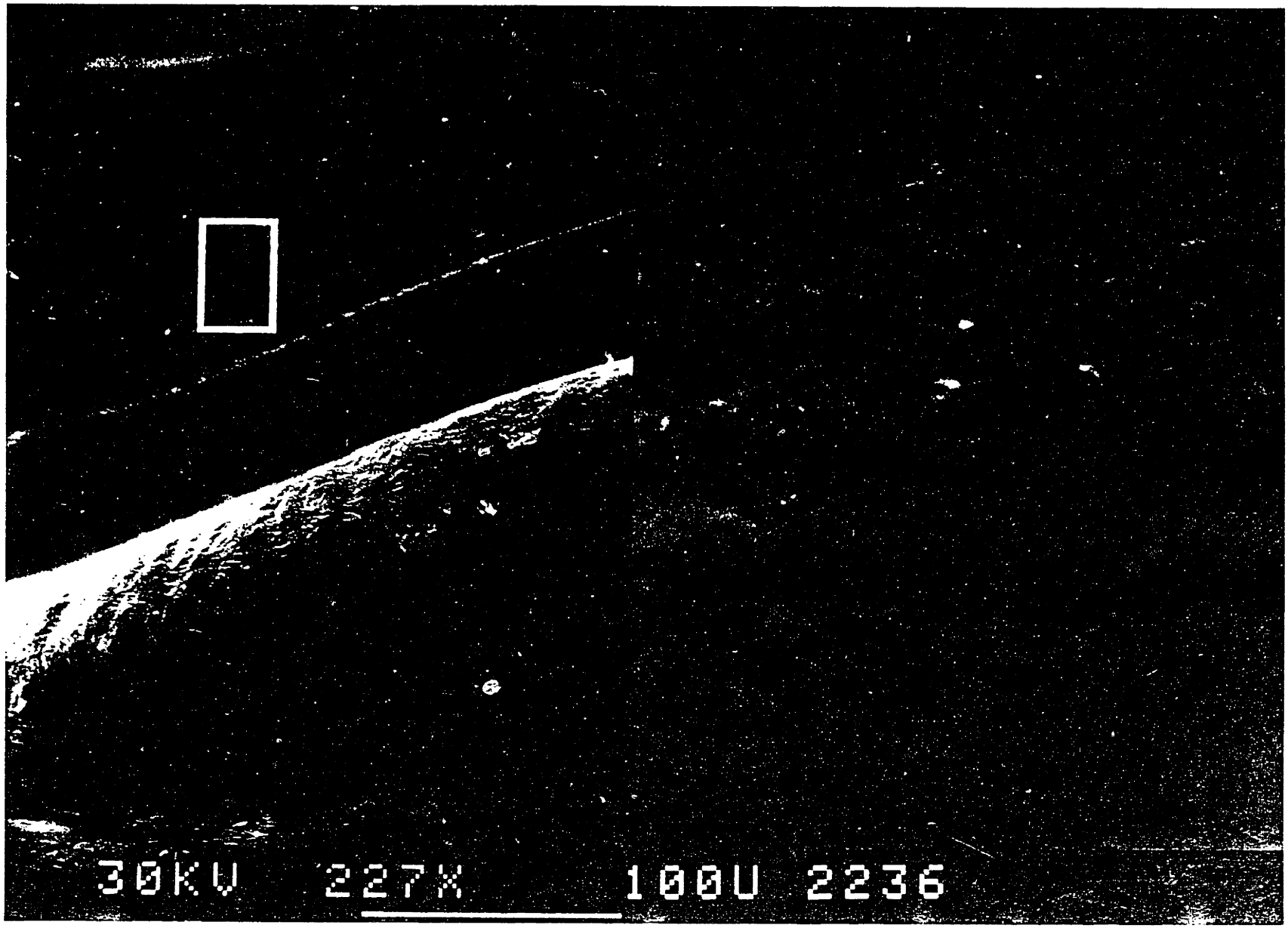

Figure 4-9. Scanning electron micrograph of surface of PEO gel. Gel was fully swollen in water and critical point dried before SEM. Right side is 10x magnification of small box on left.

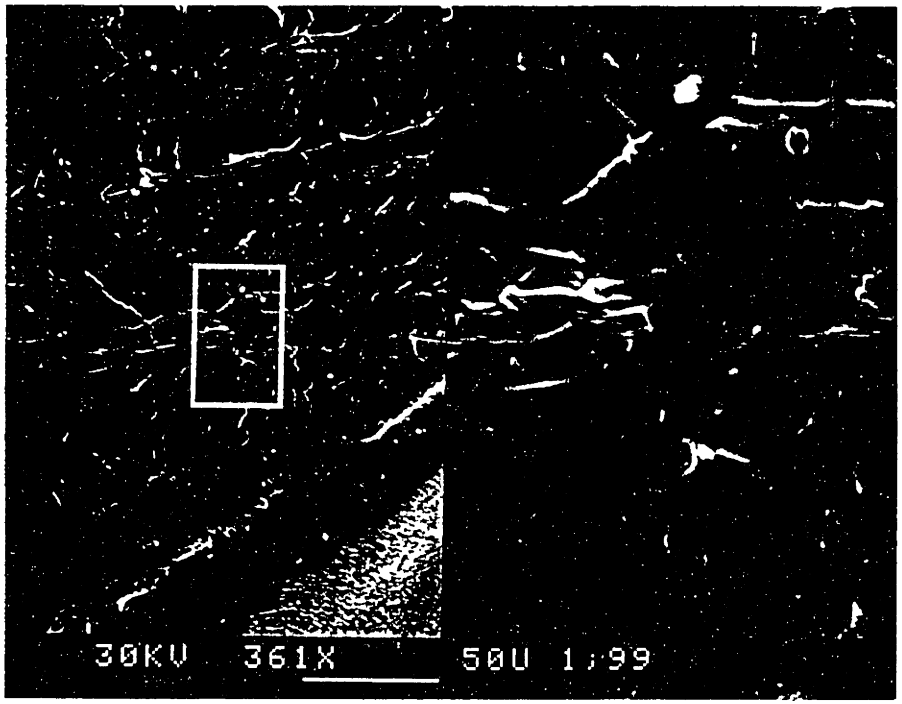

Figure 4-10. Scanning electron micrograph of cross-section of gel in figure 4-9. Striations are probably an artifact of cutting the cross-section.

is a cross-section. There was no evidence in any of the SEM work of network inhomogeneities or pores (other than the macroscopic gas bubbles trapped in the irradiation procedure). There was also no evidence for differences between the two surfaces (one formed against glass, the other against air) of the gel.

4.1.4. Differential Scanning Calorimetry.

A series of DSC measurements was carried out on the some of the gels discussed in section 4.1.3. The gels were vacuum dried prior to measurement. (A couple of attempts were made to look at crystallinity of swollen gels by using an equivalent amount of water as the reference. There was no evidence for any crystallinity in the swollen gels, but the quality of the data was not high enough to rule it out completely.) A typical trace of heat input as a function of temperature for a dried network is shown in figure 4-11. Two things were extracted from the traces: the melting temperature and the heat input, which was converted to the fraction of the polymer that was crystalline using a value for the molar heat of fusion from the literature. The results are summarized along with some of the properties of the networks used in table 4-3. The melting point decreases with increasing crosslink density. This is in qualitative agreement with the melting point depression theory of Flory [19] in which the crosslink is treated as one of the two types of units in a copolymer, which serves to disrupt the crystallinity of the other unit. The decrease in melting point may also be a reflection of the decreasing length of the network chains available to form crystallites as

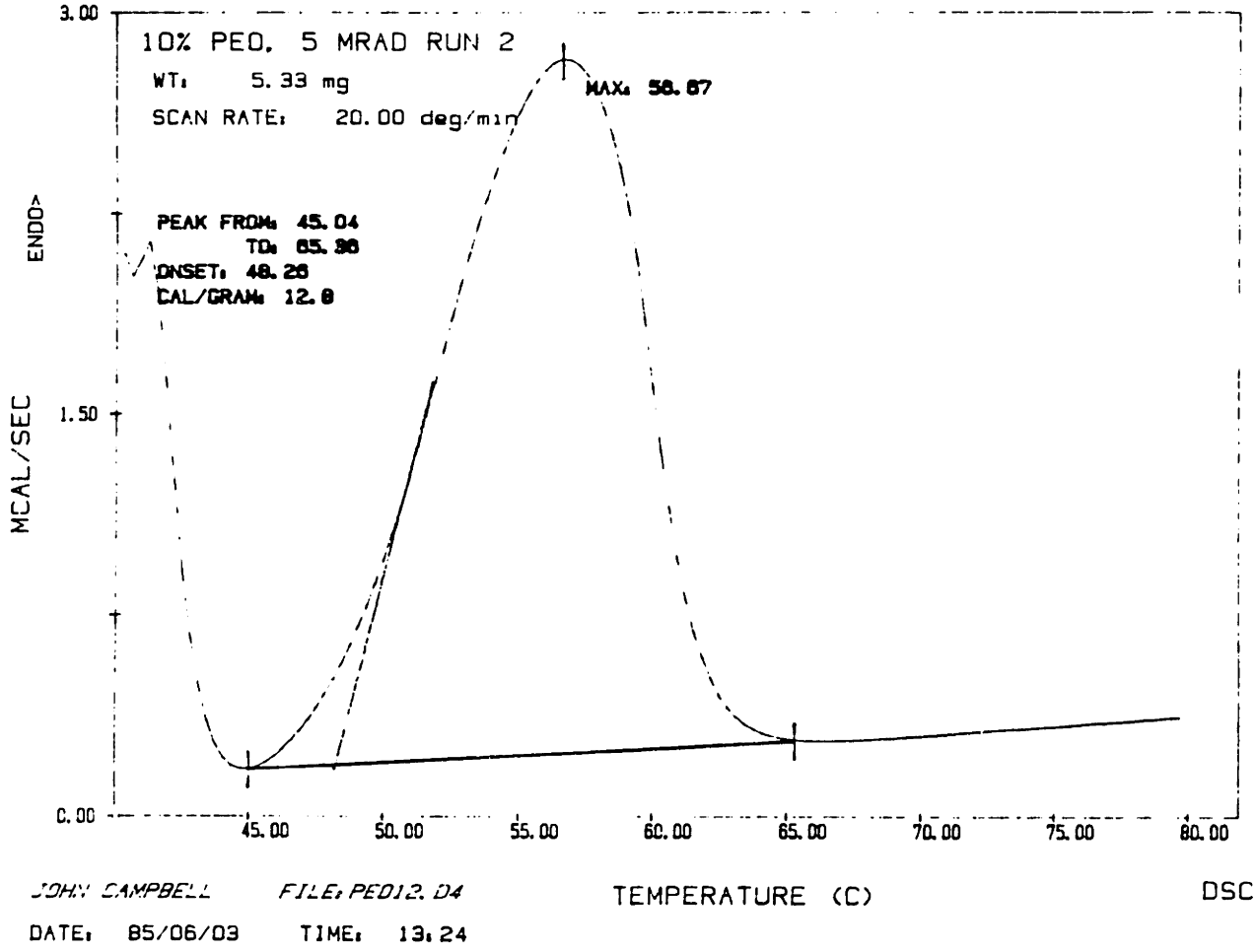

Figure 4-11. Typical trace of heat input as a function of temperature from differential scanning calorimetry. Sample was a gel synthesized at 100 g/l, 5 Mrad.

Conc (g/l)	Dose (Mrad)	v_{2s}	M_c	T_m (°C)	% Crystallinity
30	2.5	0.0174	6684	56	47.1
30	5.0	0.0306	3230	48	41.3
30	7.5	0.0357	2680	39	3.0
50	2.5	0.0134	10536	58	44.8
50	5.0	0.0276	4913	50	43.8
50	7.5	0.0360	3293	50	37.5
50	10.0	0.0463	2230	45	32.9
50	12.5	0.0602	1772	36	23.9
100	2.5	0.0080	14854	59	48.9
100	5.0	0.0216	9503	58	44.9
100	7.5	0.0330	6146	53	46.7
100	10.0	0.0451	3876	51	43.8
100	12.5	0.0538	2826	47	39.5
100	15.0	0.0626	2152	46	35.3
200	5.0	0.0158	13486	58	50.3
200	7.5	0.0283	9751	56	48.3
200	10.0	0.0383	7461	57	51.1
200	12.5	0.0448	6196	55	45.8
200	15.0	0.0559	4563	50	45.6
200	17.5	0.0620	3872	49	40.3
200	20.0	0.0741	2882	49	40.1
PEO CONTROL - Unirradiated PEO Sample -				73	92.0

Table 4-3. Summary of results from differential scanning calorimetry measurements on crosslinked PEO gels. The melting temperature reported is the temperature at which the peak maximum occurs. The fraction of crystalline material (% crystallinity) is found from the area of the fusion peak, the sample weight, and the molar heat of fusion.

the melting point increases with chain molecular weight for linear PEO molecules. The fractional crystallinity is also a function of the degree of crosslinking. This is illustrated in Figure 4-12, where the % crystallinity is plotted as a function of the gel properties M_c and v_{2s} and the melting temperature T_m is plotted as a function of M_c. It is interesting that the crystallinity seems to be a function only of the molecular weight between crosslinks as measured from the affine deformation swelling theory. It is probably reasonable to assume that the degree to which these gels develop crystalline regions on drying would be a function of how long the chain segments between crosslinks are as well as the mobility of those chain segments during the drying process. The crystallinity data thus suggest two things. First, this data suggests that the relationship between swelling properties and interjunction molecular weight used to calculate the interjunction molecular weight has the correct dependencies on v_{2s} and v_{2r}, because the data collapse to a single line when plotted against M_c. When considered in terms of the previous observation that the low degree of crosslinking predictions seemed to have the correct magnitude, it suggests that the relationship is correctly predicting M_c. Secondly, it appears that the mobility of the chains at the point in the drying process at which crystallites are forming is controlled only by the interjunction molecular weight. This does not necessarily imply that the polymer volume fraction is not important in determining chain mobility in the fully swollen state, but M_c is probably also important under those conditions.

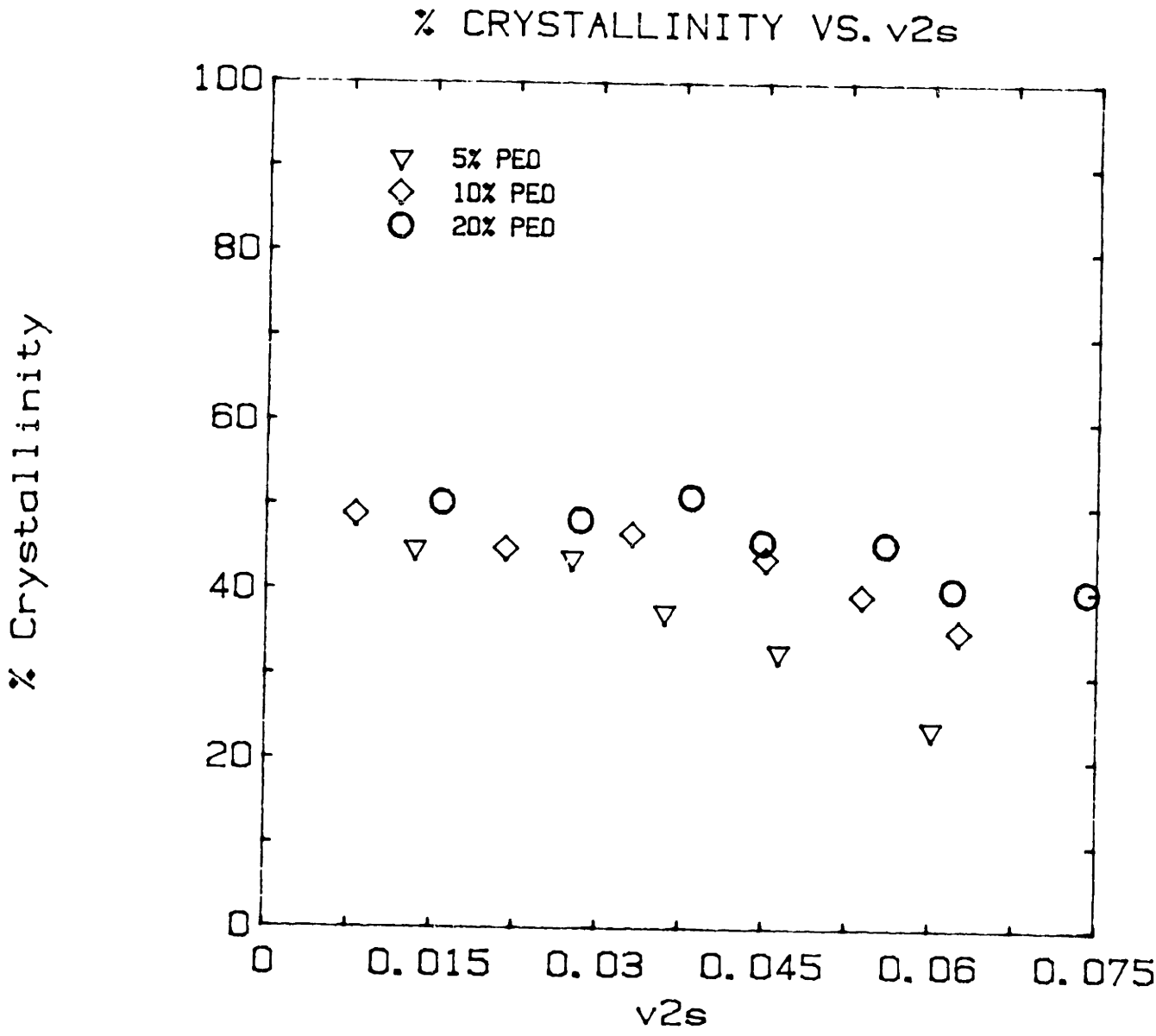

Figure 4-12. a. Degree of crystallinity of a set of dried PEO networks as measured by DSC as a function of the polymer volume fraction v_{2s} of the networks when fully swollen in water.

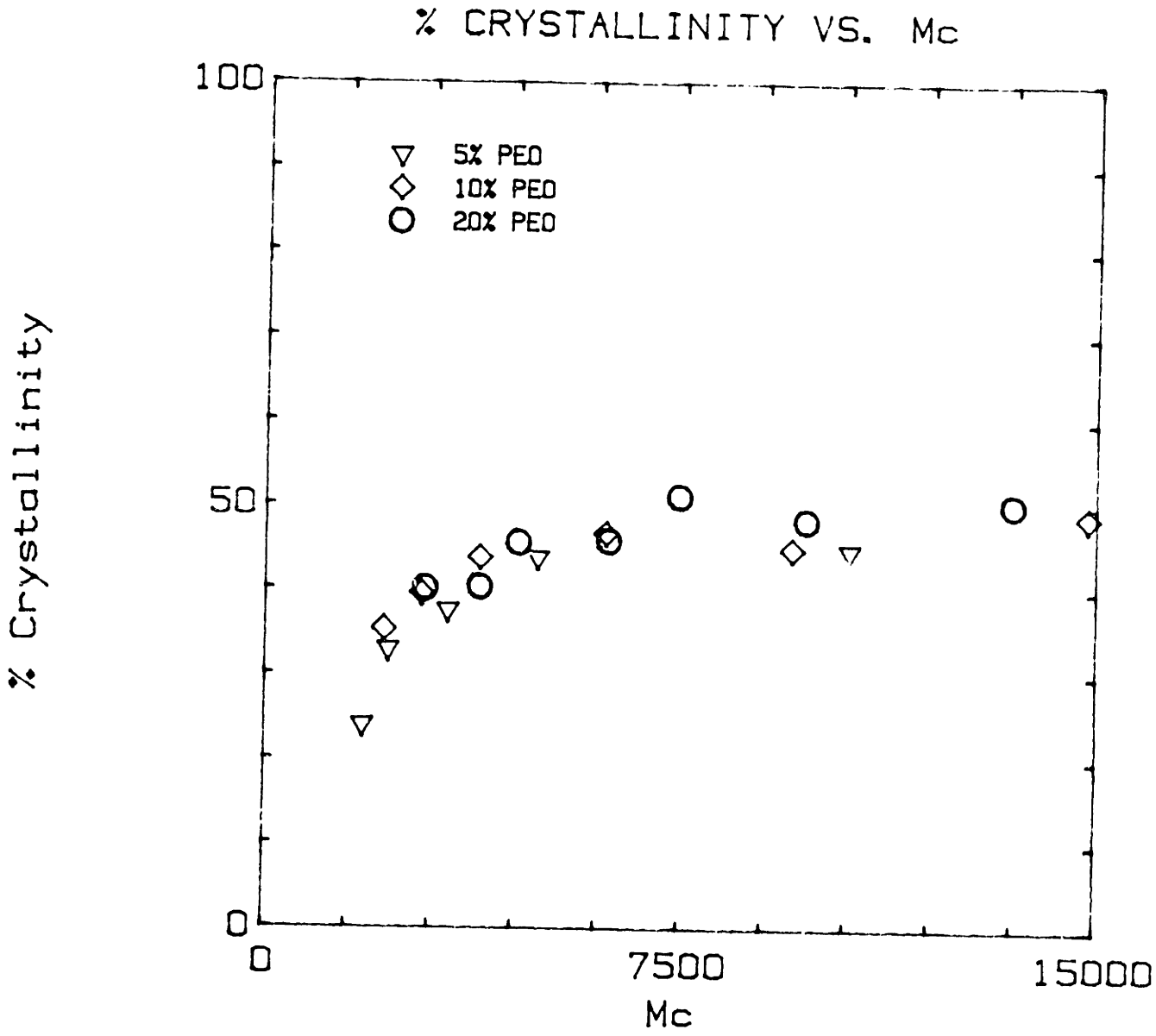

Figure 4-12. b. DSC data of figure 4-12a replotted as a function of the interjunction molecular weight M_c as calculated using the Flory-Bray affine swelling theory.

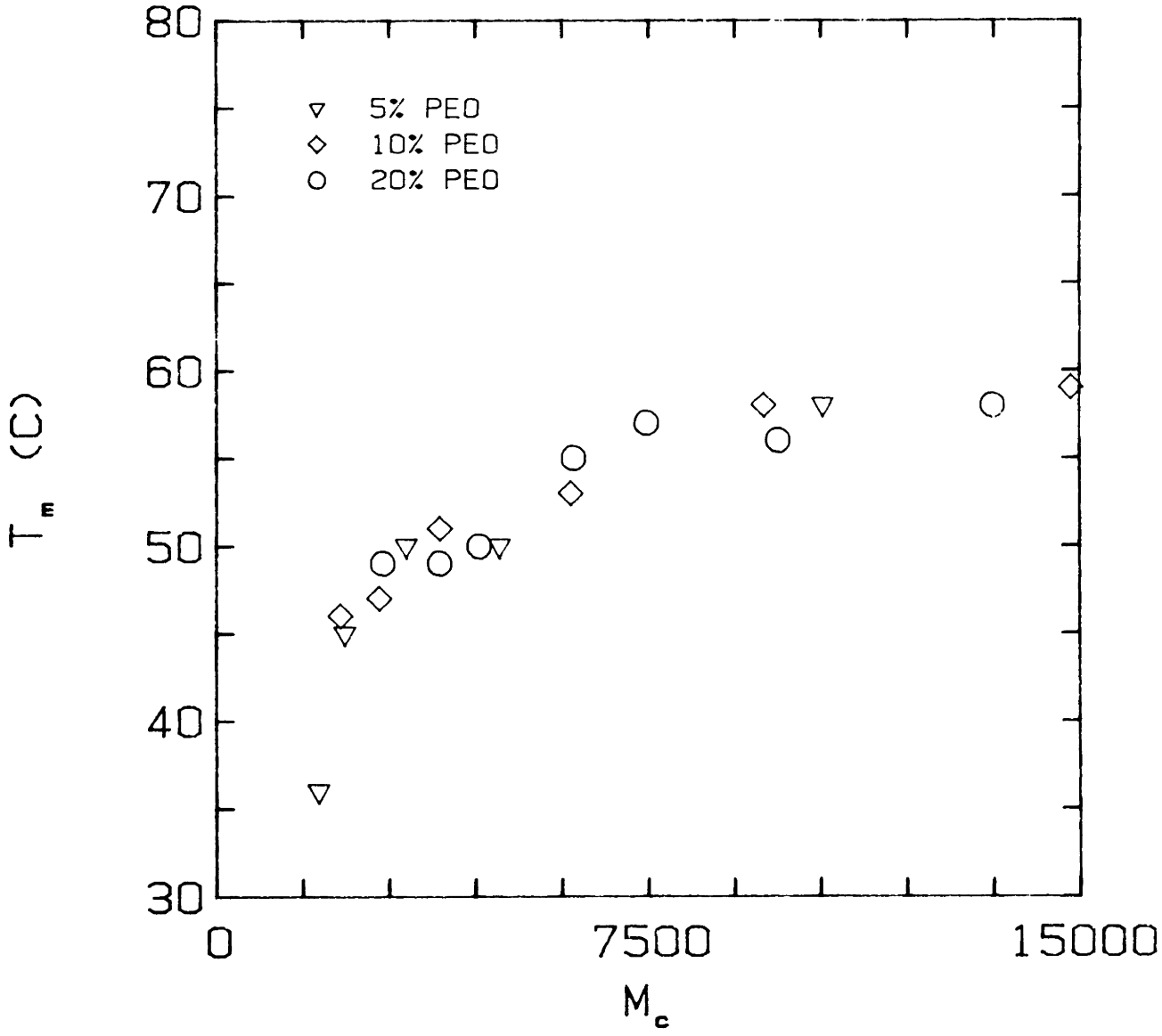

Figure 4-12. c. Melting temperature as measured by differential scanning calorimetry as a function of the interjunction molecular weight M_c.

4.2. Chemical Characterization of Radiation Crosslinking

4.2.1. Spectroscopy.

Figure 4-13 is an infrared spectrum of 20000 molecular weight PEO deposited onto an NaCl crystal from a chloroform solution. The major peaks are labelled with the molecular motion associated with the peak [12]. This spectrum is entirely consistent with those found in the literature for PEO cast from solution. Figure 4-14 is a spectrum of a PEO network formed from a 10% solution of 35000 molecular weight PEO given 10 Mrad total dose. The spectrum was obtained using the multiple internal reflectance technique. Note that this spectrum is virtually identical with the non-crosslinked spectrum except for a slight broadening of some of the peaks, which is probably due to the lower degree of crystallinity of the network (see reference 12 for a comparison of crystalline and amorphous spectra). Figure 4-15 is a spectrum of a sample of a 1% solution of PEO 35000 in water which was given a 0.5 Mrad dose (which did not cause gelation), vacuum dried at about 70°C, redissolved in $CHCl_3$, and deposited on an NaCl crystal. In this spectrum a peak is beginning to appear at about 1700 cm^{-1}, which is in the carbonyl range. This is probably indicative of an oxidative process which occurred during the somewhat harsh drying procedure, as a control (unirradiated) PEO solution dried in the same way also showed this peak. The infrared spectroscopy work indicates that there are no major changes in the basic chemical nature of PEO during the irradiation process. However, chemical changes outside the range of sensitivity of IR

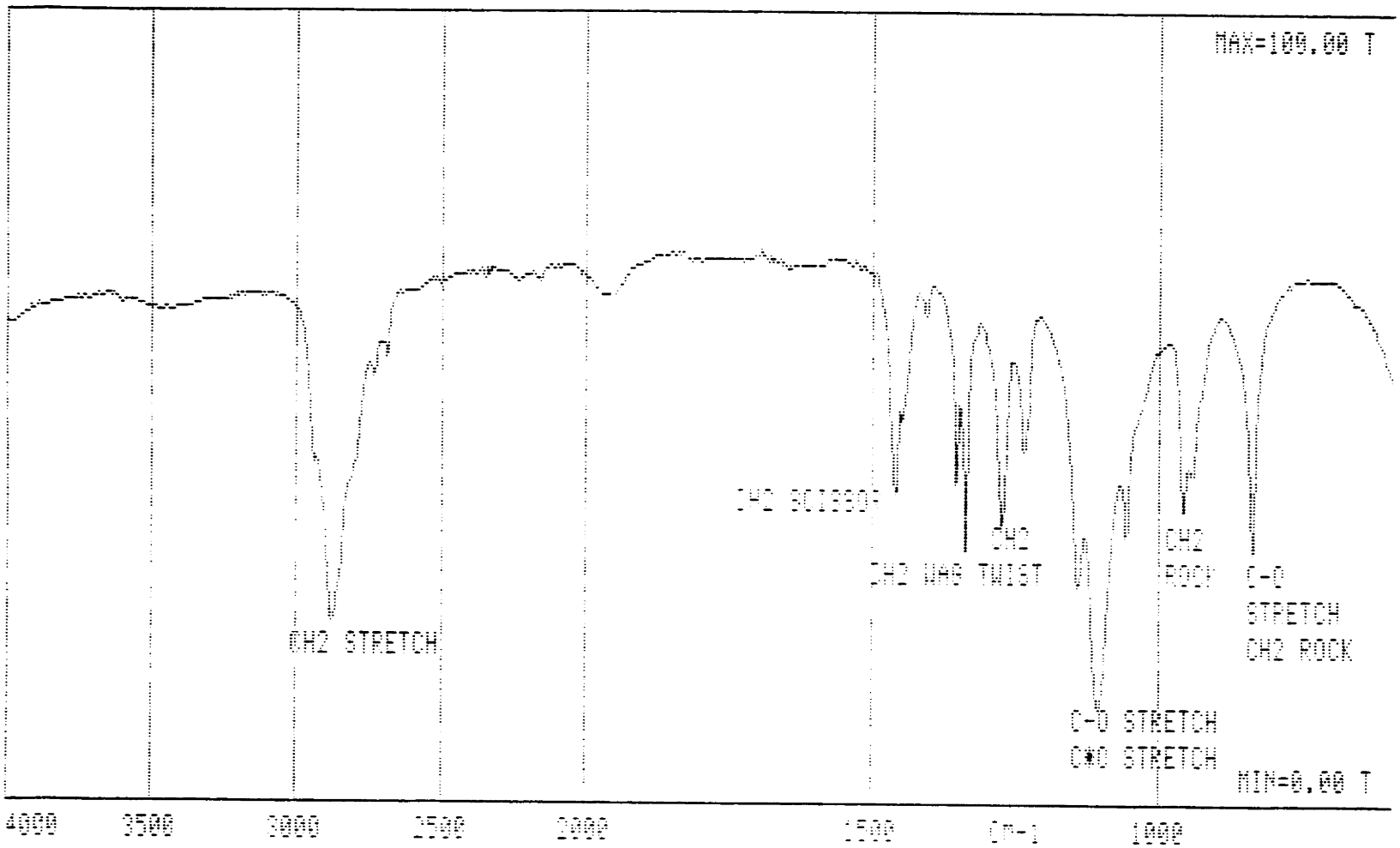

Figure 4-13. Infrared transmittance spectrum of a control PEO sample. Sample was dissovled in $CHCl_3$ and film deposited on a NaCl crystal. Prominant peaks are labelled with the molecular motion associated with the absorbance.

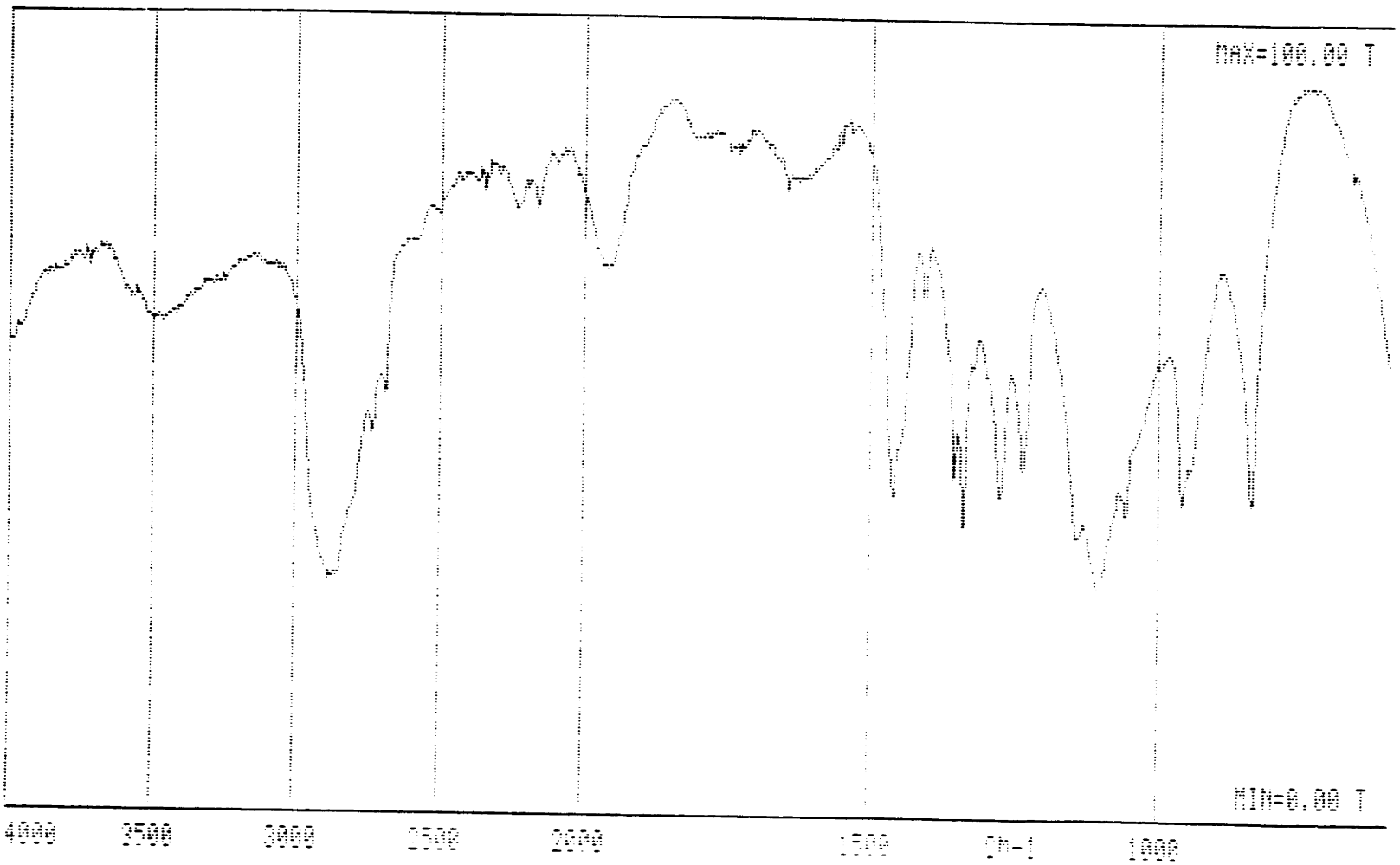

Figure 4-14. Multiple internal reflectance infrared spectrum of a crosslinked PEO network. Sample was crosslinked at 50 g/l PEO 35000, 10 Mrad total dose, allowed to swell fully in water, and vacuum dried. Peaks at 3500 and just below 2000 cm^{-1} are indicative of bound water in the sample.

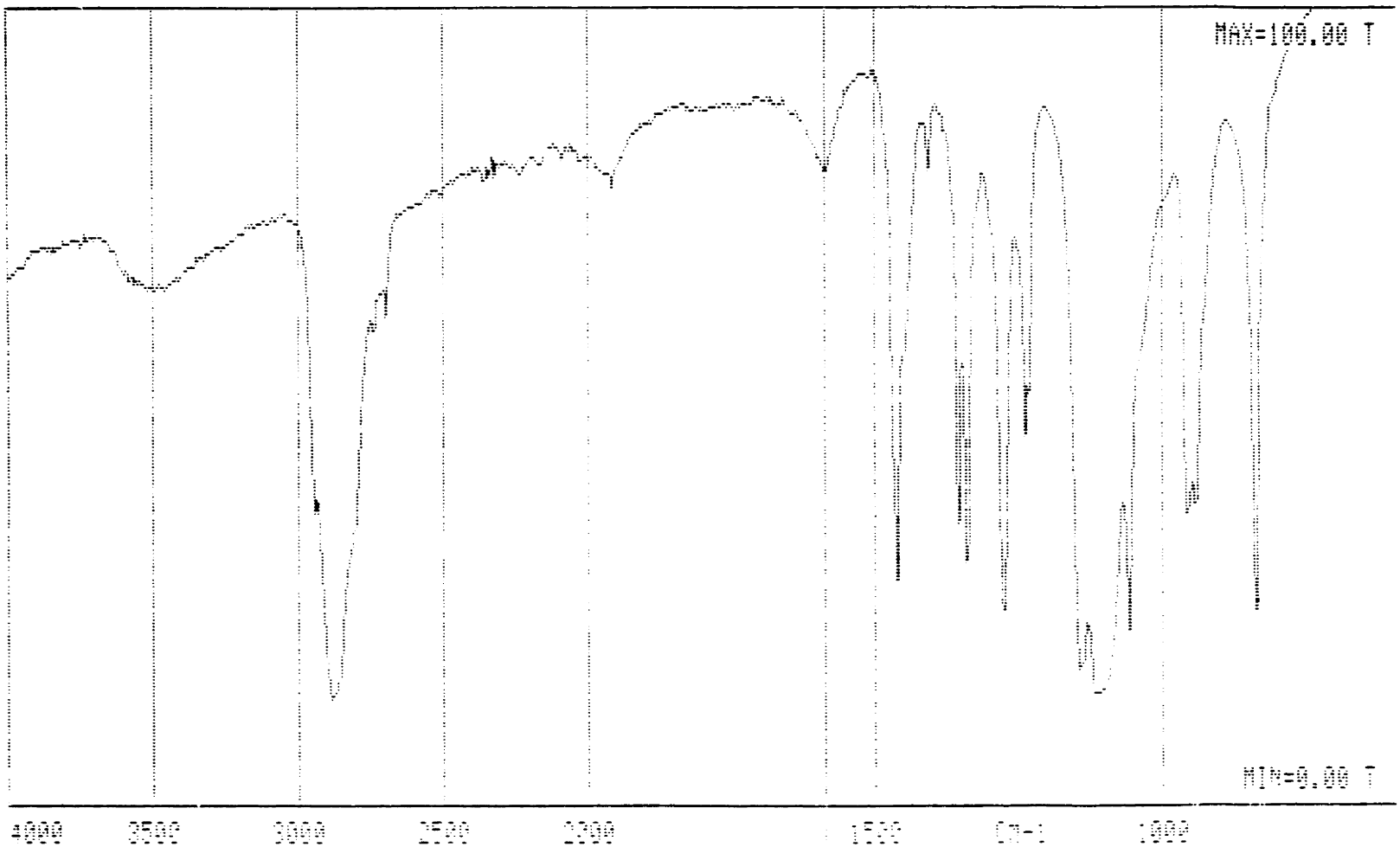

Figure 4-15. Infrared spectrum of a 1 g/l solution of PEO 35000 given 0.5 Mrad total dose in pure water at pH 7. Water was removed by vacuum drying and sample dissolved in $CHCl_3$ and deposited on a crystal. Marked peak is at 1788 cm^{-1}, which is in the carbonyl region.

spectroscopy are certainly taking place. For instance, it is evident that crosslinking is occurring during irradiation, but there is no evidence for this in the spectra obtained.

Nuclear magnetic resonance spectroscopy on solutions that were irradiated, dried, and resolvated in deuterated chloroform were equally uninformative about the chemistry of the irradiation process. Figure 4-16 shows ^{1}H spectra of irradiated and control PEO solutions, and 4-17 is the corresponding ^{13}C spectra. There are no real differences between the control and irradiated samples in either pair of spectra, but again this is probably due to lack of sensitivity rather than the absence of chemical changes.

4.2.2. Size Exclusion Chromatography of Irradiated Solutions.

A set of SEC measurements were made on solutions of PEO that had been irradiated sufficiently to produce changes in the molecular weight distribution but not enough to lead to gelation. Several things were varied in the set of measurements, including PEO concentration, total dose, dose rate, solution pH, gaseous atmosphere, and solution additives (i.e. salts, etc). Figure 4-18 is typical of the type of results obtained. The data are plotted as mass fraction as a function of molecular weight, with molecular weight on the x-axis on a log scale. This plot is for a 0.1% solution of PEO 35000, pH 7, irradiated to different total doses at a dose rate of 10000 rad/s. The distribution shifts to lower and lower molecular weights as the total dose is

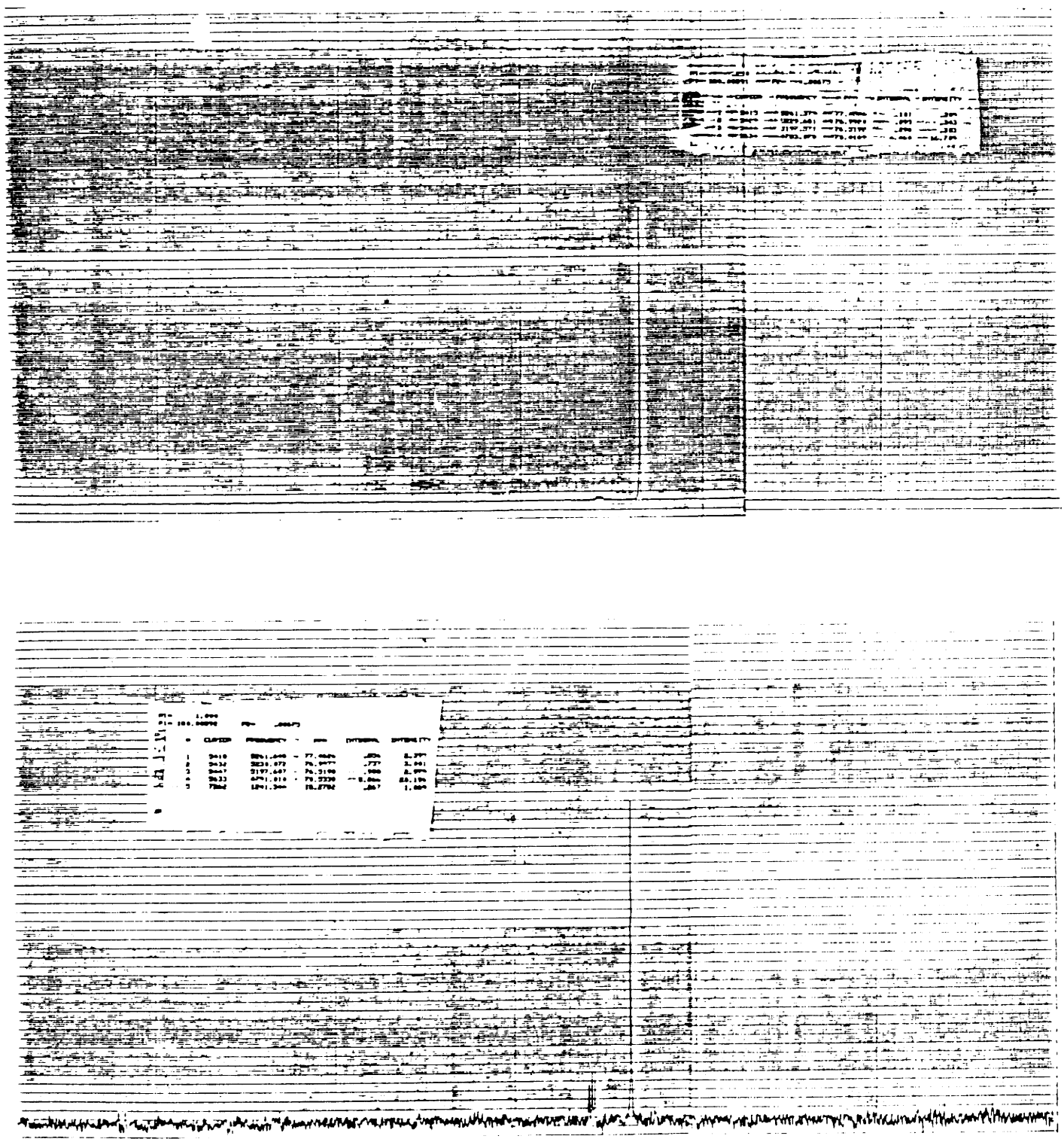

Figure 4-16. ^{1}H nuclear magnetic resonance spectra for an unirradiated PEO sample (upper spectrum) and a sample given 0.5 Mrad total dose at 1 g/l in pure water, pH 7. Spectroscopy was done at about 0.1 g/l in $CDCl_3$.

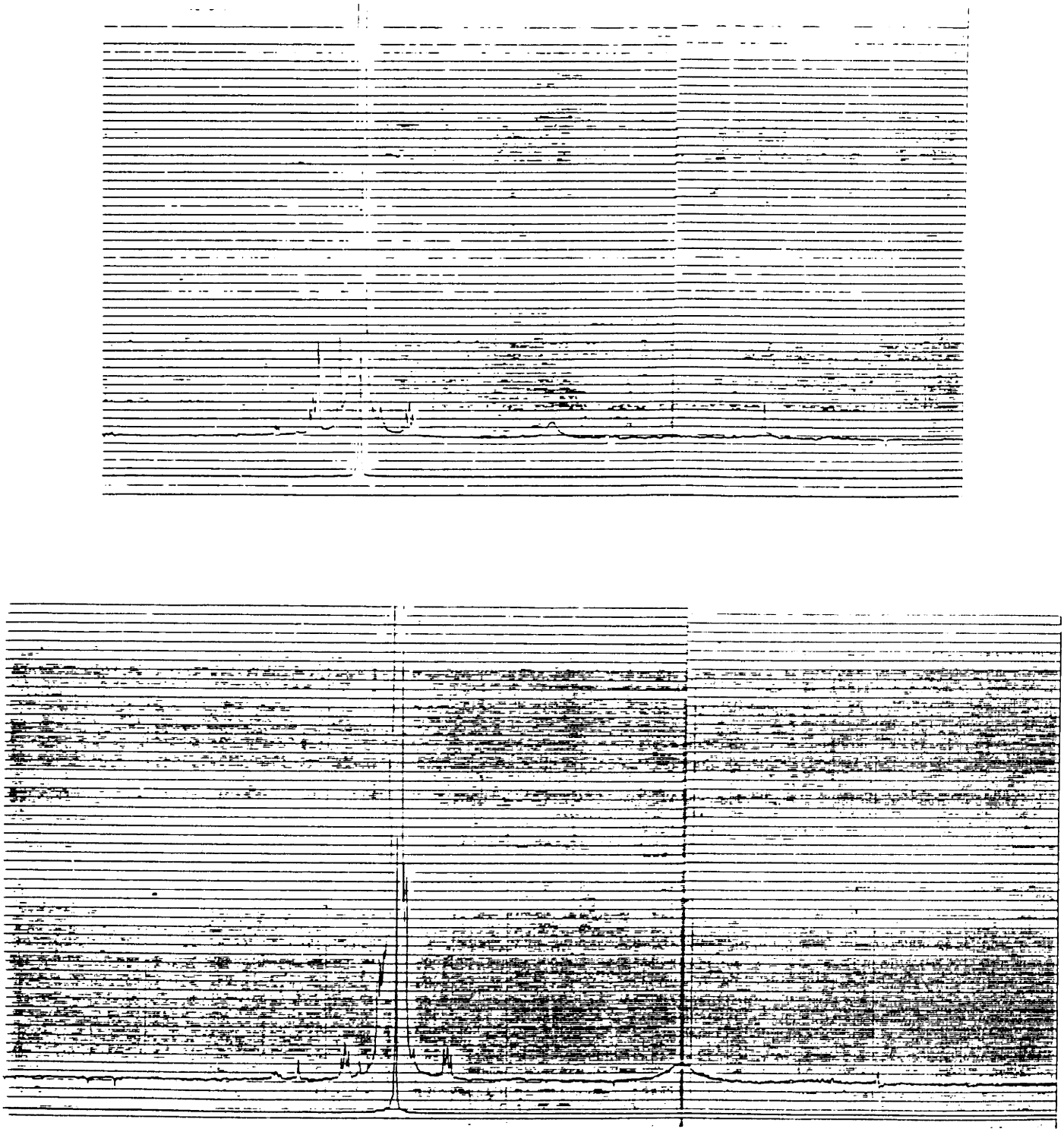

Figure 4-17. ^{13}C spectra for the same samples as figure 4-16. Control is again the upper spectrum.

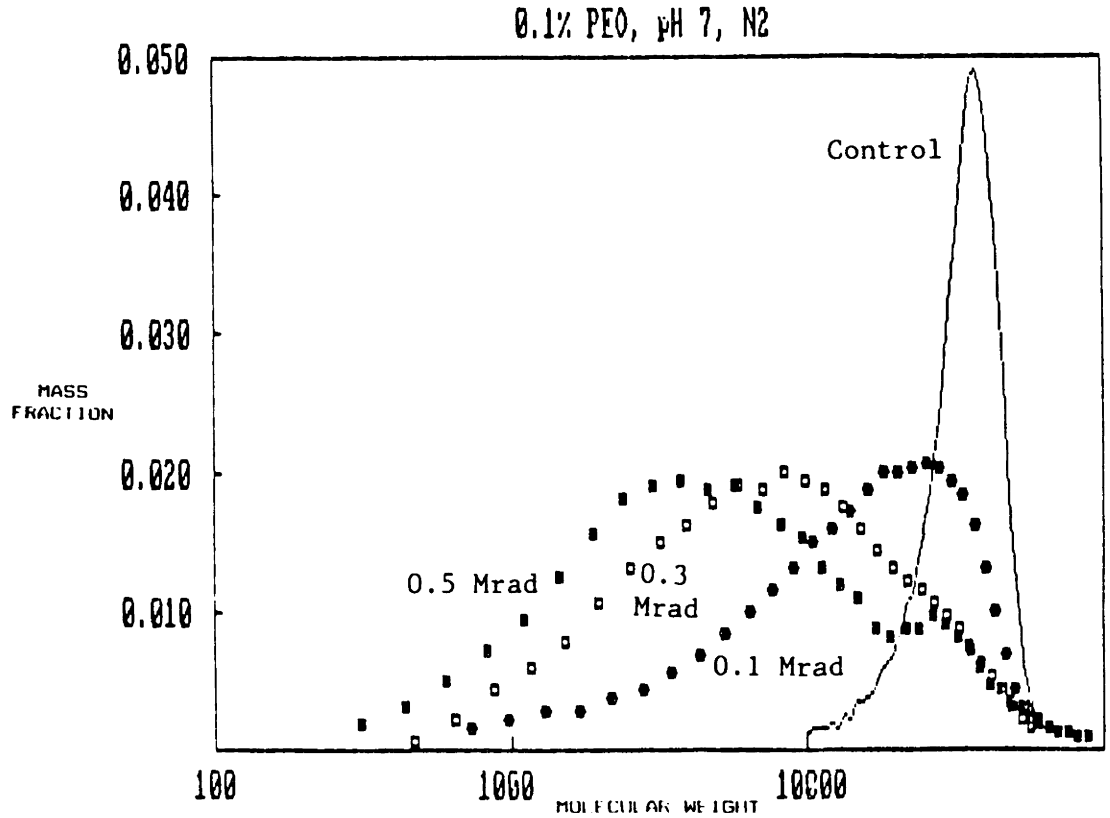

Figure 4-18. Example of SEC results. Data is presented as mass fraction as a function of molecular weight. The solid line is the unirradiated control, and the symbols have been irradiated to the total doses indicated. All samples were 1 g/l PEO in pure water at pH 7 in a nitrogen atmosphere.

increased, which is clearly evidence for chain scission taking place during the irradiation process. As can be seen, under these conditions there is no evidence of crosslinking. It is interesting to compare the measured molecular weight distribution with that calculated for a pure random scission. Basedow et al [83] have developed a kinetic model for chain scission which assumes that scission is a first order process. For the case of random scission an analytical solution for the molecular weight distribution as a function of time can be obtained, and for radiation induced changes time can be related to total dose. To make the calculations, the initial polymer molecular weight distribution was fit to a generalized exponential function. This function was plugged into the model and the simulation of degradation was allowed to continue until the number average molecular weight of the predicted distribution was the same as that of the measured post-irradiation distribution. The predictions obtained in this way are plotted with the corresponding measured distributions in figure 4-19. The poorness of the fit suggests that the process occurring during irradiation is not pure random scission. There are a number of possibilities for the actual process. Basedow et al noted that for the hydrolytic cleavage of dextran there were departures from random scission, but since it has been demonstrated in other systems that radiation-induced scission is indeed a random process [84] the most likely explanation is that there is some degree of crosslinking taking place. Clearly the level of crosslinking relative to scission is small, as there is no evidence for molecular weights higher than that of the starting material, but there could still be a considerable number of bonds being formed between chains. This will

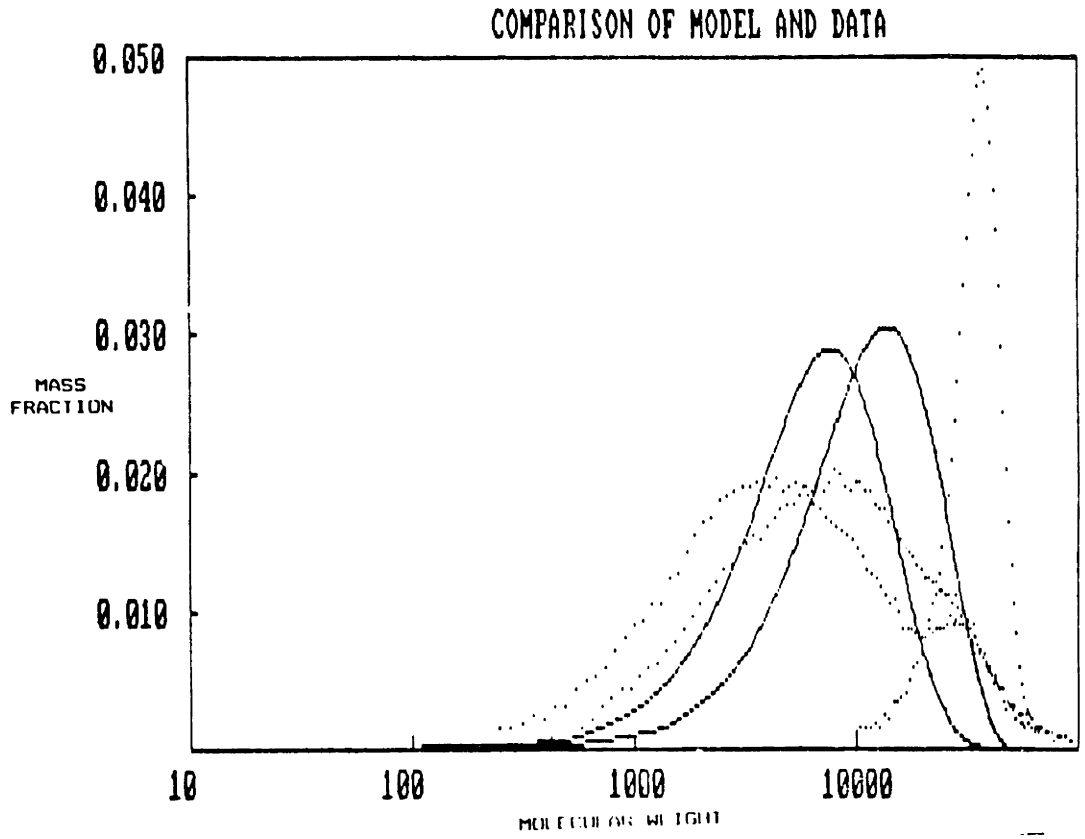

Figure 4-19. Data from figure 4-18 plotted with the predictions of the scission model of Basedow et al [38]. The dotted lines are the data for the unirradiated, 0.3 Mrad, and 0.5 Mrad total dose samples. The solid lines are model predictions for the same $\bar{M}_n$ as the two irradiated samples.

change the apparent molecular weight distribution because of the presence of branches in some of the molecules as well as affecting the actual distribution.

As already mentioned, a number of parameters were varied in addition to total dose in this study. Additional plots of mass fraction versus molecular weight for a number of variations are included in appendix 4. Unfortunately, because of the aforementioned effect of branching on the apparent molecular weight distribution, valid numbers for average molecular weights cannot be calculated. Consequently, reliable quantitative estimates for the ratio of crosslinking to scission and the efficiency of the irradiation process cannot be made. It is possible to determine trends, however, and these are reported here. The ratio of crosslinking to scission was found simply by comparing areas with molecular weights above and below that of the starting material. The overall efficiency was assumed to be proportional to the area lost from the area under the initial distribution curve. By looking at these two simple things, the following trends were found.

pH effect. The overall efficiency was highest at neutral pH and fell as the pH was either increased or decreased, although it fell more as the pH was increased. The ratio of crosslinking to scission was highest at high pH and fell as pH was decreased. It was noted that there was some degradation taking place in unirradiated solutions at very low pH over the same time scale as the SEC experiment. One possible explanation for the effect of pH is the equilibrium shown in reaction 6 of table 2-1. At

high pH, this equilibrium is driven further to the right, eliminating ·OH radicals. This should decrease the importance of reaction 2, producing less H_2O_2. If degradation reaction 9, which requires the interaction of a PEO main chain radical with H_2O_2 is important, decreasing the amount of H_2O_2 should decrease the amount of chain scission and increase the ratio of crosslinking to scission. However, as ·OH is the active species in forming main chain radicals, the efficiency of the process should be somewhat decreased by reducing the number of hydroxyl radicals available. See reference [33] for more information.

Dose rate. The overall efficiency changed very little with dose rate, increasing only very slightly with a five-fold increase in dose rate. The ratio of crosslinking to scission, however, increased considerably with increasing dose rate. This can be explained simply by the fact that crosslinking is bimolecular in main chain radicals and scission is unimolecular. A higher dose rate should give a higher concentration of main chain radicals at any time, thus allowing crosslinking to compete more successfully with scission. However, the same dose should produce the same total number of radicals regardless of dose rate, so the overall efficiency should be unchanged.

PEO concentration. Both the overall efficiency and the ratio of crosslinking to scission increased with increasing PEO concentration. This can also be explained in terms of the rate of production of radicals. In the concentration range used in this study (less than 10 g/l PEO) the concentration of water does not change appreciably, so the

number of active radicals produced by water radiolysis should not change much. However, the PEO concentration changes by an order of magnitude, so the ability of PEO chains to compete with other species in reactions with the active radicals would be increased as the concentration increases, producing more main chain radicals per unit dose. This would clearly increase the overall efficiency, and in the same way as explained above, would also increase the ratio of crosslinking to scission.

Gaseous atmosphere. Three atmospheres were looked at in this study: O_2, N_2, and N_2O. No appreciable difference was found between O_2 and N_2 atmospheres, either in overall efficiency or in ratio of crosslinking to scission. The effect of N_2O was to increase the overall efficiency and decrease the ratio of crosslinking to scission. It should be noted that these measurements were carried out at a concentration and dose rate which did not allow any measurable crosslinking in even the N_2 solution. It is somewhat surprising that the presence of O_2 had virtually no effect on the ratio of crosslinking to scission, in light of previous studies which found that O_2 appreciably decreased the ease with which a solution was crosslinked. However, these earlier studies were done using gamma radiation at 2 to 3 orders of magnitude lower dose rates than in this study. It is reasonable to expect that at the lower dose rates the solution could stay saturated with the surrounding gaseous atmosphere, while at the dose rates used in this study it is unlikely. Therefore, only the O_2 originally present in the solution can have an effect on the irradiation process. Also, no information on the kinetics of the various important reactions are available; it is possible that at the dose rates

used in this study the kinetics of the reactions using oxygen cannot compete. The increased efficiency in the presence of N_2O is probably due to the following reaction between N_2O and an aqueous electron.

$$N_2O + H_2O^{-\cdot} \longrightarrow N_2OH^{\cdot} + OH^{-}$$

$N_2OH^{\cdot}$ has been shown to be capable of abstracting hydrogen from a PEO chain, producing a main chain radical.

Solution additives. In order to look more carefully at some of the possible chemical and physical effects important in irradiation, some studies were done on solutions of PEO to which other species had been added. The first attempt was to add a catalyst for the degradation of H_2O_2. Unfortunately, all the peroxide degradation catalysts examined caused considerable degradation of PEO even in the absence of irradiation, so it was impossible to gain any useful information about the possible interaction of H_2O_2 and PEO. It was next attempted to add H_2O_2 to look for acceleration of degradation. It was again observed that unirradiated samples showed degradation, but not enough to prevent conclusions from being drawn from the results. It was found that with H_2O_2 present, the amount of radiation-induced degradation was considerably less than in the absence of H_2O_2, both at pH 7 and at pH 13. There was no evidence in any of the measurements suggesting any crosslinking, but the overall efficiency was considerably decreased in the presence of H_2O_2, especially at pH 13. One possible explanation is that peroxide is scavenging radicals that would otherwise be interacting with PEO. This is supported by a report that less water radiolysis products are produced in water irradiated with H_2O_2 present than in pure

water [93]. Another possible explanation is that the solvent quality is reduced by the addition of H_2O_2 or NaOH (used to adjust pH). The evidence for this is that phase separation of the PEO solutions was observed to take place at room temperature at high enough concentration of either of the two species. Reducing the solvent quality would cause the conformation of the chains to change from highly open to much tighter coils, which would be less penetrable by the solvent. This might make it less likely for the chains to interact with water radiolysis products. As a check on this, a set of irradiations was done using various amounts of K_2SO_4 as additive. The cloud points of these solutions were also measured to give a ranking of solvent quality; see section 4.5. The SEC work on these samples was done in aqueous K_2SO_4 solutions to avoid the desalting problem. The results support the hypothesis that decreasing the solvent quality decreases the irradiation efficiency. It should be noted that at the conditions of this study the PEO chains exist as discrete, non-interpenetrating coils, and the results might be quite different at higher concentrations.

4.3. Supported Membranes.

4.3.1. Thickness of PEO Layer.

Figure 4-20 is a scanning electron micrograph of a supported PEO membrane. The fibrous material is the non-woven polyester (Remay) support. The layer on top is the PEO coating. The PEO layer has collapsed somewhat in thickness during the dehydration and drying

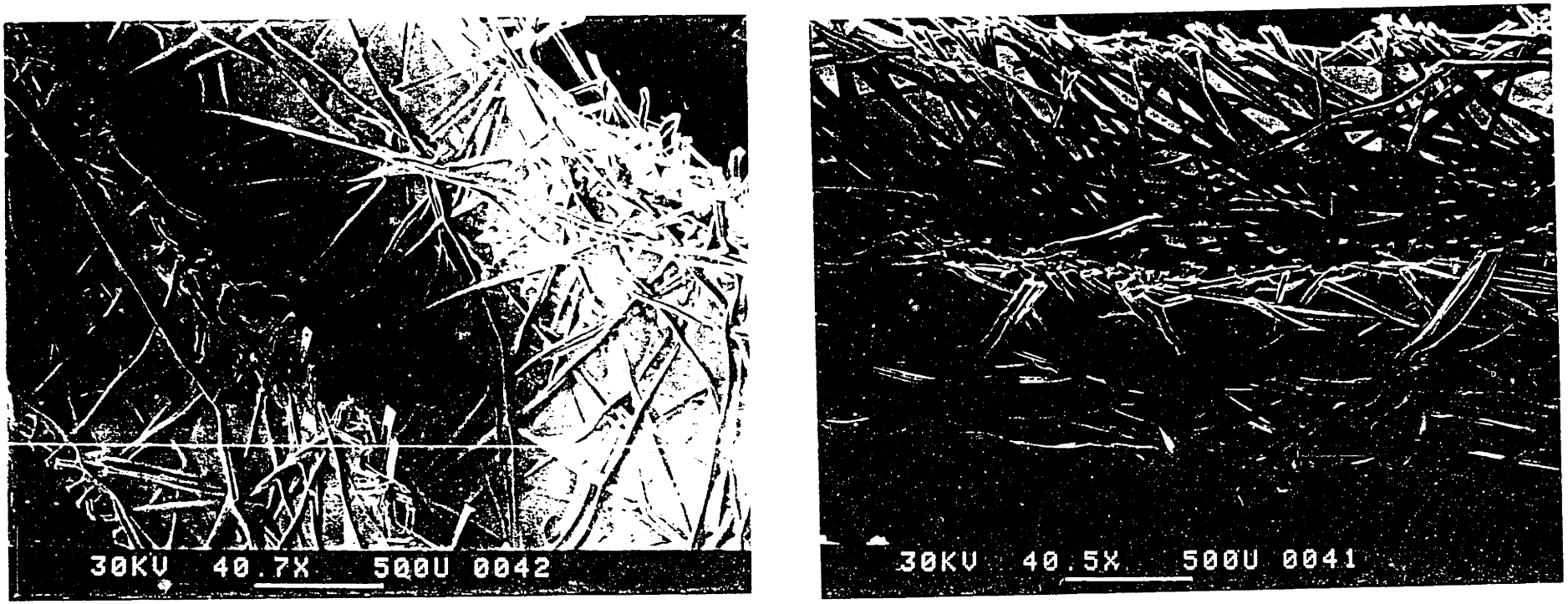

Figure 4-2. Scanning electron micrograph of Kemav-supported PEC membrane. Left photo shows the PEC side of the membrane and right photo shows the Kemav side, with the PEC showing through the fibers.

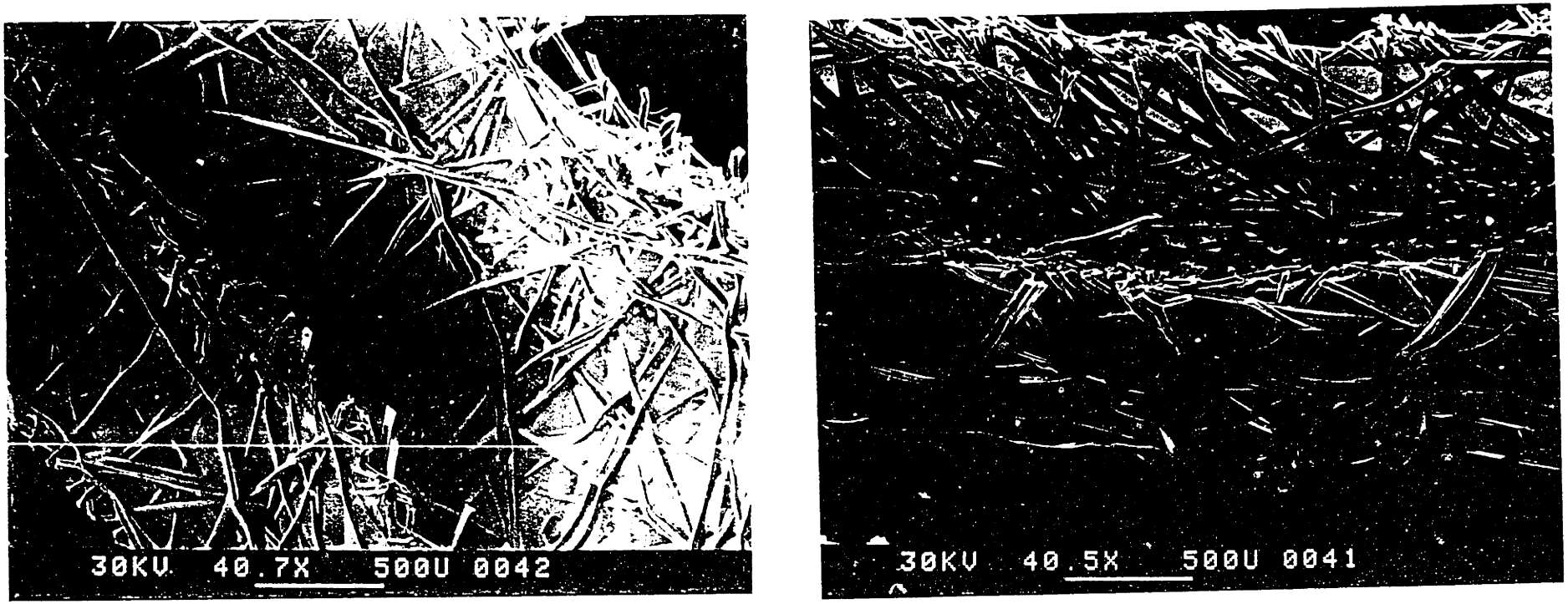

Figure 4-20. Scanning electron micrograph of Remay-supported PEO membrane. Left photo shows the PEO side of the membrane and right photo shows the Remay side, with the PEO showing through the fibers.

process, as it would be about half the thickness of the support when swollen. The PEO-coated side of the membrane is the side that was formed in contact with the glass plate. From this micrograph it appears that the PEO layer is restricted to one surface of the support and penetrates only slightly if at all into the support. This is also seen in light microscopy on swollen gels. Also, multiple internal reflectance IR spectroscopy indicates a virtually complete gel layer on one side and no PEO on the other. Because the layer is confined mostly to the surface, it is possible to get a measure of the PEO layer thickness by subtracting the support thickness from the composite membrane thickness. The thickness of the PEO layer ranged from about 50 to about 150 μm, depending on the initial concentration and dose.

4.3.2. Swelling of Supported Membranes.

The swelling characteristics of a set of supported membranes were measured and compared with those of the unsupported gels made using the same conditions. Two conditions were used, and four membranes were made at each condition and the results averaged. For a 200 g/l solution given 10 Mrad, the unsupported gel had an equilibrium polymer volume fraction of 0.0383, while the supported membrane v_{2s} was 0.0666. The supported membrane is swelling only about 60% as much as the unsupported gel. For 200 g/l at 20 Mrad, the unsupported v_{2s} was 0.0741 and the supported v_{2s} was 0.0832, which means the supported gel is swollen to 90% of the unsupported value. Since there is no real reason to think the irradiation process would be greatly different for the supported and

unsupported gels, and thus the crosslink density should be the same for the two, the difference in degree of swelling must be due to the presence of the non-swelling support material. If the chains are attached to the support either physically or chemically at the initial polymer volume fraction, which is higher than the equilibrium value by a factor of two or more, there is probably some addition to the elastic retractive forces generated close to the support due to the high modulus fibers holding the gel down. There is some evidence for anisotropic swelling in the most highly swollen gels, which tend to curl slightly with the PEO on the convex surface.

4.3.3. Integrity Testing.

The integrity testing indicated that in general the attempt to make supported membranes was unsuccessful. All membranes of any initial concentration given 7.5 Mrad or higher doses had pinholes. The success rate for membranes give 2.5 or 5.0 Mrad was higher, ranging from 50 to 75% non-leaky, with the highest success rate at the highest concentration. The relationship with total dose leads to the conclusion that it is probably either holes produced by trapped gas bubbles or small uncrosslinked regions caused by evaporation due to the temperature rise that are causing the membranes to leak. Gas bubbles are very evident in unsupported gels made at high doses, and while there are no bubbles entirely trapped in the gel layer of the supported membranes because of the thinness of the layer, it is quite possible that a bubble could be trapped between the membrane and the glass plate during irradiation and

extend far enough into the membrane to completely penetrate the gel layer.

4.4. Porous PEO Gels.

4.4.1. Scanning Electron Microscopy.

Figure 4-21 is a scanning electron micrograph of a PEO gel made by irradiating a solution of 50 g/l PEO 35000 in 0.5 M K_2SO_4. The total dose was 5 Mrad at a dose rate of 250000 rad/s. There is a very open pore structure in the gel, with pores of around 10 μm diameter. A series of gels were made by varying the K_2SO_4 concentration and the dose rate, while leaving the total dose and PEO concentration constant. Figure 4-22 is a qualitative summary of the results of this series. The micrographs are found in appendix 5. It appears that porous gels can be produced only in a limited range of K_2SO_4 concentration and dose rate. At high salt concentrations and low dose rates, the solutions phase separate before the network structure is locked in, which is obvious from an inspection of the samples both before and after irradiation. The structures resulting from irradiation have macroscopic droplets of clear (homogeneous) PEO gel in a pool of cloudy solution. At low salt concentrations and high dose rates, gels which appear homogeneous in scanning electron micrographs and are clear on visual inspection are produced. These gels look similar to the gels produced by irradiation in pure water. In the range of K_2SO_4 concentrations and dose rates in between, gels with pores of slightly varying sizes are produced. These

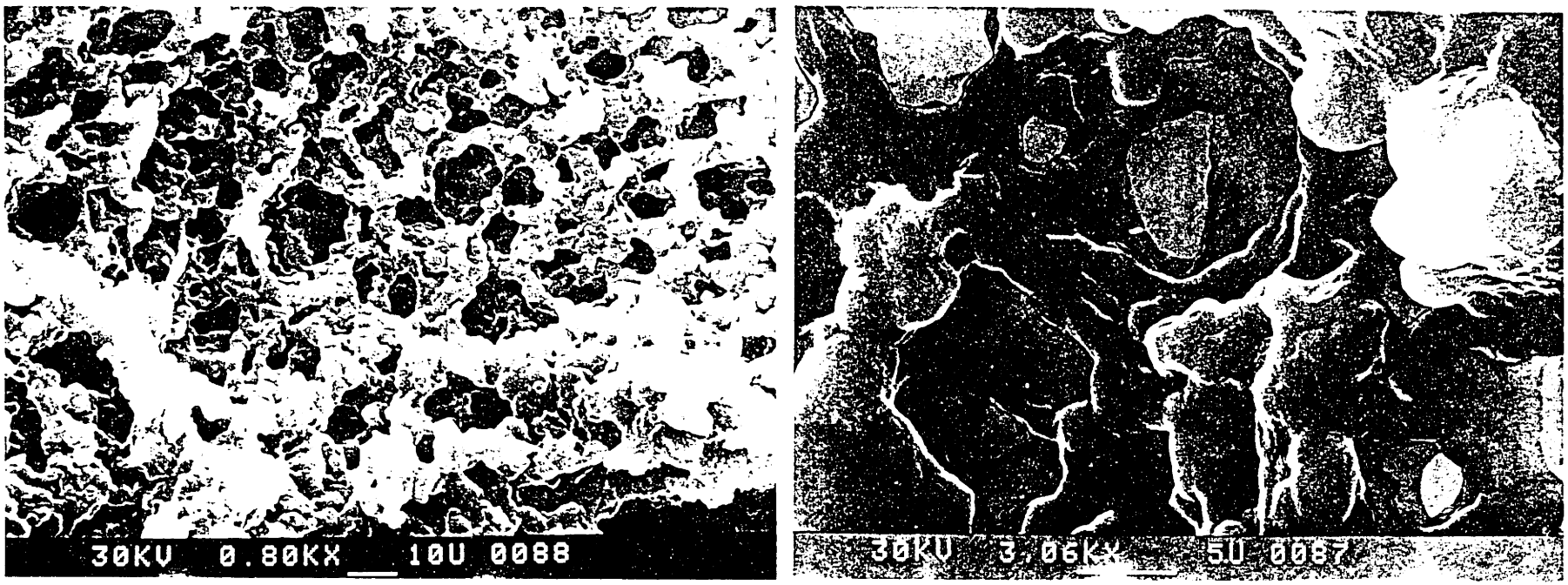

5% PEO 35000, 5 Mrad, 0.5 M K_2SO_4, 100,000 rad/sec

Figure 4-21. Scanning electron micrograph of a cross-section of a gel synthesized in K_2SO_4 solution showing the porous nature of the gel.

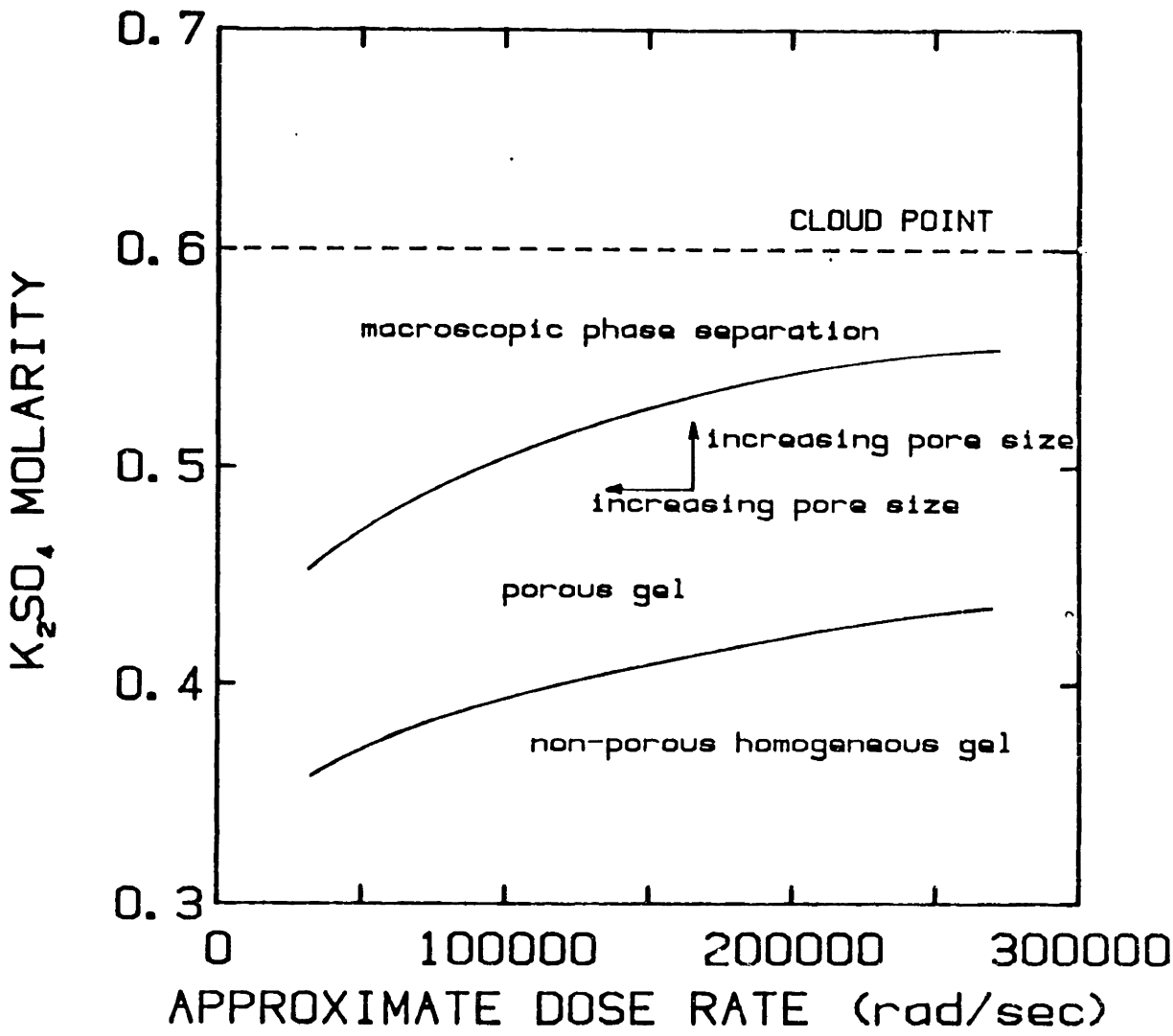

Figure 4-22. Diagram of gel types resulting from irradiation of 5% PEO 35000 under different conditions. Total dose constant at 5 Mrad.

gels look cloudy on visual inspection, which is a sign of inhomogeneities of size on the order of the wavelength of light or larger. Figure 4-23 shows micrographs of opposite surfaces of the same gel. The surfaces have been somewhat arbitrarily designated upper and lower, but these designations may not correspond to the surfaces away from and next to the glass during irradiation. There is clearly a difference between the two surfaces. The lower surface is much less porous than the upper. This membrane would clearly have transport properties similar to asymmetric membranes made by the traditional techniques of phase-inversion. Transport would be controlled by the thin (see cross-sections in appendix 5) but tight skin layer, and the rest of the membrane would serve mostly as spacer. The cause for the asymmetry is not clear because the upper and lower designations are arbitrary. Because of the affinity of PEO for glass as well as the density difference between PEO and water, the less porous surface is probably the one formed on the bottom, against the glass.

4.4.2. Swelling Measurements.

Swelling measurements were done on the series of gels. Because of the presence of the pores, the equilibrium solvent volume fraction included not only the water swelling the gel but also the water filling the pores. The measured polymer volume fractions thus cannot be used in the theory relating degree of swelling and crosslink, so interjunction molecular weights could not be obtained. Figure 4-24 is a plot of the measured volume fraction of polymer as a function of crosslinking conditions. For

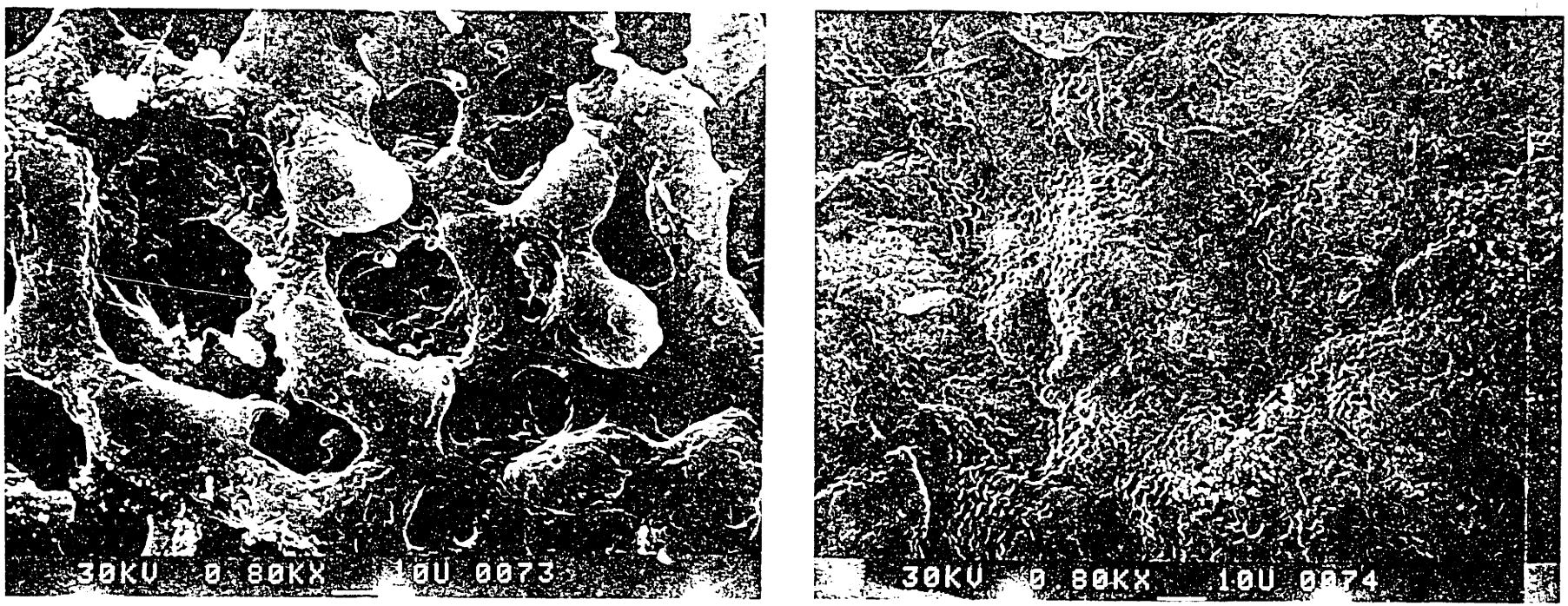

Top Surface

Bottom Surface

5% PEO 35000, 5 Mrad, 0.5 M K_2SO_4, 250,000 rad/sec

Figure 4-23. Scanning electron micrograph showing upper and lower surfaces of porous PEO gel. Upper and lower surfaces are designated somewhat arbitrarily; see text.

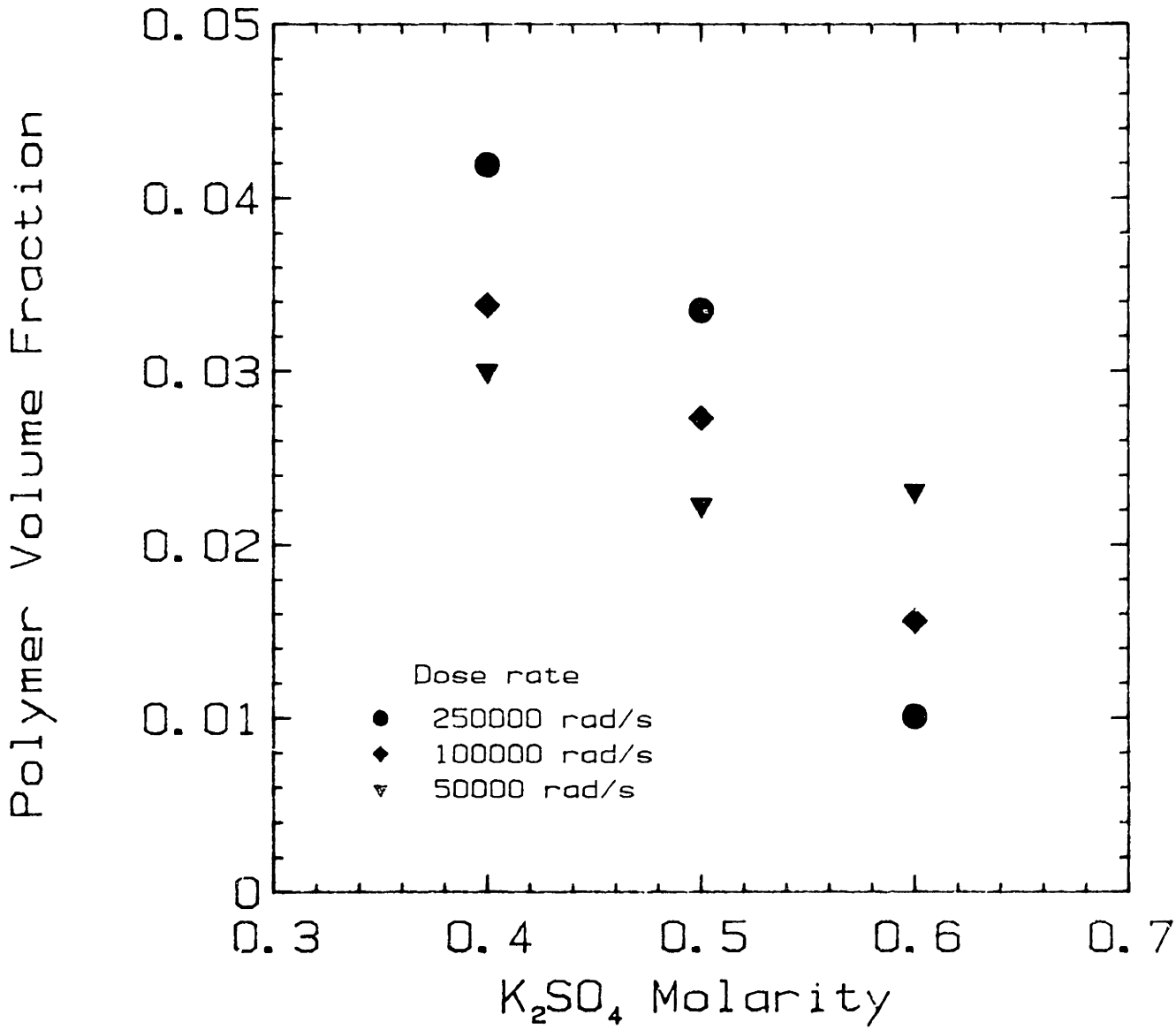

Figure 4-24. Volume fraction of polymer in the gel in equilibrium with pure water as a function of K_2SO_4 concentration in the irradiated solution.

comparison, v_{2s} for a gel made at the same concentration and total dose at 250000 rad/s in pure water would be about 0.0275. The gels made at the highest K_2SO_4 concentration swelled considerably more than the control. This is probably because phase separation took place prior to crosslinking and the part of the sample crosslinked actually had a considerably higher concentration of PEO than 50 g/l. The lower K_2SO_4 concentration samples showed an increase in v_{2s} with increasing dose rate, and all samples showed an increase in v_{2s} with decreasing K_2SO_4 concentration.

The samples were reswollen after vacuum drying at 40°C for about 24 hr. It was found that none of the samples swelled as much after drying as they did originally. This is in contrast to gels crosslinked in pure H_2O, which reswell to the original degree after vacuum drying. The gels also tended to be less opaque after reswelling and were considerably stronger. Figure 4-25 is a plot of the swelling data for the reswollen gels, and table 4-4 summarizes the conditions used and the swelling results for the gels synthesized in K_2SO_4 solutions.

4.4.3. SEM on Reswollen Gels.

It was suspected that the reason for the decrease in degree of swelling after drying the gels was a result of an irreversible collapse of the pores. To further investigate this, a series of scanning electron micrographs was taken on gels that had never been dried, gels that had been dried and reswollen, and gels that had been freeze dried and

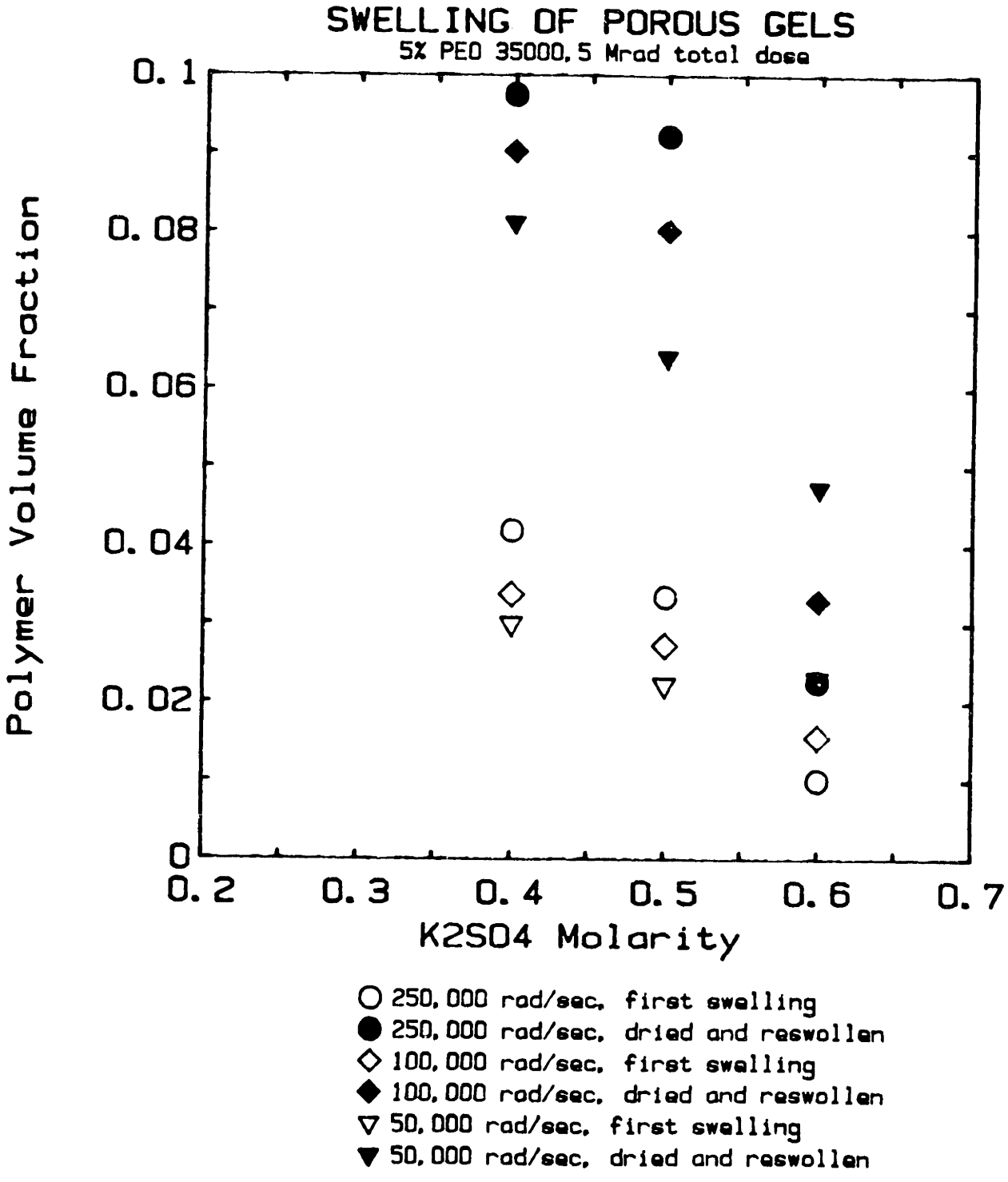

Figure 4-25. Polymer volume fraction of gels in equilibrium with pure water both before and after drying, illustrating irreversible collapse of the structure during drying. The x -axis is the K_2SO_4 concentration in which the PEO was irradiated.

K_2SO_4 (mol/l)	Dose rate (rad/s)	v_{2s} initial	v_{2s} reswollen
0.4	50000	0.0300	0.0812
0.4	100000	0.0338	0.0902
0.4	250000	0.0419	0.0975
0.5	50000	0.0223	0.0641
0.5	100000	0.0273	0.0802
0.5	250000	0.0335	0.0922
0.6	50000	0.0231	0.0474
0.6	100000	0.0156	0.0330
0.6	250000	0.0101	0.0227

Table 4-4. Summary of swelling results for gels made in K_2SO_4 solution. Initial PEO concentration was 50 g/l and total dose was 5 Mrad for all samples. Initial v_{2s} is the polymer volume fraction in gel fully swollen in pure water after irradiation. Reswollen v_{2s} is the polymer volume fraction of the same gel after being vacuum dried and re-equilibrated with pure water.

reswollen. All gels were dehydrated and critical point dried identically prior to SEM. Figure 4-26 shows micrographs of the surface of a piece of gel that was not vacuum dried (control) and a piece of the same gel that was vacuum dried and reswollen. While the surface shot does not clearly show the collapse of the gel on drying, it is apparent in figure 4-27, which shows cross-sections of the same gel. As the micrographs are at the same magnification, the most striking thing about the two samples is the difference in thickness. The dried sample has become much thinner. However, the loss of thickness was not accompanied by a corresponding loss of diameter of the sample, that is, the collapse of the gel was not isotropic. It can also be seen from this sample that the pores have indeed collapsed to a considerable extent. (Additional micrographs are included in appendix 5). The difference between the upper and lower surfaces of the gel appears to be much less after drying and reswelling. Gels that were freeze-dried and reswollen did not show the same loss of volume as the vacuum dried gels, and microscopy revealed no apparent changes in pore structure from the undried samples. The SEM work on the dried gels tends to support the conclusion that the change in degree of swelling caused by drying is indeed due to irreversible collapse of the pore structure. Attempts to measure the change in porosity using albumin as a probe were unsuccessful, apparently due to evaporation of some of the solution introduced (see section 3.6.2 for procedure used).

From the results of all the studies on the porous gels, it appears that the structure is the result of liquid-liquid phase separation and crosslinking occurring simultaneously. The process can be envisioned as

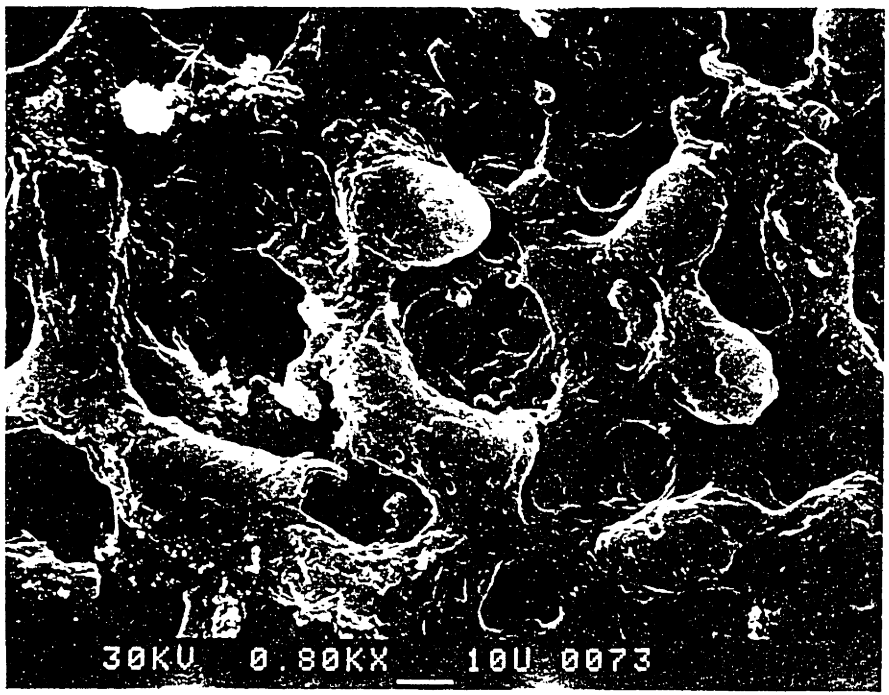

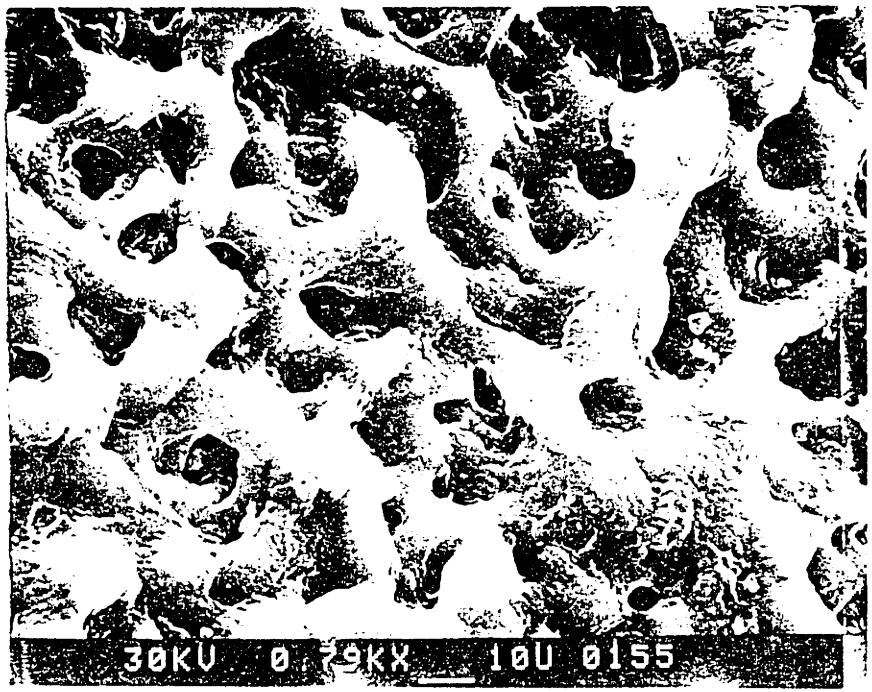

Control

Vacuum Dried

5% PEO 35000, 5 Mrad, 0.5 M K_2SO_4, 250,000 rad/sec

Figure 4-26. Scanning electron micrograph showing the surface of two pieces of the same gel. The photo marked control was kept swollen until critical point drying, and the one marked vacuum dried was vacuum dried and reswollen, then critical point dried.

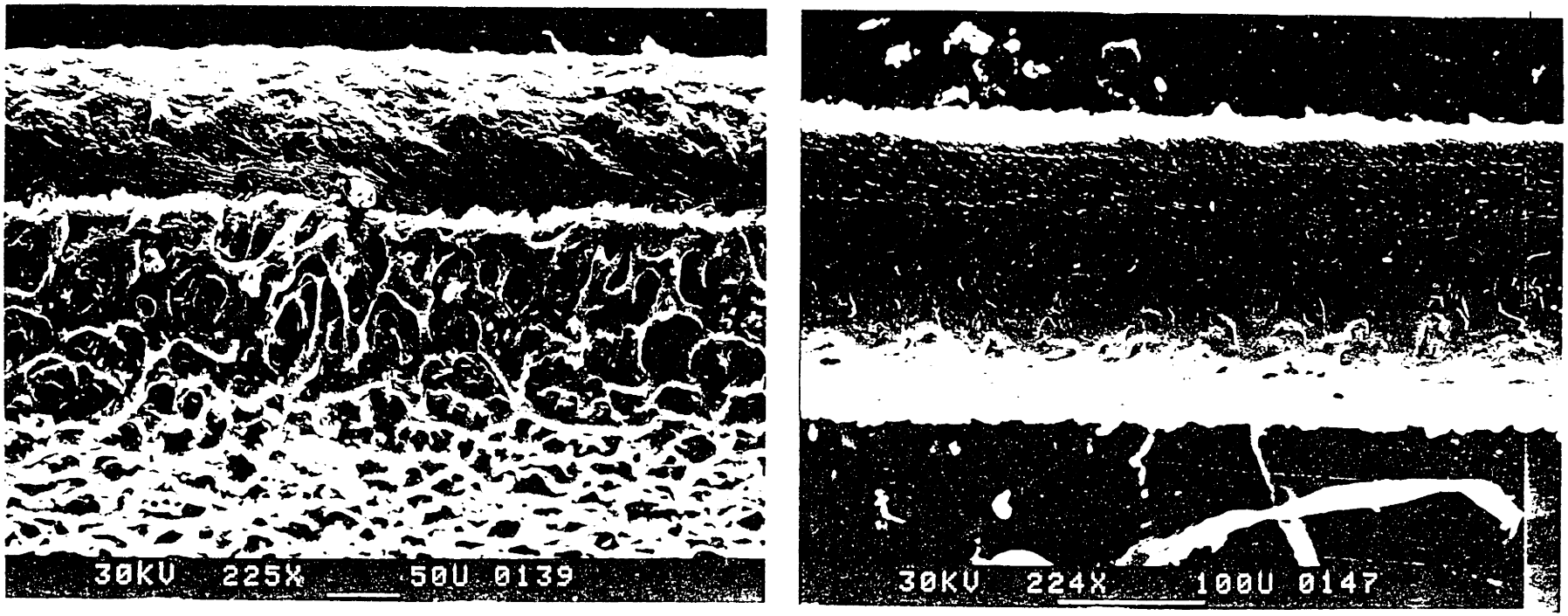

Control

Vacuum Dried

5% PEO 35000, 5 Mrad, 0.5 M K_2SO_4, 250,000 rad/sec

Figure 4-27. Scanning electron micrograph of a cross-section of the same pieces of gel as figure 4-26.

follows. Irradiation starts, producing a few crosslinks. Something in the irradiation process causes phase separation to start, causing large local differences in PEO concentration. The high PEO concentration regions continue to crosslink, at an accelerated rate because of the increased concentration, while the low concentration regions, containing mostly solvent, do not crosslink appreciably. The highly crosslinked regions lock in the solvent regions, creating pores. Clearly the kinetics of the crosslinking and phase separation processes are critical, hence the differences in structure observed at different dose rates. It is not clear from this work exactly why the phase separation occurs. There are several possible reasons, all of which are addressed in section 4.5 on PEO - salt solution interactions. First, it is known that the temperature of the samples increases during irradiation. Perhaps the increase is sufficient to reach the cloud point of the solutions used after some relatively small dose. A second possibility is that sufficient crosslinking has taken place prior to phase separation to increase the effective molecular weight enough to reach the cloud point. It is also possible that the early stages of crosslinking produce enough concentration fluctuations in the solution to cause local phase separation, which would be a self-accelerating process, leading to large scale phase separation. Clearly there must be sufficient crosslinking occuring to lock in some structure before the phase separation progresses too far to produce a porous structure. If the crosslinking process is too slow relative to phase separation, macroscopic phase separation occurs, leading to a non-porous structure. However, if the structure is completely locked in before phase separation starts, solvent is expelled

from the network as in syneresis rather than an actual phase separation occurring, leading to a homogeneous structure.

4.5. PEO - Salt Solution Interactions.

4.5.1. Phase Separation in K_2SO_4 Solutions.

The cloud point (phase separation temperature) was measured for a series of PEO and K_2SO_4 concentrations. The results are presented in figure 4-28. It is interesting that the expected change from negative to positive dependence of cloud point on concentration is not observed, especially as lattice theory [19] predicts a critical concentration for this polymer ($\bar{M}_n$ = 37000) of about 4 g/l. This may be in part due to crystalline phase separation taking place at higher PEO and K_2SO_4 concentrations as the solvent quality decreases. It was noted that there appeared to be three phases present in some of the high PEO concentration samples. One was clearly a crystalline PEO phase, and the others were two amorphous liquid phases. Also, as discussed earlier, the applicability of lattice theory to the three-component PEO - salt - water system is questionable.

Cloud point measurements were also made at a single PEO and salt concentration for a number of other salts. Because previous work suggests that PEO interacts with cationic species, the cation concentration was held constant at 0.6 mol/l. The results of these measurements are summarized in table 4-5, along with the salt partitioning results addressed in the next section. It is interesting

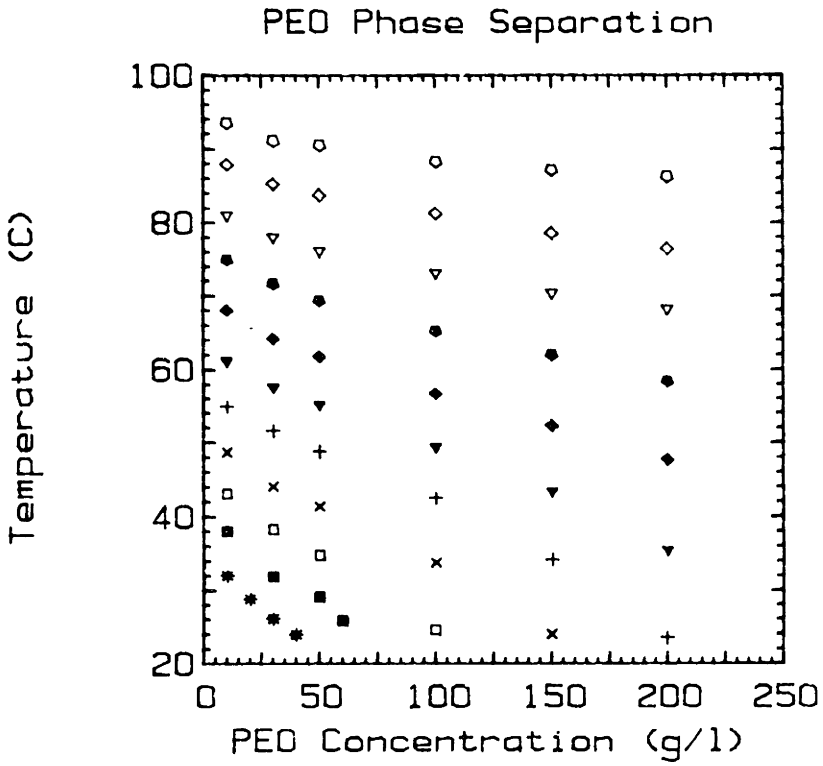

Figure 4-28. Phase separation temperature as a function of PEO concentration for solutions of 35000 molecular weight PEO in water with various concentrations of K_2SO_4. The symbols are as follows.

- ○ 0.10 M K_2SO_4
- ◇ 0.15 M
- ▽ 0.20 M
- ● 0.25 M
- ◆ 0.30 M
- ▼ 0.35 M
- \+ 0.40 M
- × 0.45 M
- □ 0.50 M
- ■ 0.55 M
- ✱ 0.60 M

Salt	Partition Coefficient	Cloud Point (°C)	$v_{2,salt}$
H_2SO_4	2.34	> 100	0.0458
KI	1.58	> 100	0.0489
NaI	1.39	> 100	0.0462
LiCl	1.39	> 100	0.0463
NaCl	1.29	92	0.0498
Na_2HPO_4	1.24	65	0.0712
$CaCl_2$	1.15	94	0.0460
Na_2CO_3	1.12	66	0.0652
K_2SO_4	1.04	68	0.0634
$MgSO_4$	0.99	38	0.0963
Pure Water	-	> 100	0.0458

Table 4-5. Results of salt partitioning and cloud point measurements. Salt partitioning is between water and a PEO gel synthesized from a 150 g/l solution of PEO 35000 in pure water given 10 Mrad of electron irradiation. The resulting gel had a polymer volume fraction at equilibrium in pure water of 0.0458 and an interjunction molecular weight of about 5000. Cloud point measurements were on a 10 g/l solution of PEO 35000. All salt solutions were 0.6 mol cation/l.

that at the PEO molecular weight and concentration used (35000 and 10 g/l), some of the salts did not depress the cloud point below 100°C. This is quite different from the results of Bailey and Callard [23], who used 4000000 molecular weight PEO at a concentration of 5 g/l, but the difference can be attributed to the difference in molecular weight. The presence of salt in the samples used in this study probably lowered the cloud point, but the phase separation temperature for this PEO in pure water is well above 100°C, so this was not observed.

4.5.2. Salt Partitioning.

The use of loosely crosslinked PEO gels provides a simple way of looking at salt partitioning between PEO and water, which may shed some light on the question of what type of interactions cause the salting out phenomena discussed above. Partitioning measurements were done using the same salts at the same constant cationic molarity as in the cloud point measurements. Two pieces of information were obtained from these measurements: the equilibrium distribution or partition coefficient between water and PEO gel for each salt and the swelling ratio for the gel (pieces of the same gel were used in all measurements) in each salt. These results are included in table 4-5. There is a good correlation between the polymer volume fraction of the gel fully swollen in the salt solution and the phase separation temperature for linear PEO in salt solution. This decrease in swelling ratio (increase in polymer volume fraction) is evidence collapse of the PEO coils due to the decrease in effective solvent quality and is the same effect seen by Bailey and

Callard [23] in their intrinsic viscosity measurements. It is interesting that the salts which preferentially partition into the PEO gel are not the ones which cause phase separation. Previous workers [12,25] have suggested that the opposite should be the case, based on the assumption that the PEO coil must collapse to put the cationic species in the right location for complexation. The current work also indicates that it is the anionic species that is important in determining salt partitioning, and to some extent the solvent quality. This is also somewhat at variance with previously reported work, which suggests that the cationic species is the one interacting with the polymer coil. If this were the case, it would be expected that the cation would control the salt distribution between polymer and solvent.

Of the two theories previously put forward to explain the salting out effect of salts added to aqueous PEO solutions, one based on the disruption of water structure and the other on the complexation of salt by the PEO chain, the results of this study could be viewed as supporting the water-structure disruption theory. This is because the salts which are most interactive with the polymer chain, i.e., the ones that are complexing with PEO, cause the least salting out effect. It therefore appears that salting out is due to an effect on the water. If the theory based on chain collapse due to ionic complexation with the PEO chain were correct, the most highly partioning salts should show the greatest decrease in phase separation temperature, and this is clearly not the case. It thus appears that salt complexation by the chain does not cause the observed decrease in solvent quality. In fact, complexation of salts

with PEO may increase the solvent quality and offset some of the water-structure disruption. If this is the case, it will help explain the differences observed in salting out behavior and ranking in the Hofmeister series of various salts. If the PEO chain is strongly complexing with an ionic species, it may begin to behave in a manner approximating a polyelectrolyte coil. Increasing the number of complexed charges would tend to expand the coil and increase its solubility. Another way in which salts which complex with the chain could be viewed as causing an increase in solvent quality is in the effect on water associated with the PEO chains. It is this association, leading to a negative excess entropy of mixing, which is assumed to be responsible for the lower critical solution temperature of PEO [12]. Salts which are associated with the PEO chain should decrease the degree to which water in the vicinity of the chain is ordered, thus decreasing the negative entropy of mixing, and offsetting the salting out effect of the salt in solution. It appears from this study that the anionic species is more important than the cationic in controlling this behavior, although there is insufficient data to draw a definite conclusion. It is not clear why this would be the case.

4.5.3. PEO - Salt Solution Interactions and Porous Cel Synthesis.

It is interesting to reexamine the results of the porous gel synthesis measurements in terms of the phase separation temperature measurements done on PEO in K_2SO_4 solutions to try to determine which of the three proposed mechanisms for inducing phase separation is correct. The three

suggested causes for phase separation were increase in temperature, increase in molecular weight, and local increase in concentration. From the K_2SO_4 cloud point measurements it appears that porous gels are produced in samples that have cloud points ranging from about 30 to 50°C, depending on the dose rate. The highest cloud points correspond to samples that phase separated only at the lowest dose rate. Temperature measurements on samples during the irradiation process indicate that the temperature in the sample increases about 6°C/Mrad at low doses. This suggests that the samples producing porous structures at high dose would do so as a consequence only of temperature effects, as the temperature rise during the initial stages of irradiation (the first pass) would be sufficient to lead to phase separation and the dose would be enough to cause gelation in the same time frame. The samples at the lowest K_2SO_4 concentrations would not reach phase separation temperature during the first pass of 2.5 Mrad but would receive sufficient dose to cause gelation, locking in a homogeneous structure. It is not completely clear whether temperature alone could explain the porous gel structure seen in high cloud point, low dose rate samples. The dose required to raise the temperature to the cloud point would be about 3 Mrad. At a dose rate of 125000 rad/s in pure water the gel dose for a 50 g/l PEO solution is about 1.5 Mrad; it is not clear whether the presence of K_2SO_4 and the decrease of dose rate to 50000 rad/s would lower the crosslinking efficiency enough to increase the gel dose to 3 Mrad. However, the increase in molecular weight and local concentration fluctuations mentioned above may now start to have an effect on lowering the phase separation temperature, so it is probably some combination of the three

effects which is operative at these lower dose rates.

4.6. Effective Diffusivity Measurement Results.

Table 4-6 contains a summary of the interjunction molecular weight M_c and the equilibrium polymer volume fraction v_{2s} in both water and phosphate-buffered saline (PBS, the solvent used in all diffusivity measurements) for the gels used in the transport measurements. It was desirable to produce a set of gels with as wide a variation in the structural parameters v_{2s} and M_c as possible. Two factors limited the range that could be used. The necessity of remaining in the regime where the solution-diffusion theory should be valid limited the polymer volume fraction to values below 0.1. Additionally, it was necessary that the gels be sufficiently strong to permit testing, which further limited the range available. It was also desirable to be able to independently vary M_c and v_{2s}. Since the two are related, there was a fairly limited range over which this was possible. Figure 4-29 is a plot of interjunction molecular weight as a function of polymer volume fraction for the gels used for diffusivity measurements, which illustrates the limited ability to vary the two independently.

Figure 4-30 is an example of the diffusivity results obtained for a single gel. The effective diffusivity in the gel D_{eff} for each solute was measured in triplicate with variations on the order of 10 to 20% between the three values. It was very difficult to measure diffusion coefficients below about 10^{-12} cm^2/s, and the estimated error in the

Gel	PEO Conc.	Irradiation Dose	v_{2s}(Water)	v_{2s}(PBS)	M_c
3%,2.5	30 g/l	2.5 Mrad	0.0172	0.0229	6926
3%,5	30 g/l	5.0 Mrad	0.0272	0.0349	3648
5%,2.5	50 g/l	2.5 Mrad	0.0137	0.0166	10425
5%,5	50 g/l	5.0 Mrad	0.0269	0.0386	5229
10%,2.5	100 g/l	2.5 Mrad	0.0074	0.0092	14655
10%,5	100 g/l	5.0 Mrad	0.0198	0.0232	10119
10%,10	100 g/l	10.0 Mrad	0.0461	0.0616	3752
10%,15	100 g/l	15.0 Mrad	0.0618	0.0849	2196
15%,5	150 g/l	5.0 Mrad	0.0187	0.0207	11671
15%,10	150 g/l	10.0 Mrad	0.0458	0.0616	4898
15%,15	150 g/l	15.0 Mrad	0.0639	0.0866	2898
20%,5	200 g/l	5.0 Mrad	0.0147	0.0175	13723
20%,10	200 g/l	10.0 Mrad	0.0483	0.0657	5436
20%,15	200 g/l	15.0 Mrad	0.0623	0.0840	3804

Table 4-6. Equilibrium polymer volume fraction v_{2s} in water and phsophate-buffered saline and interjunction molecular weight M_c of gels used in effective diffusivity measurements. M_c is determined from v_{2s} and the initial concentration using the swelling properties and the Flory-Bray affine deformation theory.

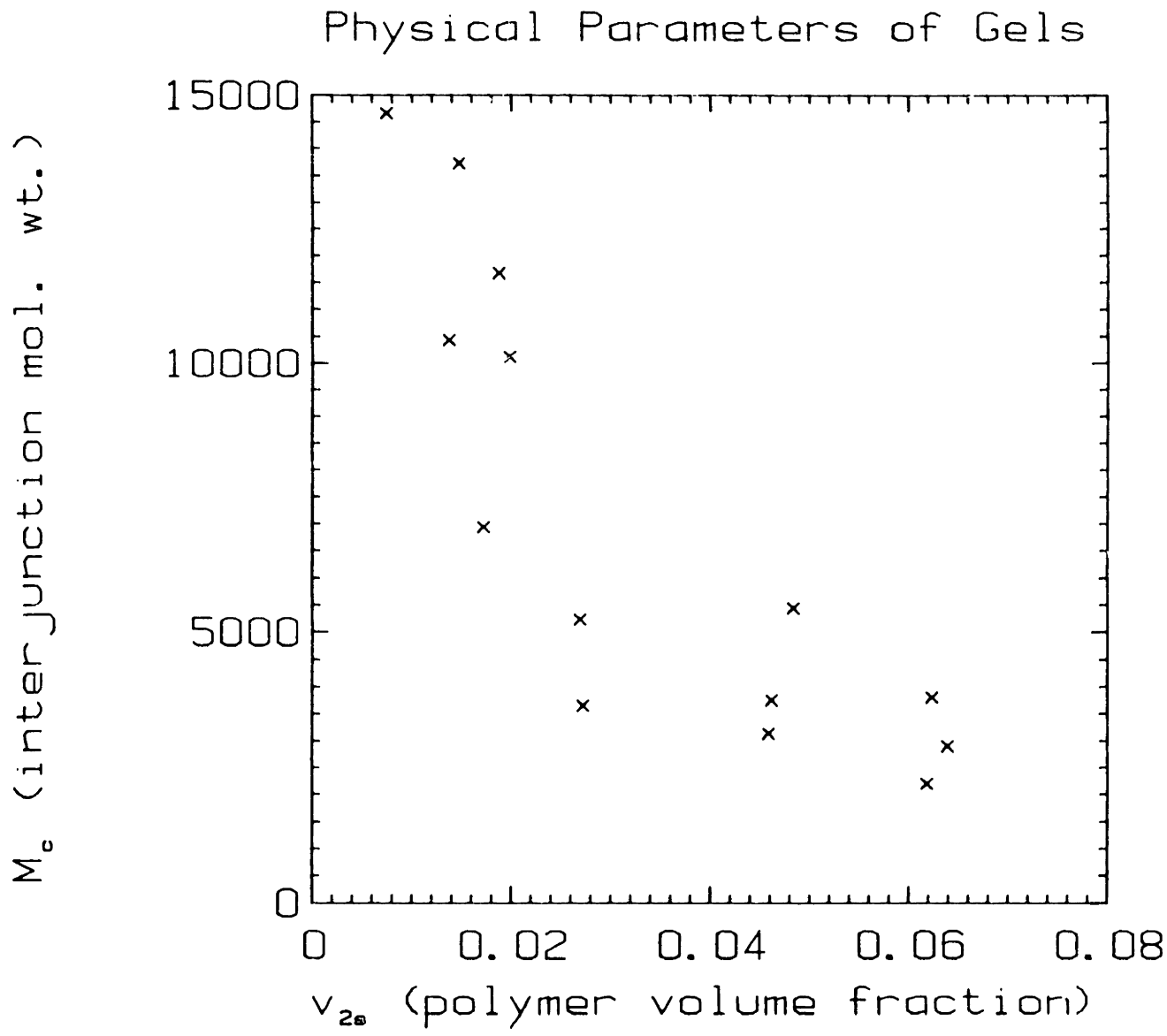

Figure 4-29. Interjunction molecular weight as a function of polymer volume fraction for the gels used in the effective diffusivity measurements, illustrating the ranges of these parameters available.

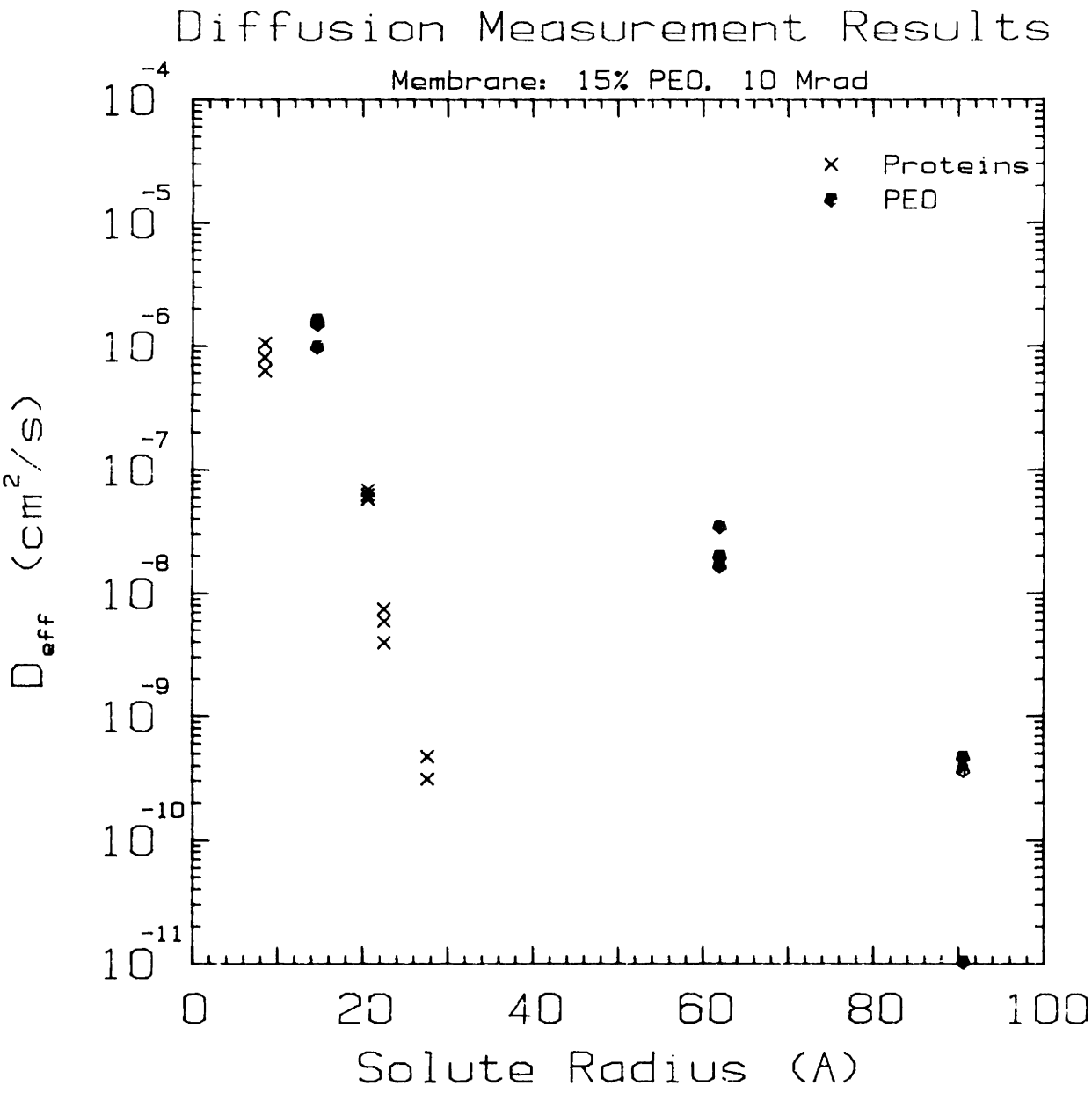

Figure 4-30. Effective diffusivity as a function of solute size for a 15% PEO, 10 Mrad gel. M_c = 4898, v_{2s}(PBS) = 0.0616.

measurements increases from around 20% for higher values of D_{eff} to about 50% for the lowest values, due mainly to protein denaturation and solvent evaporation caused by the longer times required to measure low diffusivities. A value of $D_{eff} = 0$ indicates that the diffusivity was too low to be measured, i.e., below 10^{-12}, for all three samples. Plots similar to figure 4-30 for the other networks are included in appendix 6.

4.6.1. Partition Coefficients.

The partition coefficient K was measured for each solute in each gel. It was found that there was no systematic difference in partition coefficient with gel except for those gels which completely excluded certain solutes and thus the non-zero values were averaged for each solute and the average values used for subsequent calculations. These values are summarized below. The partition coefficient reported here is defined as the ratio of the concentration of solute in the solvent in the gel to the concentration of solute in the external solution. Only a single number is reported for PEO as all three samples partitioned identically.

Solute	K
Cyanocobalamin	1.10
Lysozyme	0.85
Chymotripsinogen	1.05
Ovalbumin	1.15
Albumin	1.05
PEO	1.20

It should be noted that a value near unity indicates that the solute does not prefer to be either in or out of the gel, that is, there are no interactions between the solute and the polymer, which is one of the requirements for use of the solution-diffusion theory of transport in polymer networks. It is not clear whether the differences from unity of these partition coefficients or the differences in partition coefficient for the different solutes are significant or a result of experimental error, which is estimated to range from about 10% for the smaller solutes to 20% for the largest. The value of 1.2 for PEO confirms the observation from liquid lattice theory that while phosphate-buffered saline is a reasonably good solvent for PEO the energy of interaction between two PEO chain segments is less than the energy of interaction between a PEO chain segment and the solvent (i.e., water), so the chains preferentially partition into the gel. (In lattice theory this is reflected by a value of χ_1, the Flory-Huggins interaction parameter, greater than zero but less than 0.5.) It is possible to make an estimate for the partition coefficient of a solute between pure solvent and a polymer solution based only on the effect of steric exclusion using principles of liquid lattice theory [94]. This calculation always predicts a partition coefficient less than 1, which suggests that the values slightly larger than one observed here do reflect some small enthalpic interaction.

Previous workers, in particular Wisniewski and Kim [50] working with polyHEMA, have reported a dependence of partition coefficient on the properties of the gel. They noted a decrease in partition coefficient

(defined as the ratio of solute concentration in the solvent fraction of the gel to concentration in the solvent) with increasing polymer volume fraction, which they attributed to changes in the relative amounts of bound and free water. They developed a model of water structure within the gel which suggested that the solutes were partitioning only into the bulk water portion of the water in the gel. This effect is not seen in the present work, and there are two reasons why it would be important in the system used by Wisniewski and Kim and not in this study. One reason is the large difference in swelling ratio between the two types of gels, which will affect the relative amounts of bound and bulk water. If one assumes that three water molecules associate with each ethylene oxide unit in the PEO chain, that the molar volume of water is 18 cm^3/mol, and that the molar volume of an ethylene oxide unit is about 37 cm^3/mol, there would be a volume ratio of bound water to PEO of about 1.46, that is, the volume fraction of bound water is $1.46(v_{2s})$. The volume fraction of bound water would thus range from about 0.025 to 0.125 for these gels, and the fraction which is bound of the total water in the gel would be about 0.025 to 0.137. These amounts and the differences from one gel to another are relatively insignificant, especially when the amount of error in the measurements is considered. The polyHEMA gels of Wisniewski and Kim had much higher polymer volume fractions, around 0.45, and the bound water was up to 50% of the total water in these gels, so there would be a much more significant contribution of bound water in their gels. The other possible factor is the enthalpic interactions that may be taking place between the polymer and solutes. In the present study, the bulk of the solutes are proteins, which would be expected to have some small

attractive interaction with the chains. Wisniewski and Kim used mostly small neutral molecules which would be less likely to be either attracted to or repulsed by the polymer chains, although certain of the solutes were. If there are interactions with the polymer, the results of partitioning measurements clearly will not reflect only the structure of water in the chains.

4.6.2. PEO Effective Diffusivities.

Table 4-7 is a summary of the results of the effective diffusivity measurements with PEO as solute. The diffusion coefficient in the gel (in cm^2/s) and the ratio of diffusivity in the gel to diffusivity in water are both given in the table. The trend of decreasing diffusion coefficient in the gel with increasing solute molecular weight (and hence molecular size) is clear. In order to determine which of the structural parameters M_c and v_{2s} is more important in controlling diffusion of these random coils through the swollen network, the data were plotted as a function of both M_c and v_{2s} in figure 4-31. From these plots it appears that the polymer volume fraction v_{2s} is the property of the gel that is controlling the rate of diffusion of the random coils. This is consistent with a reptation model of diffusion of random coils through a polymer network. In this model, suggested by deGennes [53], it is assumed that the coil moves through the gel matrix not as a basically spherical glob (as such coils behave in solution) but in a snake-like manner, with a few segments moving into the gel and the rest following along in a somewhat extended conformation. The decrease in effective

Gel	PEO 1000	PEO 8000	PEO 20000
20%,5	2.42×10^{-6}	6.05×10^{-8}	7.70×10^{-9}
	0.862	0.0736	0.0129
20%,10	2.54×10^{-6}	1.14×10^{-8}	2.21×10^{-10}
	0.904	0.0139	3.71×10^{-4}
20%,15	1.28×10^{-6}	4.04×10^{-9}	0
	0.456	4.91×10^{-3}	0
15%,5	2.19×10^{-6}	1.16×10^{-7}	7.18×10^{-9}
	0.779	0.141	0.0120
15%,10	1.38×10^{-6}	2.41×10^{-8}	2.85×10^{-10}
	0.491	0.0293	4.78×10^{-4}
15%,15	1.29×10^{-6}	4.43×10^{-9}	0
	0.459	5.39×10^{-3}	0
10%,5	2.54×10^{-6}	8.45×10^{-8}	5.27×10^{-9}
	0.904	0.103	8.84×10^{-3}
10%,10	1.26×10^{-6}	1.45×10^{-8}	2.21×10^{-10}
	0.449	0.0176	3.71×10^{-4}
10%,15	1.06×10^{-6}	1.33×10^{-8}	1.34×10^{-10}
	0.377	0.0162	2.25×10^{-4}
3%,5	1.41×10^{-8}	7.21×10^{-8}	3.19×10^{-9}
	0.502	0.0877	5.35×10^{-3}

Table 4-7. Summary of effective diffusivity measurements using linear PEO as solute. The top line of data for each membrane is the effective diffusivity in cm^2/s and the second line is the ratio of diffusivity in the gel to diffusivity in pure solvent. Properties of the PEO samples used are given in table 3-2.

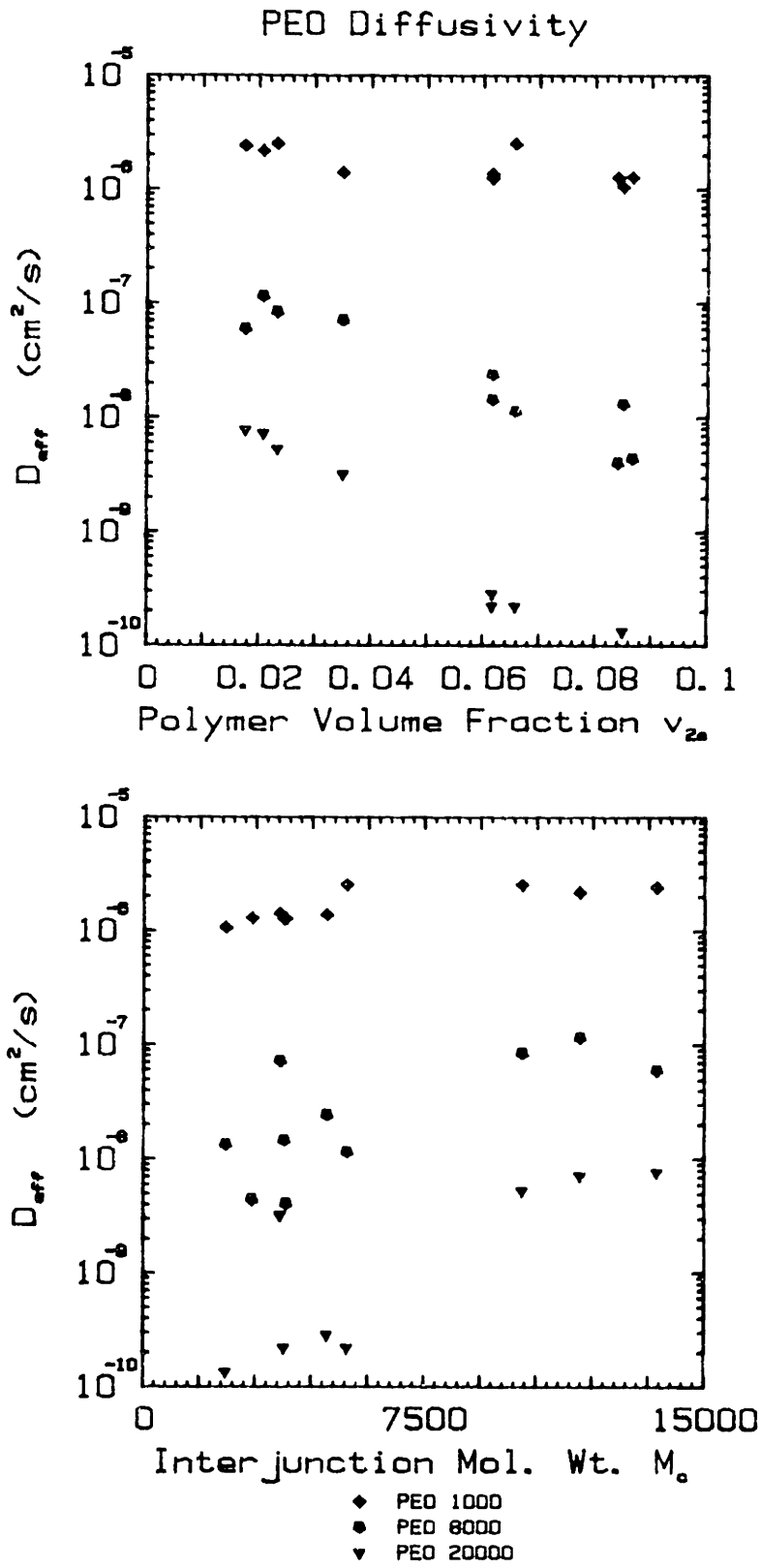

Figure 4-31. Diffusivity of linear PEO samples in the networks as a function of the network parameters M_c and v_{2s}, illustrating the stronger dependence of D_{eff} on the polymer volume fraction. Three different PEO molecular weights were used.

diffusivity with increasing molecular size is due to the greater length of the molecule moving through the gel leading to more entanglements with chain segments in the gel, and the decrease in diffusivity with increasing polymer volume fraction could result from more restricted chain motion due to higher polymer concentration or more entanglements (for the same reason). Unfortunately, not enough different chain lengths were used and the scatter in the data is too great to determine if the decrease in diffusivity with solute size is a function of solute chain molecular weight, length, area, or volume. It is expected qualitatively that length would be the controlling factor if the reptation concept is correct. DeGennes [95] has developed a theoretical model of diffusion of a linear polymer through an unswollen network of the same polymer, and arrives at a dependence of diffusivity D on the linear chain molecular weight M of $D \sim M^{-2}$. However, it is likely that the scaling would be changed by the expansion of both the chain and the network that occurs in a good solvent.

From figure 4-30 it is obvious that based on the Einstein-hard-sphere hydrodynamic radius (see appendix 2) PEO random coils diffuse through the gel networks at a much higher rate than globular solutes of the same radius, and that the maximum size molecule which can penetrate a network is much greater for the random coils. This is further evidence that the random coils are diffusing by reptation rather than as spherical globs. The phenomenon of higher diffusivity for random coils than globular solutes has been observed by previous workers [87] for diffusion in porous media. They suggest that the coils were behaving as free-draining

coils, that is, each chain segment was individually contributing to the hydrodynamic resistance based on its own radius. This is probably not the case in the present study, as a free-draining coil still requires a space for diffusion large enough to permit movement of the entire coil, which is not experimentally observed in the present study. Also, a more recent investigation of random coil diffusion in porous media [88] showed that the random coil diffusivity increases when the coils go from a concentration regime in which they are isolated coils to one in which they are overlapped and entangled. The coils were also able to penetrate pores with radius smaller than the coil radius at the concentrated condition but not as isolated coils. It is suggested that this may be the result of concentration dependent partitioning, but it could also be viewed as evidence in favor of the reptation model, as a scaling approach [53] suggests that more highly concentrated coils would be more successful at reptation. However, there is no reason to think the same mechanisms are responsible for transport in swollen polymer networks and porous media. The most important conclusion that can be drawn from the data and comparison with previous work is that the solution-diffusion model of transport as described in section 2.5.2 is unlikely to apply to diffusion of random coils through swollen polymer network.

4.6.3. Effective Diffusivity of Globular Solutes.

Table 4-8 summarizes the effective diffusivity results for the 5 globular solutes in 10 different networks. It is clear from this table that diffusivity and molecular weight cut-off (the upper limit on the size of

Membrane	Cyanocobalamin	Lysozyme	Chymotripsinogen	Ovalbumin	Albumin
20%,5	3.29×10^{-6}	2.80×10^{-7}	1.15×10^{-7}	3.74×10^{-9}	3.01×10^{-10}
	0.867	0.296	0.121	4.82×10^{-3}	5.07×10^{-4}
20%,10	1.78×10^{-6}	4.02×10^{-7}	7.34×10^{-8}	1.52×10^{-9}	0
	0.469	0.387	7.73×10^{-2}	1.95×10^{-3}	0
20%,15	5.45×10^{-7}	2.74×10^{-8}	2.69×10^{-9}	2.18×10^{-10}	0
	0.144	2.64×10^{-2}	2.83×10^{-3}	2.82×10^{-4}	0
15%,5	9.43×10^{-7}	5.04×10^{-7}	1.33×10^{-7}	8.81×10^{-9}	6.83×10^{-10}
	0.249	0.485	0.140	1.14×10^{-2}	1.15×10^{-3}
15%,10	8.25×10^{-7}	6.29×10^{-8}	5.84×10^{-9}	3.96×10^{-10}	0
	0.218	6.05×10^{-2}	6.24×10^{-3}	6.68×10^{-4}	
15%,15	4.84×10^{-7}	3.01×10^{-8}	4.33×10^{-9}	3.78×10^{-11}	0
	0.128	2.89×10^{-2}	4.55×10^{-3}	4.86×10^{-5}	0
10%,5	9.78×10^{-7}	2.03×10^{-7}	2.35×10^{-8}	1.05×10^{-8}	0
	0.258	0.195	2.47×10^{-2}	1.35×10^{-2}	0
10%,10	9.83×10^{-7}	5.92×10^{-8}	2.55×10^{-9}	7.00×10^{-11}	0
	0.259	5.69×10^{-2}	2.68×10^{-3}	9.02×10^{-5}	0
10%,15	4.42×10^{-7}	4.09×10^{-8}	4.72×10^{-9}	0	0
	0.117	3.92×10^{-2}	4.97×10^{-3}	0	0
3%,5	2.53×10^{-7}	1.44×10^{-7}	-	2.67×10^{-8}	0
	6.67×10^{-2}	0.138	-	3.44×10^{-2}	0

Table 4-8. Summary of results of effective diffusivity measurements for globular solutes. The first line for each membrane is the diffusivity in the gel in cm^2/s and the second line is the ratio of diffusivity in the network to diffusivity in pure solvent.

a solute that will penetrate the gel) are both highly dependent on the conditions of synthesis of the gel. There are several observations that can immediately be made. In general, a membrane with low polymer volume fraction and high interjunction molecular weight has higher diffusivities than one with high polymer volume fraction and low interjunction molecular weight. This is addressed in more detail in section 4.6.4. When compared with the data of Colton [66] on a traditional cellophane dialysis membrane, it appears that for the same small solute (i.e. cyanocobalamin) diffusivity, a PEO hydrogel can have a lower, possibly zero, large solute (i.e. albumin) diffusivity. Conversely, a PEO gel with the same albumin diffusivity as a cellophane membrane has a higher cyanocobalamin diffusivity. Also, a much wider range of molecular weight cut-offs are observed in the PEO gels made using different conditions than in the set of cellulosic membranes Colton studied, but the comparison may be unfair as the membranes he used were all ostensibly for hemodialysis applications. However, it is reasonable to say that the size selectivity of highly swollen PEO hydrogel membranes used in this study is greater than that of traditional dialysis membranes. It also appears that the size selectivity is greater than in standard microporous membranes [96], although the differences in molecular weight cut-off make the comparison difficult.

4.6.4. Factors Controlling Transport.

It is of interest to look at the possible factors controlling transport to try and understand why the diffusive properties of these networks are

different from more traditional networks, and also to try and shed some light on the network structure. As with the random coil solutes, plots of diffusivity as a function of interjunction molecular weight and polymer volume fraction were made to try to determine which parameter was more important in controlling diffusion. Figure 4-32 is an example of these plots for chymotripsinogen, and the behavior is typical of the other solvents as well. It seems clear that neither parameter is independently controlling diffusion of the globular solutes in these gels. There are two possible reasons for this. One is that both M_c and v_{2s} are affecting transport, and thus plotting against some combination of the two (which may represent some other structural feature, for example the chain mobility) would collapse the data to a single line. The other possibility is that there is some additional structural feature that is important in controlling mass transport that is not directly related to either (or both) M_c or v_{2s}, and thus no combination of the two would collapse the data. It is not obvious what this property would be, as most of the features expected to affect transport in the gel, such as chain mobility, chain overlap, and interjunction distance, are expected to be controlled by M_c and v_{2s}.

The most obvious guess for the structural feature controlling transport given that neither M_c or v_{2s} is appropriate is the distance between junctions. As discussed in section 2.4.2, there are two different interjunction distances: the distance between topologically connected junctions d_t and the distance between spatially closest junctions d_s. The procedure for determining an average value for d_t is outlined in

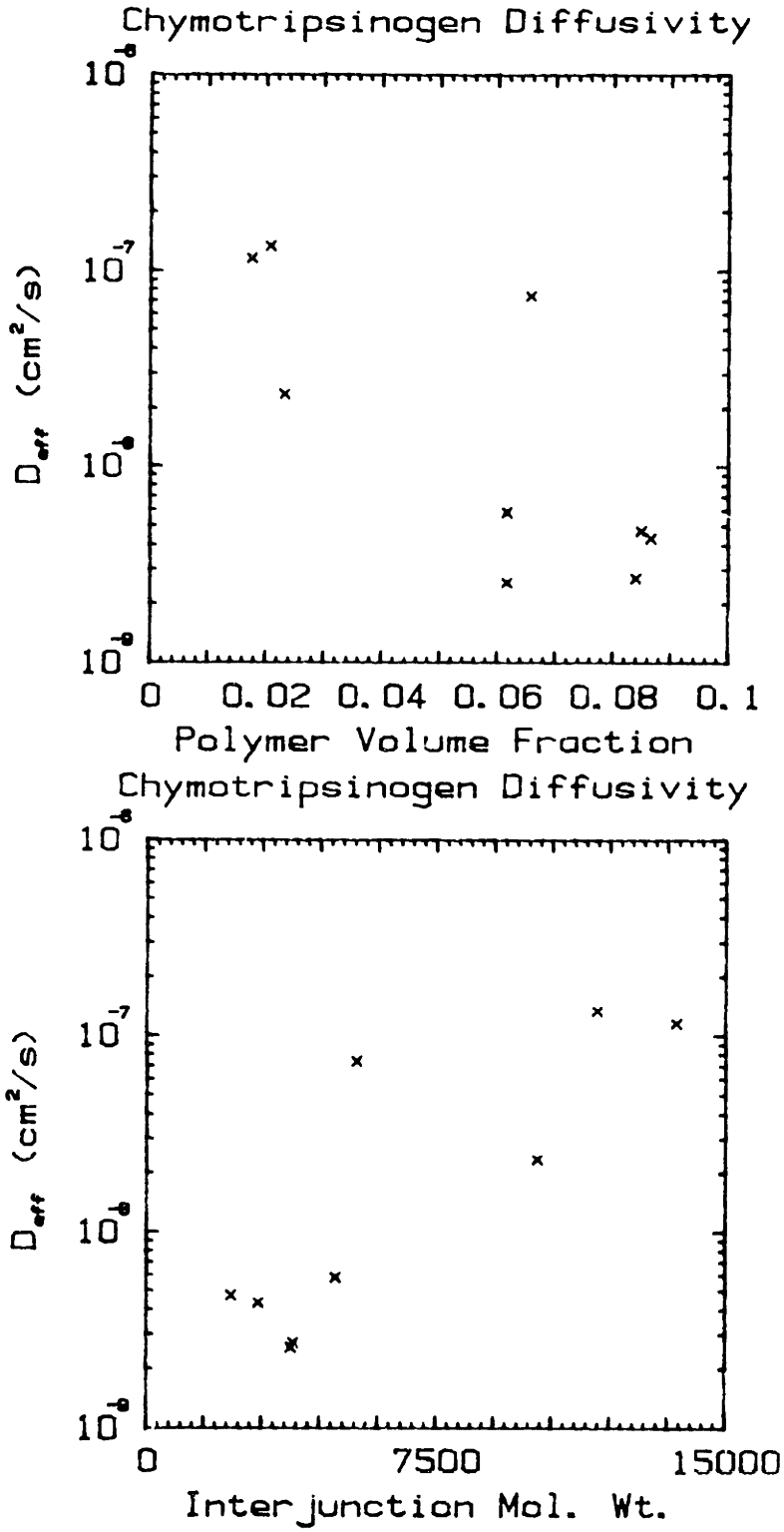

Figure 4-32. Effective diffusivity of chymotripsinogen as a function of the interjunction molecular weight and polymer volume fraction of the networks.

section 3.3.1.2. The average distance between spatially nearest junctions is found from the average volume of swollen network per crosslink, $V_{crosslink}$, which is calculated from

$$V_{crosslink} = \frac{\phi M_c}{2 v_{2s} \rho_p N_{av}} \qquad (4\text{-}2)$$

where ϕ is the junction functionality, M_c is the interjunction molecular weight, v_{2s} is the equilibrium polymer volume fraction, ρ_p is the polymer density, and N_{av} is Avogadro's number. (The volume per crosslink is $\phi/2$ times the volume per chain in the network, as there are $\phi/2$ chains per junction.) The distance between crosslinks is assumed to be the cube root of the volume per crosslink. This leads to the following scaling laws for the two distances: $d_t \sim M_c^{1/2}/v_{2s}^{1/3}$, $d_s \sim (M_c/v_{2s})^{1/3}$. The calculated average values of d_t and d_s for the networks used in the diffusivity measurements are listed in table 4-9. Also included in table 4-9 is the overlap factor, OF, which is the ratio of d_t to d_s and is a function only of the interjunction molecular weight, not the polymer volume fraction. Figure 4-33 shows the same diffusivity data as figure 4-32 plotted as a function of d_t and d_s. It appears that again the full dependence of the diffusivity is not included. This is not surprising in light of the theoretical development of the next section, which predicts a much more complicated dependence on M_c and v_{2s}.

4.6.5. Theoretical Development.

Transport in the networks used in this study is clearly not a simple

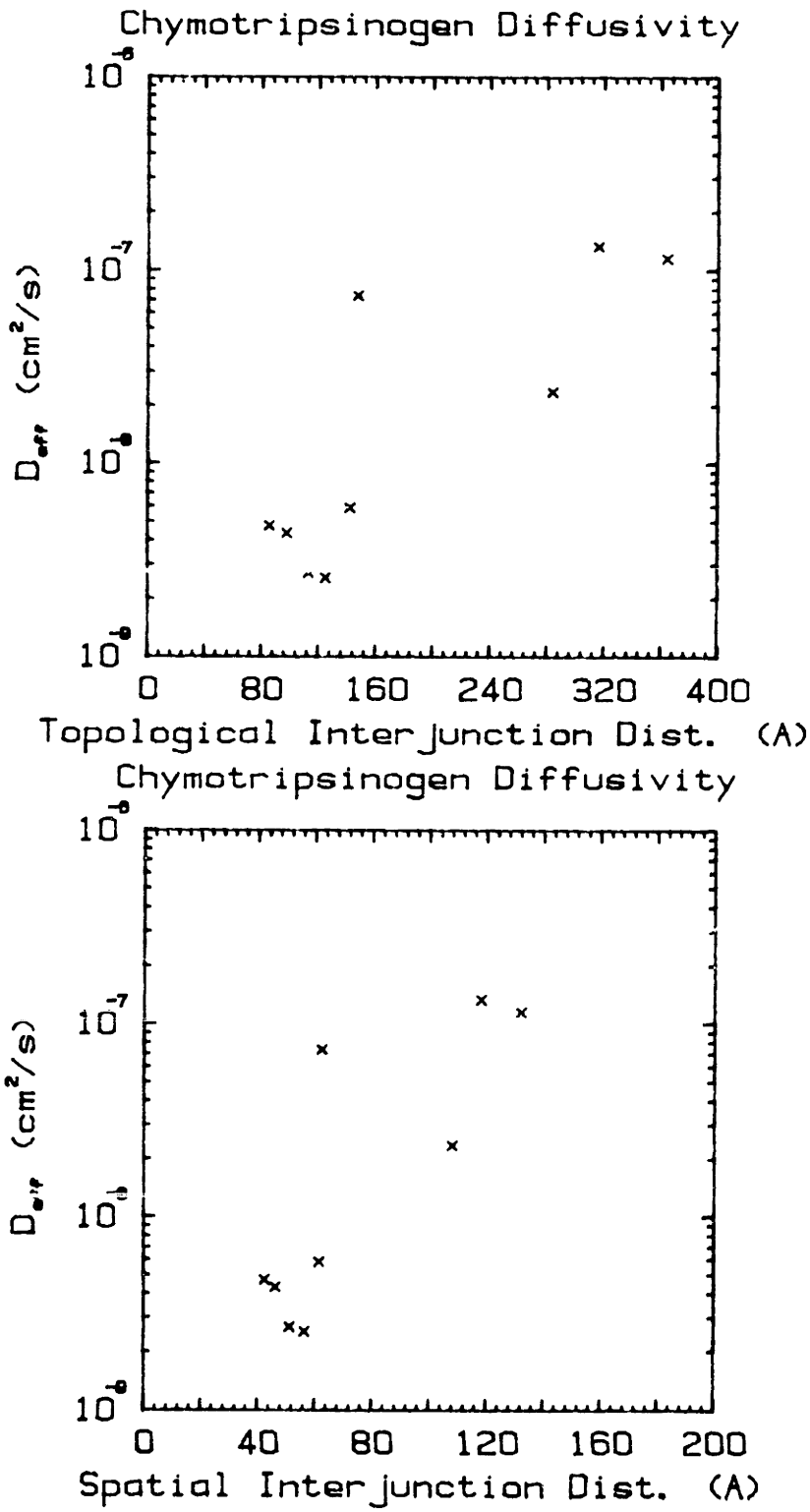

Figure 4-33. Effective diffusivity of chymotripsinogen as a function of the topological and spatial average interjunction distances of the networks.

function of either the network parameters or solute size. In an attempt to better understand how transport is controlled in these gels, an extension of the solution-diffusion model discussed in section 2.5.2 was developed. This development is described briefly here, with some additional details included in appendix 7. While the bulk of the theoretical development focused on the sieve effect, it was also necessary to slightly modify the free volume term of the solution-diffusion equation, which will be discussed first. Through a somewhat different derivation of this term it was possible to include the appropriate measure of the solvent free volume. The free volume is here defined as the volume available to each molecule in excess of the volume the molecule actually occupies. The approach parallelled the development of Cohen and Turnbull [97] for the distribution of sizes of free volume elements in a two-component (solute and polymer) system. The expression they arrive at is

$$P(v) = \exp(-\gamma v/v_f) \qquad (4\text{-}3)$$

where P(v) is the probability of a space of size v or larger existing in the medium through which diffusion is taking place, v_f is the average size of a free volume element per molecule in the medium (i.e., the average amount of volume available for each molecule in excess on the space occupied by the molecule) and γ is a factor between 0.5 and 1 which accounts for the overlap of free volume elements. Previous workers typically have followed the suggestion of Fujita [98] and misinterpreted the average size of a free volume element as the fractional free volume f, i.e., as the ratio of total free volume in the system to total system

volume. The concept of the fractional free volume is useful in going from a two-component (i.e., polymer - solute) system to a three-component system (i.e., polymer - solvent - solute) where there are two components in the medium through which diffusion is taking place; however, a more reasonable approach is to assume that the fractional free volume is the ratio of the free volume per molecule to the actual volume per molecule. That is, $f = v_f N_{av}/\bar{V}$, where $\bar{V}$ is the molar volume of the medium through which diffusion is taking place. For a medium with two components, the total fractional free volume will be the sum of the fractional free volumes of each component weighted by their volume fractions. For the present case, using the subscripts 1 and 3 to denote solvent and polymer respectively,

$$f_{13} = N_{av}\left(\frac{v_{f1}}{\bar{V}_1} v_{1s} + \frac{v_{f3}}{\bar{V}_2} v_{3s} \right) \qquad (4\text{-}4)$$

where v_{1s} and v_{3s} are the equilibrium solvent and polymer volume fractions, respectively. As the membranes are always highly swollen, and as v_{f3} will be much smaller than v_{f1} because polymer free volumes are generally small [98], the second term can be neglected, so $f_{13} = v_{1s} f_1$. Equation 4-3 can be written twice, once for the swollen network and once for pure solvent. By using the assumption of Yasuda et al [70] that the enthalpic contributions to the diffusivity are the same for both the network and solvent, and taking the ratio of diffusivity in the network to diffusivity in pure solvent, only the free volume terms remain. This leads to the following expresssion for the ratio of the diffusion coefficient of a solute in a solvent-swollen polymer network, $D_{2,13}$, to that in pure solvent, $D_{2,1}$,

$$\frac{D_{2,13}}{D_{2,1}} = \exp\left[\frac{-\gamma v}{v_f (Q-1)}\right] \qquad (4\text{-}5)$$

v = characteristic volume of the solute
γ = free volume overlap correction
v_f = average size of a free volume element in solvent
Q = swelling ratio = $1/v_{2s}$

It should be noted that this expression is also the solution-diffusion model prediction for the diffusion coefficient ratio in a polymer solution, where 1 refers to the solvent, 2 refers to the solute, 3 refers to the polymer, and v_{2s} is the polymer volume fraction in solution.

Since previous work [70] has indicated that the solute area, not volume, is the important parameter in controlling transport, v in equation 4-5 can be replaced by $\lambda\pi r_s^2$, where r_s is the solute radius and λ is the diffusional jump length. Using the definition of the average free volume element size of Meares [99] and Goldhamer's Rule, it is possible to calculate a number for the average free volume size of water of 5.21 Å^3. This leaves λ and γ as the unknown parameters.

In order to determine the appropriateness of this expression to the data collected in this study, Colton's data [66] for an Avisco wet gel membrane with Q = 5.6 were fit to this equation using a linear best fit of the log of the diffusion coefficient ratio versus solute area. According to the assumptions under which this equation was derived, γ, λ, and v_f depend only on the solvent, and thus the value for $\gamma\lambda/v_f$ obtained

from the fit to Colton's data should be valid for the present study. This value is 3.07×10^{-3} Å^{-2}. Using the aforementioned value of 5.21 Å^3 for v_f, $\gamma\lambda = 1.6 \times 10^{-2}$ Å, which implies that the diffusional jump length is on the order of 0.02 Å. Figure 4-34 is a plot of the diffusivity data for the 15%, 10 Mrad membrane as diffusivity ratio as a function of solute area with the prediction from the solution diffusion model using the value for $\gamma\lambda$ from Colton's data. Clearly the prediction is not correct. The overprediction of the diffusivity by this model suggests that in the case of diffusion through these highly swollen but fairly tightly crosslinked networks the sieve effect is important.

4.6.5.1. Sieve Effect.

Since the sieve effect appears to be important in transport in these gels, the development of an expression to quantify it was undertaken. Two restrictions were placed on the form such an expression could take. First, only structural parameters that were known or for which values could be independently assumed were included, so that a priori prediction of diffusivity based only on these parameters would be possible. Second, the expression should be based in polymer physics and physical chemistry rather than an empirical correlation. Working within these restrictions, a variety of expressions was developed. The common starting point was that the sieve effect term $f(V_2)$ in the solution-diffusion equation as derived by Yasuda et al [70] is the probability of finding a space in the mesh formed by restrictions to transport due to the network structure at least large enough for a solute species of volume V_2 to enter it. The

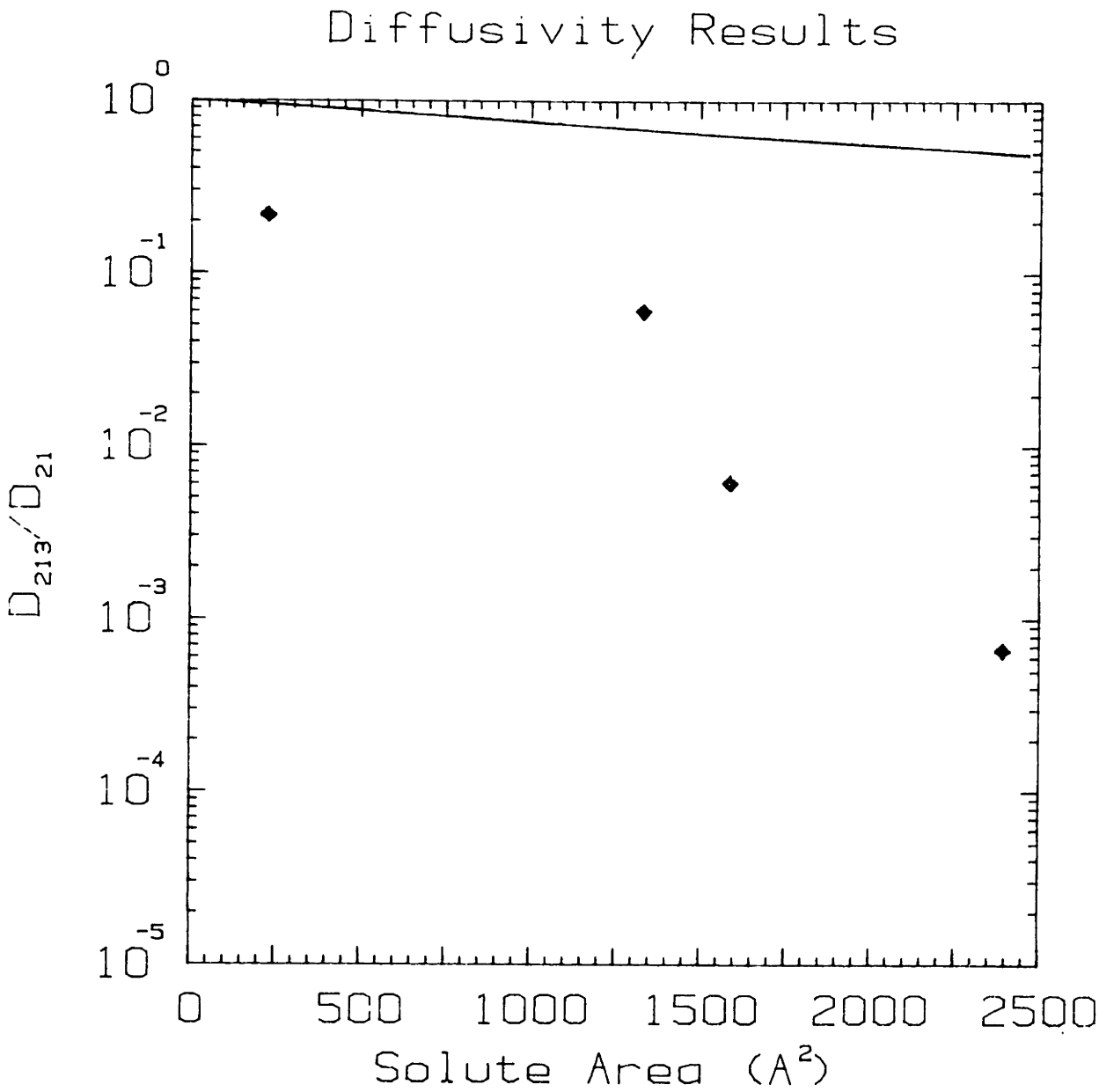

Figure 4-34. Ratio of diffusion coefficient of the globular solutes in the gel to that in pure solvent as a function of the solute area for 15%, 10 Mrad gel. Solid line is the predicted diffusivity ratio using the solution-diffusion model with $f(V_2) = 1$.

second assumption common to all the expressions derived was that the mesh is defined by the network junctions, that is, the junctions are the restrictions to transport. Two different approaches were used in determining how the spaces between the junctions are distributed, and within these two approaches a number of variations were investigated. Figure 4-35 shows schematically how all of the attempts are related.

In order to simplify the discussion, only one of the expressions will be derived in detail here. The other models are derived in appendix 7, and the differences between them will be mentioned. The expression for the sieve effect that will be discussed here is derived assuming that the topological interjunction distance is the appropriate measure of the mesh size and including distributions of both the interjunction molecular weight and the end-to-end distances of a chain of a fixed molecular weight. The distribution of interjunction molecular weights is assumed to follow the most-probable distribution. This was shown to be the case for radiation induced crosslinking of molecules of infinite primary molecular weight [35] and is a reasonable assumption for the present situation with finite but monodisperse primary chains. The expression for the probability of an interjunction chain having a specific number of units x for a given average interjunction molecular weight is

$$p(x) = \left[1 - M_0 \left(\frac{1}{\bar{M}_c} - \frac{1}{\bar{M}_n} \right) \right]^{x-1} M_0 \left(\frac{1}{\bar{M}_c} - \frac{1}{\bar{M}_n} \right) \qquad (4\text{-}6)$$

In this expression, x is the number of units in a network chain, M_0 is the repeat unit molecular weight, $\bar{M}_c$ is the number average interjunction

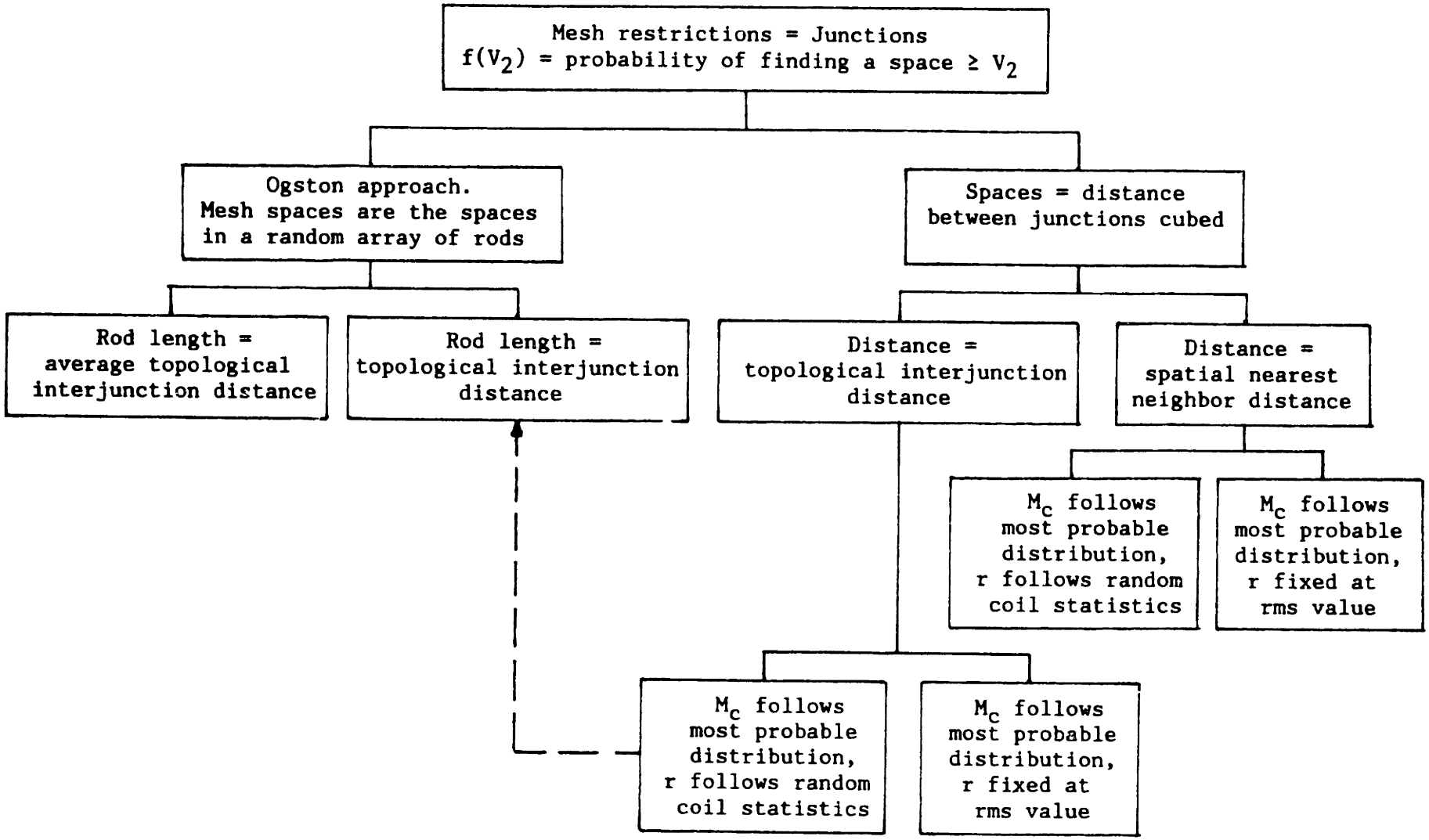

Figure 4-35. Diagram illustrating relationship between approaches used for the calculation of the sieve effect term $f(V_2)$ in the solution-diffusion model.

molecular weight, and $\bar{M}_n$ is the number average molecular weight of the primary molecules. The distribution of distances between junctions r for a given interjunction degree of polymerization x is obtained from the expression for the radial distribution of chain ends [19], assuming that the network chains are behaving as random coils. The probability of an end-to-end distance r given degree of polymerization x is thus given by

$$p(r/x) = 4\pi r^2 \left(\frac{3}{2\pi \langle \bar{r}^2 \rangle} \right)^{3/2} \exp \left[\frac{-3r^2}{2\langle \bar{r}^2 \rangle} \right] \qquad (4\text{-}7)$$

In this expression, $\langle \bar{r}^2 \rangle$ is the mean square end-to-end distance and is given by

$$\langle \bar{r}^2 \rangle = 3\alpha^2 C x \ell^2 \ . \qquad (4\text{-}8)$$

C is the characteristic ratio for the polymer, ℓ is the bond length, and α is the chain expansion factor. For an isolated random coil, α is the intramolecular expansion factor and depends on the solvent quality and chain molecular weight [19], but for the present case, α is just the linear expansion of a network chain above its unperturbed dimensions, and since network expansion is assumed to be affine (the distances between junctions expand proportionally to the macroscopic network), $\alpha^3 = Q = 1/v_{2s}$.

The desired distribution is that for the length r for a network with average interjunction molecular weight $\bar{M}_c$. This is obtained from the other distributions using a form of the Bayes Theorem,

$$p(r) = \Sigma \ p(r/x)p(x). \qquad (4\text{-}9)$$

The summation accounts for all possible values of x, which is an integer

quantity, and goes from 1 to ∞. Since the desired expression is for the probability of the mesh size (the linear dimension - in this case the distance between topologically connected junctions) being size ξ or larger, equation 4-9 is integrated over r from ξ to ∞. Putting equations 4-6 and 4-7 for the probabilities in to equation 4-9 and performing the integration leads to the following expression for $\Phi(\xi)$, the probability of the mesh size being ξ or larger.

$$\Phi(\xi) = \frac{B}{2D^{3/2}} A \sum_{x=1}^{\infty} [1-A]^{x-1} \left[\Gamma(3/2) - \sum_{n=0}^{\infty} \frac{(-1)^n \left[\frac{D}{x} \xi^2\right]^{n+1/2}}{n!\ (n+3/2)} \right] \quad (4\text{-}10)$$

with

$$A = M_0 \left(\frac{1}{M_c} - \frac{1}{M_n} \right) \quad (4\text{-}11)$$

$$B = 4\pi \left(\frac{1}{2\pi\alpha^2 C\ell^2} \right)^{3/2} \quad (4\text{-}12)$$

$$D = \frac{1}{2\alpha^2 C\ell^2} \quad (4\text{-}13)$$

The other variables are as previously defined, and $\Gamma(3/2)$ is the complete gamma function of 3/2, which is numerically 0.88623.

As mentioned above, the derivation of the other models for the mesh size is included in appendix 7. From the mesh size distribution, the hole size distribution $f(V_2)$ is determined assuming that $f(V_2) = \{\Phi(\xi)\}^3$ and that ξ can be taken as the diameter of the solute species. The function $f(V_2)$ was calculated for each of the models using the computer programs found in appendix 7. Figure 4-36 is an example of this function for each

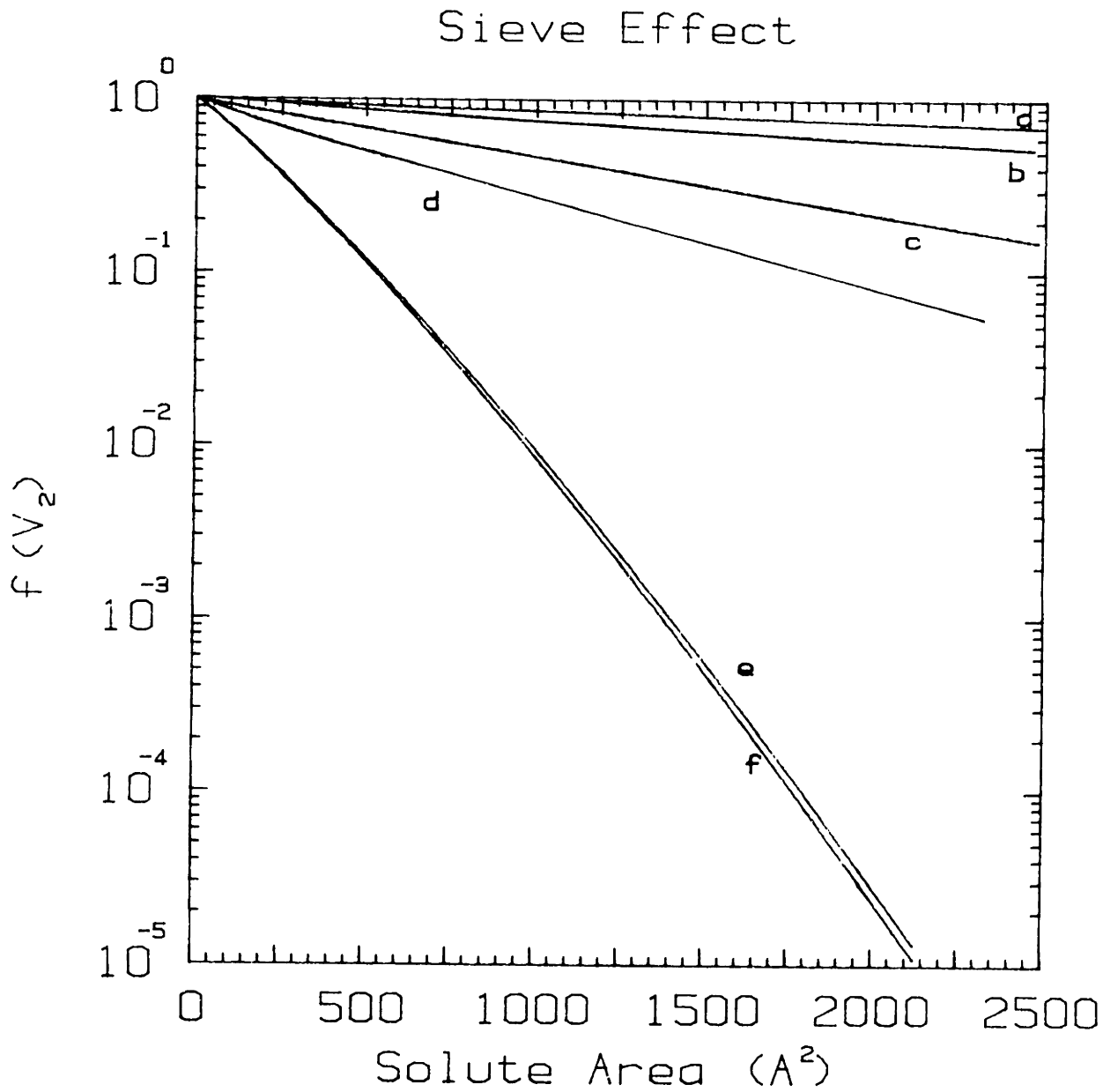

Figure 4-36. Probability of finding a space at least large enough to fit a solute of radius r_E as a function of solute area.

a. topological interjunction distance, fixed r
b. topological, distribution of r
c. spatial interjunction distance, fixed r
d. spatial, distribution of r
e. Ogston - type distribution, average d_t
f. Ogston - type, distribution of d_t as in b

of the models for a postulated network with $M_c = 5000$, $v_{2s} = 0.05$. On this plot, a model which predicts that the sieve effect is important in controlling diffusion would have lower values for $f(V_2)$ and show a greater drop-off with increasing solute area. There is a wide variation in the magnitude of the calculated values. The models based on the Ogston calculation of spaces between rods predict the largest sieve effect contribution to lowering the effective diffusivity. This is expected, as the rod length used is equal the topological interjunction distance, and the spaces in a random array of rods of a certain length must be smaller than that length cubed. Also, adding the distribution of end-to-end distances to the Ogston model makes very little difference, because of the several orders of magnitude difference in the magnitude of the probabilities. The topological interjunction distance model predicts the smallest sieve effect. The spatial interjunction distance model is different from the topological model by only by the scaling on the x-axis, which changes by a factor equal to the overlap factor squared. It is interesting to note that the topological and spatial models using the root-mean-square end-to-end distance rather than the full end-to-end distance distribution predict higher values for $f(V_2)$, that is, a smaller sieve effect. This is related to the fact that the end-to-end distance distribution is skewed toward small end-to-end distances. At the relatively small distances of interest here (compared to the average interjunction distance) the distance distribution allows for many holes smaller than the rms distance, but relatively few larger, leading to lower values for $f(V_2)$ predicted using the full distribution.

4.6.5.2. Diffusivity Predictions.

In order to make predictions of the diffusion coefficient ratio, $f(V_2)$ is inserted into equation 4-5. These predictions are shown in figure 4-37 as a function of solute area for the 15%, 10 Mrad membrane. The measured diffusion coefficient ratios for this membrane are included for comparison. It is clear from this plot that none of the models do a very good job of predicting the diffusion coefficient ratio. All of the models based on interjunction lengths overpredict the ratio, and the Ogston model underpredicts. (Note that while a single membrane was picked for purposes of illustration, the behavior is typical of the others.) As the Ogston model is based on the incorrect assumption that the junctions are connected by rigid straight chains which are barriers to transport, it is not surprising that it is incorrect; however, it is possible to achieve reasonable agreement with the data by assuming either a thickness to the rods or a different value for the solute radius (i.e., rescaling either the data or the model on the x-axis), so it may be useful as a correlative tool.

It is possible to extract some information about transport in these gels from the unsuccessful modelling work. The failure of the interjunction distance models to predict sufficiently low diffusivities suggests that these models have missed some resistance to transport. The first possibilty is that Yasuda et al [70] were correct in interpreting the sieve effect term as the probability of finding a space in the mesh at least as large as the solute and the current model is either

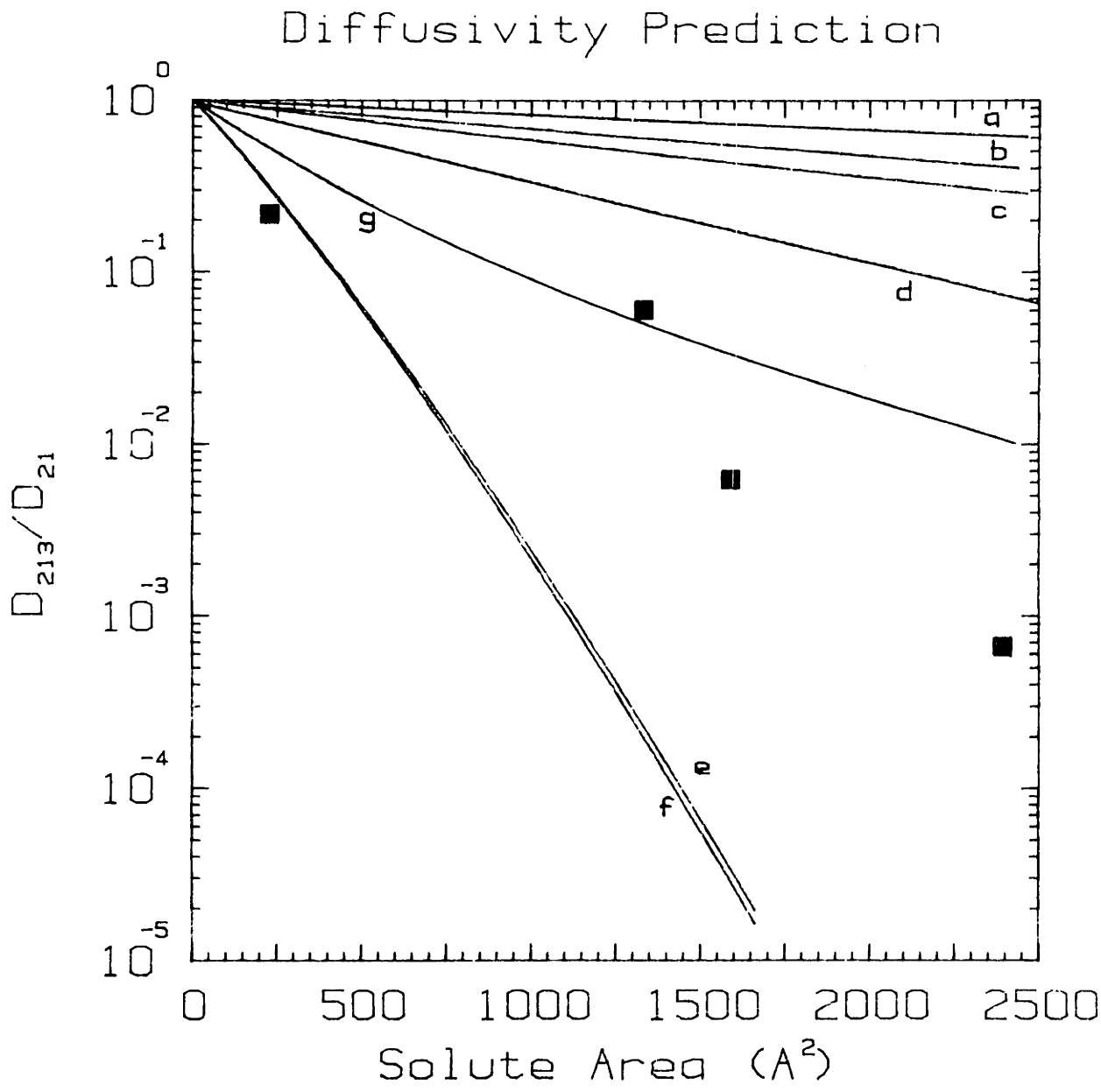

Figure 4-37. Prediction of diffusion coefficient ratio plotted with data for 15%, 10 Mrad gel. All predictions include free volume term (slope from fit to data of Colton [66]); sieve effect as follows.

a. $f(V_2) = 1$ (no sieve effect)
b. topological interjunction distance, fixed r
c. topological distance, distribution of r
d. spatial interjunction distance, fixed r
e. Ogston - type distribution, average d_t
f. Ogston - type, distribution of d_t as in c
g. spatial distance, distribution of r

overestimating the size of the spaces or underestimating the solute volume. There are a number of factors which may be contributing to underestimation of the space sizes. One of the first things to consider is that the values used for the average interjunction molecular weight are calculated from swelling data using a theory that has not been independently confirmed, and thus may not be numerically correct. If the calculated M_c is higher than the actual value by a factor of 2 or 3, the spatial interjunction model will move considerably closer to the data. However, as discussed in section 4.1.2, it is unlikely that M_c is incorrect to that large a degree.

Another possibility is that the distribution of chain lengths for a given degree of polymerization is very different for chains which are connected to junctions than for chains which are free. However, it is possible to calculate an average topological and spatial interjunction distance for each junction (see table 4-9). The average topological interjunction distance is clearly too large for any appreciable resistance to transport to be developed for the solutes used in this study if the resistance is due to solute exclusion. The average spatial distance is considerably closer to the size of the solutes used in this study, and thus the junctions could be responsible for some resistance. However, since it is an average value there are a large number of interjunction distances larger than this value, and thus the degree to which transport of a solute species with diameter equal to this value is restricted by solute exclusion is still relatively small. It should be noted that the calculation of the average spatial interjunction distance does not

Membrane	Spatial distance d_s	Topological distance d_t	Overlap Factor
20%, 5 Mrad	132 Å	364 Å	2.75
20%, 10 Mrad	62.4 Å	147 Å	2.35
20%, 15 Mrad	51.1 Å	113 Å	2.22
15%, 5 Mrad	118 Å	316 Å	2.68
15%, 10 Mrad	61.6 Å	142 Å	2.31
15%, 15 Mrad	46.2 Å	97.8 Å	2.12
10%, 5 Mrad	108 Å	284 Å	2.63
10%, 10 Mrad	56.4 Å	125 Å	2.21
10%, 15 Mrad	42.4 Å	85.7 Å	2.02
3%, 5 Mrad	67.4 Å	149 Å	2.21

Table 4-9. Summary of the average spatial and topological interjunction distances for the networks used in effective diffusivity measurements. Values were calculated as shown in the text for networks swollen to equilibrium in phosphate-buffered saline. Overlap factor is the ratio of topological to spatial interjunction distance, and is an estimate of the average number of chains occupying a single chain volume of space.

require any assumption about the behavior of the chains (other than that the crosslinks are distributed homogeneously) and thus restrictions on possible chain conformations will not affect this value.

Therefore, if the hydrodynamic radius is the correct measure of the solute radius, there must be some feature of the network other than the junctions which is decreasing the size of the spaces in the mesh. It is not completely clear that the hydrodynamic radius is appropriate in this case; the interaction between solute and mesh is not proposed to be a hydrodynamic one, but it is not at all clear what a more appropriate choice would be. Also, other possible choices for the radius tend to be smaller than the hydrodynamic radius, which will add to the discrepency. (See ref. [66] for a discussion of solute sizes.) This leaves the prospect that there is some structural feature in addition to the junctions restricting transport. The additional resistance can probably be associated with the presence of the chains. The effect of the chains in diminishing the free volume available for transport is the basis for the free volume term of the solution-diffusion equation, but the presence of the chains is not accounted for in the sieve effect calculations. There are two related ways in which the network chains may be restricting transport. First, the chains do occupy some volume of the network, which is not accounted for in the calculation of the size of the spaces in the mesh. However, at these very high degrees of swelling, the volume of chains is very small and the effect on the calculation would be minimal. The other possibilty is that chain motion is sufficiently restricted in the network that the chains can act as resistances to transport. In the

derivation it was assumed that the chains could move out of the way of a diffusing species and only the motions of the junctions were sufficiently restricted to stop a molecule. There may be situations, however, in which motion of a chain is restricted enough that it cannot move out of the way of the diffusing species and in consequence causes a transport delay. It is not at all clear how to quantify this situation.

Returning to the question of why the interjunction distance models underpredict, the second possibility that should be addressed concerns the definition of $f(V_2)$. As mentioned above, Yasuda et al [70] imply that it is the probability of a solute molecule finding a space in the mesh into which it can fit. This ignores the possibility of a molecule simply hitting the "wall" of a hole large enough for it to penetrate and being delayed by this encounter. This can be viewed as a decrease in the diffusional jump length, leading to an increase in the number of steps required to travel a certain distance and thus a decrease in the effective diffusivity. The appropriate $f(V_2)$ would thus include the probability of a species of a specific size hitting a mesh restriction, and would depend on the spatial distribution of junctions within the network.

The following results briefly summarize the modelling work.

1. The free volume term of the solution-diffusion equation, which is equivalent to the prediction for transport in a polymer solution, greatly overpredicts the diffusion coefficient ratio for globular solutes in these gels.

2. Models for the sieve effect based on the distances between junctions in the swollen network do not completely correct for the overprediction of the free volume term. That is, the diffusivity ratio is still overpredicted when the sieve effect term is included.
3. Models for the sieve effect based on the Ogston model for the distribution of sizes of spaces in a random array of rods lead to underprediction of the diffusion coefficient, but the shape of the prediction is close to correct and the model may be useful as a correlative tool.

The conclusions which can be made about transport in these gels based on the modelling work are summarized in chapter 5.

Chapter 5. Conclusions and Recommendations

There are several conclusions that can be drawn by bringing together the disparate portions of this work and viewing it as a whole. These are discussed briefly here, although all arise directly from the discussion in the previous chapter.

5.1. PEO Gel Synthesis

Homogeneous Gels. It is possible to produce homogeneous crosslinked networks of poly(ethylene oxide) by irradiating aqueous solutions of PEO with high energy electrons. By changing the conditions of the irradiation, in particular the total dose and the initial concentration of PEO, it is possible to synthesize networks with a wide variety of crosslink densities and polymer volume fractions when fully swollen. Crosslinking with high energy electrons is a much more efficient process (about 2 orders of magnitude) than crosslinking with a ^{60}Co gamma source. This is due to the several orders of magnitude higher dose rate for electron irradiation, which increases the concentration of main chain radicals and thus increases the number of crosslinks formed. The higher dose rate also increases the ratio of crosslinking to main chain scission, because crosslinking is bimolecular in main chain radicals and scission is unimolecular. This allows gelation to occur over a much broader range of conditions (pH, PEO concentration, gaseous atmosphere) than suggested by the gamma irradiation studies.

Porous Gels. It was also found that PEO gels with a highly porous structure could be produced by changing the irradiation conditions. In particular, porous gels are produced when K_2SO_4 is added to the PEO solution, which decreases the solvent quality for PEO. The porous gels result from phase separation during crosslinking, which is apparent because porous gels are produced when a solvent is used in which the phase separation temperature of the PEO is in the temperature range reached during irradiation. However, while the process in thermodynamically driven, it is kinetically controlled through the dose rate. A given PEO solution can produce a porous gel, a macroscopically two-phase system, or a homogeneous gel depending on how quickly the radiation in delivered and thus the point during the phase separation at which the network structure is locked in. The kinetics also appear to control the pore size in the porous gels, and this allows a wide range of structures to be produced quite simply.

Future Work. It would be useful to confirm that the Flory-Bray affine swelling theory is applicable to the homogeneous gels synthesized by ionizing radiation. Some of the results of this study suggest that this theory has the appropriate dependence of crosslink density on polymer volume fraction, but independent measurement of the crosslink density would be highly desirable. The most likely means of accomplishing this would be through the use of high resolution nuclear magnetic resonance spectroscopy on crosslinked gels. It should be noted that this would in be a more valuable confirmation of the theory than that possible with end-linked systems, because there should be no thermodynamic effect of

the junctions on the liquid lattice mixing terms in the present system. There are several interesting things that could be done with regard to the porous gel synthesis. These include development of a technique to measure porosity and pore size distribution, an investigation of different additives that would decrease solvent quality such as other salts or alcohols, and use of more precise control of the dose rate and the temperature change during irradiation. These things should allow a more complete understanding of the thermodynamics and kinetics of the process. It would also be interesting to be able to observe (through a video camera) the timing of phase separation relative to gelation during an irradiation.

5.2. PEO Solution Behavior

The Flory-Huggins interaction parameter χ_1 was measured for PEO in pure water at room temperature. It was found to be almost constant with volume fraction for volume fractions between 0.04 and 0.16, with an average value of 0.426. The phase separation behavior of PEO in K_2SO_4 solutions was studied as a function of PEO and K_2SO_4 concentration in pure water. The cloud point decreased with increasing PEO and K_2SO_4 concentration over the entire range studied. The decrease with increasing salt concentration is a reflection of decreasing solvent quality in this lower critical solution temperature system. The continued decrease in cloud point with increasing PEO concentration was partly due to three-phase systems at higher K_2SO_4 concentrations, with two amorphous PEO phases and crystalline PEO. A single phase could be

obtained only by heating the solution to melt the crystals and supercooling below the cloud point and the melting temperature. The study of salt partitioning between PEO gels and water suggests that the decrease in solvent quality seen when salts are added to PEO solutions is not due to complexation of the salt by the PEO chains. In fact, it appears that the salts which complex with PEO have the least effect on the solvent quality. Also, it appears that the anion may play a much more important role in determining the ability of a salt to complex with PEO than was previously thought.

Future work should focus on exploiting this unique and simple way of determining partitioning of salts and thus the enthalpic interactions between the salts and the PEO chains. It would be interesting to look at a series of salts chosen to allow differentiation between anion and cation behavior. It would also be interesting to look at competitive partitioning between two different anions or cations. Although the cloud point measurements and the change in swelling of the gels both provide some information about the solvent quality, it might be valuable to use a more fundamental measure such as intrinsic viscosity or osmometry.

5.3. Transport in Homogeneous Swollen Gels

Linear PEO. The diffusion of linear PEO in the swollen PEO networks is controlled by the polymer volume fraction. Also, the effective diffusivity of these random coils is much greater than a globular molecule of the same hydrodynamic radius. These suggest that transport

is taking place by reptation, wherein the molecule travels through the gel in a somewhat uncoiled fashion. This same type of behavior has been reported for transport of random coils in porous media.

Globular Solutes. Diffusion coefficient measurements indicate that the diffusive size separation possible with these PEO networks is sharper than that of both traditional cellophane dialysis membranes and microporous media. It is also very simple to tailor the molecular weight cut-off over a fairly wide range. When considered together with the fact that protein partition coefficients between gel and PBS are near one this suggests several important potential uses for such gels in biological separations and concentration as well as biomedical applications. In contrast to the diffusion of PEO, there is not any one obvious structural feature which appears to be most important in controlling transport of the globular solutes. This suggests that there may be a variety of factors involved, and also that the controlling parameter may be change with changes in solute size and gel structure.

Modelling Work. The attempt to predict diffusion coefficients based on the solution-diffusion model of transport suggests several things. First, neither the magnitude or the solute size dependence of the diffusivities measured were correctly predicted by the free volume term of the solution-diffusion equation, which is equivalent to the prediction for transport in polymer solutions. This suggests that there is some structural restriction to diffusion in these gels. Attempts to quantify this restriction by adding a sieve term based on the network junctions as

restrictions to transport were unsuccessful, overpredicting the diffusivity to varying degrees depending on the exact model used. This implies that transport is restricted in some way not accounted for in the models, and there are two possibilities for this additional restriction. The first is that the concept of sieving as an actual exclusion is correct and that some other structural feature, probably the chains, is limiting the size of the spaces available. The second is that the sieving concept is wrong in that it ignores the possible delays caused by the encounter of a solute molecule with an immobile junction that is not close enough to other junctions to cause solute exclusion. The second possibility is almost certainly a factor in controlling transport, but it is not clear to what extent the first possibility is important.

Future Work. Two types of studies might provide further information on the factors controlling transport in these gels. It would be interesting to look at the transport behavior of these networks swollen in non-aqueous solvents to help determine if water bound to the PEO chain is affecting transport. The other thing that might prove useful would be the development of a highly water-swellable end-linked PEO network. This would allow precise knowledge and control of the molecular weight between crosslinks and the distribution of these molecular weights. Also, the right system might allow scattering studies to determine the actual distance between crosslinks and possibly the chain and junction mobilities.

Appendix 1. SEC Data Reduction Program

The size exclusion chromatography data reported in this thesis was collected and analyzed using an IBM PC/XT with a Data Translation DT2805 analog-to-digital converter board. The board has a 12 bit converter with 8 differential analog-to-digital channels, an external trigger to start data collection, and programmable gain allowing full-scale voltages of ±20 mV, 100 mV, 1 V, and 10 V. The refractometer output of the Waters 150C ALC/GPC used for chromatography is 10 mV full scale, so the highest board gain was used. This gives a conversion accuracy of about 20 μV, or about 0.2% of the refractometer full scale output.

The programs for acquisition and reduction of the data were written in BASIC, and are attached. The techniques used for the various manipulations are briefly described below.

Data Acquisition. Data acquisition was started automatically by an external trigger sent from the 150C when an injection was made. The program was designed to collect and store up to 16 chromatograms for later retrieval and analysis, as the 150C is capable of injecting 16 different samples automatically. Conversions were made every 0.1 s for a typical 40 min SEC run. The byte values were converted to voltage using the known gain. Ten values were averaged and this average stored every second.

Baseline Correction. The voltage values as a function of time were plotted on the IBM screen, adjusting so that the full scale voltage of the plot was slightly larger than the difference in the highest and lowest data values. In order to put the baseline at 0 V, a linear regression was done on either computer selected or user selected portions of the chromatogram. The computer selected portions were the first 5 and last 2 minutes of the run. The best-fit straight line to these portions was subtracted from the entire chromatogram. All subsequent manipulations were done on the corrected chromatogram.

Peak Selection. Selection of the start and end times of peaks could also be done automatically or by the user. In the automatic selection process, the computer searches through the chromatogram for a sequence of points (typically 6) that are more than 2 standard deviations above the zero value (the baseline). This is defined as the start point of the peak. The end point is found when the voltage value falls back to within 2 standard deviations of the baseline. Because this technique is not effective on fused peaks, a manual peak selection procedure is also available. The user picks the start and end points using a cursor on the screen. Multiple peaks can be analyzed on the same chromatogram.

Integration of Peaks. The area under the peak is simply found by adding the voltage values of the baseline-corrected chromatogram for all times between the peak start and end points. The voltage values

are converted to mass fractions by dividing each by the total peak area. This can be done for individual peaks or the entire chromatogram.

Conversion to Molecular Weight. The retention times were converted to molecular weight using a third-order fit of log(molecular weight) versus retention time for a set of narrow molecular weight distribution PEO standards. Number and weight average molecular weights were computed from the slice areas (voltages) and the slice molecular weights. (Each data point was converted, so the slices had width of one second.) The resulting information about mass fraction as a function of molecular weight (the converted chromatogram) was stored as a separate file which could be used for plotting.

The first BASIC program attached is a complete package for data acquisition and reduction, including screen plotting of multiple converted chromatograms. The second program using a Direct Memory Access technique for data acquisition which allows real-time plotting of a single chromatogram as it is being collected. The data files from this program can be analyzed using the first program.

```
10 '*************************************************************************
20 '
30 '              SEC DATA REDUCTION PROGRAM
40 '
50 '
60 '                K.A.Dennison   5-24-84
70 '
80 '*************************************************************************
90 DEFINT I-N
100 ' Set up screen and variables
110 KEY OFF: SCREEN 0: COLOR 7,0: CLS
120 '
160 '
200 ' Set up main menu for selection of sub-program
210 CLS:CLOSE:CLEAR
220 LOCATE 8,11
230 PRINT "**** MAIN MENU FOR SEC DATA REDUCTION ****"
240 LOCATE 10,17
250 PRINT "Select the desired function by using function keys"
255 KEY 1,"MENU":KEY 2,"DATA":KEY 3,"INTEG":KEY 4,"DISPL":KEY 5,"END"
256 KEY 6,"EXIT":KEY 7,"":KEY 8,"":KEY 9,"":KEY 10,""
257 KEY ON
258 KEY 15, CHR$(&H4)+CHR$(&H46):KEY 16, CHR$(&H4+&H40)+CHR$(&H46)
259 KEY 17, CHR$(&H4+&H20)+CHR$(&H46):KEY 18,
CHR$(&H4+&H20+&H40)+CHR$(&H46)
260 ON KEY(15) GOSUB 5500:ON KEY(16) GOSUB 5500:ON KEY(17) GOSUB 5500
261 ON KEY(18) GOSUB 5500
270 ON KEY (1) GOSUB 200: '       RETURN TO MENU
280 ON KEY (2) GOSUB 10000: '     SEC DATA ACQUISITION
290 ON KEY (3) GOSUB 20000: '     BASELINE AND INTEGRATION
300 ON KEY (4) GOSUB 50000: '     DISPLAY OF MULTIPlE CURVES
305 ON KEY (5) GOSUB 5500: '      END PROGRAM
310 ON KEY (6) GOSUB 6500: '      EXIT TO DOS
320 '
330 LOCATE 12,20: PRINT "F1: Return to main menu"
340 LOCATE 13,20: PRINT "F2: Collect data from SEC system"
350 LOCATE 14,20: PRINT "F3: Select baseline and integrate stored data"
360 LOCATE 15,20: PRINT "F4: Display two or more curves"
370 LOCATE 16,20: PRINT "F5: End program"
375 LOCATE 17,20: PRINT "F6: Exit to DOS"
400 '
410 KEY (1) ON: KEY (2) ON: KEY (3) ON: KEY (4) ON: KEY (5) ON: KEY (6)
ON
415 KEY(15) ON:KEY(16) ON:KEY(17) ON:KEY(18) ON
420 DELAY$=INKEY$
430 IF DELAY$="" THEN 430
5500 KEY 1,"LIST ":KEY 2,"RUN"+CHR$(13):KEY 3,"LOAD"+CHR$(34):KEY
4,"SAVE"+CHR$(34)
5510 KEY 5,"CONT"+CHR$(13):KEY 6,","+CHR$(34)+"LPT1:"+CHR$(13):KEY
7,"TRON"+CHR$(13)
5515 KEY 8,"TROFF"+CHR$(13):KEY 9,"KEY ":KEY 10,"SCREEN 0,0,0"+CHR$(13)
6000 END
```

```
6500 SCREEN 0
6505 KEY 1,"LIST ":KEY 2,"RUN"+CHR$(13):KEY 3,"LOAD"+CHR$(34):KEY
4,"SAVE"+CHR$(34)
6510 KEY 5,"CONT"+CHR$(13):KEY 6,","+CHR$(34)+"LPT1:"+CHR$(13):KEY
7,"TRON"+CHR$(13)
6515 KEY 8,"TROFF"+CHR$(13):KEY 9,"KEY ":KEY 10,"SCREEN 0,0,0"+CHR$(13)
6520 SYSTEM
10000 'reading the sec runs
10002 DIM OF$(20)
10005 CLS:LOCATE 23:PRINT "
                ";
10010 PRINT:LOCATE 23,25:PRINT "INPUT SEC SYSTEM PARAMETERS"
10012 LOCATE 5,20:INPUT "Number of SEC runs";NR
10014 LOCATE 6,20:PRINT "Type the output file names"
10016 FOR K = 1 TO NR
10018 LOCATE 7+K,20:PRINT "Run ";K:LOCATE 7+K,30:INPUT OF$(K)
10020 NEXT K
10025 LOCATE 21,10:INPUT "Are the file names correct (y/n)";COR$
10027 IF COR$ = "N" OR COR$ = "n" THEN 10005
10030 CLS:LOCATE 10,20:INPUT "Total run time";TOTTIME
10040 LOCATE 11,20:INPUT "Solvent flow rate (ml/min)";FLOW
10050 LOCATE 12,20:INPUT "Injection volume (microliters)";VINJ
10060 LOCATE 14,20:INPUT "Solvent";SOL$
10070 LOCATE 15,20:INPUT "Samples";SAMP$
12010 LOCATE 23:PRINT"
                ";
12020 LOCATE 23,25:PRINT "COLLECTING DATA FRON GPC SYSTEM":CLS
12030 FOR KR = 1 TO NR
12050 OPEN OF$(KR) AS #1 LEN = 8
12055 FIELD #1, 4 AS TI$, 4 AS BI.VOLTS$
12060 '
12070 IBASE.ADDRESS =&H2EC
12080 ICOMMAND.REGISTER =IBASE.ADDRESS+1
12090 ISTATUS.REGISTER =IBASE.ADDRESS+1
12100 IDATA.REGISTER =IBASE.ADDRESS
12110 ICOMMAND.WAIT =&H4
12120 IWRITE.WAIT =&H2
12130 IREAD.WAIT =&H5
12140 '
12150 ICCLEAR =&H1
12160 ICCLOCK =&H3
12170 ICSAD =&HD
12180 ICRAD =&H8E
12190 ICSTOP =&HF
12200 ICERROR =&H2
12210 PERIOD =40000!
12220 '
12230 BASE.FACTOR =4096
12240 IBASE.CHANNELS =8
12250 IGAIN(0) =1
12260 IGAIN(1) =10
12270 IGAIN(2) =100
```

```
12280 IGAIN(3) =500
12290 '
12300 '
12310 OUT ICOMMAND.REGISTER,ICSTOP
12320 ITEMP =INP(IDATA.REGISTER)
12330 WAIT ISTATUS.REGISTER, ICOMMAND.WAIT
12340 OUT ICOMMAND.REGISTER, ICCLEAR
12350 '
12360 ' SET CLOCK RATE
12370 '
12380 WAIT ISTATUS.REGISTER, ICOMMAND.WAIT
12390 OUT ICOMMAND.REGISTER, ICCLOCK
12400 '
12410 IPERIODH =INT(PERIOD/256)
12420 IPERIODL =PERIOD-IPERIODH*256
12430 WAIT ISTATUS.REGISTER, IWRITE.WAIT, IWRITE.WAIT
12440 OUT IDATA.REGISTER, IPERIODL
12450 WAIT ISTATUS.REGISTER, IWRITE.WAIT, IWRITE.WAIT
12460 OUT IDATA.REGISTER, IPERIODH
12470 '
12480 IADGAIN=3
12490 '
12500 IADSCHANNEL=0
12510 '
12520 IADECHANNEL=0
12530 '
12540 NCONVERSIONS=TOTTIME*60/(PERIOD*.0000025)
12550 NC1=NCONVERSIONS/10
12560 '
12570 DIM IADH(NC1),IADL(NC1)
12580 '
12590 WAIT ISTATUS.REGISTER, ICOMMAND.WAIT
12600 OUT ICOMMAND.REGISTER, ICSAD
12610 '
12620 WAIT ISTATUS.REGISTER, IWRITE.WAIT, IWRITE.WAIT
12630 OUT IDATA.REGISTER, IADGAIN
12640 '
12650 WAIT ISTATUS.REGISTER, IWRITE.WAIT, IWRITE.WAIT
12660 OUT IDATA.REGISTER, IADSCHANNEL
12670 '
12680 WAIT ISTATUS.REGISTER, IWRITE.WAIT, IWRITE.WAIT
12690 OUT IDATA.REGISTER, IADECHANNEL
12700 '
12710 NUMBERH = INT(NCONVERSIONS/256)
12720 NUMBERL = NCONVERSIONS-NUMBERH*256
12730 WAIT ISTATUS.REGISTER, IWRITE.WAIT, IWRITE.WAIT
12740 OUT IDATA.REGISTER, NUMBERL
12750 WAIT ISTATUS.REGISTER, IWRITE.WAIT, IWRITE.WAIT
12760 OUT IDATA.REGISTER, NUMBERH
12770 '
12780 WAIT ISTATUS.REGISTER, ICOMMAND.WAIT
12790 OUT ICOMMAND.REGISTER, ICRAD
```

```
12800 '
12810 FOR LOOP = 1 TO NCONVERSIONS
12815 L1 = LOOP/10
12820 WAIT ISTATUS.REGISTER, IREAD.WAIT
12830 IADL(L1)=INP(IDATA.REGISTER)
12832 WAIT ISTATUS.REGISTER, IREAD.WAIT
12834 IADH(L1)=INP(IDATA.REGISTER)
12860 NEXT LOOP
12865 PRINT IADH(1),IADL(1)
12870 '
12880 WAIT ISTATUS.REGISTER, ICOMMAND.WAIT
12890 ISTATUS =INP(ISTATUS.REGISTER)
12900 OUT ICOMMAND.REGISTER, ICSTOP
12910 ITEMP=INP(IDATA.REGISTER)
12920 WAIT ISTATUS.REGISTER,ICOMMAND.WAIT :OUT ICOMMAND.REGISTER,ICERROR
12930 WAIT ISTATUS.REGISTER,IREAD.WAIT
12940 IERR1=INP(IDATA.REGISTER)
12950 WAIT ISTATUS.REGISTER,IREAD.WAIT
12960 IERR2=INP(IDATA.REGISTER)
12970 IF (ISTATUS AND &H80) THEN GOTO 13200
12980 '
12990 FACTOR =(10/4096)/500
13000 NCHAN=IADECHANNEL-IADSCHANNEL + 1
13010 IF NCHAN < 1 THEN NCHAN = NCHAN + IBASE.CHANNELS
13020 '
13025 LSET TI$ = MKS$(TOTTIME):LSET BI.VOLTS$ = MKS$(FLOW)
13027 PUT #1,1
13030 CLS
13040 FOR LOOP = 1 TO NC1
13050 '
13060 DATA.VALUE=IADH(LOOP)*256 + IADL(LOOP)
13070 UNI.VOLTS=DATA.VALUE*FACTOR
13080 BI.VOLTS=UNI.VOLTS*2-(10/500)
13090 '
13110 TIME = LOOP*10*PERIOD*.0000025/60!
13115 LSET TI$ = MKS$(TIME):LSET BI.VOLTS$ = MKS$(BI.VOLTS)
13120 PUT #1, LOOP+1
13130 IF (LOOP MOD 30)<>0 THEN GOTO 13160
13140 PRINT USING "TIME = ###.###   VOLTAGE=#.#######";TIME,BI.VOLTS
13150 PRINT
13160 NEXT LOOP
13170 '
13180 CLOSE#1
13190 GOTO 13240
13200 ' ERROR
13210 PRINT
13220 PRINT "ERROR",
13230 PRINT IERR1,IERR2
13235 END
13240 ERASE IADL
13250 ERASE IADH
13260 NEXT KR
```

```
13270 ERASE OF$
13280 RETURN 200
19995 '
19996 '
20000 'display and calculation of sec data
20002 '
20004 '
20010 SCREEN 2
20020 CLS:LOCATE 10,20:INPUT "Name of data file";IFILE$
20040 OPEN IFILE$ AS #2 LEN = 8
20060 FIELD #2,4 AS X$,4 AS Y$
20080 GET #2,1
20100 LET TOTTIME = CVS(X$)
20120 NP = TOTTIME*60
20140 DIM X(NP),Y(NP),YC(NP)
20160 FOR M = 1 TO NP
20180 GET #2,M+1
20200 LET X(M)=CVS(X$):LET Y(M)=CVS(Y$)
20220 NEXT M:CLOSE 2
20240 FOR M = 1 TO NP
20260 IF M = 1 THEN YMAX=Y(M):YMIN=Y(M)
20280 IF Y(M)>YMAX THEN YMAX=Y(M):XMAX=X(M)
20300 IF Y(M)<YMIN THEN YMIN=Y(M):XMIN=X(M)
20320 NEXT M
20340 XMAX = TOTTIME
20360 XMIN = 0!
20380 YMAX = YMAX + ABS(YMAX)*.1
20400 YMIN = YMIN - ABS(YMIN)*.5
20420 CLS:LINE(80,150)-(560,20),,B
20460 FOR M = 1 TO NP
20480 PX=80+((X(M)-XMIN)/(XMAX-XMIN))*480
20500 PY=140-((Y(M)-YMIN)/(YMAX-YMIN))*120
20520 PSET(PX,PY)
20540 NEXT M
20545 DEF SEG = &HB800
20547 BSAVE "D:screenbl",0,&H4000
20550 GOTO 20560
20552 DEF SEG = &HB800
20554 BLOAD "d:screenbl",0
20560 LOCATE 23,20:INPUT "Automatic baseline determination (y/n)";ABL$
20580 IF ABL$ ="y" OR ABL$ ="Y" THEN GOSUB 30000
20600 LOCATE 23,10:PRINT;"USE THE CURSOR TO SELECT THE TIMES FOR BASELINE
DETERMINATION";
20620 LOCATE 20,1:PRINT;"Left and right arrows move cursor; up arrow sets
bl start; down arrow sets end";
20640 LOCATE 21,1:PRINT;"Put start and stop at each portion of the data
to be used to calculate baseline";
20650 LOCATE 22,25:PRINT "Press space bar when finished";
20660 LOCATE 19,11:PRINT "-":LINE(80,150)-(80,120)
20680 K=1:L=1:Y=11
20700 ON KEY(11) GOSUB 21000
20720 ON KEY(14) GOSUB 22000
```

```
20725 ON KEY(12) GOSUB 23000
20730 ON KEY(13) GOSUB 24000
20740 KEY(11) ON:KEY(14) ON:KEY(12) ON:KEY(13) ON
20760 CHECK$=INKEY$:LINE(80,150)-(80,120)
20780 IF CHECK$ = " " THEN  20800 ELSE 20760
20800 KEY(11)OFF:KEY(12)OFF:KEY(13)OFF:KEY(14)OFF:LOCATE 19,Y:PRINT "
";:LINE(80,150)-(560,150):FOR I = 1 TO K
20820 LINE(S1(I),150)-(E1(I),145),,BF
20840 NEXT I
20843 GOSUB 20900
20845 LOCATE 23,20:INPUT "Is the baseline correct (y/n)";C1$
20850 IF C1$ = "n" OR C1$ = "N" THEN LINE(81,149)-(559,140),0,BF:GOTO
20550
20860 GOTO 25000
20900 LINE (0,200)-(640,151),0,BF:RETURN
21000 S(K) = Y-1:S1(K)=S(K)*8!
21010 LINE(S1(K),150)-(S1(K),142):K=K+1
21020 RETURN 20760
22000 E(L) = Y-1:E1(L)=E(L)*8!
22010 LINE(E1(L),150)-(E1(L),142):L=L+1
22020 RETURN 20760
23000 Y=Y-1:LOCATE 19,Y:PRINT "-";:LOCATE 19,Y+1:PRINT " ";
23010 LINE(80,150)-(560,150)
23020 RETURN 20760
24000 Y=Y+1:LOCATE 19,Y:PRINT "-";:LOCATE 19,Y-1:PRINT " ";
24010 LINE(80,150)-(560,150)
24020 RETURN 20760
25000 SX=0:SY=0:SXY=0:SXS=0:SYS=0:NUM=0
25010 GOSUB 20900:LOCATE 23,20:PRINT "Finding best fit line for baseline"
25020 FOR I = 1 TO K-1
25040 N1 = ((S(I)-10)/60)*NP:N2 = ((E(I)-10)/60)*NP
25060 FOR M = N1 TO N2
25080 SX=SX+X(M):SY=SY+Y(M):SXY=SXY+X(M)*Y(M):SXS=SXS+X(M)*X(M):
SYS=SYS+Y(M)*Y(M):NUM=NUM+1
25100 NEXT M
25120 NEXT I
25140 'calculating regression parameters
25160 REGM=NUM*SXS-SX*SX:REGN=NUM*SYS-SY*SY:PREG=NUM*SXY-SX*SY
25180 AREG=PREG/REGM
25200 BREG=(REGM*SY-PREG*SX)/(NUM*REGM)
25220 SD1=REGN/(NUM*(NUM-1)):SDY=SQR(SD1)
25240 RREG=PREG/SQR(REGM*REGN)
25260 GOSUB 20900
25280 LOCATE 21,23:PRINT "Linear regression of baseline"
25300 LOCATE 22,25:PRINT USING "Y = #.##^^^^ X + #.##^^^^";AREG;BREG
25320 FOR J = 1 TO NP
25340 YBL=AREG*X(J)+BREG:YC(J)=Y(J)-YBL:NEXT J
25360 'display of corrected chromatogram
25380 CLS:LINE(80,150)-(560,20),,B
25382 LOCATE 22,20:PRINT "Chromatogram with baseline subtracted"
25396 YCMAX = YMAX - AREG*XMAX+BREG:YCMIN = YMIN - AREG*XMIN+BREG
25400 FOR M = 1 TO NP
```

```
25420 PX=80+((X(M)-XMIN)/(XMAX-XMIN))*480
25440 PY=140-((YC(M)-YCMIN)/(YCMAX-YCMIN))*120
25460 PSET(PX,PY)
25480 NEXT M
25485 PY0=140-((0-YCMIN)/(YCMAX-YCMIN))*120
25490 LINE(80,PY0)-(560,PY0)
25500 GOSUB 20900
25540 GOSUB 20900:LOCATE 22,20:INPUT "Recalculate baseline (y/n)";RCB$
25560 IF RCB$ = "y" OR RCB$ = "Y" THEN CLS:GOTO 20552
25600 ERASE Y:GOTO 40000
29995 '
29996 '
30000 'automatic baseline selection
30002 '
30004 '
30010 SX=0:SY=0:SXY=0:SXS=0:SYS=0:NUM=0
30020 GOSUB 20900: LOCATE 22,10: PRINT "Baseline determined using the
first 5 and last 2 minutes of run"
30040 N1(1)=0:N2(1)=300:N1(2)=NP-120:N2(2)=NP
30060 FOR I = 1 TO 2
30080 FOR M = N1(I) TO N2(I)
30100 SX=SX+X(M):SY=SY+Y(M):SXY=SXY+X(M)*Y(M):SXS=SXS+X(M)*X(M):
SYS=SYS+Y(M)*Y(M):NUM=NUM+1
30120 NEXT M
30140 NEXT I
30160 RETURN 25140
39995 '
39996 '
40000 ' integration of chromatogram
40002 '
40004 '
40010 GOSUB 20900
40012 DEF SEG = &HB800:BSAVE "d:screen",0,&H4000
40015 LOCATE 23,20:INPUT "Computer selection of peaks (y/n) ";CP$
40017 IF CP$ = "n" OR CP$ = "N" THEN 41510
40020 LOCATE 23,15:PRINT "Finding the beginning and end of each peak"
40100 'locating peaks (departure from baseline)
40110 K = 0:KE=0:L=0:M=0:J=0
40120 FOR I = NP/3 TO NP
40140 IF YC(I)<2*SDY THEN 40500
40150 L = 0
40155 IF KE <> K THEN 41000
40160 IF N = 6 THEN K=K+1:PST(K)=X(I-6)
40180 IF M=I-1 THEN N=N+1
40200 M=I
40220 GOTO 41000
40500 N=0
40520 IF K=KE THEN 41000
40540 IF L = 3 THEN KE=KE+1:PEND(K)=X(I-6)
40560 IF J = I-1 THEN L=L+1
40580 J=I
40600 GOTO 41000
```

```
41000 NEXT I
41300 K=KE:'display of peak start and end times
41310 GOSUB 20900
41315 LOCATE 20,10 :PRINT "Cursors show peak location"
41320 FOR IP = 1 TO K
41340 PXS=80+((PST(IP)-XMIN)/(XMAX-XMIN))*480
41360 PXE=80+((PEND(IP)-XMIN)/(XMAX-XMIN))*480
41380 LINE(PXS,140)-(PXS,20):LINE(PXE,140)-(PXE,20)
41390 LINE(PXS,140)-(PXE,135),,BF
41397 LOCATE 19+IP,5 :PRINT "Start and end for peak ";IP;":
";PST(IP);PEND(IP);
41400 NEXT IP
41420 LOCATE 20,55:INPUT "Integrate Peaks (y/n)";CSP$
41440 IF CSP$ = "Y" OR CSP$ = "y" THEN 42000
41445 CLS:DEF SEG = &HB800:BLOAD "d:screen",0
41450 'CLS:LINE(80,150)-(560,20),,B
41460 'FOR M = 1 TO NP
41470 'PX=80+((X(M)-XMIN)/(XMAX-XMIN))*480
41480 'PY=140-((YC(M)-YCMIN)/(YCMAX-YCMIN))*120
41490 'PSET(PX,PY)
41500 'NEXT M
41505 'LINE(80,PY0)-(560,PY0)
41510 GOSUB 20900:LOCATE 20,20:PRINT "Use Cursors to Select Integration
Limits"
41520 LOCATE 21,25:PRINT "One or more areas may be selected"
41530 LOCATE 22,2:PRINT "Left & right arrows move cursor; up arrow starts
integration; down arrow ends"
41540 LOCATE 23,20:PRINT "PRESS SPACE BAR TO END"
41560 X=81:J=0:K=0
41570 ON KEY(11) GOSUB 41700
41580 ON KEY(12) GOSUB 41750
41590 ON KEY(13) GOSUB 41800
41600 ON KEY(14) GOSUB 41850
41610 KEY(11) ON:KEY(12) ON:KEY(13) ON:KEY(14) ON
41615 PT=(X-80)*NP/(60*480):LOCATE 5,12:PRINT "Cursor Location:";PT
41620 CHECK$=INKEY$:IF CHECK$ = " " THEN 41630 ELSE 41615
41630 KEY(11) OFF:KEY(12) OFF:KEY(13) OFF:KEY(14) OFF
41640 GOTO 42000
41700 J=J+1:PS(J)=X:PST(J)=(X-80)*NP/(60*480):LINE(X,150)-(X,20):RETURN
41750 X=X-5:LINE(X,149)-(X,145):LINE(X+5,149)-(X+5,145),0:RETURN
41800 X=X+5:LINE(X,149)-(X,145):LINE(X-5,149)-(X-5,145),0:RETURN
41850 K=K+1:PE(K)=X:PEND(K)=(X-80)*NP/(60*480):LINE(X,150)-(X,20):RETURN
42000 'integration of computer selected peaks
42010 DIM AREA(K):TOTAREA=0!
42015 GOSUB 20900
42016 NP1 = 2
42020 FOR IP = 1 TO K
42025 NP1 = NP1 + (PEND(IP) - PST (IP))*12
42030 AREA(IP) = 0!
42040 FOR M = PST(IP)*60 TO PEND(IP)*60
42060 AREA(IP) = AREA(IP) + YC(M)
42080 NEXT M
```

```
42090 LOCATE 19+IP,5:PRINT USING "Area of peak ## is
#.####^^^^";IP;AREA(IP);
42095 TOTAREA=TOTAREA+AREA(IP):NEXT IP
42100 LOCATE 22,45:PRINT USING "Total area is #.####^^^^";TOTAREA
42101 LOCATE 23,40:INPUT "Reselect peak start and end (y/n)";RP$
42103 IF RP$="y" OR RP$ = "Y" THEN ERASE AREA:GOTO 41445
42105 IF RM$ ="Y" OR RM$ = "y" THEN ERASE YMF:ERASE WM
42107 LOCATE 23,40:PRINT "                                          "
42110 LOCATE 23,15:INPUT "Convert all peaks to mass fractions (y/n)";CO$
42115 IF CO$ = "N" OR CO$ = "n" THEN 42220
42120 'conversion of y values to mass fractions
42140 'average of 5 points taken
42145 L=0:DIM YMF(NP1),WM(NP1):SUMW=0:SUMN=0
42150 'conversion of retention time to molecular weight
42155 GOSUB 20900:LOCATE 20,5:INPUT "Type the calibration coefficients
(A+BX+CX^2+DX^3)";A,B,C,D
42156 FOR IP = 1 TO K
42160 FOR J = PST(IP)*60+3 TO PEND(IP)*60+3 STEP 5
42180 L=L+1:YMF(L)=(YC(J-2)+YC(J-1)+YC(J)+YC(J+1)+YC(J+2))/(TOTAREA)
42190 WM(L)=10^(A+B*X(J)+C*X(J)^2+D*X(J)^3)
42192 SUMW=SUMW+YMF(L)*WM(L):SUMN=SUMN+YMF(L)/WM(L)
42195 LOCATE 22,50:PRINT YMF(L);WM(L)
42200 NEXT J:NEXT IP
42202 SUMN=1/SUMN
42205 GOSUB 20900:LOCATE 20,5:PRINT "Weight Ave. MW = ";SUMW
42210 LOCATE 21,5:PRINT "Number Ave. MW = ";SUMN
42212 LOCATE 23,15:INPUT "Recalculate with different peaks";RM$
42215 IF RM$ = "Y" OR RM$ = "y" THEN 42101 ELSE 42300
42220 GOSUB 20900:LOCATE 20,15:INPUT "Peak number of peak to be
converted";IP
42225 L=0:DIM YMF(NP1),WM(NP1):SUMW=0:SUMN=0:SUMC=0
42230 LOCATE 21,5:INPUT "Type the calibration coefficients
(A+BX+CX^2+DX^3)";A,B,C,D
42240 FOR J = PST(IP)*60+3 TO PEND(IP)*60+3 STEP 5
42250 L=L+1:YMF(L)=(YC(J-2)+YC(J-1)+YC(J)+YC(J+1)+YC(J+2))/(AREA(IP))
42260 WM(L)=10^(A+B*X(J)+C*X(J)^2+D*X(J)^3)
42265 SUMW=SUMW+YMF(L)*WM(L):SUMN=SUMN+YMF(L)/WM(L)
42270 NEXT J
42275 SUMN=1/SUMN
42280 GOSUB 20900:LOCATE 20,5:PRINT "Weight Ave. MW = ";SUMW
42285 LOCATE 21,5:PRINT "Number Ave. MW = ";SUMN
42290 LOCATE 23,15:INPUT "Recalculate with different peaks";RM$
42295 IF RM$ = "Y" OR RM$ = "y" THEN 42101
42300 'temporary plotting file
42310 LOCATE 23,15:PRINT "                                                  "
42320 LOCATE 23,15:INPUT "Plotting file name";PF$
42340 OPEN PF$ FOR OUTPUT AS #3
42350 PRINT #3,L
42360 FOR J1 = 1 TO L
42380 PRINT #3,WM(J1);YMF(J1)
42400 NEXT J1
42420 CLOSE 3:ERASE X:ERASE YC:ERASE YMF:ERASE WM:ERASE AREA
```

```
42500 RETURN 200
49995 '
49996 '
50000 'Screen plotting of converted chromatograms
50002 '
50004 '
50010 CLS:SCREEN 2
50015 KEY OFF
50020 INPUT "How many files do you wish to plot";N
50030 FOR I = 1 TO N
50040 PRINT
50050 PRINT "Type the name of file ";I
50060 INPUT;A$(I)
50070 NEXT I
50080 PRINT:PRINT:PRINT "Open circles - type OC"
50090 PRINT "Filled circles - type FC"
50100 PRINT "Open squares - type OS"
50110 PRINT "Filled squares - type FS"
50120 PRINT "Points - type P"
50125 PRINT "Lines - type L"
50130 FOR I = 1 TO N
50140 PRINT: PRINT "Pick the desired symbol for file number";I
50150 INPUT;SY$(I):NEXT I
50160 PRINT:PRINT "Type the title for the plot":INPUT;TITLE$
50170 LOCATE 24,30:PRINT "Reading the data files....."
50180 FOR J = 1 TO N
50190 OPEN A$(J) FOR INPUT AS #1
50200 INPUT#1,NP
50210 DIM X1(NP),Y(NP),X(NP)
50220 FOR I = 1 TO NP
50230 INPUT#1,X1(I),Y(I):X(I)=(LOG(X1(I)))/2.3026
50240 IF J = 1 THEN IF I = 1 THEN XMAX = X(I):YMAX =
Y(I):YMIN=Y(I):XMIN=X(I)
50250 IF X(I)>XMAX THEN XMAX = X(I)
50260 IF X(I)<XMIN THEN XMIN = X(I)
50270 IF Y(I)>YMAX THEN YMAX=Y(I)
50280 IF Y(I)<YMIN THEN YMIN = Y(I)
50290 NEXT I:CLOSE 1:ERASE X:ERASE Y:ERASE X1:NEXT J
50300 CLS:LINE(100,19)-(600,179),,B
50310 YMIN=0!
50320 IF YMAX>.8 THEN YMAX=1!:YTIC=.2:GOTO 50430
50330 IF YMAX>.5 THEN YMAX=.8:YTIC=.2:GOTO 50430
50340 IF YMAX>.2 THEN YMAX=.5:YTIC=.1:GOTO 50430
50350 IF YMAX>.1 THEN YMAX=.2:YTIC=.05:GOTO 50430
50360 IF YMAX>.08 THEN YMAX=.1:YTIC=.02:GOTO 50430
50370 IF YMAX>.05 THEN YMAX=.08:YTIC=.02:GOTO 50430
50380 IF YMAX>.02 THEN YMAX=.05:YTIC=.01:GOTO 50430
50390 IF YMAX>.01 THEN YMAX=.02:YTIC=.005:GOTO 50430
50400 IF YMAX>8.000001E-03 THEN YMAX=.01:YTIC=.002:GOTO 50430
50410 IF YMAX>.005 THEN YMAX=8.000001E-03:YTIC=.002:GOTO 50430
50420 YMAX=.005:YTIC=.001
50430 YT=YTIC:NTY=INT(YMAX/YTIC)
```

```
50440 XMIN=INT(XMIN):XMAX=INT(XMAX)+1
50450 FOR K=XMIN TO XMAX-1
50460 XPTIC=100+((K-XMIN)/(XMAX-XMIN))*500
50470 LINE (XPTIC,179)-(XPTIC,174)
50480 TIC=XPTIC*80/640
50490 LOCATE 24,TIC-3
50500 PRINT USING "########";10^K;
50503 FOR J = 2 TO 9
50504 XPT = LOG(10^K*J)/2.303:XPTIC = 100+((XPT-XMIN)/(XMAX-XMIN))*500
50505 LINE (XPTIC,179)-(XPTIC,176)
50506 TIC=XPTIC*80/640
50507 LOCATE 24,TIC
50509 NEXT J
50510 NEXT K
50520 FOR L = 1 TO NTY
50530 YPTIC=179-((YTIC-YMIN)/(YMAX-YMIN))*160
50540 LINE (100,YPTIC)-(104,YPTIC)
50550 TIC=(YPTIC*25/200)+1
50560 LOCATE TIC,7
50570 PRINT USING "#.#####";YTIC
50580 YTIC=YTIC+YT
50590 NEXT L
50600 FOR J = 1 TO N
50610 OPEN A$(J) FOR INPUT AS #1
50620 INPUT#1,NP
50630 DIM X(NP),Y(NP),X1(NP):IC=0
50640 FOR I=1 TO NP
50650 INPUT#1,X1(I),Y(I):X(I)=(LOG(X1(I)))/2.3026
50655 IF Y(I) < 0 THEN 50800
50660 PX=100+((X(I)-XMIN)/(XMAX-XMIN))*500
50670 PY=179-((Y(I)-YMIN)/(YMAX-YMIN))*160
50680 IF SY$(J) ="OC" GOTO 50730
50690 IF SY$(J)="FC" GOTO 50740
50700 IF SY$(J)="OS" GOTO 50750
50710 IF SY$(J)="FS" GOTO 50770
50720 IF SY$(J)="P" GOTO 50790
50725 IF SY$(J) = "L" GOTO 50795
50730 IF I MOD 2 <> 0 THEN 50800
50732 CIRCLE (PX,PY),3:GOTO 50800
50740 IF I MOD 2 <> 0 THEN 50800
50742 CIRCLE (PX,PY),3:PAINT (PX,PY) :GOTO 50800
50750 IF I MOD 2 <> 0 THEN 50800
50752 PX1=PX+4:PY1=PY+2:PX2=PX-4:PY2=PY-2
50760 LINE(PX2,PY1)-(PX1,PY2),,B:GOTO 50800
50770 IF I MOD 2 <> 0 THEN 50800
50772 PX1=PX+4:PY1=PY+2:PX2=PX-4:PY2=PY-2
50780 LINE(PX2,PY1)-(PX1,PY2),,BF:GOTO 50800
50790 PSET(PX,PY)
50795 IF IC = 1 THEN 50797
50796 PSET(PX,PY):IC = 1:GOTO 50800
50797 LINE -(PX,PY)
50800 NEXT I:CLOSE 1
```

```
50810 ERASE X:ERASE X1
50820 ERASE Y:NEXT J
50830 CLOSE 1
50840 LOCATE 2,35:PRINT TITLE$
50850 RETURN 400
```

```
10 '    PROGRAM FOR SEC DATA ACQUISITION
20 '          --- K.A.DENNISON ---
30 '
40 '    Program is set up to collect 10 data points, 0.2 msec apart,
50 '    average the values, convert to voltage, write the voltage value
60 '    to an array, wait a predetermined number of seconds, and repeat
70 '    the process for the specified run time.  The user inputs the
80 '    total run time and the number of seconds between data points.
90 '    After all the data is collected, it is written to a file.
100 '
110     CLS:LOCATE 5,15:PRINT "DATA COLLECTION PROGRAM"
120     LOCATE 8,7:INPUT "TOTAL DATA COLLECTION TIME (in minutes) ",TTIME
130     TINT = CINT(TTIME*60/1000):IF TINT = 0 GOTO 150:NDP =
TTIME*60/TINT
140 NDP = TTIME*60/TINT
150     LOCATE 10,7:PRINT "THE TIME INTERVAL BETWEEN DATA POINTS (in
seconds) IS ";TINT
160 IF TINT = 0 GOTO 180
170 LOCATE 11,10:PRINT USING "This interval collects #### points.";NDP
180     LOCATE 13,7:INPUT "DO YOU WISH TO CHOOSE A DIFFERENT INTERVAL
(y/n)";W$
190     IF (W$ = "n") OR (W$ = "N") THEN 215
200     LOCATE 15,7:INPUT "INPUT THE DESIRED INTERVAL (in seconds) ",TINT
210     NDP = CINT(TTIME*60/TINT):NUM = 0
215 LOCATE 18,7:INPUT "External trigger (y/n)";ET$
220 LOCATE 21,15:INPUT "DATA FILE NAME: ",DF$
225 'LOCATE 24,15:PRINT "DON'T FORGET TO PUT A DISK IN A:"
230 FOR I = 1 TO 100:L = L + I:NEXT I
260     GOSUB 500
270     DIM DARRAY(NDP)
271 IF ET$ = "n" OR ET$ = "N" THEN 280
272     CRAD = &H9E:GOSUB 1090
274     CRAD = &H1E
280     ON TIMER(TINT) GOSUB 1090
290     TIMER ON
300 '  Real-time screen plotting of data as it is collected.
310 KEY OFF
320    SCREEN 2:CLS:LINE(0,179)-(600,179):LOCATE 1,1:PRINT "TIME:
min":WHILE NUM<NDP+1
330    IF NUM = 0 THEN 410
340 ' YMAX sets the fullscale voltage for the screen.
350    XMAX = NDP:YMAX = .01
360 IF CK = NUM + 2000 THEN 420
370    X = NUM/XMAX:Y = DARRAY(NUM)/YMAX
380 CK = NUM +2000
390    PSET (X*600,179-Y*179)
392 LOCATE 1,7:PRINT USING "##.##";NUM*TINT/60
400 IF NUM = NDP THEN NUM = NDP+1
410 '  WHILE NUM<NDP
420    COUNT = COUNT + 1
430    WEND
435 OPEN DF$ AS #1 LEN = 8
```

```
436 FIELD #1, 4 AS T$, 4 AS D$
437 'OPEN "A:"+DF$ FOR OUTPUT AS #2
438 LSET T$ = MKS$(TTIME):LSET D$ = MKS$(TINT)
439 PUT #1,1
440    FOR I = 1 TO NDP
442 LSET T$ = MKS$(TINT*I/60):LSET D$ = MKS$(DARRAY(I))
444 PUT #1,I+1
450 ' PRINT #2, TINT*I;",";DARRAY(I)
460 '  PRINT #1, TINT*I;",";DARRAY(I)
462 NEXT I
470 LOCATE 24,25:PRINT "Press space bar to continue";
480 E$ = INKEY$:IF E$ <> " " THEN 480
490    KEY ON:END
500 '  BOARD SET-UP SUBROUTINE
510    BASE.ADDRESS      = &H2EC
520    COMMAND.REGISTER  = BASE.ADDRESS + 1
530    STATUS.REGISTER   = BASE.ADDRESS + 1
540    DATA.REGISTER     = BASE.ADDRESS
550    COMMAND.WAIT      = &H4
560    WRITE.WAIT        = &H2
570    READ.WAIT         = &H5
580 ''
590    CSTOP             = &HF
600    CCLEAR            = &H1
610    CERROR            = &H2
620    CCLOCK            = &H3
630    CSAD              = &HD
640    CRAD              = &H1E
650    DUMMY             = 5
660 ''
670 '' Define DMA constants for DMA channel 1.
680 ''
690 '' The memory to be used for DMA starts at memory address &H0
700 '' on memory page 4.
710 ''
720    DMACHANNEL   = 1
730    DMAMODE      = &H45
740    BASEREG      = 2
750    COUNTREG     = 3
760    PAGEREG      = &H83
770    DMABASEL     = 0
780    DMABASEH     = &H0
790    DMAPAGE      = 4
800 ''
810 '  Period and frequency set internal clock - period is the number of
820 '   cycles between data samples and frequency is the cycle frequency.
830 '   Frequency is fixed at 400000 (2.5 microseconds/cycle).
840 '  Factor, range, and offset are used in conversion to voltage.
850 '
860    FACTOR# = 4096
870    PERIOD# = 80
880    FREQUENCY# = 400000!
```

```
890    GAIN(0) = 1 : GAIN(1) = 10
900    GAIN(2) = 100 : GAIN(3) = 500
910    RANGE=20:OFFSET=10
920 ''
930 '' Print out conversion rate.
940 ''
950 '  PRINT
960 '  PRINT "          The internal clock is set to a frequency of ";
970 '  PRINT USING "#####";FREQUENCY#/PERIOD#; : PRINT " Hertz."
980 ''
990    GAIN.CODE = 3  ''' Sets full scale to 100 millivolts
1000 ''
1010 '  Start.channel and end.channel specify the A/D channel to be used.
1020 '  Both are set to the same number to sample only one channel.
1030    START.CHANNEL = 0: END.CHANNEL = 0
1040 ''
1050    NUM.CONV = 10  '' Number of samples to be collected and averaged.
1060    RETURN
1070 '  Subroutine for collecting num.conv data points and averaging
them.
1080 '
1090 '' Check for legal Status Register.
1100    NUM = NUM + 1
1110    STATUS = INP(STATUS.REGISTER)
1120    IF NOT((STATUS AND &H70) = 0) THEN GOTO 2400
1130 ''
1140 '' Stop and clear the DT2801.
1150 ''
1160    OUT  COMMAND.REGISTER, CSTOP
1170   TEMP = INP(DATA.REGISTER)
1180    WAIT STATUS.REGISTER,  COMMAND.WAIT
1190    OUT  COMMAND.REGISTER, CCLEAR
1200 ''
1210 '' Set up the A/D converter.
1220 '' Write SET A/D PARAMETERS command.
1230 ''
1240    WAIT STATUS.REGISTER,  COMMAND.WAIT
1250    OUT  COMMAND.REGISTER, CSAD
1260 ''
1270 '' Write A/D gain byte.
1280 ''
1290    WAIT STATUS.REGISTER,  WRITE.WAIT, WRITE.WAIT
1300    OUT  DATA.REGISTER,    GAIN.CODE
1310 ''
1320 '' Write A/D start channel byte.
1330 ''
1340    WAIT STATUS.REGISTER,  WRITE.WAIT, WRITE.WAIT
1350    OUT  DATA.REGISTER,    START.CHANNEL
1360 ''
1370 '' Write A/D end channel byte.
1380 ''
1390    WAIT STATUS.REGISTER,  WRITE.WAIT, WRITE.WAIT
```

```
1400    OUT  DATA.REGISTER,    END.CHANNEL
1410 ''
1420 '' Write two bytes, dummy number of conversions.
1430 ''
1440    WAIT STATUS.REGISTER,  WRITE.WAIT, WRITE.WAIT
1450    OUT  DATA.REGISTER,    DUMMY
1460    WAIT STATUS.REGISTER,  WRITE.WAIT, WRITE.WAIT
1470    OUT  DATA.REGISTER,    DUMMY
1480 ''
1490 '' Set internal clock rate.
1500 '' Write SET CLOCK PERIOD command.
1510 ''
1520    WAIT STATUS.REGISTER,  COMMAND.WAIT
1530    OUT  COMMAND.REGISTER, CCLOCK
1540 ''
1550 '' Write high and low bytes of PERIOD#.
1560 ''
1570    PERIODH = INT(PERIOD#/256)
1580    PERIODL = PERIOD# - PERIODH * 256
1590    WAIT STATUS.REGISTER,  WRITE.WAIT, WRITE.WAIT
1600    OUT  DATA.REGISTER,    PERIODL
1610    WAIT STATUS.REGISTER,  WRITE.WAIT, WRITE.WAIT
1620    OUT  DATA.REGISTER,    PERIODH
1630 ''
1640 '' Set-up DMA controller
1650 ''
1660    DMACOUNT  = (NUM.CONV * 2) - 1
1670    DMACOUNTH = INT(DMACOUNT/256)
1680    DMACOUNTL = DMACOUNT - DMACOUNTH * 256
1690 ''
1700    OUT 11,DMAMODE              ' set DMA mode
1710    OUT 12,0                    ' clear byte flip-flop
1720    OUT BASEREG,DMABASEL        ' set DMA memory base address
1730    OUT BASEREG,DMABASEH        '
1740    OUT COUNTREG,DMACOUNTL      ' set DMA byte count
1750    OUT COUNTREG,DMACOUNTH      '
1760    OUT PAGEREG,DMAPAGE         ' set DMA memory page
1770    OUT 10,DMACHANNEL           ' enable DMA channel mask
1780 ''
1790 '' Check for ERROR.
1800 ''
1810    WAIT STATUS.REGISTER,  COMMAND.WAIT
1820    STATUS = INP(STATUS.REGISTER)
1830    IF (STATUS AND &H80) THEN GOTO 2160
1840 ''
1850 '   Starting conversions.
1860 ''
1870    WAIT STATUS.REGISTER,  COMMAND.WAIT
1880    OUT  COMMAND.REGISTER, CRAD
1890 ''
1900 '' Check for ERROR.
1910    WAIT STATUS.REGISTER,  COMMAND.WAIT
```

```
1920    STATUS = INP(STATUS.REGISTER)
1930    IF (STATUS AND &H80) THEN GOTO 2160
1940 ''
1950 '' Calculate and print the A/D readings in volts.
1960 ''
1970 ''
1980 '  The data values are read form the assigned memory locations.
1990    DEF SEG = &H4000
2000 ''
2010    SUM# = 0
2020    FOR LOOP = 1 TO NUM.CONV
2030 ''
2040    ADDRESS = (LOOP - 1) * 2
2050    DATA.VALUE# = PEEK(ADDRESS)
2060    DATA.VALUE# = DATA.VALUE# + PEEK(ADDRESS + 1) * 256
2070    IF DATA.VALUE# > 32767 THEN DATA.VALUE# = DATA.VALUE# -65536!
2080    SUM# = SUM# +DATA.VALUE# : NEXT LOOP : DATA.VALUE# =
SUM#/NUM.CONV
2090 ''
2100    VOLTS# = ((RANGE * DATA.VALUE#/FACTOR#) - OFFSET)/GAIN(GAIN.CODE)
2110 ''
2120    DARRAY(NUM) = VOLTS#
2130    IF NUM = NDP THEN TIMER OFF  ' Stops looping after all data
collected
2140    RETURN
2150    PRINT : PRINT : PRINT "FINISHED" : GOTO 2480
2160 ''
2170 '' Fatal board error.
2180 ''
2190    PRINT
2200    PRINT "FATAL BOARD ERROR"
2210    PRINT "STATUS REGISTER VALUE IS ";HEX$(STATUS);" HEXIDECIMAL"
2220    PRINT : BEEP : BEEP : GOSUB 2270
2230    PRINT "ERROR REGISTER VALUES ARE:"
2240    PRINT "      BYTE 1 -   ";HEX$(ERROR1);"  HEXIDECIMAL"
2250    PRINT "      BYTE 2 -   ";HEX$(ERROR2);"  HEXIDECIMAL"
2260    PRINT : GOTO 2480
2270 ''
2280 '' Read the Error Register.
2290 ''
2300    OUT  COMMAND.REGISTER, CSTOP : TEMP = INP(DATA.REGISTER)
2310 ''
2320    WAIT STATUS.REGISTER, COMMAND.WAIT
2330    OUT COMMAND.REGISTER, CERROR
2340 ''
2350    WAIT STATUS.REGISTER, READ.WAIT
2360    ERROR1 = INP(DATA.REGISTER)
2370    WAIT STATUS.REGISTER, READ.WAIT
2380    ERROR2 = INP(DATA.REGISTER)
2390    RETURN
2400 ''
2410 '' Illegal Status Register.
```

```
2420 ''
2430    PRINT
2440    PRINT "FATAL ERROR - ILLEGAL STATUS REGISTER VALUE"
2450    PRINT "STATUS REGISTER VALUE IS ";HEX$(STATUS);" HEXIDECIMAL"
2460    BEEP : BEEP
2470 ''
2480    PRINT : PRINT
2490   END
```

Appendix 2. Characterization of PEO

Size Exclusion Chromatography.

All PEO samples were characterized using size exclusion chromatography to obtain weight and number average molecular weights and molecular weight distributions. The chromatographic system used is the one described in section 3.4.3. The results of the SEC measurements for all the PEO samples used in this study are below.

Nominal MW	Number Average MW	Weight Average MW	$\bar{M}_w/\bar{M}_n$
300	354	418	1.18
600	690	793	1.15
1000	961	1220	1.27
1540	1553	1712	1.10
3400	3639	4129	1.13
8000	11211	11727	1.05
14000	17876	20759	1.16
20000	21340	24718	1.16
35000	37171	40098	1.08

The 35000 nominal molecular weight sample is the one used for synthesis of all gels discussed in this thesis. Figure A-1 shows the superimposed molecular weight distributions for all samples. (Each sample was run individually.)

PEO End-to-end Distance.

The root-mean-square end-to-end distance was determined for each of the PEO samples. There are a number of ways of computing end-to-end

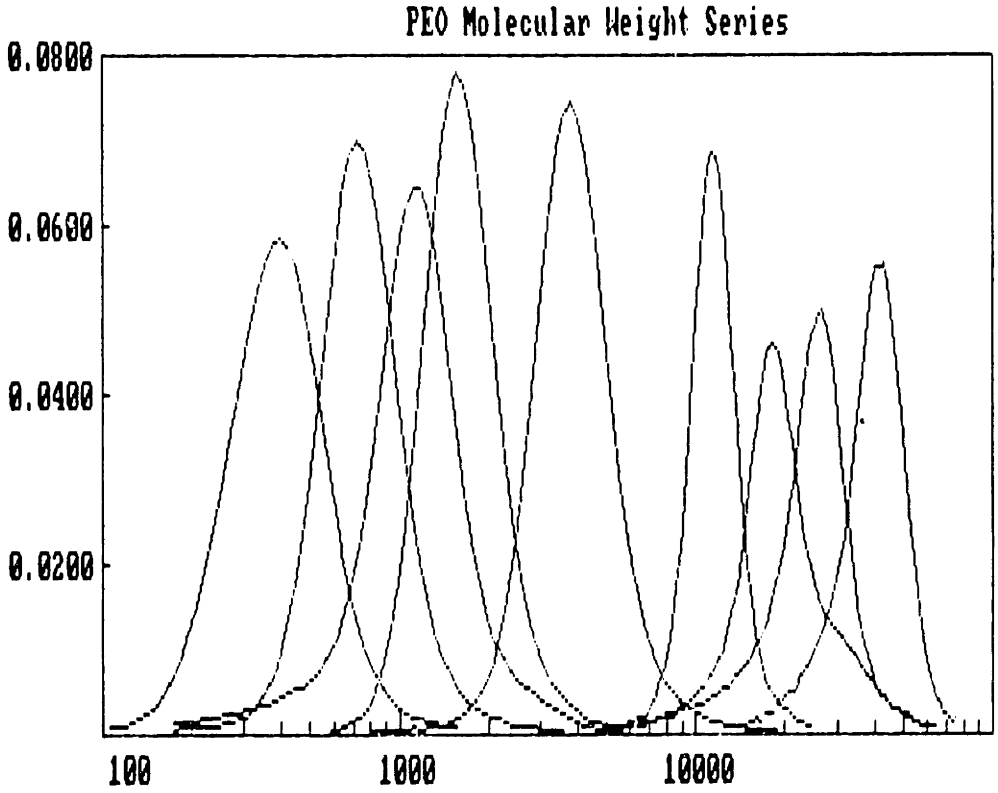

Figure A-1. Molecular weight distributions of 9 PEO samples as determined using size exclusion chromatography. Nominal and weight and number average molecular weights are given in the text.

distances [19], which all give similar results. The technique chosen is based on the intramolecular expansion of an isolated random coil, and is taken directly from Flory [19]. The rms end-to-end distance $\langle \bar{r}^2 \rangle^{1/2}$ is given by

$$\langle \bar{r}^2 \rangle^{1/2} = \alpha \langle \bar{r}^2 \rangle_0^{1/2} \qquad \text{(A-1)}$$

where α is the intramolecular expansion factor for an isolated random coil, and $\langle \bar{r}^2 \rangle_0^{1/2}$ is the unperturbed rms end-to-end length, which is defined by

$$\langle \bar{r}^2 \rangle_0 = Cn\ell^2 \qquad \text{(A-2)}$$

where C is the characteristic ratio, n is the number of bonds, and ℓ is the bond length. The intramolecular expansion factor α is defined by

$$\alpha^5 - \alpha^3 = 2C_m\psi_1(1 - \theta/T)M^{1/2} \qquad \text{(A-3)}$$

C_m is a constant for a given polymer - solvent pair, and is numerically 0.105 for PEO in water at 25°C. M is the molecular weight. Strictly speaking, the equation applies for a monodisperse sample only, but as the samples used had narrow distributions, using the number average molecular weight for M should give reasonable results. The other variables, ψ_1 and θ, are measures of the solvent quality. The values used were 95°C and -0.5, both of which were taken from data found in Bailey and Koleske [12]. Equation A-3 can be solved iteratively to find a value for α for a given

molecular weight. This can then be used in equation A-1, in which equation A-2 has been substituted, to find $\langle \bar{r}^2 \rangle^{1/2}$ for a given PEO sample. These are the values given in table 3-2 for the PEO samples used in the diffusivity measurements. For completeness, values for all the PEO samples on which chromatography was done are given here.

Nominal MW	$\langle \bar{r}^2 \rangle^{1/2}$ (Å)
300	24
600	35
1000	42
1540	56
3400	92
8000	178
14000	235
20000	261
35000	362

Diffusion Coefficient and Effective Hydrodynamic Radius.

The two other properties of the PEO samples reported in table 3-2, the diffusion coefficient in water at 25°C and the effective hydrodynamic radius under the same conditions, were determined from the measured molecular weights. The diffusivity was found using a correlation of Rossi [100], which related the diffusivity in cm^2/s to the number average molecular weight as follows.

$$D = 8.7 \times 10^{-5} \bar{M}_n^{-1/2} \qquad \text{(A-4)}$$

The effective hydrodynamic radius was computed using the suggestion of

Tanford [52] that the hydrodynamic radius of a random coiling macromolecule should be 0.85 R_g. R_g is the radius of gyration, and can be related to the end-to-end distance by

$$R_g = [\langle \bar{r}^2 \rangle / 6]^{1/2} \qquad \text{(A-5)}$$

and thus the effective hydrodynamic radius r_E was found from the previously reported values for $\langle \bar{r}^2 \rangle^{1/2}$ in water at 25°C. It should be noted that both the effective radius and the diffusion coefficient will be somewhat different in phosphate-buffered saline, the solvent used for the effective diffusivity measurements, but preliminary measurements suggest the differences will be less than 15%.

It is possible to obtain the value of $0.85R_g$ from theoretical considerations by assuming the macromolecule hydrodynamic volume is that of an equivalent sphere for which Einstein's law of viscosity holds. If one sets the Kirkwood-Riseman intrinsic viscosity expression for random coils [19]

$$[\eta] = \Phi \langle \bar{r}^2 \rangle^{3/2} / M \qquad \text{(A-6)}$$

equal to the Einstein expression for the intrinsic viscosity of a suspension of spheres [19],

$$[\eta] = (0.025) N_{av} (4\pi/3) r_E^3 / M \qquad \text{(A-7)}$$

and the constant Φ is taken to be 2.5×10^{21}, the experimentally observed value, one finds that the equivalent hydrodynamic radius

$$r_E \approx 0.35 \langle \bar{r}^2 \rangle^{1/2} \approx 0.85 R_g. \qquad \text{(A-8)}$$

Appendix 3. Analysis of Approach to Equilibrium Data

Obtaining a diffusion coefficient from the change in solution concentration from time zero (at which the gel is added) to some later time requires a solution to the diffusion equation appropriate to this situation. Crank [90] looked at this problem, which he terms diffusion from a stirred solution of limited volume, for several geometries. The one most closely approaching the situation in the present work is the infinite plane sheet. The problem is set-up as follows. An infinite sheet of the test material of thickness 2l is placed in a solution which extends a distance a from both sides of the sheet. The solution is well-mixed, and the initial concentration is C_0. The initial concentration in the sheet is 0. Therefore, a solution to the transient diffusion equation

$$\frac{\partial C}{\partial t} = D\frac{\partial^2 C}{\partial x^2} \qquad \text{(A-9)}$$

with initial condition

$$C = 0, \quad -1 < x < 1, \quad t = 0 \qquad \text{(A-10)}$$

and boundary condition

$$a\partial C/\partial t = \mp D\partial C/\partial x, \quad x = \pm 1, \quad t > 0. \qquad \text{(A-11)}$$

Any partition coefficient between sheet and solution is assumed to be included in a, i.e., $a = a'/K$ where a' is the actual solution length. The problem is non-dimensionalized and solved by means of Laplace transforms. Crank arrives at the solution

$$\frac{M_t}{M_\infty} = 1 - \sum_{n=1}^{\infty} \frac{2\alpha_k(1+\alpha_k)}{1 + \alpha_k + \alpha_k^2 q_n^2} \exp(-\theta q_n^2) \qquad \text{(A-12)}$$

The variables are

M_t = mass of solute in sheet at time t
M_∞ = mass of solute in sheet at equilibrium
α_k = ratio of solution volume to sheet volume accessible to solute
θ = dimensionless time = Dt/l^2
q_n = roots to $\tan(q_n) = -\alpha_k q_n$
t = time
D = diffusivity in sheet
l = half thickness of sheet

However, the actual samples are low aspect ratio cylinders, not infinite flat sheets. Fortunately, Ma and Evans [91] solved the diffusion problem numerically for bodies of arbitrary shape, and found that for small dimensionless times the numerical and analytical solutions all converge if the length scale used is the volume to surface ratio of the object. Therefore, l in equation A-12 is replaced with $\sigma = V/S = dh/(2d + 4h)$ where d is the gel disk diameter and h the thickness for the present situation. The error due to this approximation is expected to be less than 5% for all measurements made.

The measured solution concentration is related to the fractional uptake M_t/M_∞ as follows. At any time t, the mass of solute in the sheet (gel) M_t is $V_s(C_{si} - C_{st})$ where C_s is the concentration in solution initially (C_{si}) and at time t (C_{st}) and V_s is the volume of solution. From the definition of the partition coefficient and $\alpha_k = V_s/V_gK$,

$$M_\infty = V_g C_{si}/(1+\alpha_k) \qquad \text{(A-13)}$$

and thus

$$\frac{M_t}{M_\infty} = \frac{C_{si} - C_{st}}{C_{si}} (1+\alpha_k) \quad . \tag{A-14}$$

The only remaining unknown in equation A-12 (since the roots q_n can be found knowing α_k) is the diffusivity. In order to find D, an iterative procedure must be used. This was done using the attached BASIC program. The inputs to the program are M_t/M_∞, α_k, t, h (as d is constant), and an initial guess for θ. Because α_k is different for each sample, the roots to $\tan(q_n) = -\alpha_k q_n$ must be found for each sample. Initial calculations indicated that for the conditions in the present study 8 terms were more than sufficient for convergence of the summation in equation A-12, so the first 8 values were found using Newton's method to find the roots to

$$f = \tan(q_n) + \alpha_k q_n = 0 \tag{A-15}$$

with

$$\partial f/\partial q_n = 1/\cos^2 q_n + \alpha_k. \tag{A-16}$$

Equation A-12 was rewritten as

$$g = \frac{M_t}{M_\infty} - 1 + \sum_{n=1}^{\infty} \frac{2\alpha_k(1+\alpha_k)}{1 + \alpha_k + \alpha_k^2 q_n^2} \exp(-\theta q_n^2) = 0 \tag{A-17}$$

with

$$\frac{\partial g}{\partial \theta} = \sum_{n=1}^{\infty} \frac{-2\alpha_k(1+\alpha_k)}{1 + \alpha_k + \alpha_k^2 q_n^2} q_n^2 \exp(-\theta q_n^2) \tag{A-18}$$

and θ solved for iteratively using Newton's method with the summation in a loop inside the iteration. The summation always included 8 terms as

this was found to be sufficient. After a value for θ was found, the effective diffusivity was determined from the known time and σ, which was found from the gel dimensions. Program output was θ, D, and σ.

```
4 '
5 'PROGRAM FOR CALCULATION OF EFFECTIVE DIFFUSIVITY FROM APPROACH
6 'TO EQUILIBRIUM MEASUREMENTS
7 '
8 ' K.A.Dennison  9-1-85
9 '
10 DEFDBL A-Z
20 DIM IG(8): DIM QN(8)
30 CLS
35 ' Input of data
40 INPUT "Thickness (mm) ";H
50 INPUT "alpha ";ALPHA
60 INPUT "Time (min) ";TI
70 INPUT "Mt ";MT
80 INPUT "Initial guess for theta ";THETA
85 ' Initial guesses for first 8 qn
90 IG(1)=2.0288:IG(2)=4.9132:IG(3)=7.9787:IG(4)=11.0856:IG(5)=14.2075:
IG(6)=17.3364:IG(7)=20.45:IG(8)=23.6
100 FOR I% = 1 TO 8
110 GUESS = IG(I%)
115 'Loop for Newton's method to find qn
120 F = TAN(GUESS)+ALPHA*GUESS
130 IF ABS(F)<1E-09 GOTO 170
140 FPRIME = (COS(GUESS))^(-2)+ALPHA
150 GUESS = GUESS - F/FPRIME
160 GOTO 120
170 QN(I%) = GUESS
180 'PRINT:PRINT I%,QN(I%)
190 NEXT I%
195 'Newton's method loop for finding theta
200 SUM = 0:SUMPRIME = 0
205 'Calculation of summation using 8 terms
210 FOR I% = 1 TO 8
220 TERM = ((2*ALPHA*(1+ALPHA))/(1+ALPHA+(ALPHA^2)*(QN(I%)^2)))
*EXP(-THETA*QN(I%)^2)
230 SUM = SUM+TERM:SUMPRIME = SUMPRIME+TERM*QN(I%)^2
235 'PRINT SUM,SUMPRIME
240 NEXT I%
250 G = MT - 1 + SUM
260 IF ABS(G) < 1E-09 THEN 310
270 'PRINT G,SUMPRIME,THETA
280 GPRIME = - SUMPRIME
285 IF GPRIME = 0 THEN THETA = 0:GOTO 200
290 THETA = THETA - G/GPRIME
300 GOTO 200
305 'Calculation of sigma and Deff and output of values
310 CLS:BEEP
320 SIGMA = (1.1*H/10)/(2.2+.4*H)
330 PRINT:PRINT "Sigma = ";SIGMA
335 PRINT:PRINT "Theta = ";THETA
340 DEFF = THETA*SIGMA*SIGMA/(TI*60)
360 PRINT:PRINT "Deff (cm^2/s) = ";DEFF
362 LOCATE 20,22:PRINT "Press any key to continue"
364 C$ = INKEY$: IF C$ = "" THEN 364
```

```
370 'PRINT:PRINT:INPUT "More values at same alpha ";MV$
380 GOTO 30
390 IF MV$ = "n" OR MV$ = "N" THEN 430
400 PRINT:PRINT:INPUT "Mt ";MT
410 INPUT "Initial guess for theta ";THETA
420 GOTO 200
430 END
```

Appendix 4. SEC Study Data

Chromatograms of irradiated PEO solutions obtained under a variety of conditions are included in this appendix for reference. Each figure shows several chromatograms of PEO irradiated under slightly different conditions to allow comparison of the efficiency of irradiation and the ratio of crosslinking to scission. The conclusions that can be drawn about how irradiation conditions affect the efficiency and the ratio of crosslinking to scission are found in section 4.2.2.

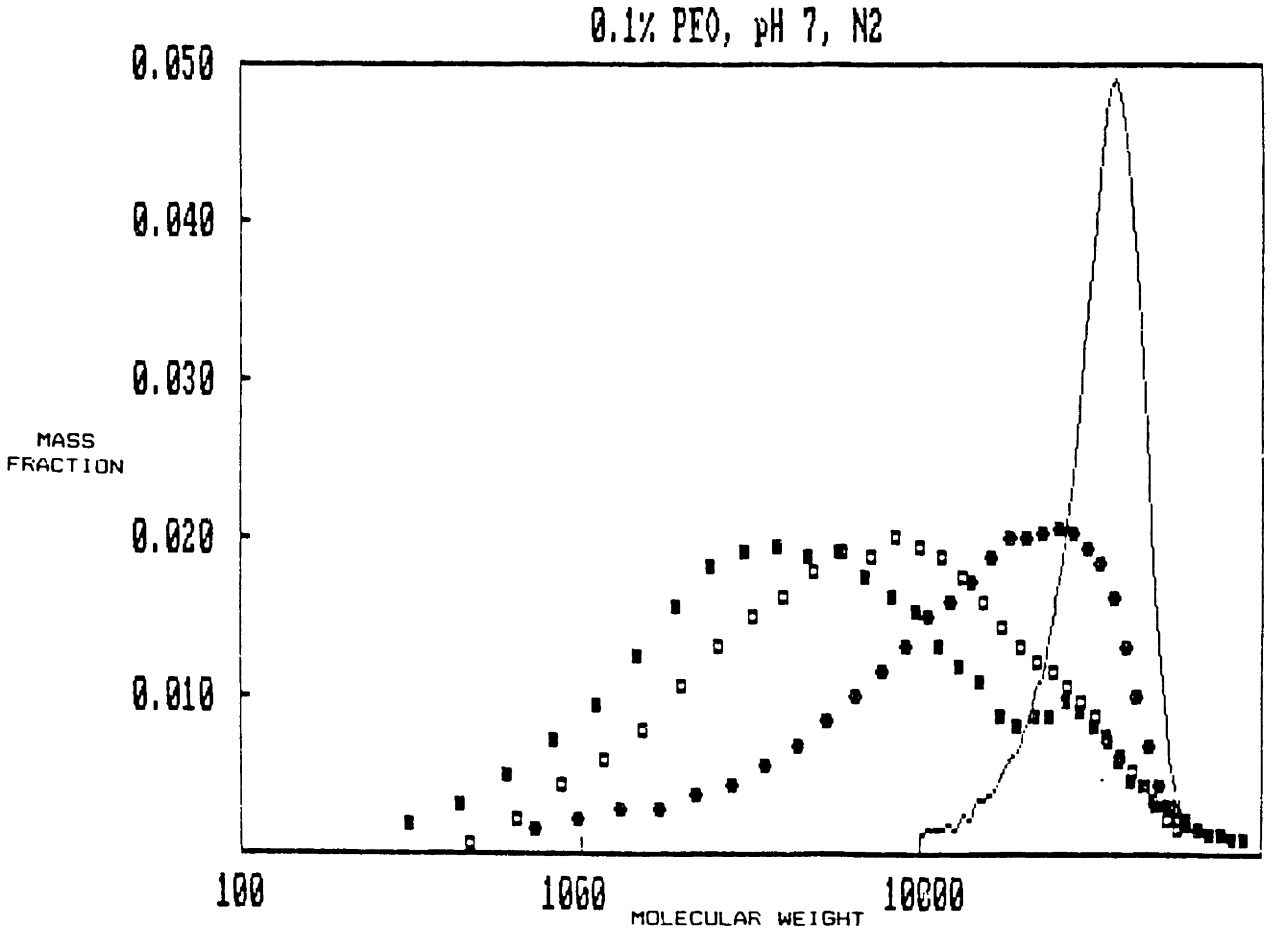

Figure 1. Molecular weight distribution for samples of 0.1% PEO, pH 7, irradiated under N_2 at a dose rate of 10000 rad/sec. ——— , unirradiated: ● , 0.1 Mrad total dose; □ , 0.3 Mrad; ■ , 0.5 Mrad.

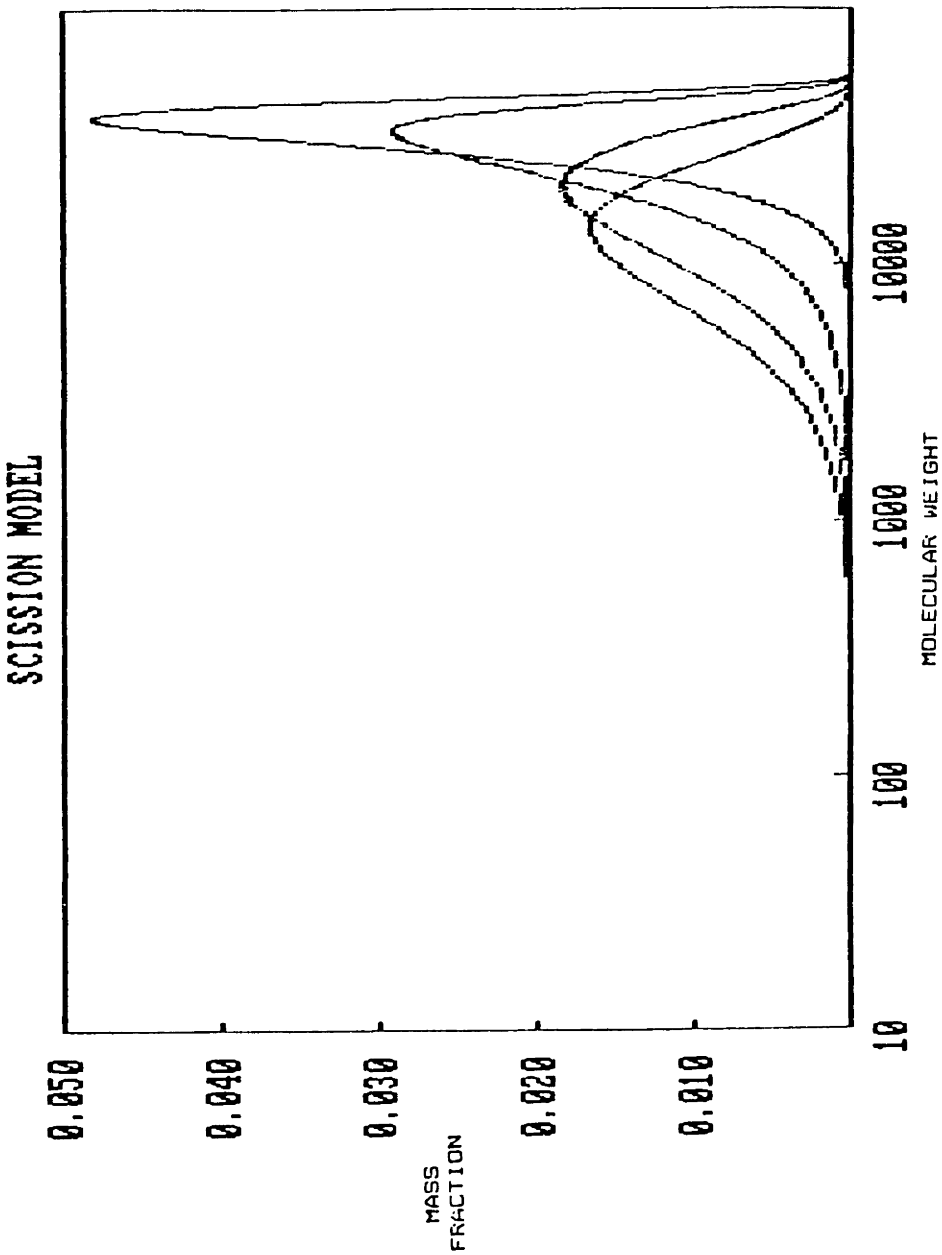

Figure 2. Random scission molecular weight distributions. See text for details.
a. Scission model predictions

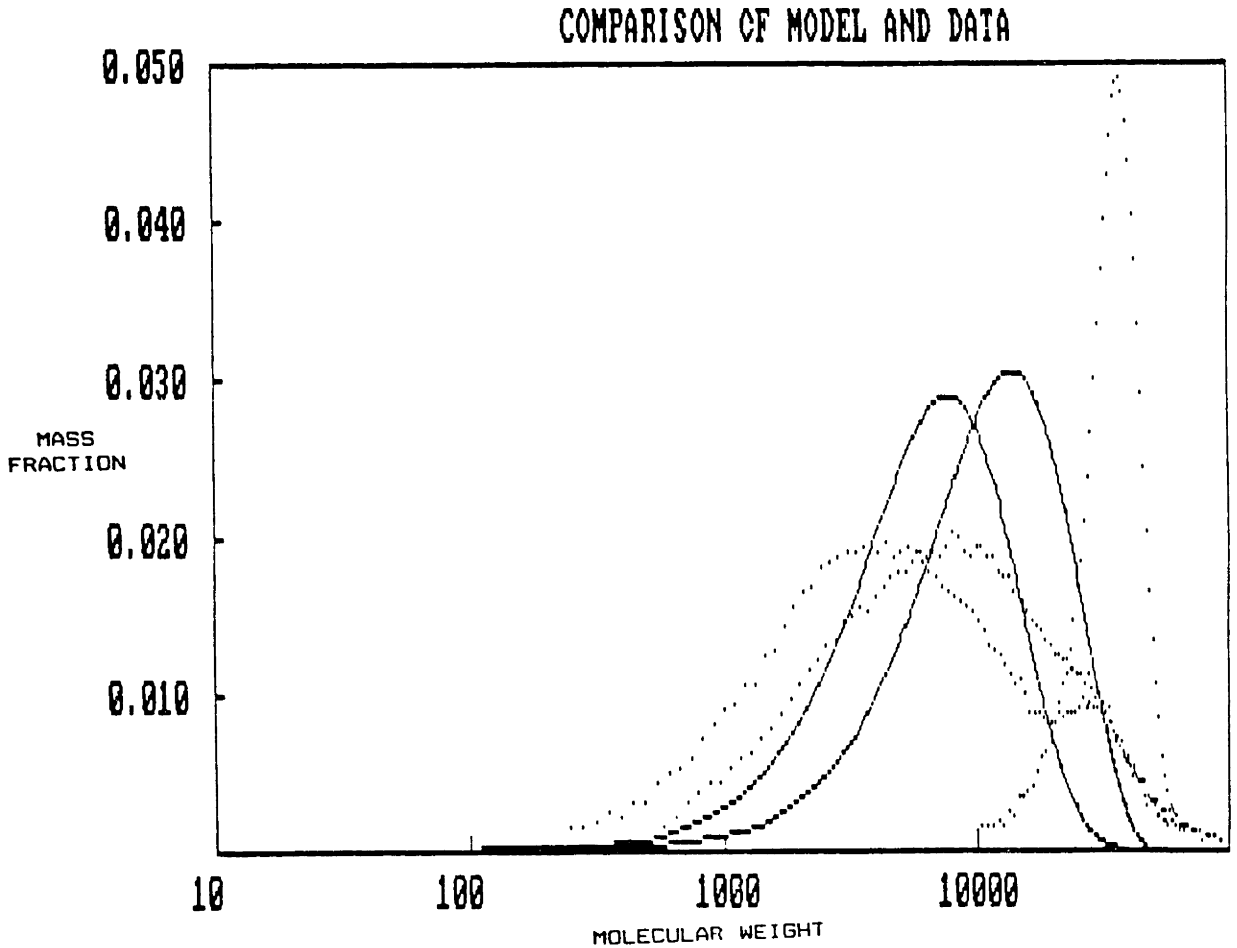

Figure 2. b. Scission model compared with data. ——, model: ···, data (0.1% PEO, pH 7)

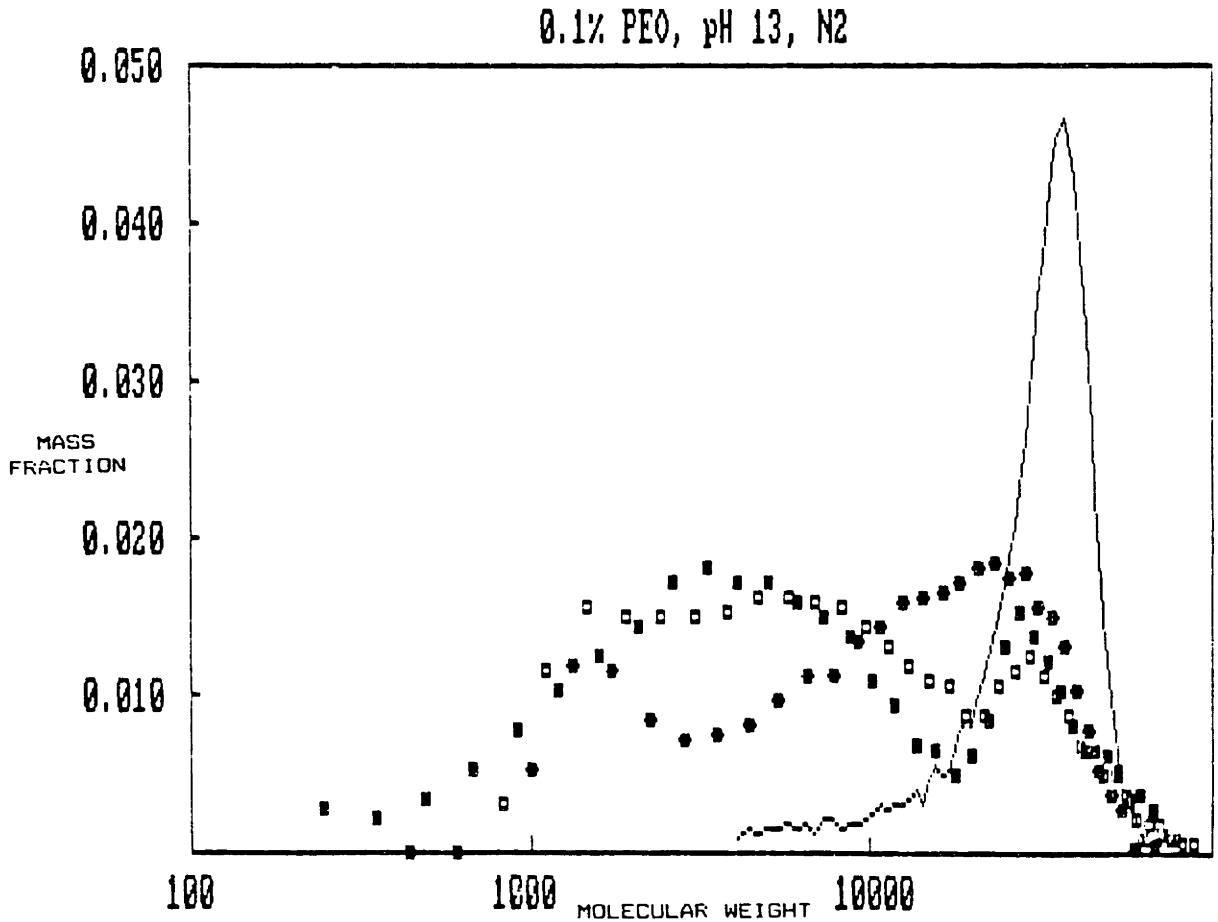

Figure 3. Molecular weight distribution for samples of 0.1% PEO, pH 13, irradiated under N_2 at a dose rate of 10000 rad/sec. ——, unirradiated; ✱, 0.1 Mrad total dose: ■, 0.3 Mrad: □, 0.5 Mrad.

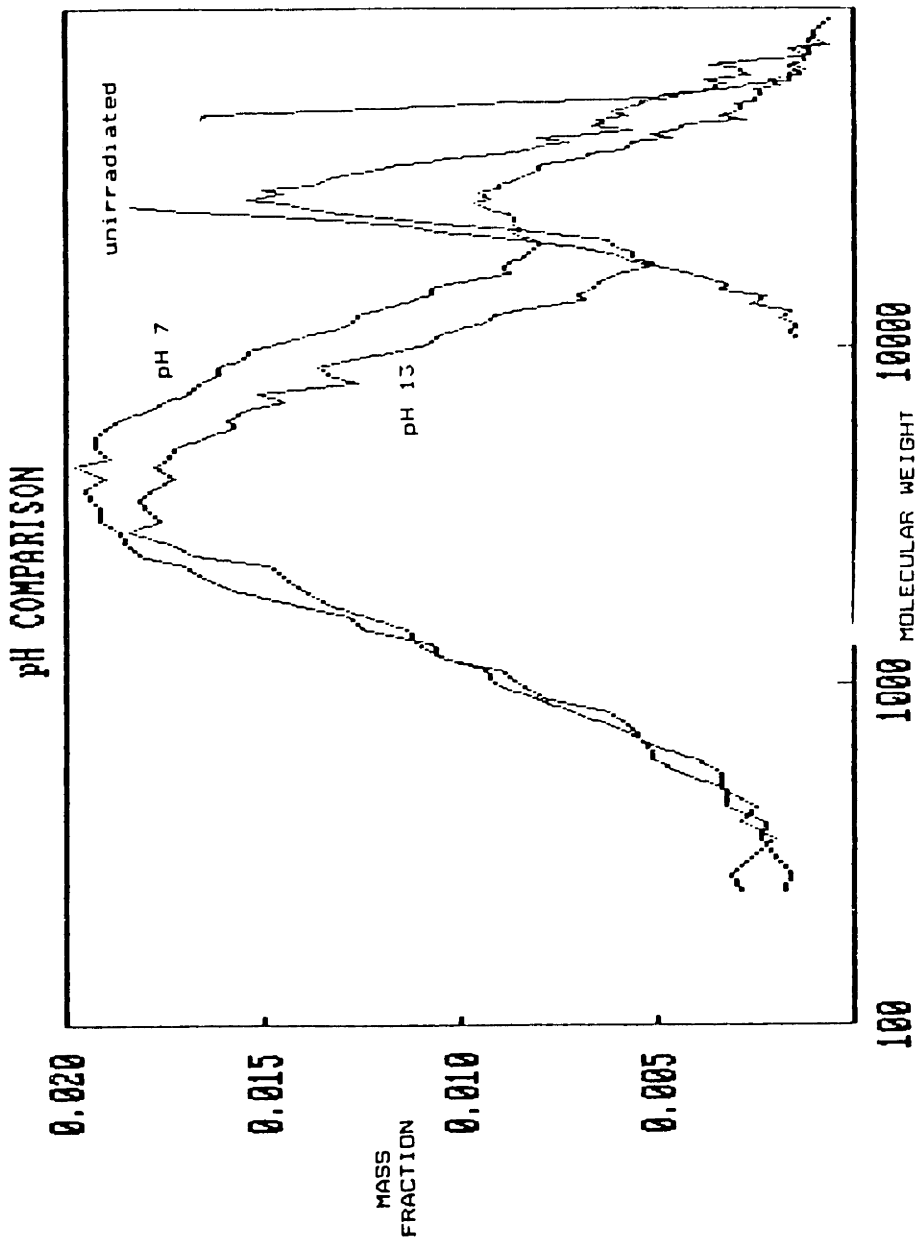

Figure 4. Effect of pH on molecular weight distribution.
a. Data at pH 7 and 13, 0.1% FEO, 0.3 Mrad total dose, plotted with initial distribution for comparison.

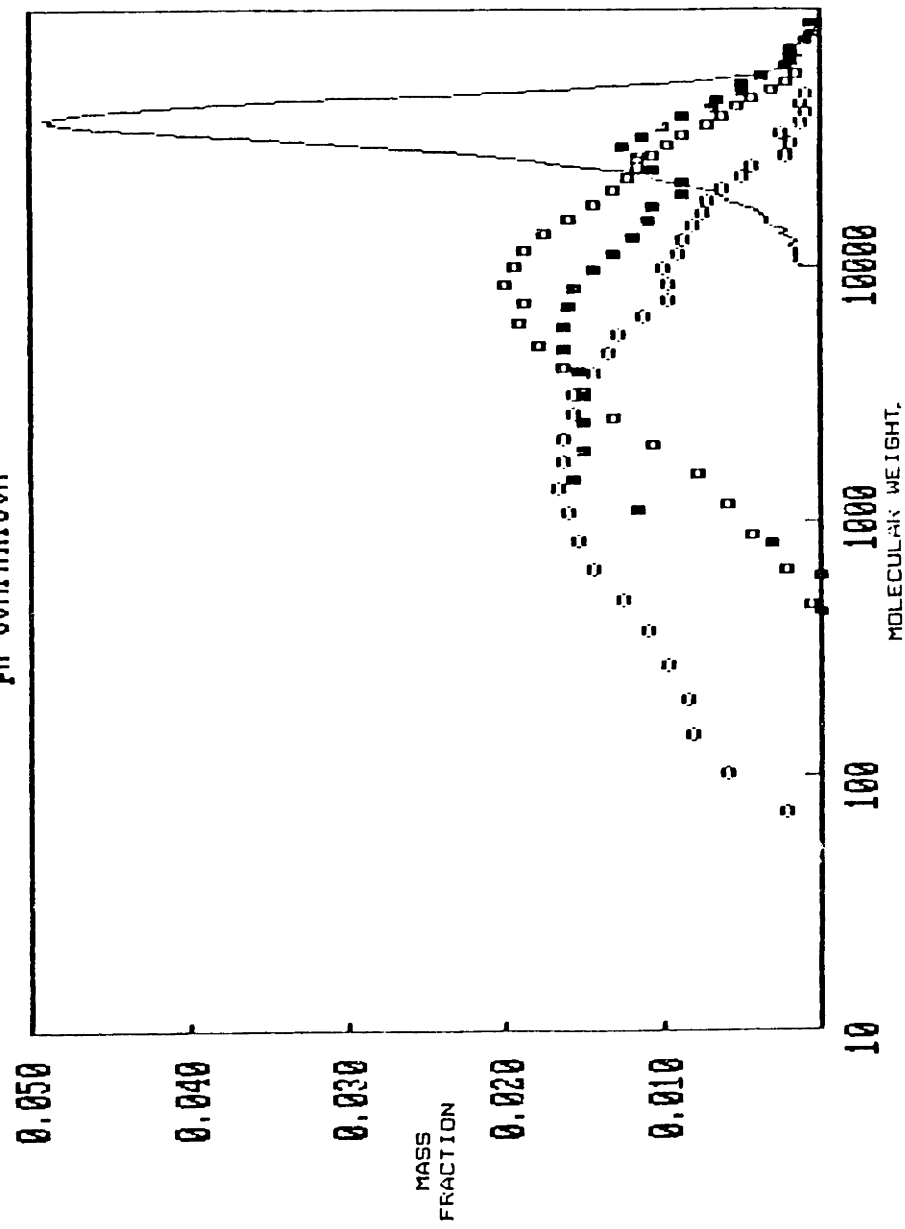

Figure 4. b. Comparison of samples of 0.1% PEO, 0.3 Mrad total dose, at three different values of pH, showing increase in degradation with decreasing pH.
——— , unirradiated; ■ , pH 13; ■ , pH 7;
■ , pH 4.

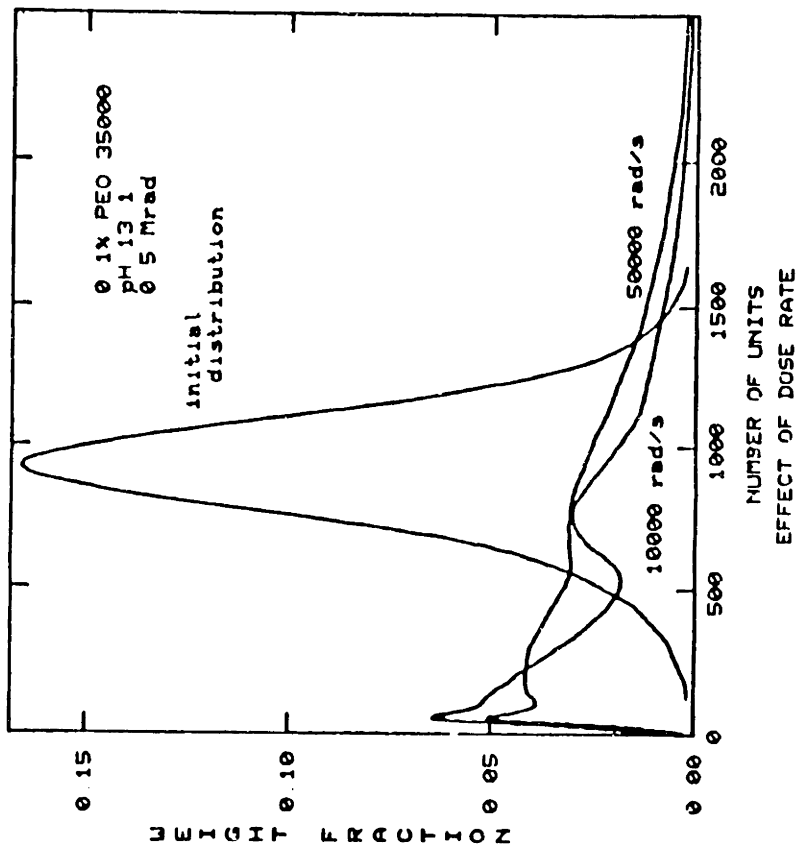

Figure 5. Effect of dose rate and PEO concentration on molecular weight distribution.
a. 0.1% PEO samples irradiated at pH 7 under N_2 at 10000 and 50000 rad/sec. Total dose 0.5 Mrad.

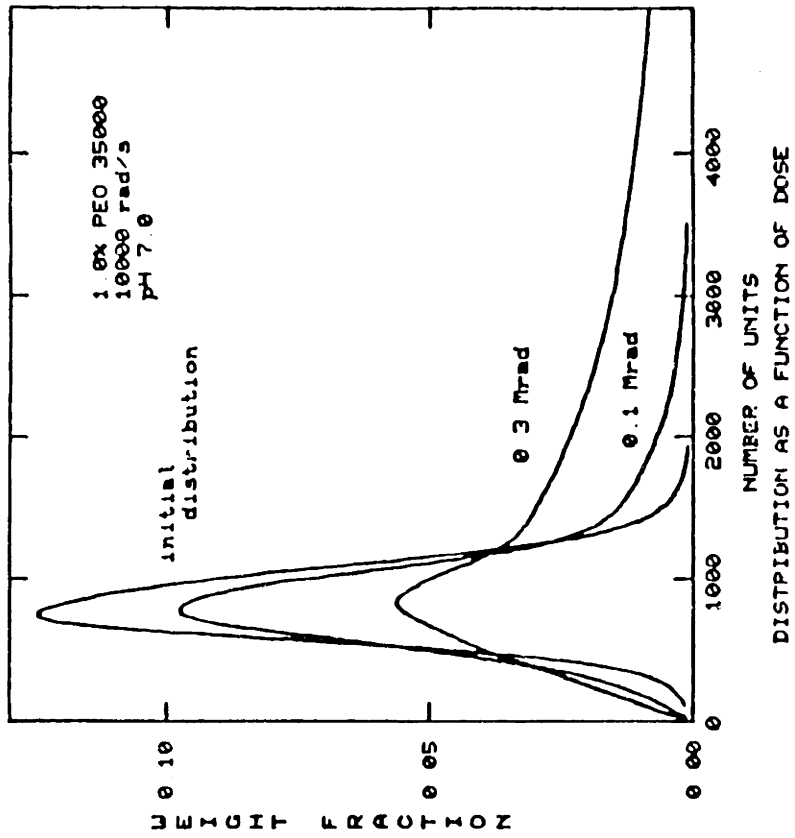

Figure 5. b. 1.0% PEO samples irradiated at pH 7 under N_2, 10000 rad/sec. Note the considerable amount of crosslinking taking place.

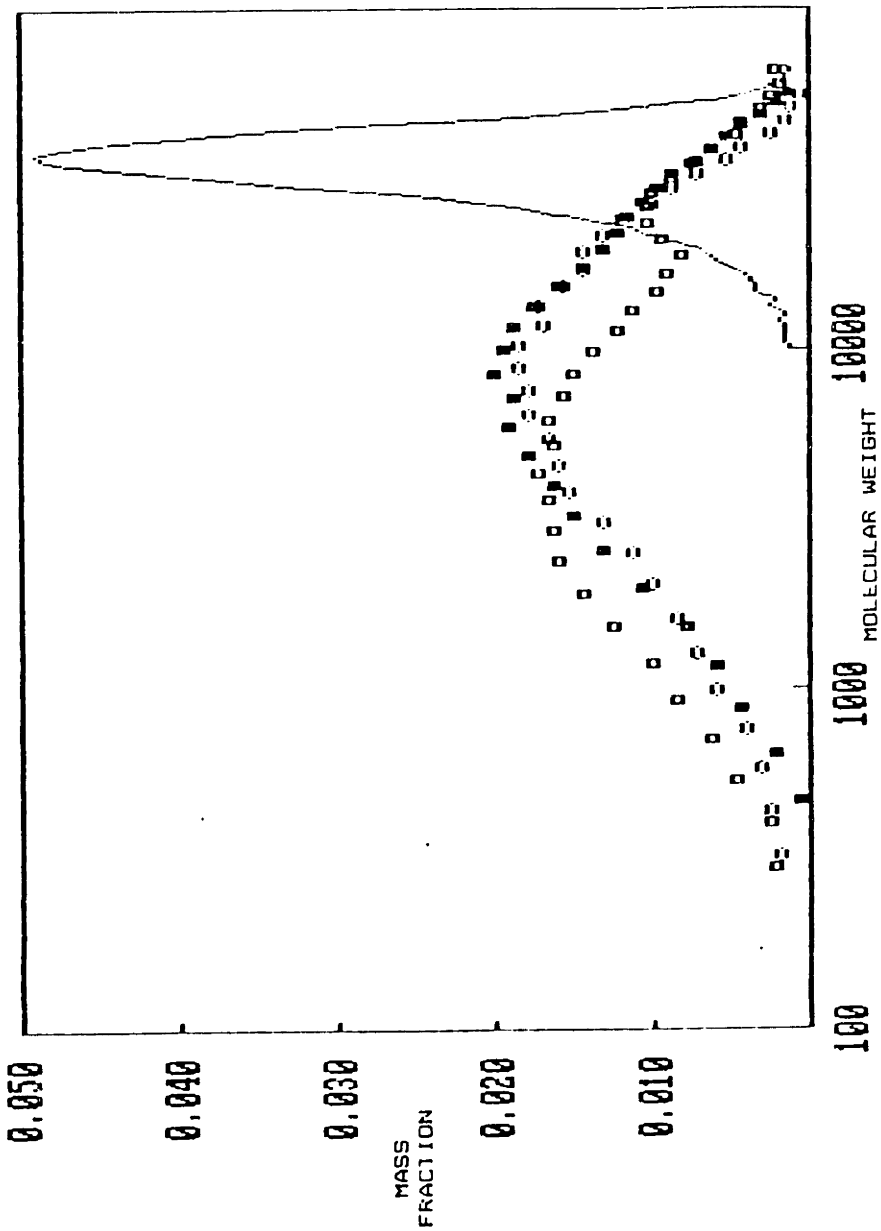

Figure 6. Molecular weight distribution for samples of 0.1% FEO, pH 7, dose rate 10000 rad/sec, total dose 0.3 Mrad, irradiated under various atmospheres. ——, unirradiated; ■, N_2; □, N_2O; ○, O_2.

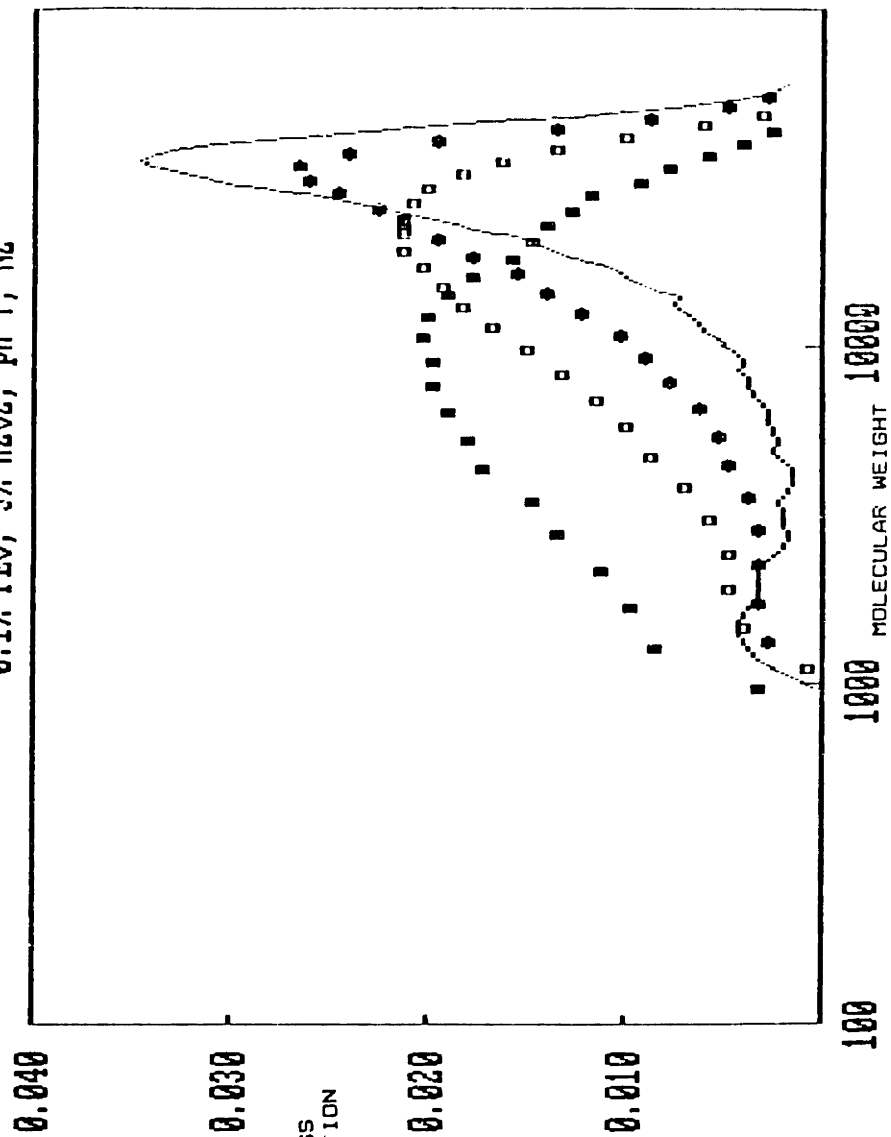

Figure 7. Irradiations done with 5% H_2O_2 added to the PEO solutions.
a. Molecular weight distribution for samples of 0.1% PEO, pH 7, irradiated under N_2 at a dose rate of 10000 rad/sec. ——— , unirradiated; ● , 0.1 Mrad total dose: □ , 0.3 Mrad; ■ , 0.5 Mrad.

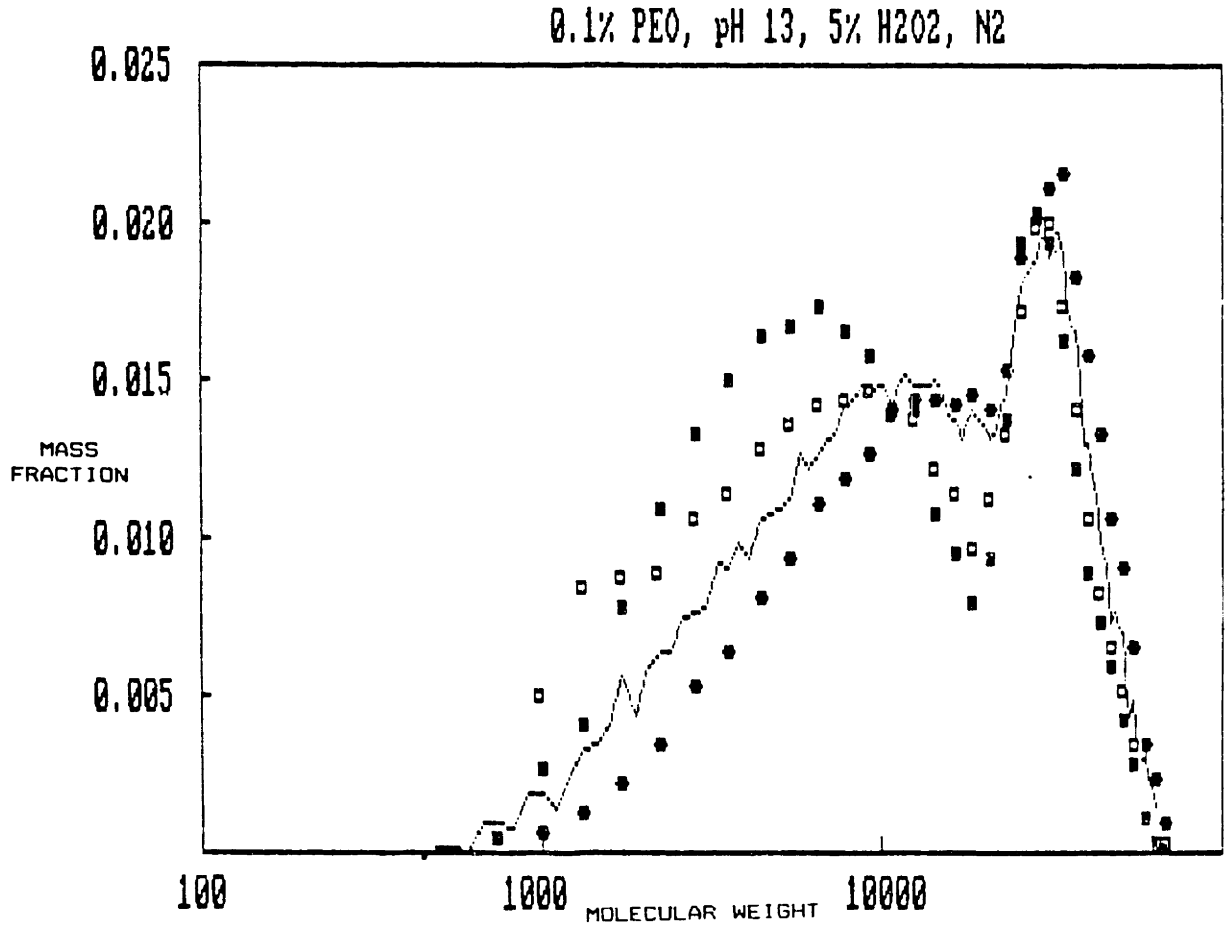

Figure 7. b. Molecular weight distribution for samples of 0.1% PEO, pH 13, irradiated under N_2 at a dose rate of 10000 rad/sec. ——, unirradiated; ▪ , 0.1 Mrad total dose; ▫ , 0.3 Mrad; ▮ , 0.5 Mrad.

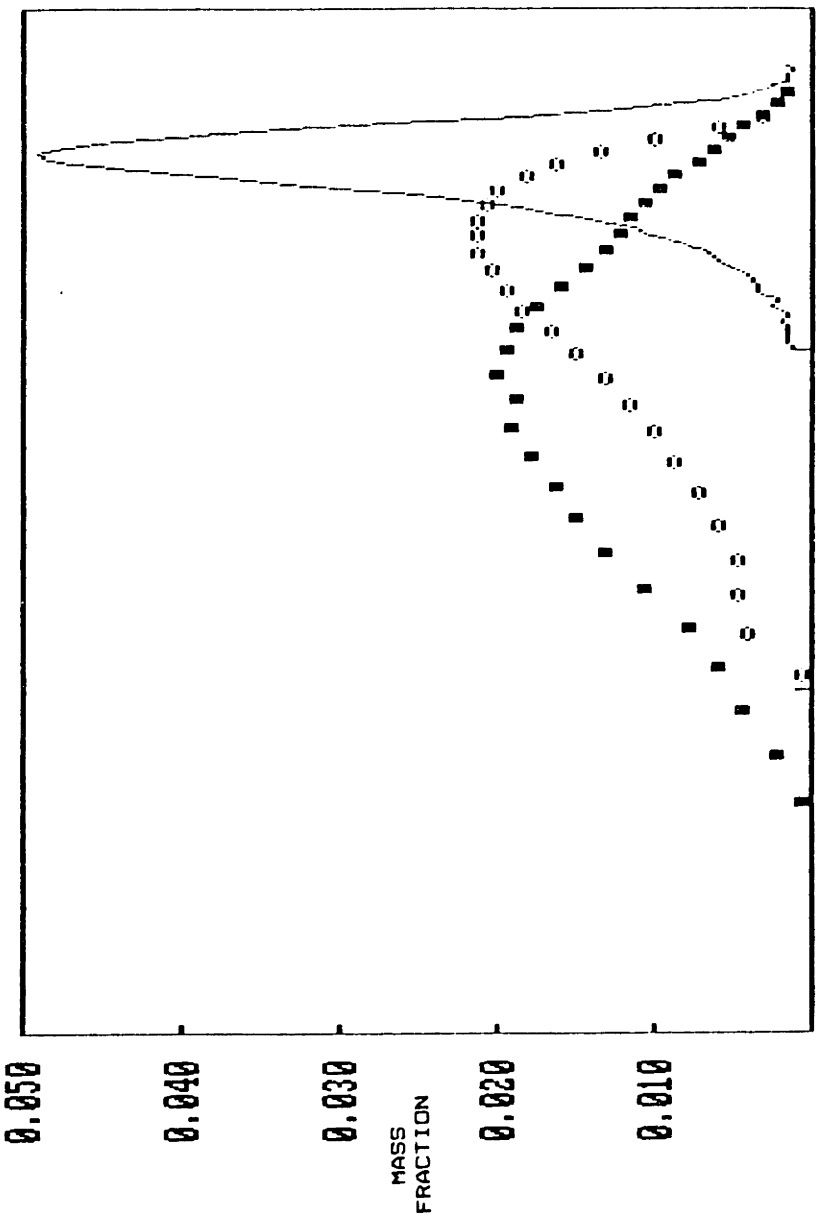

Figure 8. Effect of H_2O_2 on molecular weight distributions. All samples were 0.1% FEO, dose rate 10000 rad/sec, total dose 0.3 Mrad.
a. pH 7. ——— , unirradiated (no H_2O_2); ■ , no H_2O_2; ▫ , 5% H_2O_2.

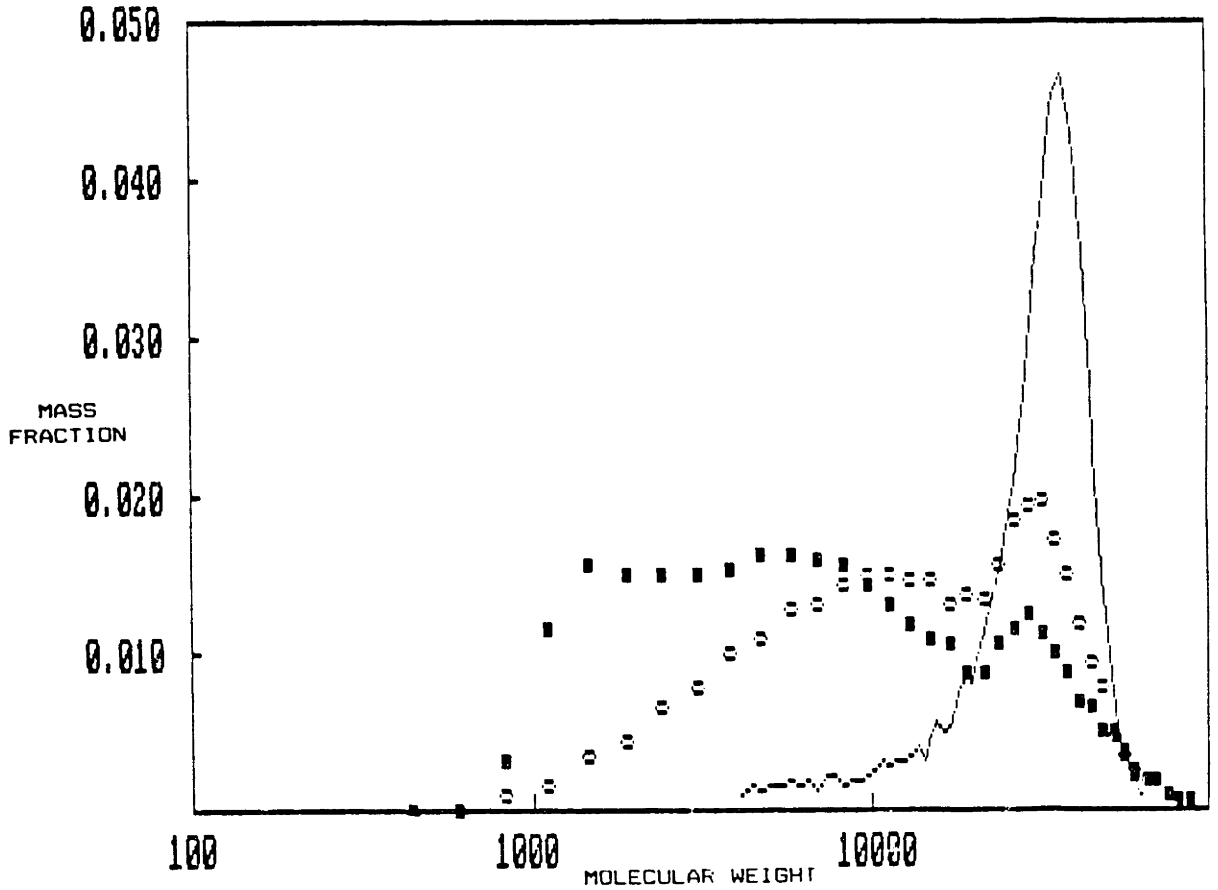

Figure 8. b. pH 13. ——, unirradiated (no H_2O_2); ▮, no H_2O_2; ⁘, 5% H_2O_2.

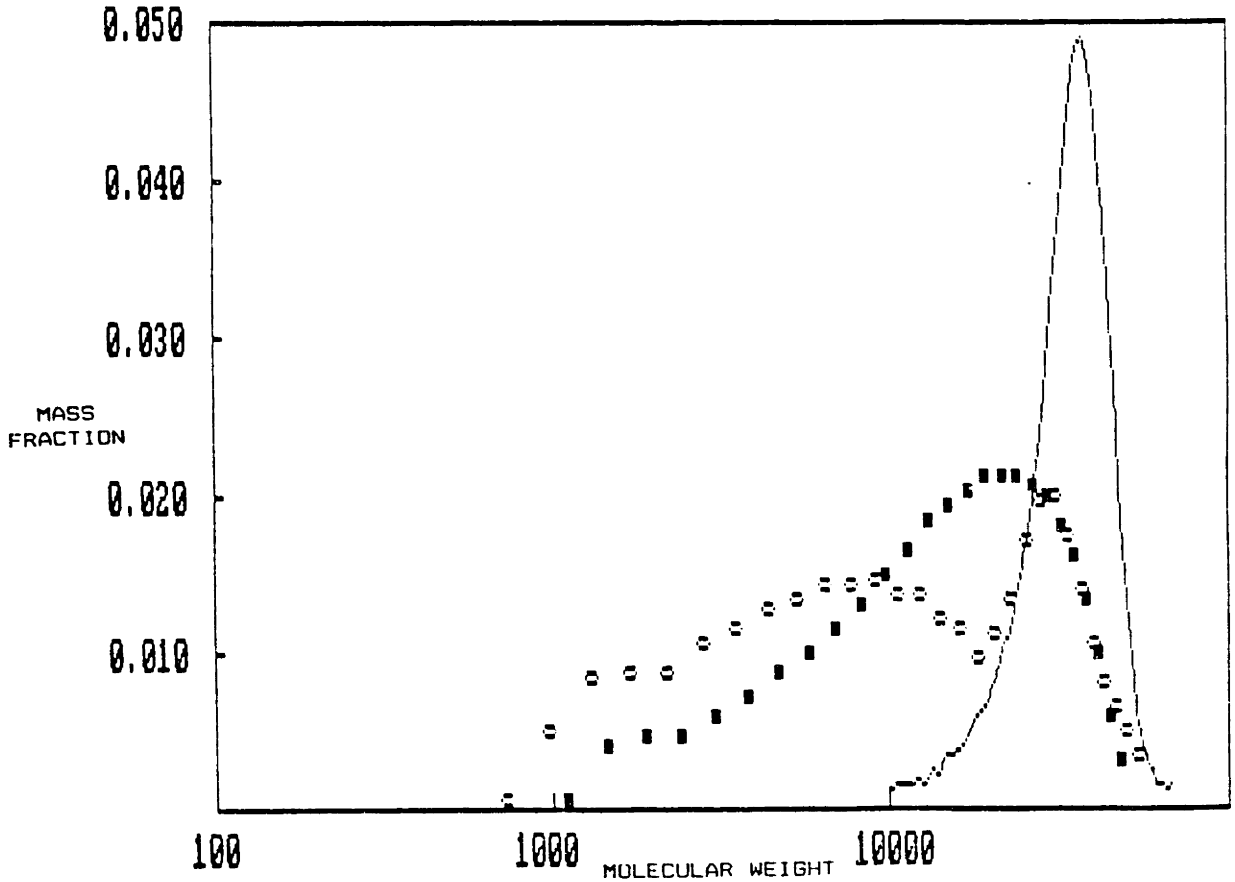

Figure 8. c. 5% H_2O_2. ——— , unirradiated (no H_2O_2): ▪ , pH 7; ▫ , pH 13.

Appendix 5. Scanning Electron Micrographs of Porous Gels

This appendix contains additional SEMs of PEO gels synthesized in K_2SO_4 solution. Each micrograph is marked with the conditions of synthesis (PEO concentration, total dose, K_2SO_4 concentration, and dose rate) and some information about the preparation and location on the gel.

5% PEO 35000, 5 Mrad, 0.5 M K_2SO_4, 250,000 rad/sec

Surface of gel

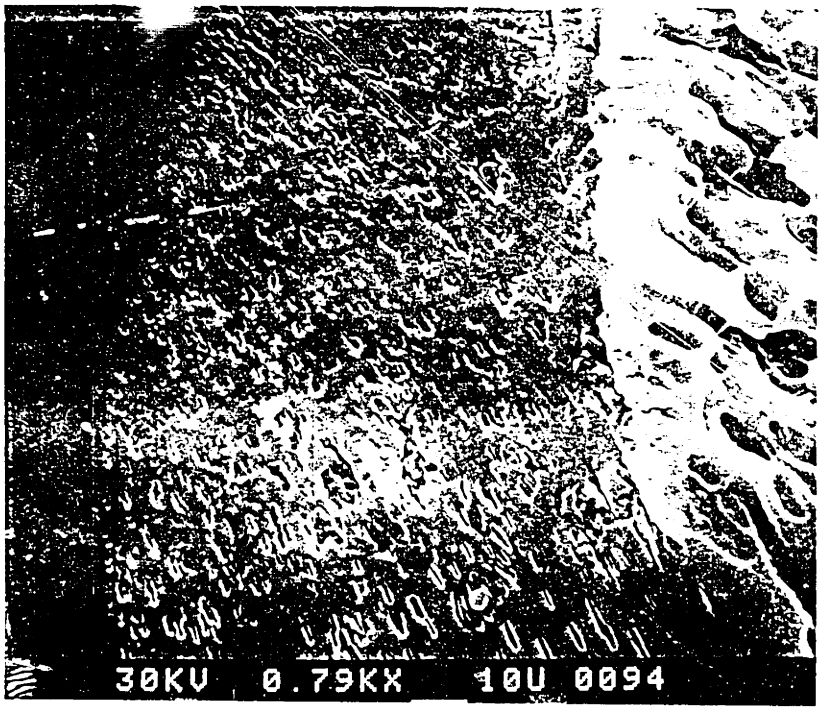

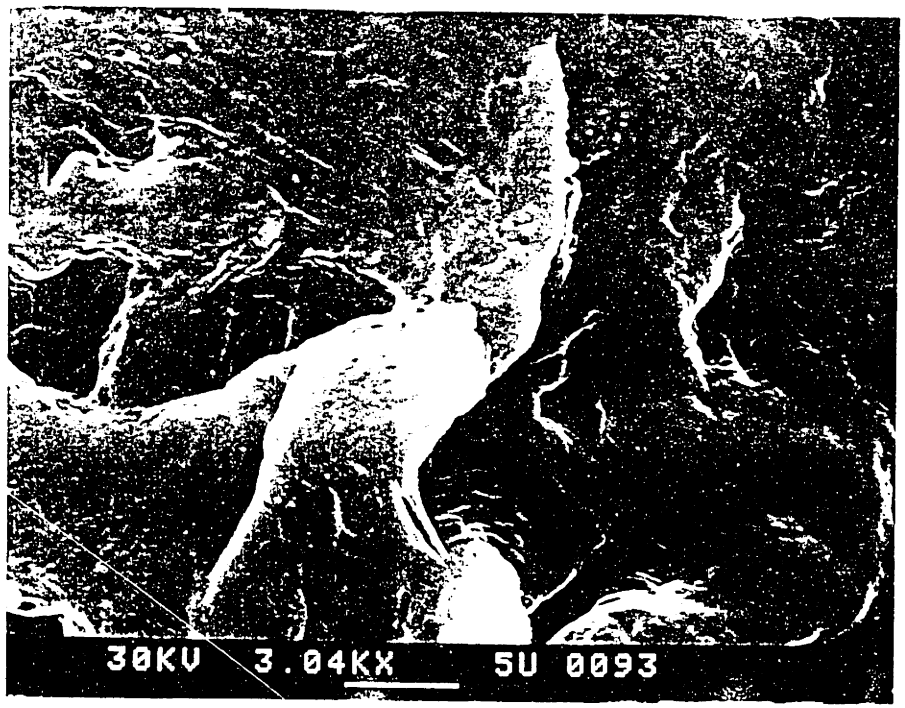

5% PEO 35000, 5 Mrad, 0.4 M K_2SO_4, 50,000 rad/sec

Surface of gel

5% PEO 35000, 5 Mrad, 0.4 M K_2SO_4, 100,000 rad/sec

Surface of gel

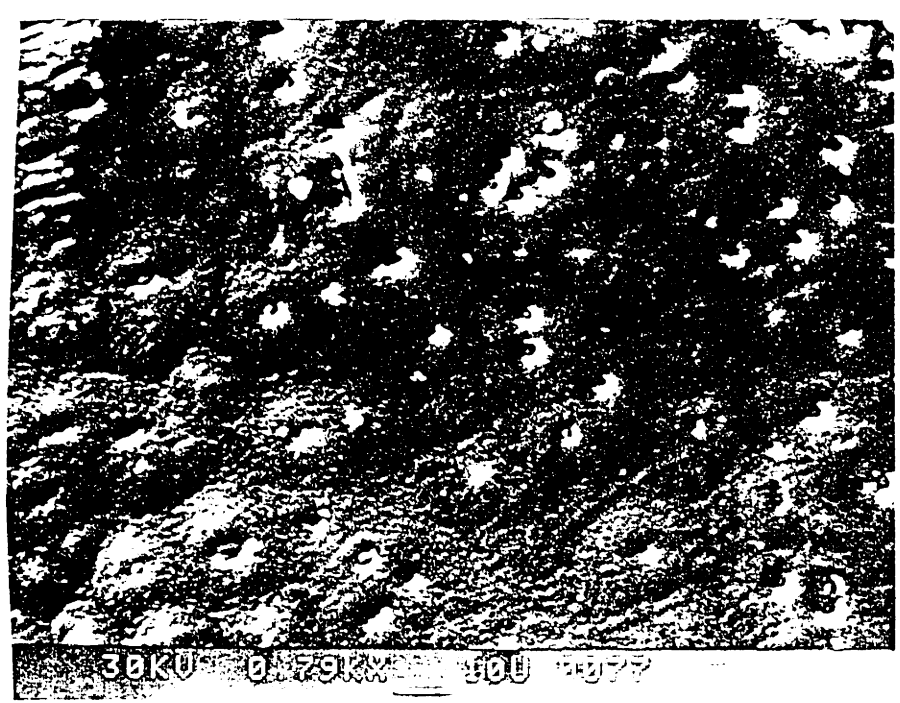

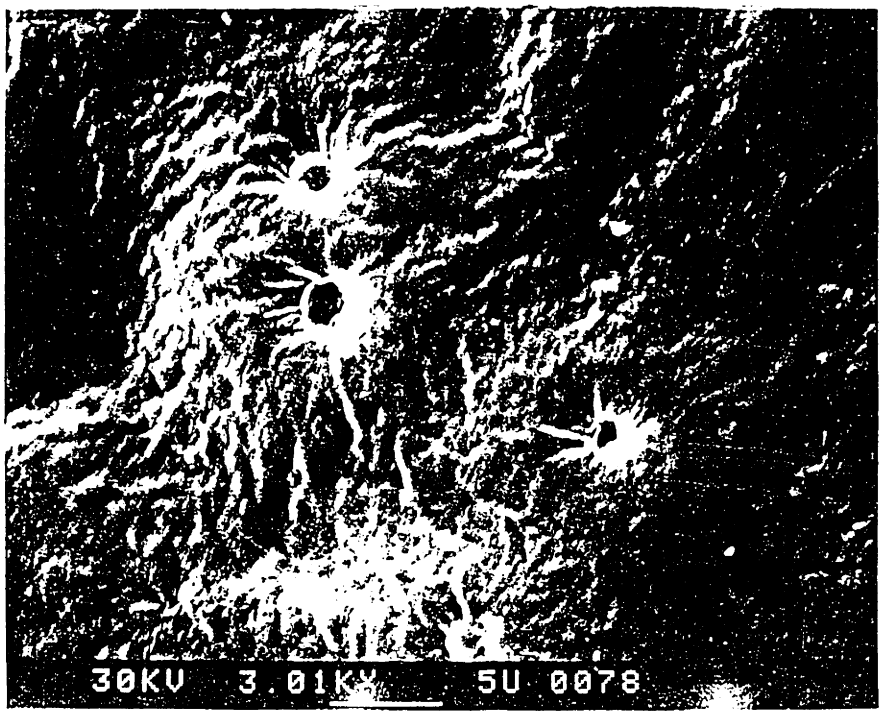

5% PEO 35000, 5 Mrad, 0.4 M K_2SO_4, 250,000 rad/sec

Surface of gel

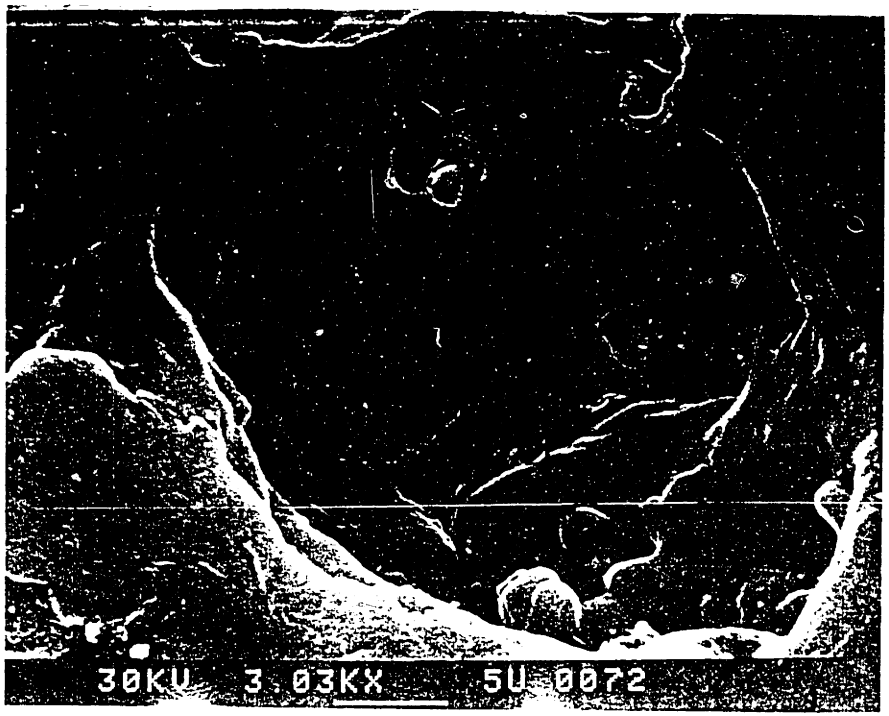

Control

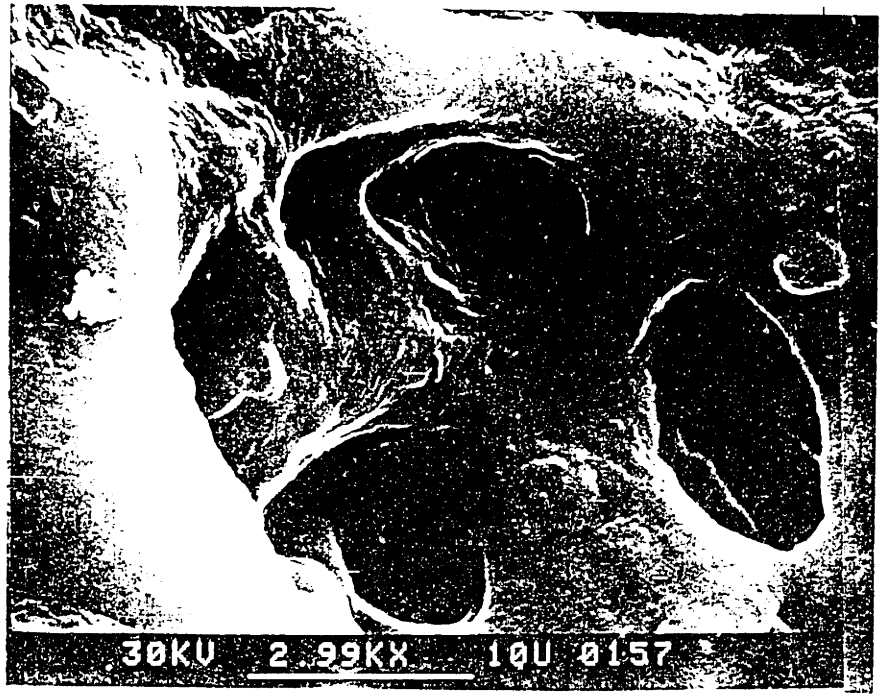

Vacuum Dried

5% PEO 35000, 5 Mrad, 0.5 M K_2SO_4, 250,000 rad/sec

Surface of gel

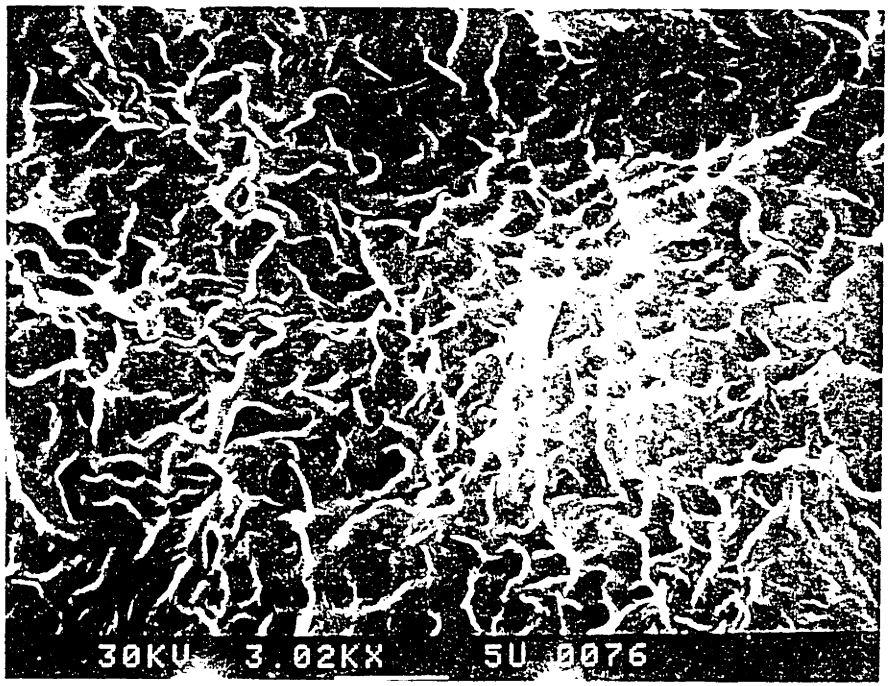

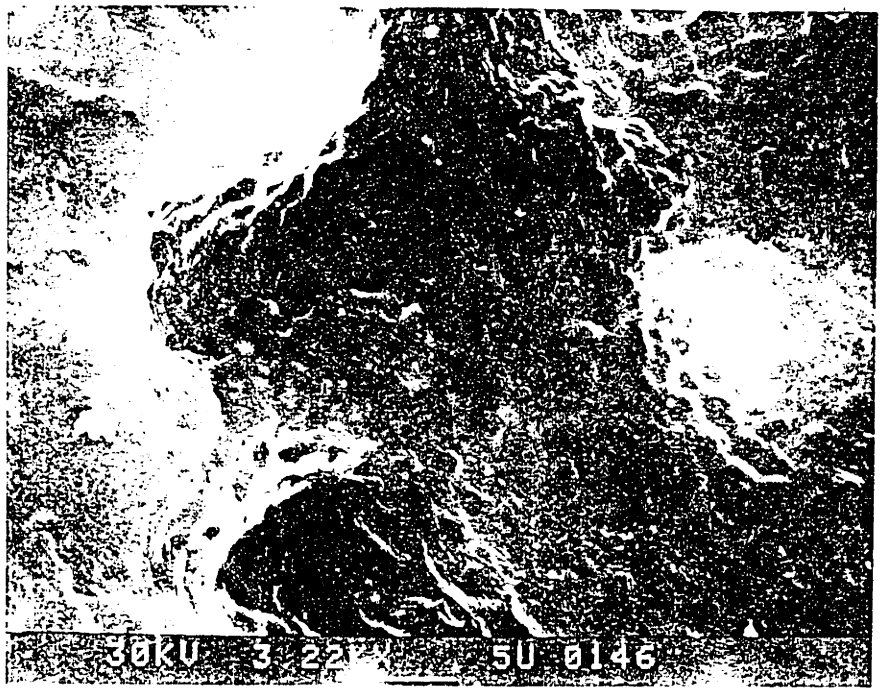

Control

Vacuum Dried

5% PEO 35000, 5 Mrad, 0.5 M K_2SO_4, 250,000 rad/sec

Surface of gel

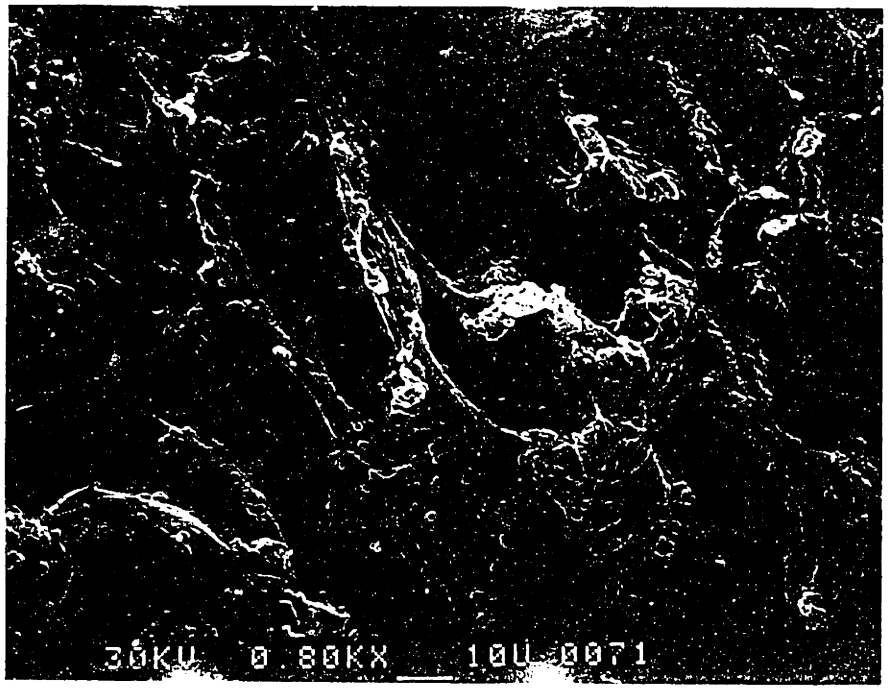

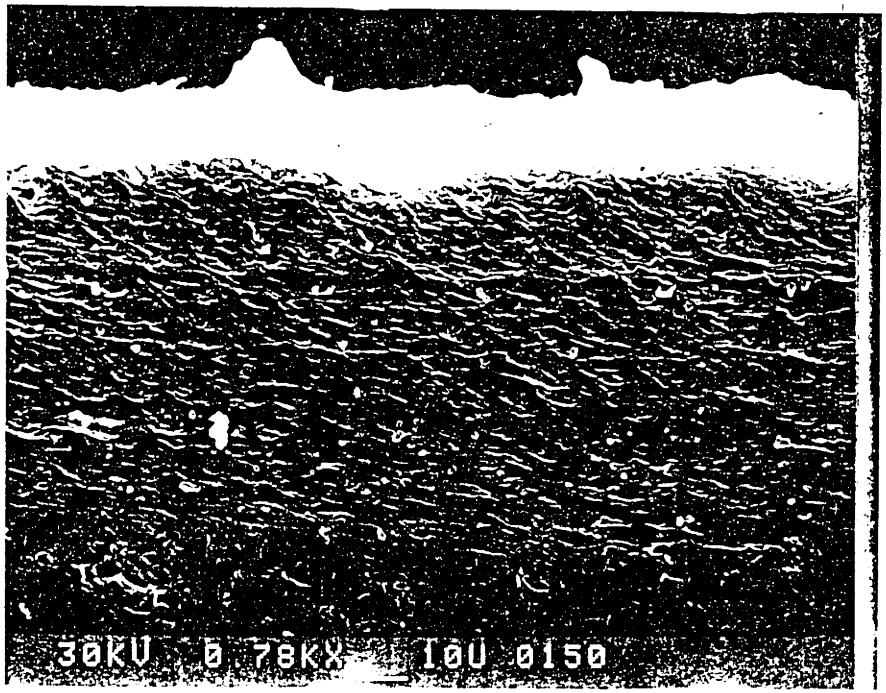

Control

Vacuum Dried

5% PEO 35000, 5 Mrad, 0.5 M K_2SO_4, 250,000 rad/sec

Cross-section of gel

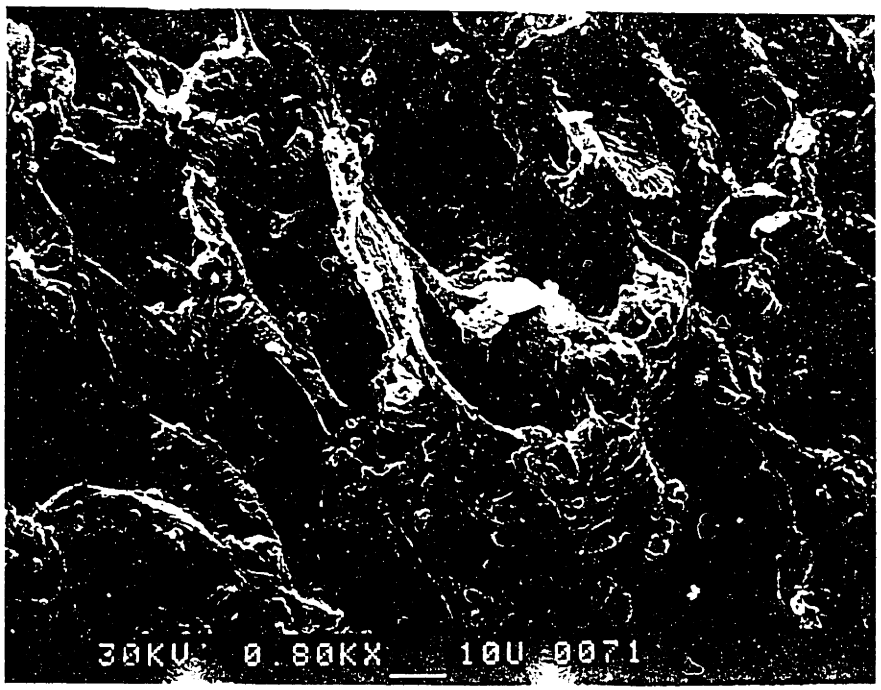

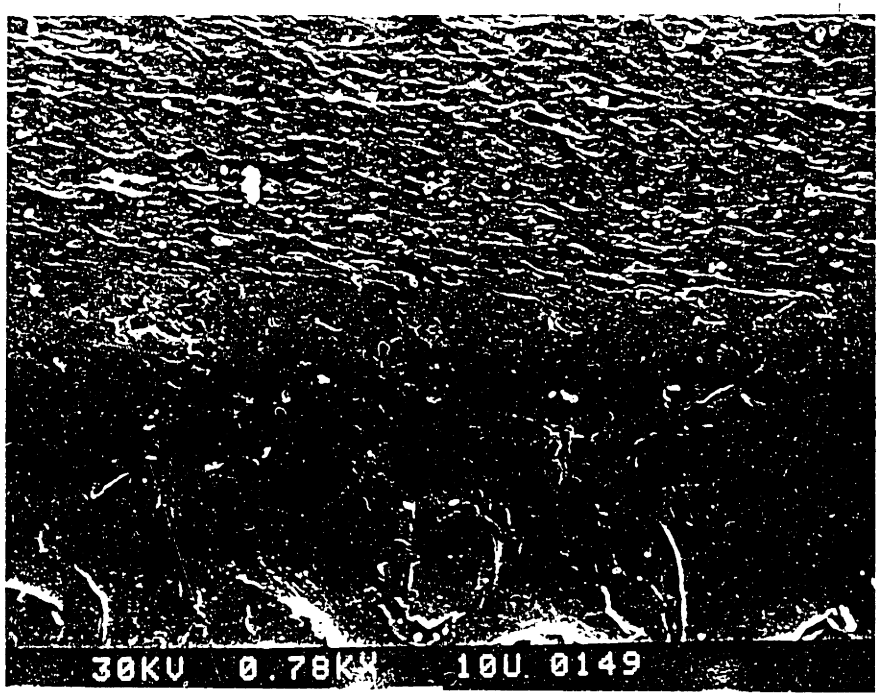

Control

Vacuum Dried

5% PEO 35000, 5 Mrad, 0.5 M K_2SO_4, 250,000 rad/sec

Cross-section of gel

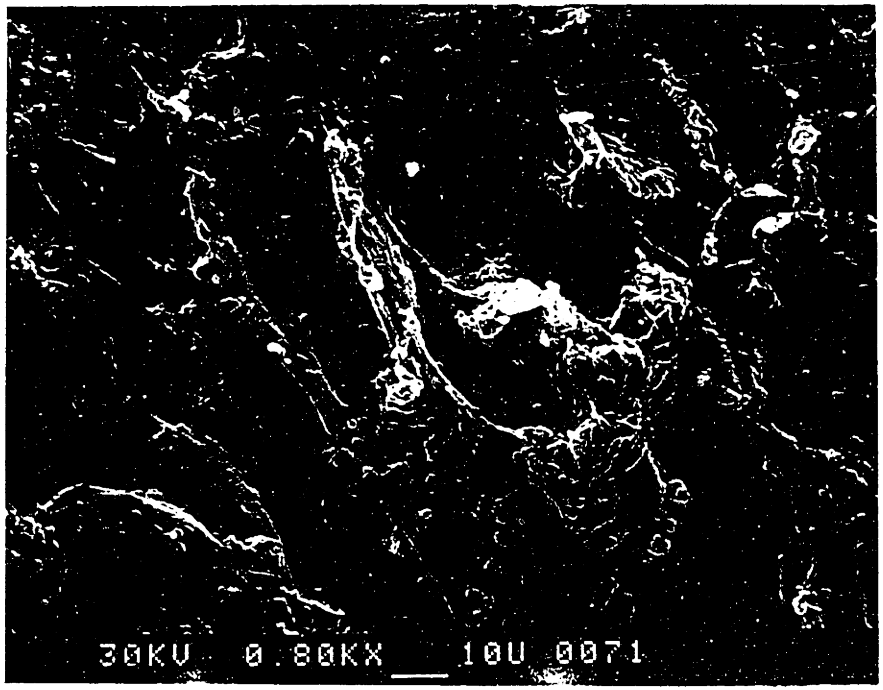

Control

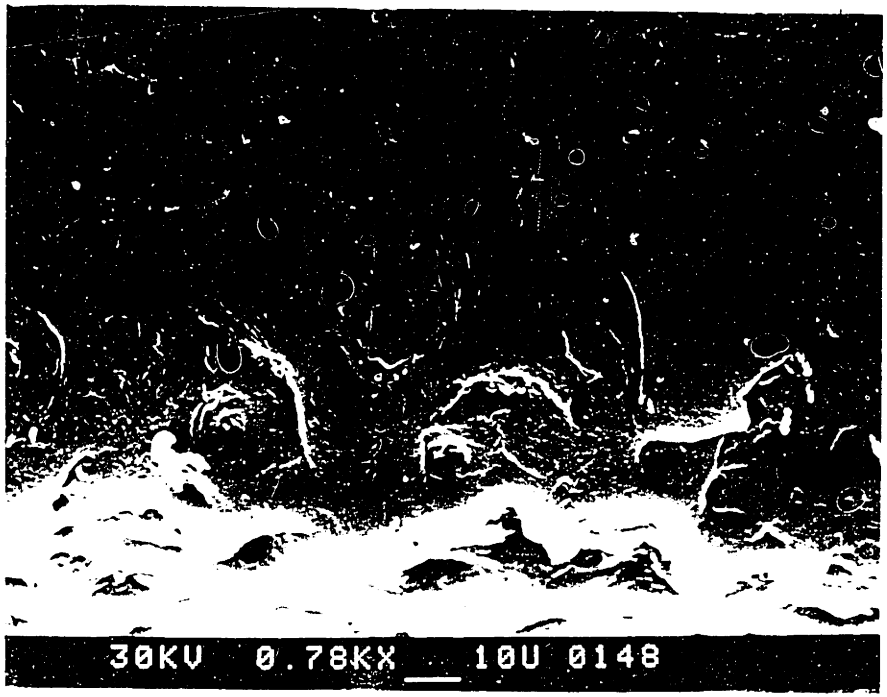

Vacuum Dried

5% PEO 35000, 5 Mrad, 0.5 M K_2SO_4, 250,000 rad/sec

Cross-section of gel

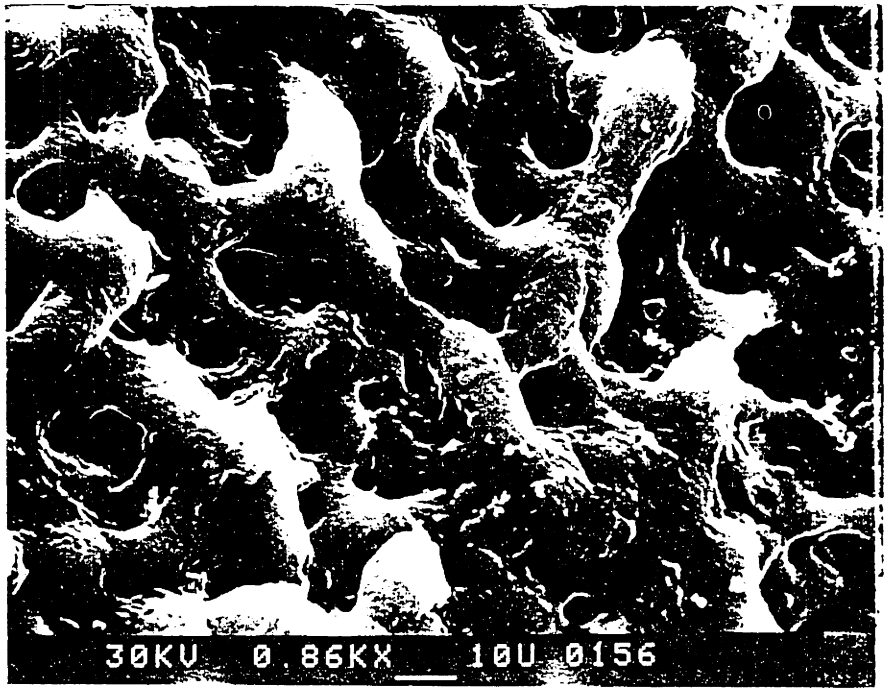

Top Surface

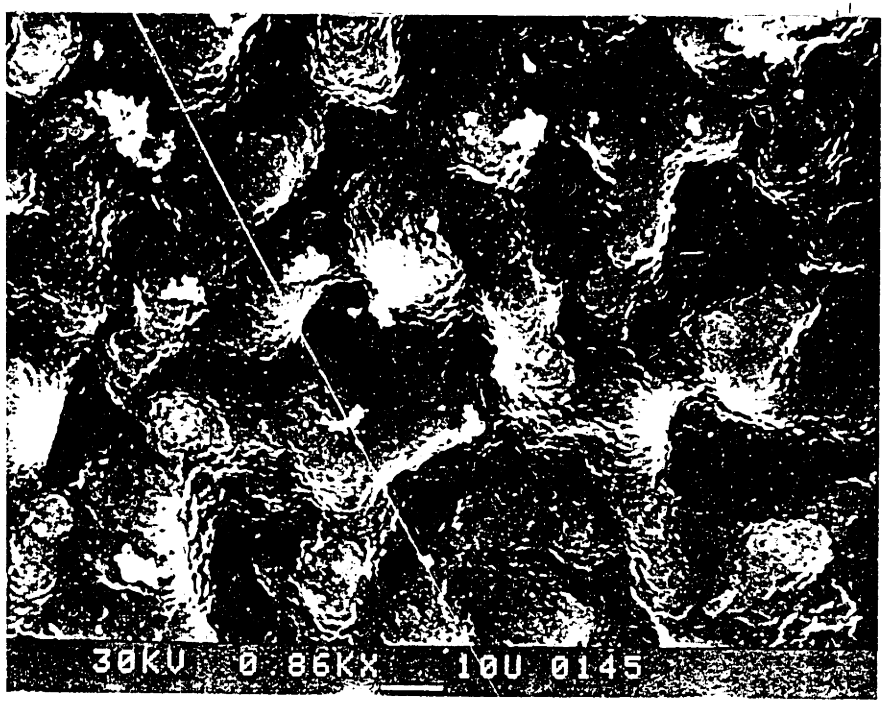

Bottom Surface

5% PEO 35000, 5 Mrad, 0.5 M K_2SO_4, 250,000 rad/sec

Vacuum dried gel

Appendix 6. Effective Diffusivity Data

Plots of effective diffusivity as a function of solute size for each of the 10 membranes used are attached. Each plot is labelled with the conditions of synthesis of the gel. Further information about the gels and the diffusivity results are included in section 4.6.

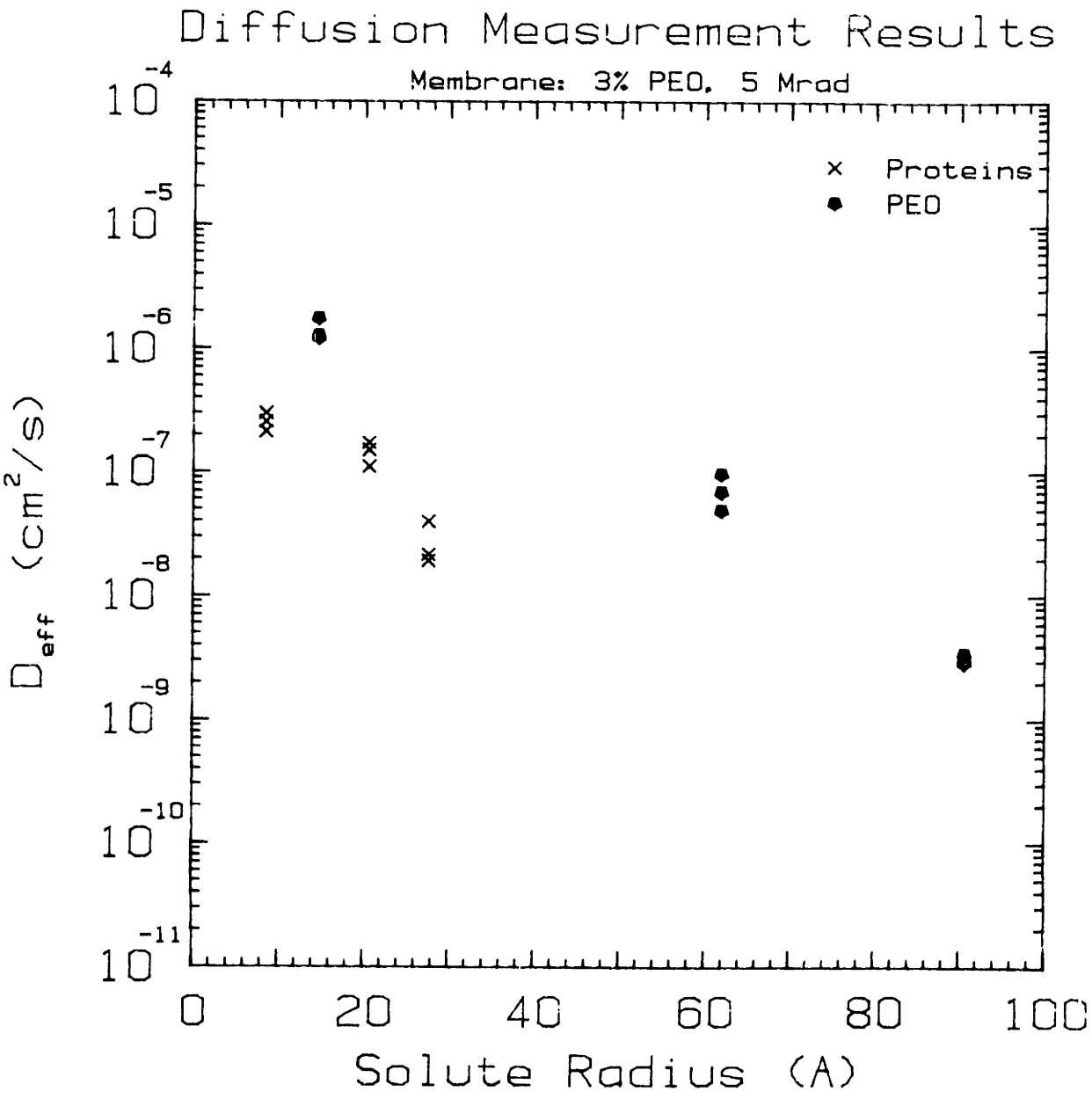
Diffusion Measurement Results
Membrane: 3% PEO, 5 Mrad
Proteins
PEO
D_{eff} (cm^2/s)
10^{-4}
10^{-5}
10^{-6}
10^{-7}
10^{-8}
10^{-9}
10^{-10}
10^{-11}
0
20
40
60
80
100
Solute Radius (A)

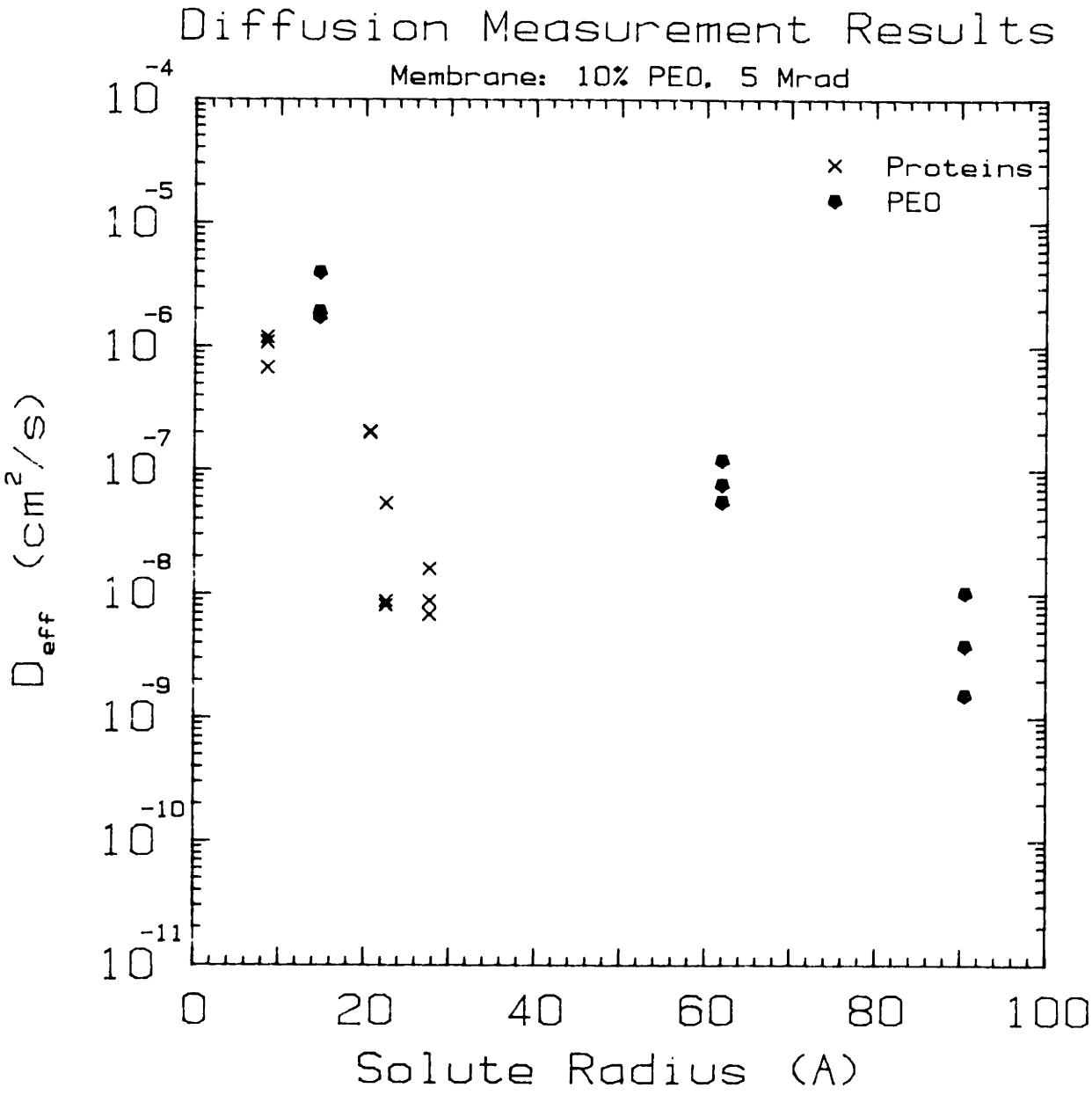
Diffusion Measurement Results
Membrane: 10% PEO, 5 Mrad
Proteins
PEO
D_{eff} (cm^2/s)
10^{-4}
10^{-5}
10^{-6}
10^{-7}
10^{-8}
10^{-9}
10^{-10}
10^{-11}
0
20
40
60
80
100
Solute Radius (A)

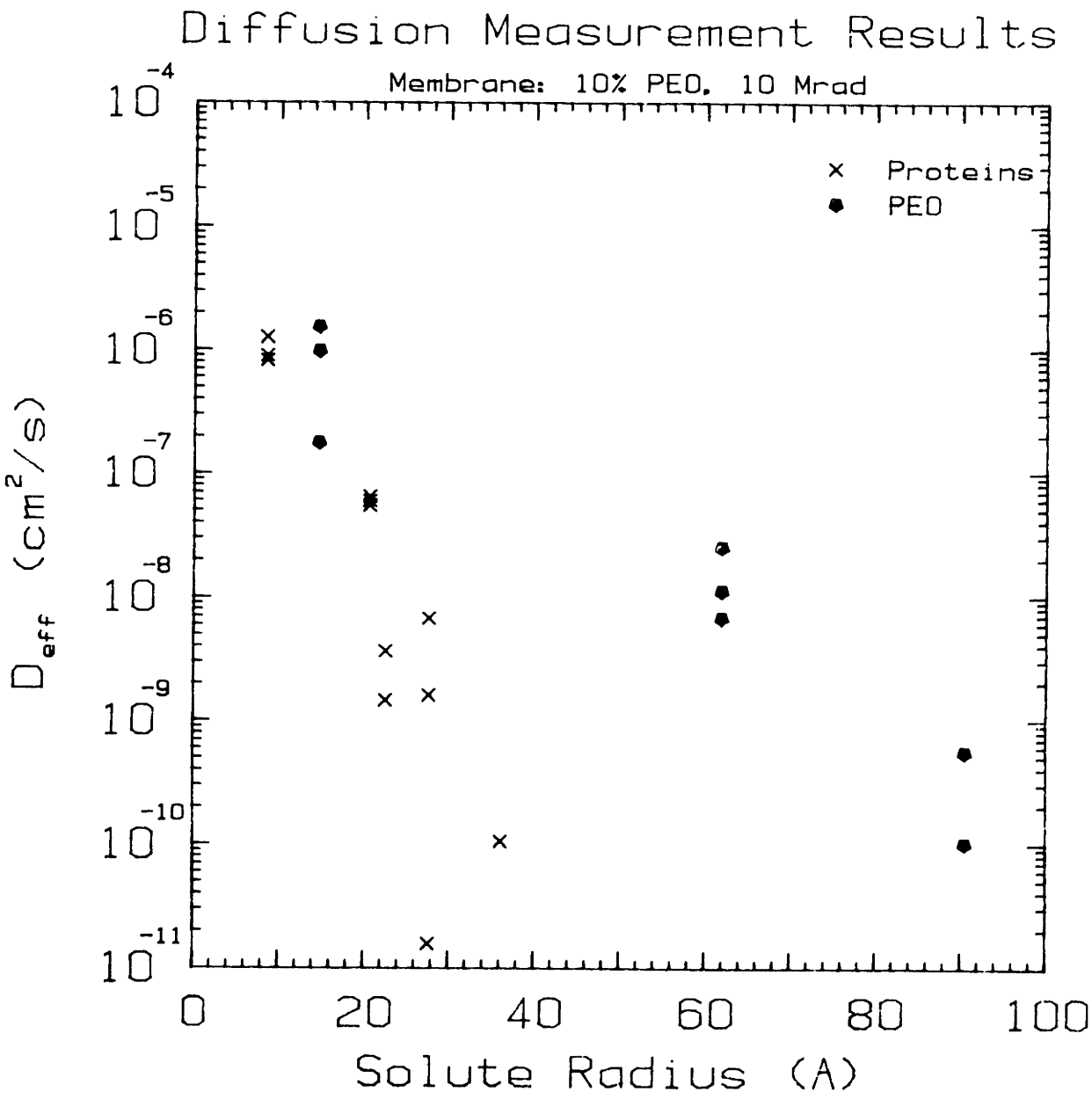
Diffusion Measurement Results
Membrane: 10% PEO, 10 Mrad
Proteins
PEO
D_{eff} (cm^2/s)
10^{-4}
10^{-5}
10^{-6}
10^{-7}
10^{-8}
10^{-9}
10^{-10}
10^{-11}
0
20
40
60
80
100
Solute Radius (A)

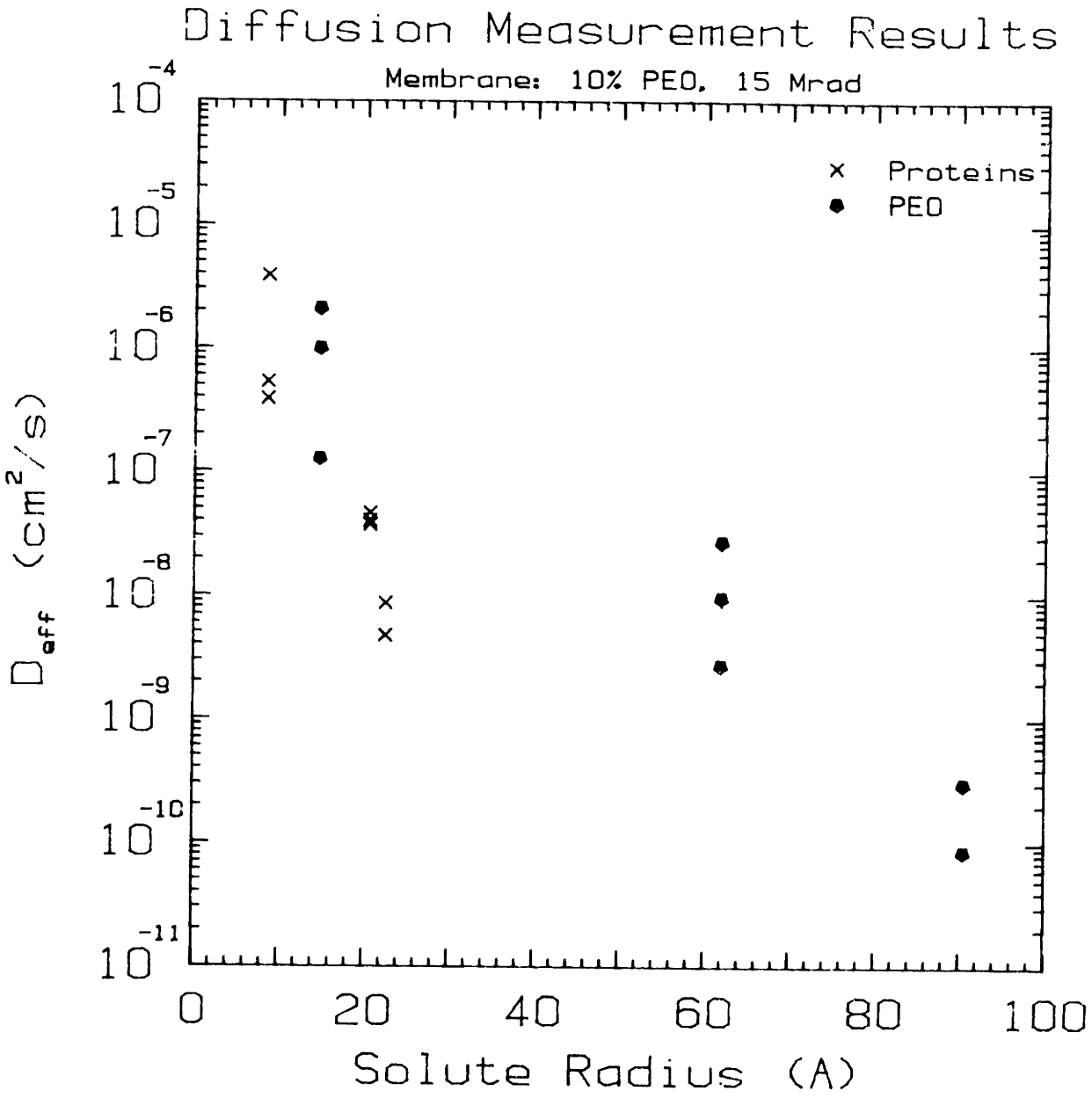
Diffusion Measurement Results
Membrane: 10% PEO, 15 Mrad
Proteins
PEO
D_{eff} (cm^2/s)
10^{-4}
10^{-5}
10^{-6}
10^{-7}
10^{-8}
10^{-9}
10^{-10}
10^{-11}
0
20
40
60
80
100
Solute Radius (A)

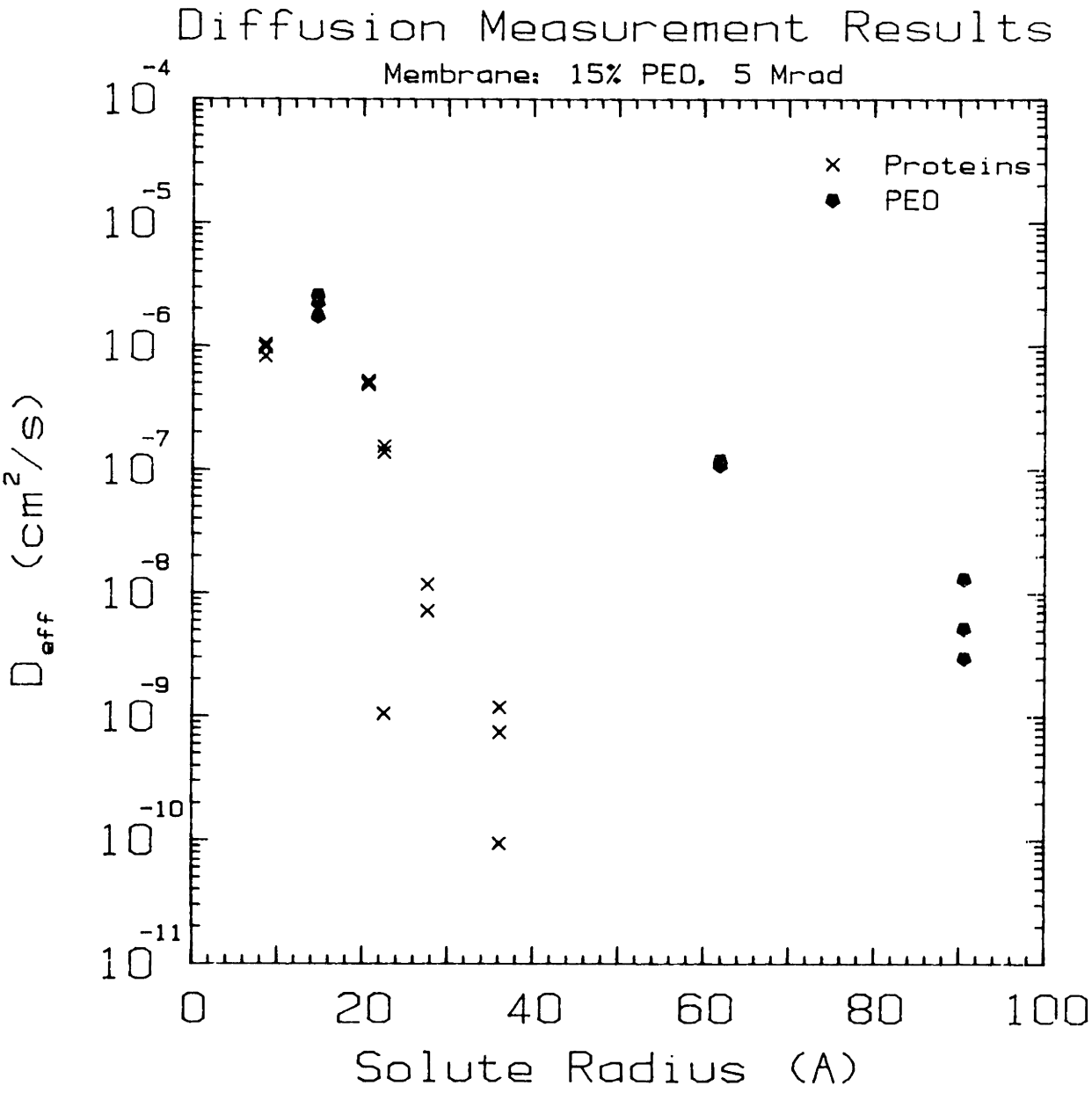
Diffusion Measurement Results
Membrane: 15% PEO, 5 Mrad
Proteins
PEO
D_{eff} (cm^2/s)
10^{-4}
10^{-5}
10^{-6}
10^{-7}
10^{-8}
10^{-9}
10^{-10}
10^{-11}
0
20
40
60
80
100
Solute Radius (A)

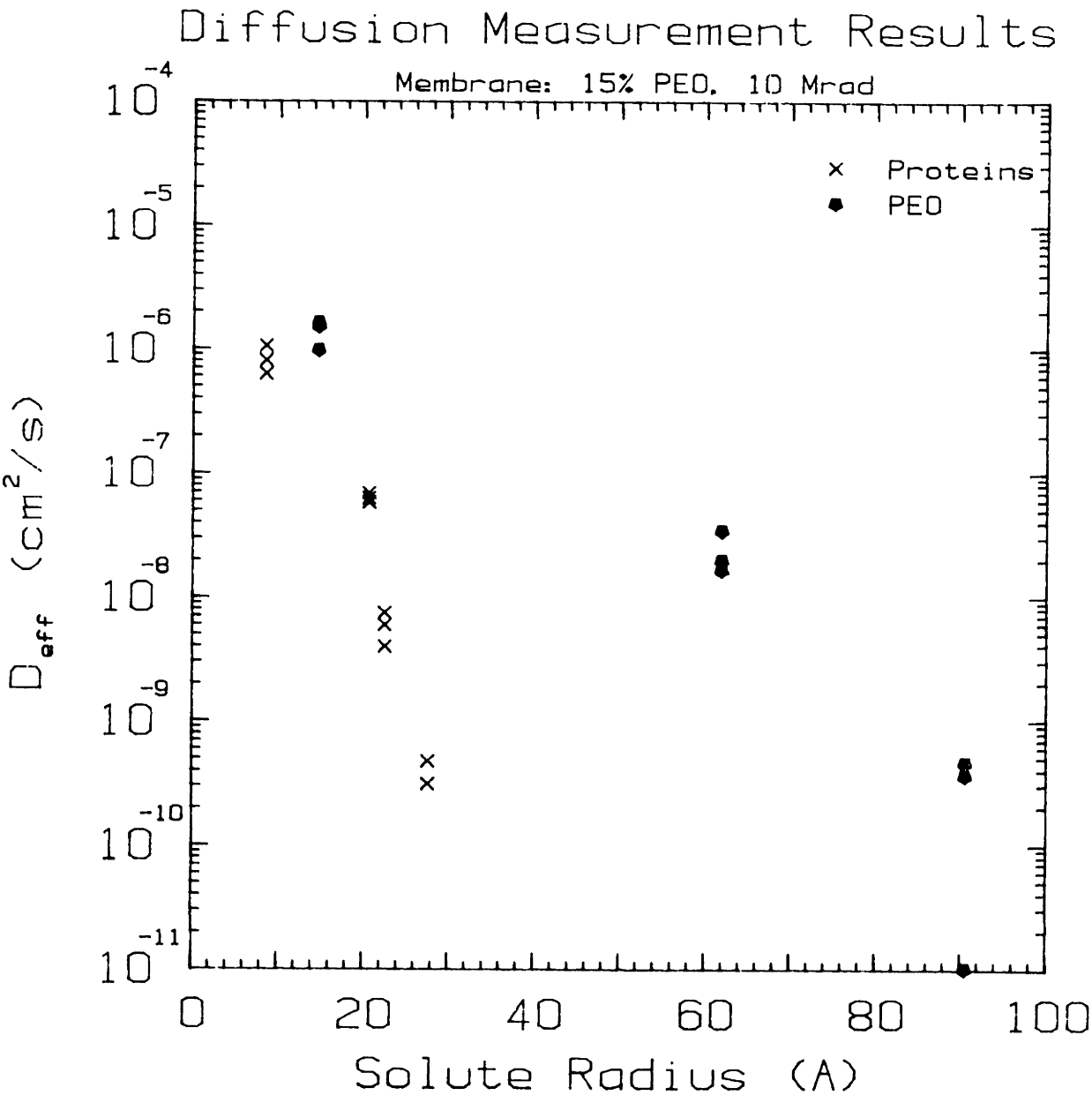
Diffusion Measurement Results
Membrane: 15% PEO, 10 Mrad
Proteins
PEO
D_{eff} (cm^2/s)
10^{-4}
10^{-5}
10^{-6}
10^{-7}
10^{-8}
10^{-9}
10^{-10}
10^{-11}
0
20
40
60
80
100
Solute Radius (A)

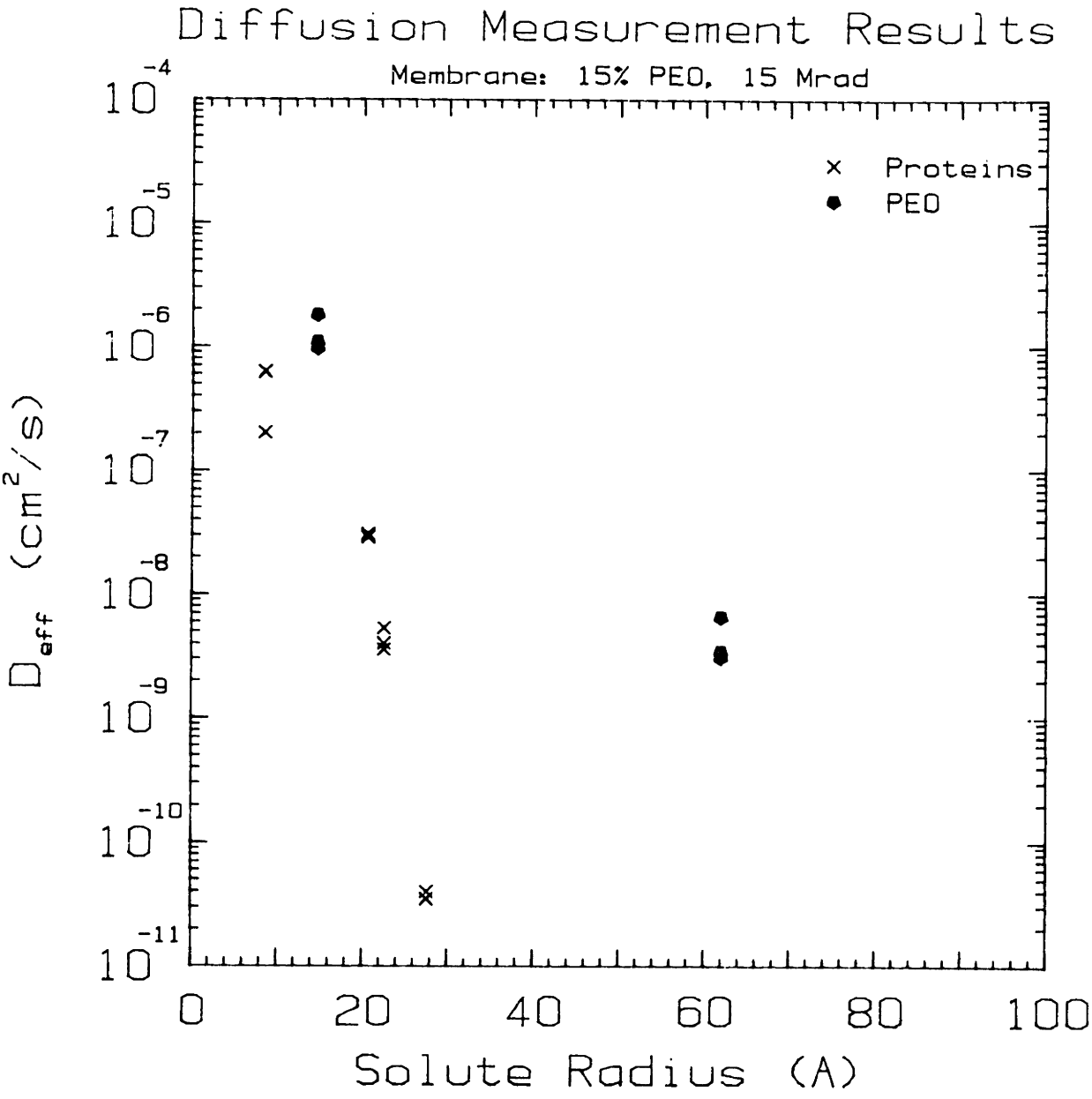
Diffusion Measurement Results
Membrane: 15% PEO, 15 Mrad
Proteins
PEO
D_{eff} (cm^2/s)
10^{-4}
10^{-5}
10^{-6}
10^{-7}
10^{-8}
10^{-9}
10^{-10}
10^{-11}
0
20
40
60
80
100
Solute Radius (A)

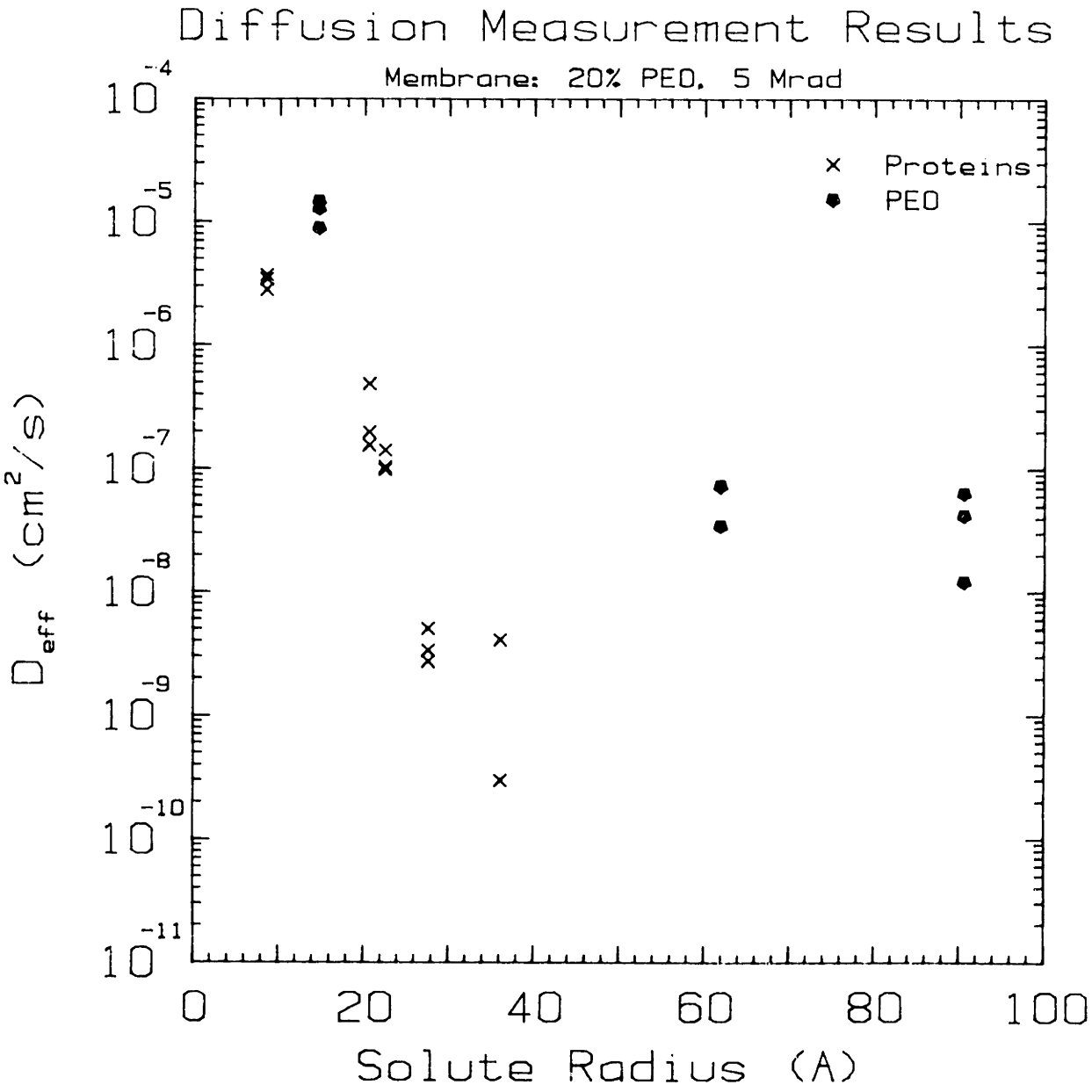
Diffusion Measurement Results
Membrane: 20% PEO, 5 Mrad
Proteins
PEO
D_{eff} (cm^2/s)
10^{-4}
10^{-5}
10^{-6}
10^{-7}
10^{-8}
10^{-9}
10^{-10}
10^{-11}
0
20
40
60
80
100
Solute Radius (A)

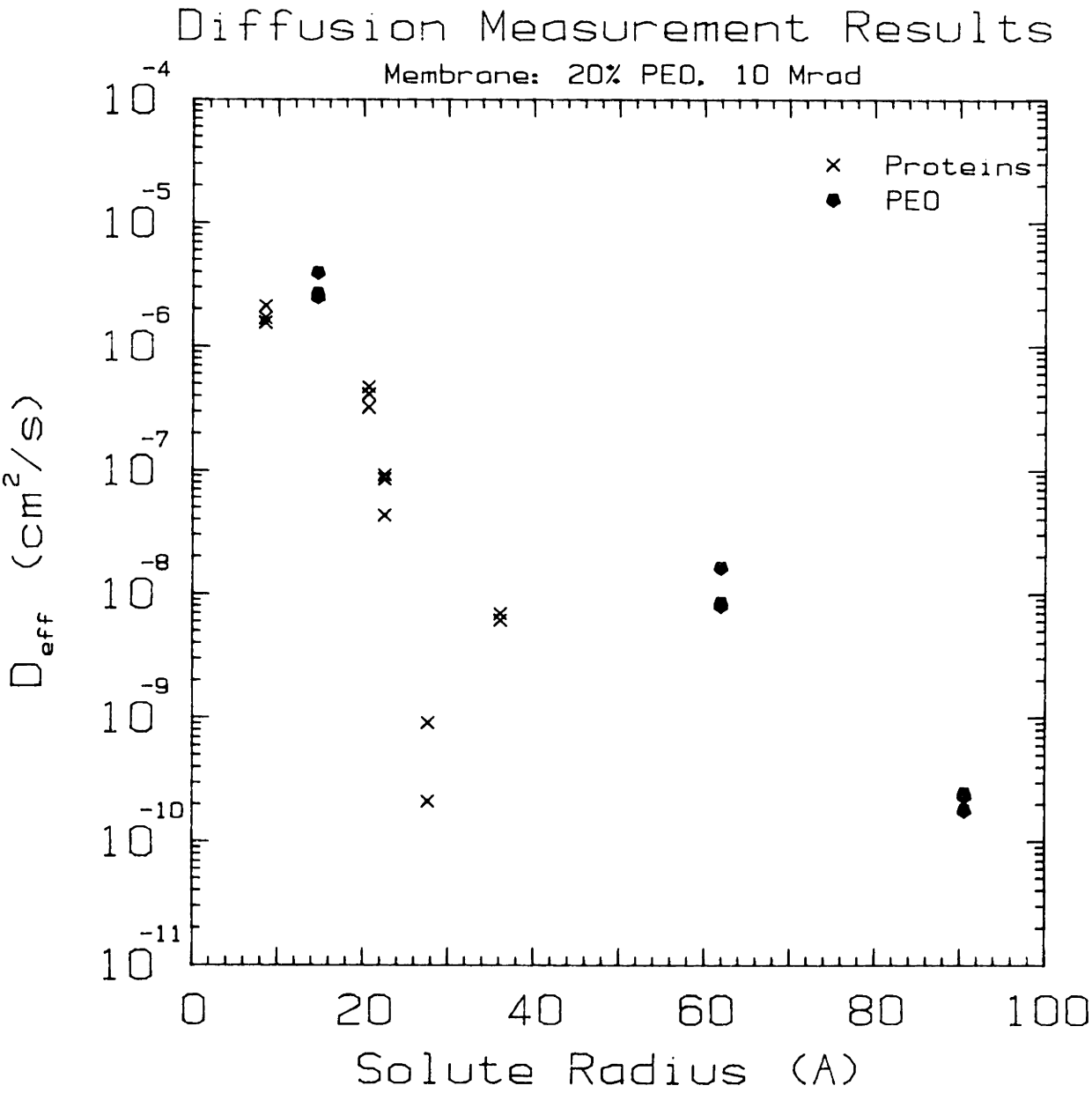
Diffusion Measurement Results
Membrane: 20% PEO, 10 Mrad
Proteins
PEO
D_{eff} (cm^2/s)
10^{-4}
10^{-5}
10^{-6}
10^{-7}
10^{-8}
10^{-9}
10^{-10}
10^{-11}
0
20
40
60
80
100
Solute Radius (A)

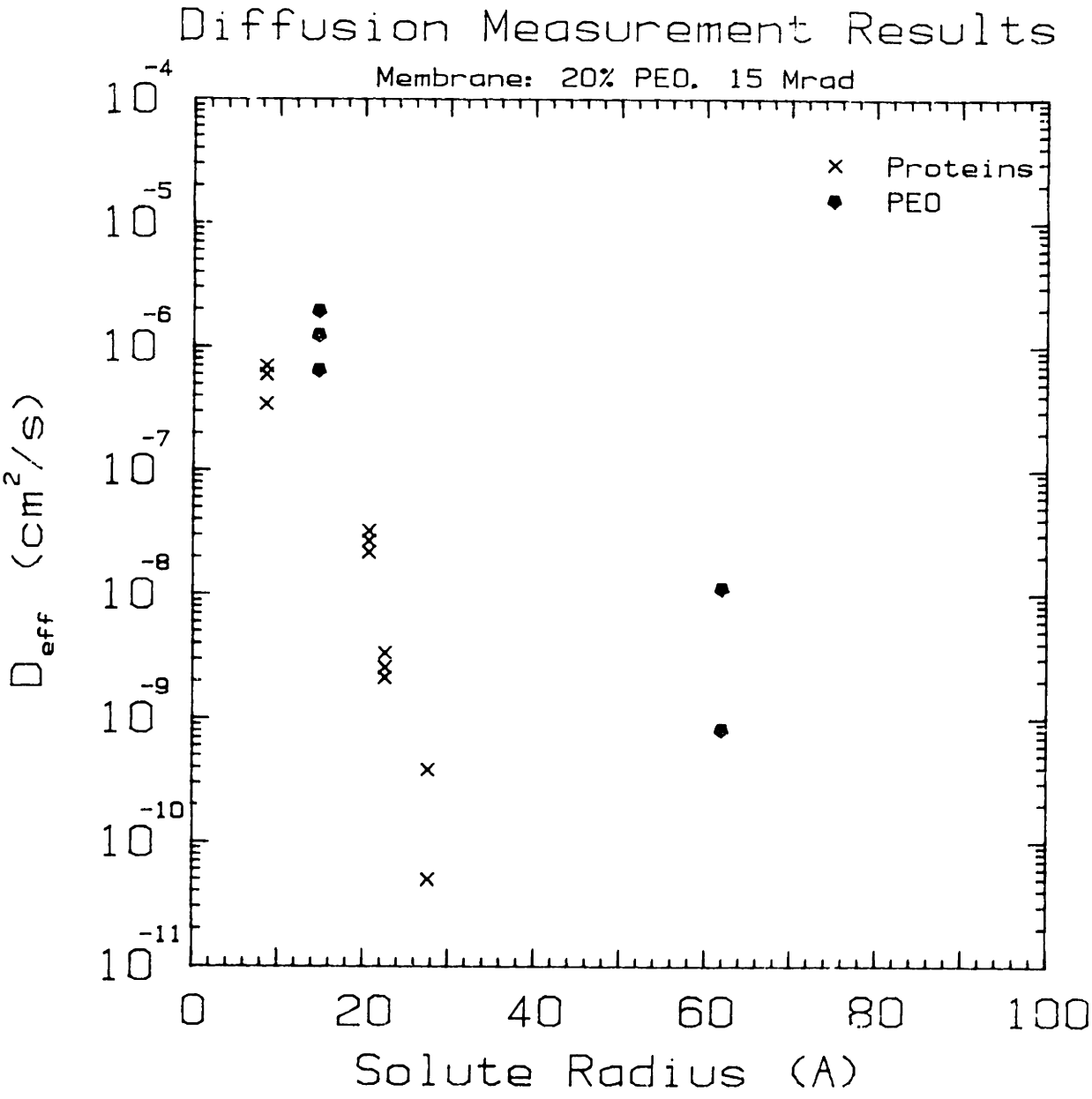
Diffusion Measurement Results
Membrane: 20% PEO. 15 Mrad
Proteins
PEO
D_{eff} (cm^2/s)
10^{-4}
10^{-5}
10^{-6}
10^{-7}
10^{-8}
10^{-9}
10^{-10}
10^{-11}
0
20
40
60
80
100
Solute Radius (A)

Appendix 7. Derivation of the Solution-Diffusion Model

In this appendix, additional details of the derivation of the solution diffusion model and the sieve effect term are given. The reader is advised to refer to sections 2.5.2 and 4.6, especially 4.6.5, for the general discussion of the assumptions and applicability of the model.

The development starts with the assumption of Yasuda et al [70] that the diffusivity can be written as a form of the Eyring rate equation [102]

$$D = \nu e^{-G/kT} = \nu e^{-S/k}\, e^{-H/kT} \qquad \text{(A-19)}$$

where ν is the translational oscillating frequency of the diffusing molecule, G is the activation free energy of diffusion, S is the activation entropy of diffusion, and H is the activation enthalpy of diffusion. The frequency term can be written as $\lambda^2 kT/h$, where λ is the diffusional jump length, k is Boltzmann's constant, h is Planck's constant, and T is the temperature. Equation A-19 can be written for both the swollen polymer network and the pure solvent. Here the polymer will be component 3, the solvent component 1, and the solute 2, so the subscript 2,1 refers to diffusion of solute in pure solvent and 2,13 refers to diffusion of solute in solvent-swollen polymer network. Since the network is assumed to be very highly swollen, the enthalpic term and the diffusional jump length are assumed to be the same for the network and the pure solvent, which leads to the following expression for the ratio of the diffusion coefficients in gel and solvent.

$$\frac{D_{2,13}}{D_{2,1}} = \frac{e^{-S_{2,13}/k}}{e^{-S_{2,1}/k}} \qquad \text{(A-20)}$$

The remaining entropic term is assumed to be purely configurational, and to consist of two parts: the probability of forming a "hole" large enough to permit passage of the diffusing molecule and the probability of finding space in the network large enough to allow the hole. The first part will be designated P(v) and the second $f(V_2)$; these will become the free volume and sieve effect terms respectively. The expression for the diffusion coefficient ratio is now

$$\frac{D_{2,13}}{D_{2,1}} = \frac{\exp\{\ln[P_{2,13}(v)] + \ln[f(V_2)]\}}{\exp\{\ln[P_{2,1}(v)]\}} \qquad \text{(A-21)}$$

The logarithm arises from the Boltzmann postulate relating the possible configurations to the entropy of the system, and the $f(V_2)$ term does not appear in the denominator because there are no mesh restrictions in pure solvent. The first term P(v), the probability of finding a hole large enough to permit diffusion, is assumed to be described by the Cohen and Turnbull model [97] for the distribution of sizes of free volume elements in liquids and glasses. They begin by defining the average free volume v_f as the total free volume in the system V_f divided by the number of molecules N. That is, v_f is the volume available for each molecule in excess of the volume it actually occupies. Assuming that the free volumes are normally distributed about the mean, the probability density p(v) of free volume of size v is

$$p(v) = \frac{\gamma}{v_f} \exp\left[-\gamma v/v_f\right] \quad . \qquad \text{(A-22)}$$

P(v), the probability of finding a hole of at least size v, is thus

$$P(v) = \int_{v}^{\infty} p(v')\, dv' = \int_{v}^{\infty} \frac{\gamma}{v_f} \exp\,[-\gamma v/v_f]$$
$$= \exp\,[-\gamma v/v_f] \qquad \text{(A-23)}$$

In these expressions γ is a factor between 0.5 and 1 which accounts for the fact that some free volume elements overlap. Substituting this into equation A-21 the free volume ratio now becomes

$$\frac{D_{2,13}}{D_{2,1}} = f(V_2)\, \frac{\exp[-\gamma v/v_{f,13}]}{\exp[-\gamma v/v_{f,1}]} \qquad \text{(A-24)}$$
$$= f(V_2)\, \exp[\gamma v(1/v_{f,13} - 1/v_{f,1})]$$

where $v_{f,13}$ is the average free volume in the network and $v_{f,1}$ is the average free volume in the solvent.

At this point, previous workers [70,77] typically have followed the suggestion of Fujita [98] and interpreted the average size of a free volume element as the fractional free volume f, i.e., as the ratio of total free volume in the system to total system volume. This is clearly not correct. However, the concept of the fractional free volume will be introduced here as it is useful in simplifying equation A-24. The fractional free volume is defined as the ratio of the free volume per molecule to the total volume available per molecule. That is,

$$f = v_f N_{av}/\bar{V} \qquad \text{(A-25)}$$

where $\bar{V}$ is the molar volume of the medium through which diffusion is taking place. For a medium with two components, such as the swollen

network, the total fractional free volume will be the sum of the fractional free volumes of each component weighted by their volume fractions. For the present case, using the subscripts 1 and 3 to denote solvent and polymer respectively,

$$f_{13} = N_{av}\left(\frac{v_{f1}}{V_1} v_{1s} + \frac{v_{f3}}{V_2} v_{3s} \right) \qquad \text{(A-26)}$$

where v_{1s} and v_{3s} are the equilibrium solvent and polymer volume fractions in the network. Since v_{3s} is assumed to be small, and v_{f3} will be smaller than v_{f1},

$$f_{13} = v_{1s} f_1 \qquad \text{(A-27)}$$

Substituting equations A-25 and A-27 into equation A-24, assuming the molar volume of the network can be taken as the molar volume of solvent, and making the substitution that $v_{3s} = 1/Q = 1 - v_{1s}$, the following expression is obtained for the diffusion coefficient ratio.

$$\frac{D_{2,13}}{D_{2,1}} = f(V_2) \exp\left[\frac{-\gamma v}{v_f (Q-1)} \right] \qquad \text{(A-28)}$$

v = characteristic volume of the solute
γ = free volume overlap correction
v_f = average size of a free volume element in solvent
Q = swelling ratio = $1/v_{2s}$
V_2 = hole size

The last assumption in the free volume term derivation is that it is the area of the solute rather than the volume that is important in controlling transport, and thus v is replaced by $\lambda \pi r_E^2$ where r_E is the effective hydrodynamic radius of the solute and λ is again the diffusional jump length.

Sieve Term. The derivation of an expression for the sieve term $f(V_2)$ in equation 4-28 will now be described. There are essentially two different approaches that were used in deriving this term. The first assumes that the junctions are causing the restrictions to transport and the size of the space available in the mesh is proportional to the distance between junctions. The second assumes that an Ogston model [101] is appropriate. This model describes the distribution of the size of the spaces in a random array of rods given the rod length, which in this case is assumed to be the topological interjunction distance. Each of the two approaches and the variations on it will be discussed separately.

Interjunction distance distribution approach. As mentioned above, in this approach to the problem of determining the distribution of sizes of spaces between restrictions in the mesh, the junctions are assumed to be restrictions. The size of the spaces is assumed to be the cube of the distance between junctions. The problem, then, is to define and find the distribution of the interjunction distances. There are two different interjunction distances, the topological and spatial distances, and two different approaches were used for finding each, leading to four different distributions of interjunction distances and thus four different expressions for $f(V_2)$.

The basic approach was to find the distribution of end-to-end lengths for the network chains, that is, the distribution of distances between topologically connected junctions. The spatial interjunction distance was assumed to have the same type of distribution but with a smaller

magnitude for the distance. The ratio of the magnitudes was assumed to be the ratio of the average values for the two interjunction distances, which are given in table 4-9. The approach to computing the distribution of end-to-end lengths was to find the distribution of the molecular weights between crosslinks for the network and the distribution of the end-to-end distances for a chain of a specific molecular weight. Given these two quantities, Bayes Theorem can be applied to give the distribution of end-to-end distances for the network. Only a single function was used for the distribution of interjunction molecular weights, but the end-to-end distance distribution was treated in two different ways: (1.) the distribution was assumed to follow the radial distribution of end-to-end lengths predicted by random coiling statistics, and (2.) the end-to-end distance for a particular chain length was assumed to be fixed at the root-mean-square value.

The distribution of molecular weights between crosslinks was assumed to follow a most probable distribution, as radiation crosslinking should be a random process [35]. For simplicity, this distribution is given here in terms of x, the number of repeat units between crosslinks. ($x = M_c/M_0$, where M_0 is the repeat unit molecular weight.)

$$p(x) = \left[1 - M_0 \left(\frac{1}{\bar{M}_c} - \frac{1}{\bar{M}_n} \right) \right]^{x-1} M_0 \left(\frac{1}{\bar{M}_c} - \frac{1}{\bar{M}_n} \right) \qquad \text{(A-29)}$$

$\bar{M}_n$ is the number average molecular weight of the primary molecules and $\bar{M}_c$ is the number average molecular weight of the interjunction chains.

Looking first at the more complicated case for the end-to-end length, the

distribution of end-to-end distances r for a chain with x units p(r/x) is given by [19]

$$p(r/x) = 4\pi r^2 \left(\frac{3}{2\pi \langle \bar{r}^2 \rangle} \right)^{3/2} \exp \left[\frac{-3r^2}{2\langle \bar{r}^2 \rangle} \right] \qquad \text{(A-30)}$$

In this expression, $\langle \bar{r}^2 \rangle$ is the mean square end-to-end distance and is given by

$$\langle \bar{r}^2 \rangle = 3\alpha^2 C x \ell^2 \ . \qquad \text{(A-31)}$$

C is the characteristic ratio for the polymer, ℓ is the bond length, and α is the chain expansion factor. For an isolated random coil, α is the intramolecular expansion factor and depends on the solvent quality and chain molecular weight [19], but for the present case, α is just the linear expansion of a network chain above its unperturbed dimensions, and since network expansion is assumed to be affine (the distances between junctions expand proportionally to the macroscopic network), $\alpha^3 = Q = 1/v_{2s}$.

Since the desired distribution is for the interjunction length of a population of network chains, Bayes Theorem is used to find p(r).

$$p(r) = \Sigma\ p(r/x)p(x). \qquad \text{(A-32)}$$

The summation accounts for all possible values of x from 0 to ∞ and is a sum rather than an integral because x can have only integer values. Combining equations A-29, A-30, and A-32, and defining A, B, and D as follows

$$A = M_0 \left(\frac{1}{\bar{M}_c} - \frac{1}{\bar{M}_n} \right) \tag{A-33}$$

$$B = 4\pi \left(\frac{1}{2\pi\alpha^2 C\ell^2} \right)^{3/2} \tag{A-34}$$

$$D = \frac{1}{2\alpha^2 C\ell^2} \tag{A-35}$$

leads to this expression for p(r)

$$p(r) = \sum_{x=1}^{\infty} B\, r^2 x^{-3/2} \exp -\left[\frac{Dr^2}{x}\right] A\,[1-A]^{x-1} \quad . \tag{A-36}$$

The desired quantity, however, is the probability of a whole being at least size ξ or larger, that is

$$\Phi(\xi) = \int_{\xi}^{\infty} p(r)\, dr \tag{A-37}$$

Substituting equation A-36 into A-37 and switching the order of integration and summation we get

$$\Phi(\xi) = \sum_{x=1}^{\infty} B\, x^{-3/2}\, A[1-A]^{x-1} \int_{\xi}^{\infty} r^2 \exp -\left[\frac{Dr^2}{x}\right] dr \tag{A-38}$$

which can be integrated to give

$$\Phi(\xi) = \frac{B}{2D^{3/2}} A \sum_{x=1}^{\infty} [1-A]^{x-1} \left[\Gamma(3/2) - \sum_{n=0}^{\infty} \frac{(-1)^n \left[\frac{D}{x}\xi^2\right]^{n+1/2}}{n!\,(n+3/2)} \right] \tag{A-39}$$

which is the distribution of the distances between topologically connected junctions in a network with average interjunction molecular weight $\bar{M}_c$. The desired function $f(V_2)$, where V_2 is the volume of the

solute, is found by assuming

$$f(V_2) = \{\Phi(\xi)\}^3 \quad . \tag{A-40}$$

The second approach to the problem of the end-to-end length is simpler. In this approach, the end-to-end distance r is assumed to be the rms end-to-end distance, so

$$r^2 = \langle \bar{r}^2 \rangle = \alpha^2 C n \ell^2 = \alpha^2 3 C \ell^2 x^2 \quad . \tag{A-41}$$

The probability of having a given end-to-end length r is thus just the probability of having degree of polymerization $x = r^2/\alpha^2 3C\ell^2$. The appropriate expression for $\Phi(\xi)$ for this case is thus

$$\Phi(\xi) = \sum_{x=\xi^2/\alpha^2 3C\ell^2}^{\infty} A\,[1-A]^x \tag{A-42}$$

Equations A-39 and A-42 thus give us the topological interjunction distance distributions for the two types of end-to-end distance distributions. To obtain the spatial interjunction distance distribution the same equations are used but the scaling of ξ is different, as discussed above. That is, $\Phi(\xi_s) = (d_s/d_t)\Phi(\xi_t)$.

Ogston model. The Ogston model [101] is essentially a geometric calculation of the sizes of the spaces in a random 3-dimensional array of ν rods of length L per unit volume. The expression given for the probability of finding a space at least large enough to fit a sphere of radius r is

$$P(r) = \exp -(2\pi\nu L r^2 + \frac{4\pi}{3}\nu r^3) \tag{A-43}$$

The task is thus to define L and ν. In the first case, L is taken to be

the average topological interjunction distance as given in table 4-9. ν is then the number of network chains per unit volume of network. This is given by

$$\nu = \frac{v_{2s}\bar{N}_{av}}{M_c \bar{v}_1} \qquad \text{(A-44)}$$

where $\bar{v}_1$ is the polymer specific volume and the other variables are as previously defined. Equations A-44 and A-43 together allow calculation of P(r), which is the equivalent of $f(V_2)$.

A slight modification was made to include the distribution of interjunction lengths. In this case, equation A-43 was taken to be P(r/L) and equation A-36 was taken as p(L), and P(r) = P(r/L)p(L).

Computation. All calculations were done by computer. A variety of programs were written to calculate a number of different distributions and values for $f(V_2)$ as a function of solute size. The two programs that are attached calculate $f(V_2)$ and the diffusion coefficient ratio for the 6 forms of the sieve term discussed here. The first program was written in Fortran 77, the second in BASIC.

```
C
C
C PROGRAM FOR CALCULATION OF EFFECTIVE DIFFUSIVITY
C IN A SWOLLEN PEO GEL, BASED ON TOPOLOGICAL AND
C NEAREST NEIGHBOR INTERJUNCTION DISTANCE DISTRIBUTIONS
C
C
      IMPLICIT DOUBLE PRECISION(A-H,M-Z),INTEGER(I-L)
C
C ***OPENING OUTPUT FILES***
C
      OPEN (20,FILE='INPUT',STATUS='OLD')
      OPEN (21,FILE='OUTRD',STATUS='FRESH')
      OPEN (22,FILE='OUTOTR',STATUS='FRESH')
      OPEN (23,FILE='OUTDC3',STATUS='FRESH')
      OPEN (24,FILE='OUTNN3',STATUS='FRESH')
      OPEN (25,FILE='OUTOG',STATUS='FRESH')
      OPEN (26,FILE='OUTOGT',STATUS='FRESH')
      OPEN (27,FILE='OUTDRAT',STATUS='FRESH')
      OPEN (28,FILE='OUTDR3',STATUS='FRESH')
      OPEN (29,FILE='OUTNDR',STATUS='FRESH')
      OPEN (30,FILE='OUTOGR',STATUS='FRESH')
C
      WRITE (21,*) "1E33,6"
      WRITE (22,*) "1E33,6"
      WRITE (23,*) "1E33,6"
      WRITE (24,*) "1E33,6"
      WRITE (25,*) "1E33,6"
      WRITE (26,*) "1E33,6"
      WRITE (27,*) "1E33,6"
      WRITE (28,*) "1E33,6"
      WRITE (29,*) "1E33,6"
      WRITE (30,*) "1E33,6"
C
C ***READING GEL PROPERTIES***
C
      READ (20,*)MC,V2S,OF
      CLOSE (20)
      QS=1/V2S
      A=44.*(1./MC-1./35000.)
C
C ***LOOP IN INTERJUNCTION DISTANCE R***
C
      DO 400  I=1,30
      R=2.*I
      XSUM=0
      X=0
   50 XSUMO=XSUM
      X=X+1
      NFAC=1.
      N=0.
```

```
      F1A=V2S**2.
      F1=F1A**(1./3.)
      F2=F1*0.0527
      F3=F2/X
      F4=R**2.
      F5=F3*F4
      F6A=F5**3.
      F6B=F6A**.5
      F6=2.*F6B/3.
      SUM=F6
  100 N=N+1.
      SUMO=SUM
      NFAC=NFAC*N**(1./4.)
      W=1/(N+1.5)
      P1=((-1.)**N)/(N+1.5)
      P2=(((0.0527*(V2S**(2./3.)))/(X*NFAC**W*NFAC**W*
     &NFAC**W*NFAC**W))*R**2.)**(N+1.5)
      SUM=SUMO+P1*P2
      IF (ABS((SUM-SUMO)/SUM) .GT. 1E-6) GO TO 100
      XSUM=XSUMO+(1.-A)**(X-1.)*(0.88632-SUM)
      IF (ABS((XSUM-XSUMO)/XSUM) .GT. 1E-6) GO TO 50
C
C ***CALCULATION OF HOLE BIGGER THAN R***
C
      PROB=XSUM*A*1.129
C
C ***CALCULATION OF HOLE AREAS AND DIFFUSION COEFFICIENTS***
C
      V=3.14159*R*R/4
      VD=V/(OF*OF)
      DRAT=EXP(-(V/326.)/(1/V2S-1)
      DOG=EXP(-(4.539*(0.8042*V2S*R*R/MC**0.5+2*V2S*R*R*R/(3*MC))))
      DOGT=DOG*PROB
      DRAT2=PROB*PROB
      DRAT3=DRAT2*PROB
      DR3=DRAT3*DRAT
      DOGR=DOG*DRAT
      DOTR=DOGT*DRAT
C
C ***OUTPUT OF RESULTS***
C
      WRITE(21,500)R,PROB
      WRITE(22,500)V,DOTR
      WRITE(23,500)V,DRAT3
      WRITE(24,500)VD,DRAT3
      WRITE(25,500)V,DOG
      WRITE(26,500)V,DOGT
      WRITE(27,500)V,DRAT
      WRITE(28,500)V,DR3
      WRITE(29,500)VD,DR3
      WRITE(30,500)V,DOGR
      PRINT *,X,R,PROB
```

```
400  CONTINUE
     CLOSE(21)
     CLOSE(22)
     CLOSE(23)
     CLOSE(24)
     CLOSE(25)
     CLOSE(26)
     CLOSE(27)
     CLOSE(28)
     CLOSE(29)
     CLOSE(30)
500  FORMAT(1X,E12.4,",",E12.4)
     STOP
     END
```

```
 2 ' Program for calculation of sieve effect
 4 ' and effective diffusivity
 6 ' for spatial and topological distributions using
 8 ' the rms value for end-to-end distance
10 OPEN "1510.nav" FOR OUTPUT AS #2
20 PRINT #2,"1e33,6"
30 OPEN "1510.tav" FOR OUTPUT AS #1
40 PRINT #1,"1e33,6"
43 OPEN "1510.dta" FOR OUTPUT AS #3
45 PRINT #3,"1e33,6"
47 OPEN "1510.dna" FOR OUTPUT AS #4
49 PRINT #4,"1e33,6"
50 INPUT "input Mc, v2s,OF  ", MC,V2S,OF
60 A=44*(1/MC-1/35000!)
70 SUM = 0 : SUMO=0 :X = 1
80 SUMO = SUM:SUM = SUMO + A*(1-A)^X
90 X = X + 1
100 IF ABS((SUM-SUMO)/SUM) > 1E-08 GOTO 80
110 R = (1/V2S)^(1/3)*1.54*12^.5*XI^.5
120 PRINT R,SUM
130 FOR XI = 1 TO 100
140 SUM = SUM - A*(1-A)^(XI-1)
150 R = (1/V2S)^(1/3)*1.54*12^.5*XI^.5
160 PRINT R,SUM
170 V=R*R*3.14159
180 VN=V/(OF*OF)
185 DIST=SUM*SUM*SUM
188 DRAT=EXP(-(V/326)/(1/V2S-1))
189 DRAN=EXP(-(VN/326)/(1/V2S-1))
190 PRINT #1,V;",";DIST
200 PRINT #2,VN;",";DIST
203 PRINT #3,V;",";DIST*DRAT
205 PRINT #4,VN;",";DIST*DRAN
210 NEXT XI
```

Appendix 8. References

1. Merrill EW; Salzman EW. Polyethylene Oxide as a Biomaterial. ASAIO J 1983, 6, 60-64

2. SaDa Costa V. "Study of Polyurethanes for Biomaterials." PhD Thesis, Massachusetts Institute of Technology, Cambridge MA. (1979)

3. Mahmud NA. "Hydrophilic Segmented Polyurethanes for Biomaterials." ScD Thesis, Massachusetts Institute of Technology, Cambridge, MA. (1983)

4. Brash JL and Uniyal S. Dependence of Albumin - Fibrinogen Simple and Competitive Adsorption on Surface Properties of Biomaterials. J Polymer Sci 1979, 66, 377

5. Lyman DJ. New Synthetic Membranes for the Dialysis of Blood. Trans Am Soc Artif Intern Organs 1964, 10, 17

6. Merrill EW, Salzman EW, SaDa Costa V, Brier-Russell D, Dincer A, Pape P, Lindon JN. Platelet Retention om Polymer Surfaces: Some in vitro Experiments. In Biomaterials: Interfacial Phenomena and Applications. Advances in Chemistry Series 199, American Chemical Society, Washington DC (1982)

7. Furasawa K, Shimura Y, Otobe K, Atsumi K, Tasuda K. Blood Compatibility of Polyether - Polyurethanes. Ronbushi Kobushu 1977, 4, 309

8. Silliman JE. "Network Hydrogel Polymers for Application to Hemodialysis." PhD Thesis, Massachusetts Institute of Technology, Cambridge, MA. (1972)

9. Reinhart CT and Peppas NA. Solute Diffusion in Swollen Membranes. Part II. Influence of Crosslinking on Diffusive Properties. J Membrane Sci 1984, 18, 227-239

10. Wisniewski S, Kim SW. Permeation of Water-soluble Solutes Through Poly(2-Hydroxyethy Methacrylate) Crosslinked With Ethylene Glycol Dimethacrylate. J Membrane Sci 1980, 6, 299-308

11. Pusch W, Walch A. Membrane Structure and its Correlation with Membrane Permeability. J Membrane Sci 1982, 10, 325-360

12. Bailey FE and Koleske JV. Poly(ethylene oxide). Academic Press, New York (1976)

13. Koenig JL and Angood AC. Raman Spectra of Poly(ethylene Glycols) in Solution. J Polymer Sci Pt A-2 1970, 8, 1787-1796

14. Brown W and Stilbs P. On the Solution Comformation of Poly(ethylene oxide). An FT-Pulsed Field Gradient NMR Self-diffusion Study. Polymer 1982, 23, 1780-1784

15. Benko B, Buljan V, Vuk-Pavlovic. Concentration Dependent Proton Magnetic Cross Relaxation in Aqueous Polyoxyethylene Solutions. J Phys Chem 1980, 84, 913-916

16. Maconnachie A, Vasudevan P, Allen G. Molecular Dynamics of Poly(ethylene oxide) in Concentrated Solution. Polymer 1978, 19, 33-38

17. Maxfield J and Shepherd IW. Conformation of Poly(ethylene oxide) in the Solid State, Melt, and Solution Measured by Raman Scattering. Polymer 1975, 16, 505-509

18. Graham NB and McNeill ME. Hydrogels for Controlled Drug Delivery. Biomaterials 1984, 5, 27-36

19. Flory PJ. Principles of Polymer Chemistry. Cornell University Press, Ithaca NY, (1953)

20. Huggins ML. Ann NY Acad Sci 1943, 44, 431

21. Ingram K. "Determination of the Flory Interaction Parameter for Polyethylene Glycol - Water and (Polyethylene Oxide-co- Tolylene Diisocyanate) - Water Systems" SB Thesis, Massachusetts Institute of Technology, Cambridge MA. (1980)

22. Malcom BN and Rowlinson JS. Trans Faraday Soc 1957, 53, 921

23. Bailey FE,Jr and Callard RW. Some Properties of Poly(ethylene oxide) in Aqueous Solution. J Applied Polym Sci 1959, 1, 56-62

24. Luck WAP. The Structure of Aqueous Systems and the Influence of Electrolytes. In Rowland SP (ed.), Water in Polymers. Advances in Chemistry Series 127, American Chemical Society, Washington, DC (1980)

25. Balasubramanian D and Chandini B. Poly(ethylene Glycol) - A Poor Chemist's Crown. J Chem Ed 1983, 60, 77-78

26. Olabisi O, Robeson LM, Shaw MT. Polymer-Polymer Miscibility. Marcel Dekker, New York, (1979)

27. Pekala RW. "Synthesis and Characterization of Polyether/Polysiloxane Networks for Blood-Interfacing Applications." ScD Thesis, Massachusetts Institute of Technology, Cambridge MA. (1984)

28. Mark JE. Bimodal Elastomeric Networks. in Mark JE and Lal J, eds., Elastomers and Rubber Elasticity, ACS Symposium Series 193, American Chemical Society, Washington DC (1982)

29. Charlesby A and Byrne M. Irradiation of Poly(ethylene oxide) Solutions Above and Below the Freezing Point. Radiat Phys Chem 1978, 12, 129-131

30. King PA and Ward JA. Radiation Chemistry of Aqueous Poly (ethylene oxide) Solutions. I. J Polym Sci Part A-1 1970, 8, 253-262

31. Stafford JW. The Radiation Induced Reactions of Aqueous Polyethylene Oxide Solutions. I.Theory of Gelation. Makromol Chem 1970, 134, 57-69

32. VanBrederode RA and Rodriguez F. Gelation of Poly(ethylene oxide) Solutions by Gamma Radiation: Effects of Molecular Weight and Irradiation Conditions. J Appl Polym Sci 1970, 14, 979-987

33. Crouzet C, Decker C, Marchal J. Caracterisation de Reactions Primaires de Degradation Oxydante au Cours de L'autoxydation des Polyoxyethylenes a 25 C: Etude en Solution Aqueuse avec Amorcage par Radiolyse du Solvent. 8.Etude Cinetique en Fonction du pH Compris Entre 1 et 13. Makromol Chem 1976, 177, 145-157

34. Hueston TG. "Effects of Environment, Concentration, and Radiation Dose on Poly(ethylene oxide) Crosslinking." SB Thesis, Massachusetts Institute of Technology, Cambridge MA. (1984)

35. Bovey FA. Effects of Ionizing Radiation on Natural and Synthetic High Polymers. Polymer Reviews 1. Interscience, New York. (1958)

36. Dole M. The Radiation Chemistry of Macromolecules. Academic Press, New York (1972)

37. Shultz AR. Radiation and Crosslinking by Radiation in Fettes EM (ed.), Chemical reactions of Polymers. Interscience, New York (1964)

38. Irradiation of Polymers. Advances in Chemistry Series 66 American Chemical Society, Washington DC (1967)

39. Wilson JE. Radiation Chemistry of Polymers, Monomers, and Plastics. Marcel Dekker, New York (1974)

40. King PA. Radiation Modification of Poly(ethylene oxide). In Irradiation of Polymers. Advances in Chemistry Series 66 American Chemical Society, Washington DC (1967)

41. Ng MKM and Freeman GR. J Am Chem Soc 1965, 87, 1935

42. Graham B. Electron Irradiation of Organic Polyethers. US Patent No. 2,964,455 (1960)

43. Charlesby A and Kopp PM. Radiation Protection of Aqueous Polyethylene Oxide Solutions by Thiourea. Proc Roy Soc (London) Ser A 1966, 291, 129-143

44. VanBrederode RA, Rodriguez F, Cocks GG. Crosslinking of Poly(ethylene Oxide) in Dilute Solutions by Gamma Rays. J Appl Polym Sci 1968, 12, 2097-2104

45. Grollman U and Schnabel W. On the Kinetics of Polymer Degradation in Solution, 9. Pulse Radiolysis of Poly(ethylene oxide). Makromol Chem 1980, 181, 1215-1226

46. Matheson MS, Mamou A, Silverman J, Rabani J. Reaction of Hydroxyl Radicals with Polyethylene Oxide in Aqueous Solution. J Phys Chem 1973, 77, 2420-2424

47. Crouzet C and Marchal J. Caracterisation de Reactions Primaires de Degradation Oxydante au Cours de L'autoxydation des Polyoxyethylenes a 25 C: Etude en Solution Aqueuse avec Amorcage par Radiolyse du Solvent. III.Mecanisme Monomoleculaire de Decomposition des Radicaux Peroxyles et Schema Cinetique de la Production des Coupures Observees par Viscosimetrie. Makromol Chem 1973, 166, 99-116

48. Bray JC. "Formation of Poly(vinyl alcohol) Hydrogels via Electron Beam Irradiation and Chrystallization - Application as a Synthetic Articular Cartilage Material." ScD Thesis, Massachusetts Institute of Technology, Cambridge, MA. (1972)

49. Yasuda H, Lamaze CE. Permselectivity of Solutes in Homogeneous Water-swollen Polymer Membranes. J Macromol Sci - Phys 1971, B5(1), 111-134

50. Wisniewski S, Kim SW. Permeation of Water-soluble Solutes Through Poly(2-Hydroxyethy Methacrylate) Crosslinked With Ethylene Glycol Dimethacrylate. J Membrane Sci 1980, 6, 299-308

51. Meyers KO. "Synthesis and Mechanical Properties of Endlinked Model Multifunctional Silicone Networks." PhD Thesis, Massachusetts Institute of Technology, Cambridge, MA. (1980)

52. Tanford C. Physical Chemistry of Macromolecules. John Wiley and Sons, New York (1961)

53. DeGennes PG. Scaling Concepts in Polymer Physics. Cornell University Press, Ithaca NY (1979)

54. Bastide J, Picot C, Candau S. Some Comments on the Swelling of Polymeric Networks in Relation to Their Structure. J Macromol Sci, Phys 1981, B19, 13

55. Doskocilova D, Schneider B, Jakes J. Dynamic Structure of Swollen Crosslinked Poly(ethylene oxide) Gels from NMR Line-shape Analysis and Magic Angle Rotation NMR. Polymer 1980, 21, 1185-1189

56. Powell RL and Schwarz WH. Rheological Properties of Polyethylene Oxide Solutions. Rheol Acta 1975, 14, 729-740

57. Candau SJ, Young CY, Tanaka T, Lemarechal P, Bastide J. Intensity of Light Scattered from Polymeric Gels: Infuence of the Structure of the Networks. J Chem Phys 1979, 70, 4694-4700

58. Munch JP, Candau S, Herz J, and Hild G. Inelastic Light Scattering by Gel Modes in Semi-dilute Polymer Solutions and Permanent Networks at Equilibrium Swollen State. J de Physique 1977, 38, 971

59. Lakshminarayanaiah N. Transport Phenomena in Artificial Membranes. Chemical Reviews 1965, 6, 491-565

60. Belfort G, ed., Synthetic Membrane Processes. Academic Press, Orlando FL, 1984

26. Peppas NA and Meadows DL. Macromolecular Structure and Solute Diffusion in Membranes: An Overview of Recent Theories. J Membrane Sci, 1983, 16, 361-377

62. Crank J, Park GS, eds., Diffusion in Polymers. Academic Press, New York, 1968

63. Paul DR. Relation Between Hydraulic Permeability and Diffusion in Homogeneous Swollen Membranes. J Polym Sci, Polym Phys 1973, 11, 289-296

64. White ML. The Permeability of an Acrylamide Polymer Gel. J Chem Phys 1960, 64, 1563-1565

65. Paul DR. Further Comments on the Relation Between Hydraulic Permeation and Diffusion. J Polym Sci, Polym Phys 1974, 12, 1221-1230

66. Colton CK. "Permeability and Transport Studies in Batch and Flow Dialyzers with Applications to Hemodialysis." PhD Thesis, Massachusetts Institute of Technology, Cambridge, MA. (1969)

67. Colton CK, Smith KA, Merrill EW, Farrell PC. Permeability Studies with Cellulosic Membranes. J Biomed Mater Res 1971, 5, 459-488

68. Paul DR, Ebra-Limo OM. Hydraulic Permeation of Liquids Through Swollen Polymeric Networks. III. A generalized Correlation. J Appl Polym Sci 1975, 19, 2759-2771

69. Cooney DO. Biomedical Engineering Principles. Marcel Dekker, New York, 1976

70. Yasuda H, Peterlin A, Colton CK, Smith KA, Merrill EW. Permeability of Solutes Through Hydrated Polymer Membranes. Part III. Theoretical Background for the Selectivity of Dialysis Membranes. Makromol Chem 1969, 126, 177-186

71. Fujita H. Diffusion in Polymer-Diluent Systems. Fortschr Hochpolym-Forsch 1961, 3, 1-47

72. Tay SW. PhD Thesis, Massachusetts Institute of Technology, Cambridge MA, 1986

73. Faxen H. Die Bewegung einer starren Kugel Langs der Achse eines mit zahrer Flussigkeit gefullen Rohres. Arkiv Mat Astron Fys 1923, 17, 27

74. Anderson JL, Quinn JA. Restricted Transport in Small Pores. A Model for Steric Exclusion and Hindered Particle Motion. Biophys J 1974, 14, 130-150

75. Ratner BD, Miller IF. Transport Through Crosslinked Poly(2-Hydroxyethyl methacrylate) Hydrogel Membranes. J Biomed Mater Res 1973, 7, 353

76. Vrentas JS, Duda JL. Molecular Diffusion in Polymer Solutions. AIChE J 1979, 25, 1-24

77. Peppas NA, Reinhart CT. Solute Diffusion in Swollen Membranes. Part I. A New Theory. J Membrane Sci 1983, 15, 275-287

78. Brandrup J, Immergut EH, eds. Polymer Handbook. John Wiley and Sons, New York (1975)

79. Cohen AL. Critical Point Drying. In Hayat MA (ed.), Principles and Techniques of Scanning Electron Microscopy. Van Nostrand Reinhold Co., New York (1974)

80. Operating Instructions, Wilks Mini-Press KBr Pellet Maker Kit. Foxboro Analytical, So. Norwalk, CT (1979)

81. Instructions, Multiple Internal Reflectance Accessory. Perkin-Elmer Corp., Norwalk, CT (1977)

82. Yau WW, Kirkland JJ, Bly DD. Modern Size Exclusion Liquid Chromatography. John Wiley and Sons, New York (1979)

83. Basedow AM, Ebert KH, Ederer HJ. Kinetic Studies on the Acid Hydrolysis of Dextran. Macromolecules 1978, 11, 774-781

84. Egusa S, Ishigure K, Tabata Y. Fast Neutron Irradiation Effects on Polymers. 1. Degradation of Poly(methyl methacrylate). Macromolecules 1979, 12, 939-944

85. Merrill EW, Horn AF. Scission of Macromolecules in Dilute Solution: Extensional and Turbulent Flows. Polym Commun 1984, 25, 263

86. Micropak TSK Exclusion Columns Manual. Varian Associates Inc., Walnut Creek CA (1982)

87. Colton CK, Satterfield CN, Lai CJ. Diffusion and Partitioning of Macromolecules Within Finely Porous Glass. AIChE J 1975, 21, 289-298

88. Guillot G, Leger L, Rondelez F. Diffusion of Large Flexible Polymer Chains through Model Porous Membranes. Macromolecules 1985, 18, 2531-2537

89. Sober HA, ed., CRC Handbook of Biochemistry. Selected Data for Molecular Biology, Chemical Rubber Co., Cleveland, OH (1968)

90. Crank J. The Mathematics of Diffusion. Clarendon Press, Oxford (1975)

91. Ma YH and Evans LB. Transient Diffusion from a Well-Stirred Reservoir to a Body of Arbitrary Shape. AIChE J 1968, 14, 956-961

92. Adamson AW. A Textbook of Physical Chemistry. Academic Press, New York (1973)

93. Byakov VM, Ershler BV, Bugaenko LT. Effects of Various Factors on the Radiolytic Product Yields from Water, in Dobo J and Hedvig P (eds), Proceedings of the Second Tihany Symposium on Radiation Chemistry. Akademiai Kiado, Publishing House of the Hungarian Academy of Sciences, Budapest (1967)

94. Baskir J. PhD Thesis (in progress). Massachusetts Institute of Technology, Cambridge, MA

95. DeGennes PG. Reptation of a Polymer Chain in the Presence of Fixed Obstacles. J Chem Phys 1971, 55, 572-579

96. Beck RE and Schultz JS. Hindrance of Solute Diffusion within Membranes as Measured with Microporous Membranes of Known Pore Geometry. Biochim Biophys Acta 1972, 255, 273

97. Cohen MH and Turnbull D. Molecular Transport in Liquids and Glasses. J Chem Phys 1959, 31, 1164-1169

98. Fujita H. Diffusion in Polymer-Diluent Systems. Fortschr Hochpolym-Forsch 1961, 3, 1-47

99. Meares P. Diffusion of Allyl Chloride in Polyvinyl Acetate. Part I. The Steady State of Permeation. J Polym Sci 1958, 27, 391-404

100. Rossi C, Bianchi E, Conio G. Proprieta' di Poliossietilenglicoli in Soluzione. Chem Ind (Milan), 1963, 45 (12), 1498-1501

101. Ogston AG. The Spaces in a Uniform Random Suspension of Fibres. Trans Far Soc, 1958, 1754-1757

102. Glasstone S, Laidler KJ, Eyring H. The Theory of Rate Processes, McGraw-Hill, New York, 1941